On the role of blood flow induced inflammation in cerebral aneurysm formation

Xizhuo Jiang[1], Daniel C. Baeriswyl[1], Maria Pikoula[1,2], Matthew B. Tessier[3], Ioanna Prionisti[4], Tom Peach[1], Grigoris Tsolkas[4], Muye Feng[1], Kok Yean Chooi[4,5], John Vardakis[1], Sandrine Morel[6], Mannekomba R. Diagbouga[6], Philippe Bijlenga[7], Hipeng Gong[8], Simon Cuhlmann[4], Robert J. Woods[3], Paul Evans[4,9], Brenda R. Kwak[6], Paul Watton[9], Kai Luo[1], Rob Krams[4,5], Yiannis Ventikos[1]

University College London[1], University of Oxford[2], Univrsity of Georgia[3], Imperial College London[4], Queen Mary University London[5], University of Geneva[6], Geneva University Hospitals[7], Tsinghua University[8], University of Sheffield[9]

Introduction

The progression of cerebral aneurysms from inception and initiation to growth and rupture (or stabilisation) involves a multitude of factors, endogenous and exogenous, that exhibit complex mechanobiological interplay. These phases are quite distinct in nature and encompass different mechanisms and processes. The exact role haemodynamics plays is debated and investigated intensely, since the magnitude and nature of loads put on the vascular wall by blood flow (pressure & Wall Shear Stress, regular or disturbed) affect the evolution of the disease, but are also a prime target for a wide class of therapies, importantly minimally invasive implantable devices.

Methods

In this study, we attempt to approach the role haemodynamics play along four scales and using two investigation techniques: we conduct experiments that involve the cellular level (i.e. endothelial culture under static and flow conditions) looking at cell mobility and NF-kB activity. We go one scale up and model populations of such cells and how they react to stimuli. We also go down a scale and model the exact manner that relevant cell molecular structures (i.e. the glycocayx) translate extracellular mechanical stumuli (flow) to intracellular signals, by conducting detailed large scale direct simulation molecular dynamics numerical experiments with emphasis on transmebrane proteins response, Figure 1. Insight acquired by such methods is then embedded in large – organ scale – mechanical models that attempt to mimic the process of whole aneurysm growth, from inception to stabilisation or to rupture.

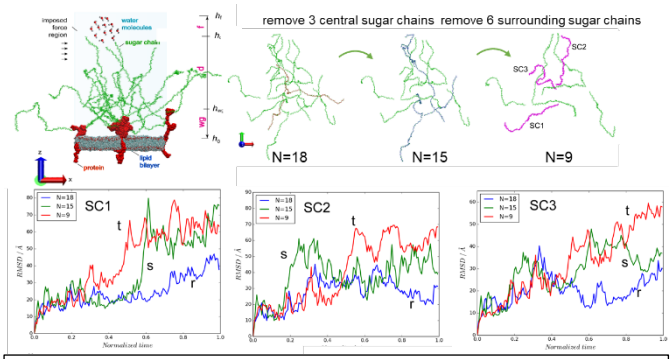

Figure 1: The direct simulation molecular dynamics system used, initially with 18 sugar chains per transmebrane protein. Subsequent simulations involved a damaged system with 15 and with 9 sugar chains per protein. Conformational patterns and the response of this system to flow, as injury levels increase is demonstrated.

Results

A multitude of findings is produced by this combination of experimental and computational techniques. At the smaller scale, the complex mechanical interplay of sugar chains, syndecan-4, the lipid bilayer and flow reveals that the transmission of information from flow to cytoskeleton happens in a highy organized manner. At the cell scale, nuclear translocation is found to coreelate well with stimuli, yet often cell populations are observed to exhibit counter-intuitive motile behavior. At the vasculature level, we can show that models of collagen deposition can mimic aneurysm growth and capture well shapes and volumes of real aneurysms, as identified though medical imaging modalities.

Conclusions

The ultimate goal of such mechanobiological studies is to achieve understanding and predictive capability to forecast the evolution of disease, with the ambition to generate risk markers useful in the healthcare management of the disease; importantly answering the question: is this a case where risk justifies intervention? Although substantial progress is achieved, we are still not in a position to answer such questions with the required certainty to translate such methodologies into a prognostic clinical tool.

A novel mechanosensor in the endothelium

Ellie Tzima
University of Oxford, UK

Shear stress imparted by blood flow on arteries is a critical determinant of vascular development and homeostasis but can also be an instigator of atherosclerosis. Endothelial cells (ECs) lining the vasculature use molecular mechanosensors to directly detect shear stress profiles that will ultimately lead to atheroprotective or atherogenic responses. This presentation will introduce our group's recent discovery of a new mechanosensor. We show that loss of this protein abolishes EC responses to shear stress *in vitro*, while endothelial-specific deletion disrupts EC alignment in the direction of flow *in vivo*, a hallmark response to atheroprotective shear stress. Loss of this protein in ECs results in reduced inflammation and deposition of plaques in areas exposed to atheroprone shear stress. Direct force application shows it acts as a mechanosensor upstream of the junctional mechanosensory complex and integrins. Our results establish a novel mechanosensor in ECs that regulates vascular function and atherosclerosis.

Piezo1 mechano-sensor in vascular physiology and disease

Professor David Beech
Leeds University

In mammals the sensing of blood flow is pivotal for embryonic maturation and adult physiology and disease. How this sensing occurs has been surprisingly difficult to decipher. We have revealed how calcium-permeable non-selective cationic channels formed by Piezo1 proteins assemble to act as sensors of blood flow and determinants of vascular structure in murine development and adult physiology (Li et al 2014 *Nature* 515, 279-; Rode et al 2017 *Nature Comms* 8, 350-). Conditional deletion has been necessary for detailed studies in the adult where we found endothelial Piezo1 was necessary for blood pressure determination in whole body physical exercise (Rode et al 2017). We suggested contribution as an exercise sensor (Beech 2017 *J Physiol* 596, 979-). In both embryo and adult there was compelling evidence for endothelial Piezo1 channels as direct sensors of force, yet exactly how they enable sensing of this force – and thus of blood flow - remains unclear. Intriguingly, Piezo1 channels present a dichotomy for the endothelium in conferring both vasodilator and vasoconstrictor capabilities, the relative importance of which may depend on context (Rode et al 2017; Evans et al 2018 *Br J Pharmacol* 175, 1744-). Small-molecule activation of Piezo1 channels has been discovered in the form of Yoda1 and our studies have started to show the tight chemical requirements for this pharmacological effect, yet there was sufficient flexibility for us to discovery a competitive antagonist of Yoda1 which we refer to as Dooku1 (Evans et al 2018). Disease-causing mutations in human *PIEZO1* have been linked to Generalized Lymphatic Dysplasia, suggesting importance in human endothelium. Our studies of tissues from patients are also suggesting relevance to human physiology and disease (Morley et al 2018 *Mol Hum Reprod* 24, 510-). While there might be potential for novel therapeutics targeted to Piezo1 it will be necessary to take account of the broad roles of Piezo1 in various cell and tissue types (Beech & Xiao 2018 *J Physiol* 596, 965-; Beech 2019 *Cell Calcium* 77, 77-78). Supported by grants from the Medical Research Council UK, Wellcome Trust and British Heart Foundation.

Cilia and their role in mechano-sensing

Julien Vermot
IGBMC, France

Cells act as force sensors and can actively trigger physical changes during embryonic patterning and growth. Defects in these processes can cause catastrophic developmental abnormalities, in particular in the cardiovascular system where blood flow is generating mechanical forces essential for cardiogenesis. Our goal is to understand the dynamics and the roles of biological flow during the development of the zebrafish. We use live imaging techniques, cell biology and genetic analysis to characterize the physical stimuli and the molecular mechanisms that specify cell responses to flow forces during embryogenesis. We will discuss our recent results assessing flow forces affect cardiovascular morphogenesis.

Evaluation of shear stress and strain in pig coronaries

Ranil de Silva
Imperial College London, UK

Identification of coronary plaques at risk of causing future acute coronary syndromes (ACS) in appropriately selected high risk patients remains a major unmet clinical challenge. We show that specific patterns of lowered and multi-directional wall shear stress cause the development of human-like advanced coronary atherosclerotic plaques, including thin cap fibroatheroma (TCFA), in hypercholesterolaemic transgenic minipigs. Like the majority of investigations in this field, we have not accounted for the interaction between pressure-wall distension and shear stress metrics. We address these limitations within the framework of subject-specific fluid-structure interaction (FSI) model to improve not only the determination of our previously developed local haemodynamic shear stress metrics but also to provide estimates of plaque wall strain and stress. We aim to use AI approaches which consider the complete biomechanical environment, as well as conventional plaque morphology criteria and local plaque biomarkers to develop models that predict the development of advanced plaque morphologies and their risk of rupture.

Spatial relationships among local endothelial shear stress, minimal luminal area, and near-infrared spectroscopy lipid signal in patients with coronary artery disease: *Implications for plaque destabilization*

Anubodh S. Varshney, MD, Ahmet U. Coskun, PhD, Gerasimos Siasos, MD, PhD,
Charles Maynard, PhD, Dimitris Fotiadis, PhD, Ryan D. Madder, MD, Peter H. Stone, MD

Aims. To explore how local endothelial shear stress (ESS) patterns, minimal luminal area (MLA), and near-infrared spectroscopy (NIRS) lipid signal spatially relate in arteries with large lipid rich plaques (LRP) versus arteries with smaller LRP.

Methods and Results. Coronary arteries imaged with invasive angiography and NIRS-intravascular ultrasound (IVUS) underwent 3D reconstruction and computational fluid dynamics calculations of local flow patterns. ESS, lumen area, and lipid core burden index (LCBI) were obtained for each 3-mm arterial segment. The locations of maximum ESS (maxESS), minimum ESS (minESS), MLA, and maximum LCBI in a 4-mm segment (maxLCBI4mm) were determined for each artery and classified as spatially concordant or discordant. Large LRP arteries were characterized by higher maxESS (9.31± 4.78 vs. 6.32 ± 5.54 Pa; p = 0.023), lower minESS (0.41 ± 0.16 vs. 0.61 ± 0.26 Pa; p = 0.007), and smaller MLA (3.54 ± 1.22 vs. 5.14 ± 2.65 mm2; p = 0.002) compared with non-large LRP arteries. The location of the maxLCBI4mm was spatially discordant from the sites of MLA (p<0.0001), maxESS (p=0.003), and minESS (p=0.003) in most arteries in both groups.

Conclusions. The locations of the MLA, maxESS, and minESS were spatially discordant from the maxLCBI4mm in most arteries, independent of the presence of large LRP. Prospective, longitudinal studies are required to determine which ESS patterns and spatial relationships between plaque elements predict plaque progression and destabilization.

Spatial relationships between location of maxLCBI and minESS, max ESS, and MLA:

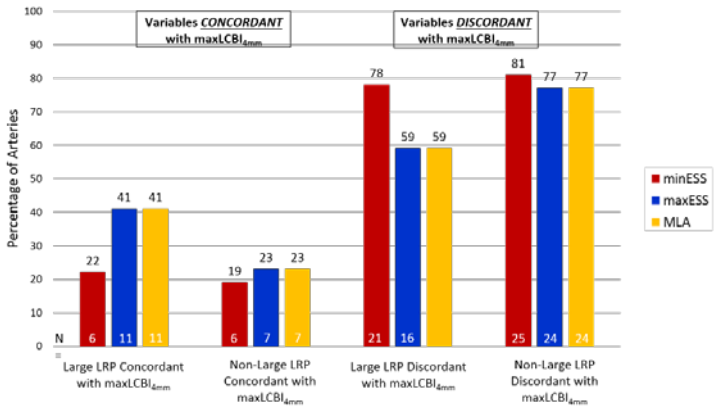

Percentage of arterial surface area of ESS categories in large and non-large LRP arteries:

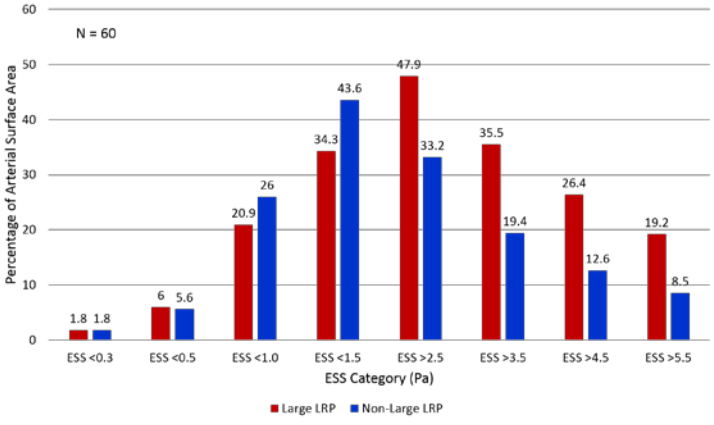

The role of NFkB in mechanotransduction

Martin Schwartz
Yale, USA and Manchester, UK

Fluid shear stress, the frictional force from flowing blood, is a critical determinant of morphogenesis and physiology in the vascular system, and a critical determinant of atherosclerosis, which arises selectively in regions of low and disturbed flow. We previously identified a complex consisting of PECAM-1, VE-cadherin and VEGFR2 that resides at cell-cell junctions and transduces forces from fluid flow into biochemical signals. We have also found that the matrix beneath the endothelial cells is a major modulator of the signals from flow, determining whether flow activates inflammatory vs. anti-inflammatory pathways and subsequent vascular remodeling or development of atherosclerotic plaque. I will present our latest work on elucidation of mechanisms by which endothelial cells sense fluid shear stress and their role in vascular remodeling and atherosclerosis.

Imaging Perivascular Fat to Predict Cardiovascular Events

Charalambos Antoniades
University of Oxford, UK

Coronary inflammation is a widely accepted driver of coronary atherosclerosis, contributing to plaque development and rupture, leading to heart attacks. Recent discoveries pointed out that the inflamed coronary arteries send signals (inflammatory cytokines) to their perivascular space, years before the development of atherosclerotic plaques. The perivascular adipocytes, sense these signals and change their morphology, composition and way they are “packed together” in the fat tissue. These biological changes lead to structural and morphological changes of perivascular fat that precede the development of coronary atherosclerosis. Similarly, the inflamed atherosclerotic plaques cause changes in the perivascular space that could differentiate the unstable (inflamed) from stable (less inflamed) plaques. We have developed an imaging technology that utilizes AI approaches to characterize these changes in the perivascular space by analysis images from standard coronary computed tomography angiography (CCTA). A new imaging biomarker, the Fat attenuation index (FAI), was developed to capture these changes in perivascular space, in a way that it identifies the inflamed coronary arteries. FAI has been tested in a recent prospective study of 4000 people undergoing cardiac CT angiography, showing that it has a striking prognostic value in identifying individuals at risk for future fatal and non-fatal heart attacks. This technology is expected to become a mainstream tool for risk stratification, in patients undergoing cardiovascular CT.

Molecular Imaging of advanced plaques

René Botnar
Kings College London, UK

Atherosclerosis is the leading cause of cardiovascular morbidity and mortality. Over the past two decades, increasing research attention is converging on the early detection and monitoring of atherosclerotic plaque. Amongst a number of invasive and non-invasive imaging modalities, magnetic resonance imaging (MRI) is emerging as a promising option. Advantages include its versatility, excellent soft tissue contrast for plaque characterisation and lack of ionizing radiation. In this talk, I will explore the recent advances in multi-contrast and multiparametric imaging sequences that are bringing the aspiration of simultaneous arterial lumen, vessel wall and plaque characterisation closer to clinical feasibility. I will also discuss the latest advances in molecular MR and multimodal atherosclerosis imaging.

Sex Differences in Autosomal DNA Methylation of Atherosclerotic Plaques from Patients Undergoing Carotid Endarterectomy

Hester M. den Ruijter
Laboratory of Experimental Cardiology, University Medical Center Utrecht, Utrecht, The Netherlands

Sex differences are evident in atherosclerosis with women having more stable plaques and plaque erosion as substrate for cardiovascular disease, as compared to men where plaque rupture is dominant. The extent to which these differences are correlated to DNA methylation (DNAm) in atherosclerotic plaques is not known. To assess sexual dimorphic autosomal DNAm at CpG-dinucleotides (CpGs) in atherosclerotic plaques from carotid endarterectomy patients, we performed an epigenome-wide association study on sex (♀ n = 180, ♂ n = 495). We applied a Bayesian method to control for latent bias and inflation. 2,464 CpG sites were differentially methylated between the sexes. As DNAm is heavily cell-type and tissue-specific, we determined how much of the found sex differences in DNAm are driven by plaque composition. The strongest effects on DNAm sex differences were observed for smooth muscle cell content and intraplaque hemorrhage, affecting 1,336 (54.2%) and 1,358 (55.1%) of the total number of differentially methylated CpGs, respectively. The majority of CpGs (80.6%) not affected by plaque composition are methylated more in females and more often located in promoters than those in males, which are more often located in gene bodies. In addition, we associated genetic data with DNAm in carotid plaques in both sexes, showing that 70.4% of differentially methylated CpGs can be affected by sex-specific genetic variation. Additional RNA-sequencing data of atherosclerotic tissue showed that genes with more promoter methylation in women have lower expression in women as well (Chi-square test p-value = 0.003). In conclusion, substantial sexual dimorphic autosomal DNAm exists in atherosclerotic plaques, partly explained by plaque composition and genetic variation. These data provide insight into the etiological differences between the sexes in atherosclerosis which may be linked to differences in DNA methylation.

Funding: This study was funded by the Dutch Heart Foundation (Queen of Hearts T084/2013).

Gender differences in Abdominal Aortic Aneurysm

T.Christian Gasser
KTH Solid Mechanics, KTH Royal Institute of Technology, Stockholm, Sweden; Faculty of Health Sciences, University of Southern Denmark, Odense, Denmark

The natural history of Abdominal Aortic Aneurysms (AAAs) is determined by the proteolytic degradation of elastin and collagen in the aortic wall, resulting in the dilatation and eventual rupture of the vessel wall. High age, smoking, male gender, family history for AAAs, Caucasian ethnicity, unfavourable blood lipid profile, hypertension and a number of connective tissue disorders increase the likelihood of developing an AAA, whilst diabetes is seen to lower it.

In an effort to prevent patients from aortic rupture, 414 open surgeries and 612 endovascular aortic repairs (EVAR) were carried out in Sweden in 2017 [1]. Whilst AAA prevalence is approximately five times lower in females than in males, the female aneurysmatic aorta has a higher risk of rupture [2][3][4]. Some studies have also reported an inferior outcome in the repair of AAA in females, even when adjusting for the older age of female patients [5][6][7]. It has been postulated that females are treated too late; only the latest European AAA treatment guideline suggests treating females at a lower diameter than males [8]. This recommendation is justified by the observation that the normal infrarenal aortic diameter correlates with parameters such as gender, age and body surface area [9][10], and additionally that the aorta in 70 year old females is considerably smaller than in males (ascending thoracic aorta: 34 vs. 40mm; descending thoracic aorta: 28 vs. 32 mm; proximal infrarenal abdominal aorta: 22 vs 24mm) [11].

The higher rupture risk of female AAAs could not be adequately explained by a more risk-prone aneurysm geometry [12]. It is suspected that the strength of the aneurysm wall is lower in females, a factor that is commonly considered by AAA biomechanical studies [13][4][18][19]. Oestrogens are thought to be a potential candidate for the alteration in aortic wall properties, a factor that would also explain the later onset of aneurysm disease in females [14][15]. Oestrogen affects the aortic collagen to elastin ratio in rats [16], and elastase perfusion of the infrarenal aorta showed less medial destruction, less macrophage infiltration, and lower levels of MMP 9 in females compared to male rats [17]. However, solid clinical material to study aneurysm disease in females in very limited, and females are often underrepresented in clinical studies: the Chichester study, the Multicenter Aneurysm Screening Study (MASS), the West Australia Screening Study, and the Viborg Study contain only 4 to 7% females. Females are also underrepresented in EVAR studies (Dutch Randomized Endovascular Aneurysm Management DREAM: 8% United Kingdom EVAR trial 1: 9%: Open versus Endovascular Repair OVER: <1%). In conclusion, the contributing factors behind the gender difference in AAA disease are poorly understood and a great deal more research is needed [20], if a gender equivalent treatment of this disease is to be fully realised.

References

[1] Vascular Registry in Sweden, Swed. Soc. Vas. Surg., 2018.
[2] Heikkinen M. et al., J. Vasc. Surg. 37, 291-296, 2003.
[3] Brown L.C. and Powell J.T., Ann. Surg. 230, 289-296, 1999.
[4] Polzer S. et al., J. Vasc. Surg. (in press)
[5] McPhee J.T. et al., J. Vasc. Surg. 45, 891-899, 2007.
[6] Hultgren R. et al., Eur. J. Vasc. Endovasc. Surg. 33, 556-560, 2007.
[7] Norman P.E. et al., BMJ 317, 852-856, 1998.
[8] Wanhainen A. et al., Eur. J. Vasc. Endovasc. Surg. 57, 8-93, 2019.
[9] Sonesson B. et al., Eur. J. Vasc. Endovasc. Surg. 8, 89-95, 1994.
[10] Pearce W.H. et al., Surg. 114, 691-697, 1993.
[11] Wanhainen A. et al., J. Vasc. Surg. 47, 504-512, 2008.
[12] Larsson E. et al., J. Vasc. Surg. 54, 295-299, 2011.
[13] Vande Geest J.P. et al., Ann. N. Y. Acad. Sci. 1085, 11-21, 2006.
[14] Mureebe L. et al., J. Vasc. Surg. 48, 1101-1107, 2008.
[15] Best V.A. et al., Br. J. Surg. 90, 1510-1515, 2003.
[16] Fischer G.M. and Swain M.L., Am . Physiol. 232, H617-H621, 1977.
[17] Ailawadi G. et al., Arteriosc. Thromb. Vasc. BIol. 24, 2116-2122, 2004.
[18] Lindquist Liljeqvist M. et al., J. Vasc. Surg. 65, 1014-1021, 2017.
[19] Gasser T.C., Aorta 4, 42-60, 2016.
[20] Larsson E. PhD thesis, Karolinska Institute, Stockholm, Sweden, 2010.

Sex differences in blood flow-mediated remodeling

Françoise Lenfant[1], Jean-François Arnal[1], Daniel Henrion[2]
I2MC, INSERM U 1048, University of Toulouse III, Toulouse, France
MITOVASC Institute, UMR INSERM 1083, UMR CNRS 6015, Université d'Angers, France

Resistance arteries (RA) control local blood flow to organs and are able to adapt in responses to changes in hemodynamic conditions. A chronic increase in blood flow in these vessels induces outward hypertrophic remodeling that normalizes shear stress. This arterial blood flow-remodeling (FMR) occurs in physiological conditions such as growth, chronic exercise or pregnancy as well as ischemic disorders, where they contribute to collateral arteries growth and reperfusion of the tissue. In recent years, more attention has been paid to on the impact of biological sex and hormonal status in physiology and pathophysiology. Although estrogens and androgens are viewed as female and male sex hormones respectively, they also influence numerous physiological processes in circulation. Blood flow-remodeling was studied in animals in one mesenteric RA after ligating side arteries. Two weeks later, arterial structure and reactivity were measured *in vitro* in high (HF) and normal flow (NF) arteries. We found an obligatory role of E2 in FMR of female resistance arteries *in vivo* both in female rats and mice. Thanks to mice selectively inactivated for either the nuclear or the membrane Estrogen Receptor alpha (ERα), we found an essential role of E2 in FMR of female resistance arteries. In contrast, the rapid activation of endothelium nitric oxide (NO)- dependent dilatation as well as flow-mediated dilation both rely on membrane ERα activation (unpublished). FMR was also studied in 3- and 12-month-old male and female rats and mice. E2 deprivation, rather than age, led to decline in FMR, which can be prevented by early exogenous E2. However, delayed E2 replacement was ineffective on FMR, underlining the importance of timing of this estrogen action. FMR of resistance arteries remains efficient in 12-mo-old female rats compared with age-matched male. Moreover, testosterone promoted FMR in male rats through the complementary actions of estrogenic (through aromatization) and androgenic actions, with a prominent effect of the androgenic action (demonstrated using di-hydrotestosterone). Sex hormones thereby contributed to the prevention of skin necrosis in a model of skin-flap ischemia.
Together, these studies emphasize an important role of sex hormones in the vascular adaptation to flow, a finding with potential major medical implications. The physiological significance of these observations will be discussed during the meeting.

References:

1 Chenu, C. *et al.* Testosterone Prevents Cutaneous Ischemia and Necrosis in Males Through Complementary Estrogenic and Androgenic Actions. *Arterioscler Thromb Vasc Biol* **37**, 909-919, doi:10.1161/ATVBAHA.117.309219 (2017).

2 Tarhouni, K. *et al.* Key role of estrogens and endothelial estrogen receptor alpha in blood flow-mediated remodeling of resistance arteries. *Arterioscler Thromb Vasc Biol* **33**, 605-611, doi:10.1161/ATVBAHA.112.300334 (2013).

3 Tarhouni, K. *et al.* Determinants of flow-mediated outward remodeling in female rodents: respective roles of age, estrogens, and timing. *Arterioscler Thromb Vasc Biol* **34**, 1281-1289, doi:10.1161/ATVBAHA.114.303404 (2014).

4 Arnal, J. F. *et al.* Membrane and Nuclear Estrogen Receptor Alpha Actions: From Tissue Specificity to Medical Implications. *Physiol Rev* **97**, 1045-1087, doi:10.1152/physrev.00024.2016 (2017).

Molecular origins of aortic aneurysms

Michael Simons

Yale University

Molecular mechanisms responsible for aortic aneurysm development remain poorly understood. We developed a genetic model of aortic aneurysm development that fully phenocopies human disease without any requirement for mechanical injury. To gain an understanding of molecular factors driving aneurysm development we carried out a time course analysis of changing smooth muscle cell gene expression patterns using single cell RNAseq (scRNAseq). Results point to the existence of a distinct SMC population in the normal aorta, prior to aneurysms induction, that is largely responsible for its growth. RNAseq and scRNAseq analyses of human aortas and aneurysms confirmed these findings. Molecular characteristics of this cell population and translational implications of these findings will be discussed.

Future Direction for Wave Intensity Analysis

Kim H Parker
Department of Bioengineering, Imperial College, London, UK

Introduction

Wave intensity analysis provides information about the magnitude and direction of waves in the arteries. The method was first published 40 years ago although the name 'wave intensity' was first used a few years later. It has proven to be a useful method in theoretical studies of the vasculature and its clinical use is growing. It seems timely to speculate about future direction for the method.

Methods

Sometimes the way forward can be found by looking backward and so the history of wave intensity analysis will be explored for ideas that have been forgotten or under-exploited. Early studies stressed the temporal nature of the analysis, it does not rely upon the 'periodicity' of the cardiac waveforms and can therefore be used to study transient behaviour. An early study analysing the effect of a Valsalva manoeuvre is one example. Other transient phenomena are important clinically, for example the mechanical sequelae of atrial fibrilation, and wave intensity analysis may be useful in that and similar areas of pathology.

Results

Originally wave intensity analysis was carried out using simultaneous measurements of pressure and velocity in the vessel. These measurements are usually invasive and there have been a number of studies exploring variants involving properties that can be measured non-invasively. These variant forms of wave intensity are discussed and they suggest new avenues for clinical application of wave intensity.

There are an increasing number of clinical studies correlating the results of wave intensity with various pathologies. Examples including the chronic effects of mitral valve repair, the effect of left ventricular outflow tract occlusion in patients with hypertrophic cardiomyopathy and the comparison of wave intensity waveforms in the pulmonary artery in patients with primary pulmonary hypertension and chronic thromboembolic pulmonary hypertension will be shown. These studies provide a good indicator of the future of wave intensity analysis clinically; providing useful clinical information about diseases involving the derangement of the mechanical behaviour of the cardiovascular system.

The role of wave intensity analysis in the development of instantaneous wave-free ratio (iFR) as a clinical indicator for the stenting of coronary artery stenoses will be discussed. This method seems likely to supplant functional flow reserve (FFR) which requires the administration of a vasodilator. It also points to other possible directions for the use of wave intensity analysis; the indication of times or periods during the cardiac cycles when critical measurements can be taken.

A relatively recent outgrowth of wave intensity analysis is the idea of separating the arterial pressure waveform into a reservoir pressure, which is determined by the whole arterial network, and an excess pressure that depends on local, transient waves. Several recent epidemiological studies have found that indices related to reservoir pressure are indicators of the risk of cardiovascular events. We have also studied the effect of vasoactive drugs on the reservoir pressure in dogs; work that may improve pharmacological treatment of hypertension. The utility of the reservoir-wave hypothesis is yet to be determined but, if proven, it will open a whole new direction for future applications of wave intensity analysis.

Conclusions

Wave intensity analysis is based on fundamental mechanical principles, the conservation of mass and momentum. It is carried out in the time domain, enabling its results to be directly related to events happening during the cardiac cycle. It also enables us to separate arterial waves into their forward and backward components, which provides further information about the origin of disturbances. Given the complexity of cardiovascular pathology, it is most likely that the clinical utility of wave intensity analysis will depend upon clinical trials, at least in the immediate future. However, in the longer term it may also provide the means for providing causal information about the correlations that are observed.

A new method for non-invasive measurement of arterial wave speed, intensity and reflection

Ethan K. Rowland, Kai Riemer, Kevin Lichtenstein, Meng-Xing Tang and Peter D. Weinberg

Department of Bioengineering, Imperial College London, London UK

Introduction

Ventricular ejection generates a forward-going compression wave in the arterial system. Slowing of ejection leads to a forward-going expansion wave. The waves contain clinically useful information: their magnitude varies with cardiac performance, their speed depends on arterial stiffness, and their reflection is affected by conduit artery tone. These properties can be studied using Wave Intensity Analysis (WIA) [1]. However, the need for high temporal resolution, simultaneous and spatially coincident recordings of arterial pressure and blood velocity is restrictive; measurements must be catheter based or introduce errors, assumptions and/or restrictions. Here we describe and validate a new, non-invasive method that avoids these problems.

Methods

The method employs the novel WIA formulation of Feng and Khir [2] based on velocity and diameter rather than velocity and pressure. That enables all necessary data to be obtained from the same B-mode ultrasound images, using ultrasound imaging velocimetry (UIV) [3] for velocity measurement. In vitro experiments employed blood driven through a latex tube by a pulsatile pump; capillary tubes and air-filled reservoirs gave appropriate resistance and compliance. In vivo experiments were conducted by imaging the abdominal aorta of 24 terminally anesthetised rabbits, some of which were administered esmolol, a short-acting cardioselective beta-blocker, to induce ventricular dysfunction. Experiments complied with the Animals (Scientific Procedures) Act 1986 and were approved by Imperial's Animal Welfare and Ethical Review Board. In vitro and in vivo, a Verasonics ultrafast plane-wave imaging system gave frame rates in the kHz range, microbubble contrast agents were used in some experiments, and data were compared with conventional WIA based on pressure and Doppler velocity measurements from an invasive, catheter-based system (Volcano).

Results

In vitro, UIV with contrast agent gave the same velocity waveform as the catheter-based method. Native blood speckle could be used in place of contrast agent speckle if blood and tissue signals were separated by singular value decomposition. In vivo, flow waveforms obtained by UIV with contrast agent or with native blood speckle and singular value decomposition were essentially identical, and WIA using the new method gave the same results as WIA using the gold-standard method. Changes in peak intensities could be detected after administration of esmolol.

Conclusions

The new method enables wave speeds, intensities and reflections to be obtained simply, reliably and non-invasively at single points in the arterial system using existing ultrasound scanners. It could provide a clinically useful way to detect arterial stiffening, heart failure, and alteration of arterial tone.

(Supported by a BHF Centre of Research Excellence Award and MRC Confidence-in-Concept funds)

References

1. Parker KH. Med Biol Eng Comput. 2009;47:175-188
2. Feng J, Khir AW. J Biomech. 2010;43:455-462
3. Leow CH et al. Ultrasound Med Biol. 2015;41:2913-2925

Ventricular dynamics is a main determinant of the augmentation index: An in *in vivo* and *in silico* study

Sam Vennin[1,2], Ye Li[1], Jorge Mariscal-Harana[2], Peter Charlton[2], Jordi Alastruey[2], Phil Chowienczyk[1]

[1]Department of Clinical Pharmacology, King's College London, UK [2]Department of Biomedical Engineering, King's College London, UK

Introduction

The role of pulse wave reflections in the increase of the augmentation pressure and, in turn, pulse pressure (PP) with ageing has been recently challenged as recent studies have highlighted the potential importance of ventricular ejection properties in determining blood pressure pulsatile components [1,2]. The first systolic shoulder (P1) of the pressure waveform is proportional to the product between the aortic pulse wave velocity (PWV) and aortic flow at time of P1 (U1) [3], and the usual peak pressure (P2) to the product between PWV and the volume of blood (V2) ejected at the time of P2 [4]. Both V2 and U1 can be approximated respectively by stroke volume (SV) and peak flow (U_{max}). Assuming proportionality between proximal and distal PWV and noticing the close relationship between the augementation index (AIx) and the ratio P2/P1, we investigate the relationship between AIx and a new index based entirely on ventricular mechanics, QIx, defined as SV/U_{max}.

Methods

The study involved patients from a normotensive (n=164, 126 men, age 49±8 years, blood pressure 110±16/69±10 mmHg, means±SD) and hypertensive (n=156, 83 men, age 46±17 years, blood pressure 130±23/83±13 mmHg) cohort. Reflected waves were quantified using the reflection coefficient Γ, *i.e.* the ratio of backward to forward pressure component. A Least Absolute Shrinkage and Selector Operator (LASSO) analysis was performed to statistically identify the main contributors to AIx among a set of cardiac and arterial parameters (Age, PWV, Γ, QIx, MBP, PP). To determine the relative contribution to AIx of arterial (Γ) and cardiac (QIx) properties, variations of AIx with QIx for an approximately fixed Γ were assessed, and *vice versa*. A sensitivity analysis of changes in AIx to QIx and Γ was also performed using an *in silico* model of blood flow in the larger arteries of the upper thoracic aorta.

Results

The LASSO analysis identified QIx, MBP and Γ as the main determinants of AIx with standardised coefficients of 0.32, 0.22 and 0.17, respectively ($p>0.001$ in each case). *In vivo* studies confirmed QIx was more correlated than Γ with AIx (Pearson coefficient, R= 0.71 vs R=0.53 in the normotensive group; R=0.52 VS R=0.37 in the hypertensive group). The sensitivity analysis also confirmed QIx have a greater impact on AIx than Γ.

Conclusions

We have proposed a new index based entirely on ventricular ejection dynamics and studied its relationship with AIx. The results of this part-*in-silico*/part-*in-vivo* study further challenge the role of reflection waves in the increase of AIx, as our new index was as correlated, if not more, to AIx than Γ.

References

[1] Torjessen AA, Wang N, Larson MGn Hamburg NM, Vita JA, Levy D, Benjamin EJ, Vasan RS, Mitchell GF, Forward and backward wave morphology and central pressure augmentation in men and women in the Framingham Heart Study, *Hypertension*, 64(2):259-265, 2014

[2] Fok H, Guilcher A, Li Y, Brett S, Shah A, Clapp B, Chowienczyk P, Augmentation Pressure Is Influenced by Ventricular Contractility/Relaxation Dynamics, *Hypertension*, 63(5):1050-1055, 2014

[3] Vennin S, Mayer A, Li Y, Fok H, Clapp B, Alastruey J, Chowienczyk P. Noninvasive calculation of the aortic blood pressure waveform from the flow velocity waveform: a proof of concept, *Am J Physiol Heart Circ Physiol*, 309(5):H969-76, 2015

[4] Vennin S, Li Y, Willemet M, Fok H, Gu H, Charlton P, Alastruey J, Chowienczyk P. Identifying hemodynamic determinants of pulse pressure. A combined numerical and physiological approach, *Hypertension*, 70(6):1176-1182, 2017

Wall shear stress and plaque development: did we buy a pig in a poke?

Patrick Segers[1], David De Wilde[1], Bram Trachet[1], Guido De Meyer[2]

[1]IBiTech-bioMMeda, Ghent University, Ghent, Belgium;
[2]Division of Physiopharmacology, University of Antwerp, Antwerp, Belgium

Hemodynamics is thought to play a role in the initialization and development of atherosclerosis, with zones experiencing low and oscillatory shear stresses being more prone to the development of atherosclerosis. However, it is not straightforward to link shear stress patterns to atherosclerosis development, as atherosclerosis develops slowly with the disease altering arterial geometry, hereby changing the shear stress distributions that occur. Follow-up studies in humans that could demonstrate a causal link between shear stress and plaque development is virtually impossible.

We therefore undertook such endeavor in N=4 female ApoE-/- mice. Animals were fed a Western type diet (TD88137, Harlan Teklad, Madison, Wis, USA) from the age of 6 to 26 weeks. At weeks 10, 15 and 20 after the start of the diet (mice aged 16, 21 and 26 weeks), the animals underwent an imaging protocol consisting of µCT and ultrasound. Hemodynamic wall parameters were obtained from mouse-specific Fluid-Structure Interaction simulations at week 10 in all 4 animals, and for both the left and right carotid territory.

Overall, our study indicated that (i) the association between hemodynamics and atherosclerosis is most apparent when assessed at the level of the entire carotid bifurcation; the association is much weaker when assessed at the individual branch level; (ii) the association is stronger for the data measured at week 20 than week 15; (iii) the association is stronger for the population compared to individual carotid bifurcations; (iv) of all parameters tested, the strongest spatial correlation between hemodynamics and atherosclerosis development was observed for the relative residence time and time averaged wall shear stress; (v) aggregating the data leads to an overestimation of the correlation.

Our study does provide evidence supporting the low and oscillatory shear stress hypothesis. At the same time, despite that the correlations that were found were statistically significant (on a population level), they still remain very low. Atherosclerosis is a complex process involving different mechanisms and hemodynamics provides, at best, only a partial explanation of the localized nature of atherosclerosis.

References

Shear Stress Metrics and Their Relation to Atherosclerosis: An In Vivo Follow-up Study in Atherosclerotic Mice. De Wilde D, Trachet B, De Meyer GR, Segers P. Ann Biomed Eng. 2016 Aug;44(8):2327-38.
Assessment of shear stress related parameters in the carotid bifurcation using mouse-specific FSI simulations. De Wilde D, Trachet B, Debusschere N, Iannaccone F, Swillens A, Degroote J, Vierendeels J, De Meyer GRY, Segers P. J Biomech. 2016 Jul 26;49(11):2135-2142
Vulnerable plaque detection and quantification with gold particle-enhanced computed tomography in atherosclerotic mouse models. De Wilde D, Trachet B, Van der Donckt C, Vandeghinste B, Descamps B, Vanhove C, De Meyer GR, Segers P. Mol Imaging. 2015;14. doi: 10.2310/7290.2015.00009.

Wall shear stress and plaque structural stress in plaque growth and composition

Martin R. Bennett
University of Cambridge

Background
The focal distribution of atherosclerotic plaques suggests that local biomechanical factors may influence plaque development. Wall shear stress (WSS) is determined by geometry and flow, and plaques develop and progress faster at sites of low WSS. In contrast, plaque structural stress (PSS) is determined by plaque composition and structure, and plaques rupture when PSS>structural strength of the plaque. We have also shown that plaques that rupture, cause acute coronary syndromes, and multiple cardiovascular events have higher PSS than plaques that don't.

Methods and Results
We studied 40 patients at baseline and over 12 months by virtual-histology intravascular ultrasound and bi-plane coronary angiography. We calculated plaque structural stress (PSS), defined as the mean of the maximum principal stress at the peri-luminal region, and wall shear stress (WSS), defined as the parallel frictional force exerted by blood flow on the endothelial surface, in areas undergoing progression or regression. Changes in plaque area (PA), plaque burden (PB), necrotic core (NC), fibrous tissue (FT), fibrofatty tissue (FF) and dense calcium (DC) were calculated for each co-registered frame. A total of 4029 co-registered frames were generated. In areas with progression, high PSS was associated with larger increases in NC and small increases in FT vs. low PSS (difference in ΔNC: 0.24±0.06mm^2; p<0.0001, difference in ΔFT: -0.15±0.08 mm^2; p=0.049). In areas with regression, high PSS was associated with increased NC and decreased FT (difference in ΔNC: 0.15±0.04; p=0.0005, difference in ΔFT: -0.31±0.06mm^2; p<0.0001). Low WSS was associated with increased PB vs. high WSS in areas with progression (difference in ΔPB: 3.3±0.4%; p<0.001) with a similar pattern observed in areas with regression (difference in ΔPB: 1.2±0.4%; p=0.004). PSS and WSS were largely independent of each other (R^2 =0.002; p=0.001).

Conclusions
Areas with high PSS are associated with compositional changes consistent with increased plaque vulnerability. Areas with low WSS are associated with more plaque growth in areas that progress and less plaque loss in areas that regress. The interplay of PSS and WSS may govern important changes in plaque size and composition.

JCAD, a human coronary artery disease gene, is a novel regulator of endothelial hippo signaling

Thomas Webb
University of Leicester

Genome-wide association studies have associated 164 chromosome loci with increased risk of coronary artery disease (CAD). Notably, many of these loci do not contain genes previously linked to atherosclerosis. The CAD-associated variants at chromosome 10 p11.23 fall in *JCAD*, which encodes an uncharacterised endothelial junction protein. Analysis of gene expression datasets showed that the risk allele of the lead disease variant is also associated with increased expression of *JCAD* in vascular and atherosclerotic tissue. Knockdown of *JCAD* in endothelial cells caused pro-atherosclerotic phenotypes including reduced migration and proliferation and increased apoptosis, adhesion molecule expression and monocyte recruitment. JCAD has recently been shown to interact with LATS2, a core kinase of the hippo signalling pathway. We therefore sought to determine if the regulation of endothelial cell function by JCAD occurs via hippo pathway regulation. We confirmed the physical interaction between JCAD and LATS2 and demonstrated that JCAD acts via RhoA to regulate phosphorylation and nuclear localisation of YAP, the transcriptional effector of the hippo pathway. Co-expression analysis of RNA-seq data from normal and atherosclerotic blood vessels revealed JCAD as a key driver of YAP signalling. Various extracellular signals including cell-cell contact, GPCR and integrin signalling and mechanotransduction regulate the hippo pathway and induction of YAP activity by disturbed blood flow was recently shown to promote atherosclerotic plaque formation. Our data show that JCAD is a new regulator of Hippo signalling in endothelial cells and suggest that the variants at the 10 p11.23 CAD locus act through JCAD to increase CAD risk via YAP.

Shear stress, notch and atherosclerosis

Paul C. Evans
University of Sheffield, UK

Although atherosclerosis is associated with systemic risk factors such as age, high cholesterol and obesity, plaque formation occurs predominantly at branches and bends that are exposed to disturbed patterns of blood flow. These regions are susceptible because endothelial cells (EC) are prone to injury and pro-inflammatory activation compared to EC at atheroprotected sites. The focal nature of endothelial cell injury and activation is related to wall shear stress (WSS), a force exerted on endothelial cells by flowing blood that varies in time, magnitude and direction according to vascular pulsatility and anatomy. Notch signalling is a critical regulator of vascular development and homeostasis. I will describe our recent data using cultured EC, porcine and murine models showing that Notch signalling drives endothelial dysfunction and atherosclerosis at sites of disturbed flow. These studies may lead to the identification of novel therapeutic targets to treat atherosclerosis.

Synchrotron-based quasi-static pressure inflation of the mouse carotid artery

Bram Trachet[1,2], M. Ferraro[2], G. Lovric[3], L. Aslanidou[2], G. Logghe[1], P. Segers[1], N. Stergiopulos[2]

[1]IBiTech-bioMMeda, Ghent University, Ghent, Belgium; [2]Institute for Bioengineering, EPFL, Lausanne, Switzerland;

[3]Swiss Light Source, Paul Scherrer Institute, Villigen, Switzerland

Introduction

Recent synchrotron-based pre-clinical evidence has demonstrated that thoraco-abdominal aortic dissections initiate as micro-structural ruptures of the aortic lamellae in Ang II-infused mice [1]. Unfortunately, the contribution of micro-structural mechanics to cardiovascular disease initiation is still poorly understood. State-of-the-art 3D imaging techniques such as in vivo micro-CT and MRI cannot visualize these micro-structural components, while multiphoton imaging has a limited field of view [2]. Synchrotron-based imaging, on the other hand, would allow for more detailed 3D models but is typically based on scans of non-pressurized, ex vivo aortic samples. In order to overcome this limitation we developed a synchrotron-compatible pressure inflation device that allows for quasi-static imaging of the mouse carotid artery at different pressure levels.

Methods

Six wild type (WT) and six ApoE-/- mice, all male and on a C57Bl6/J background, were used for this study. After mounting the left carotid artery on the device, pressure was increased quasi-statically with a syringe pump, from 0 to 120 mmHg. Synchrotron-based phase-propagation imaging was performed at 25m source-to-sample distance, at 25 cm sample-to-detector distance and at 21 keV. A scientific CMOS detector (pco.Edge 5.5) was used in combination with a 4x magnifying visible-light optics and a 20 µm thick scintillator. The effective voxel size was 1.625 μm^3. During the scans the axial stretch was kept at the in vivo value. Images were segmented using an in-house developed automated segmentation algorithm. Aortic diameter, length, straightness and thickness were quantified at each pressure level.

Results

All three lamellar layers straightened and stretched simultaneously when aortic pressure was increased, confirming earlier reports [2]. The most important increase in lamellar straightness occurred between 0 and 30 mmHg. We did not find significant differences in straightness between the three different lamellar layers. The lamellar length increased quasi-linearly in all three lamellae and the decrease in thickness of the wall was equally distributed between lamellar and interlamellar layers. We did not find any statistically significant difference between WT and ApoE $^{-/-}$ mice. Segmented 3D models include both the medial lamellae and the tunica adventitia.

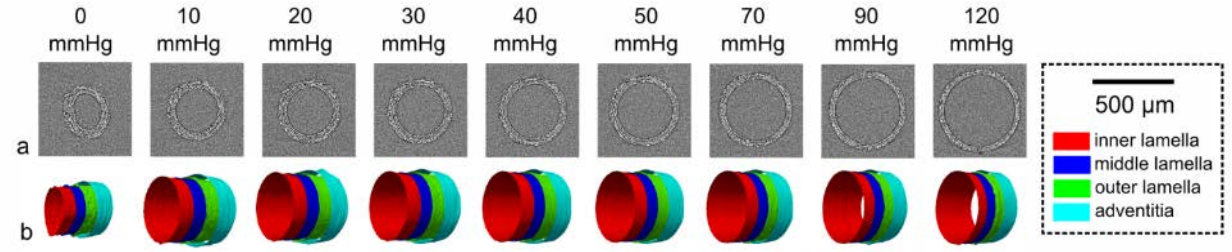

Figure 1. Synchrotron images (a) and corresponding 3D segmentations (b) of aortic lamellae and tunica adventitia in the mouse left carotid artery.

Conclusions

On the long term the results presented in this work might lead to a breakthrough in micro-structural computational biomechanics of the arterial wall. Ultimately, we hope that this will contribute to a better understanding of how the micro-structure affects the initiation and propagation of cardiovascular disease.

References

[1] Trachet B, Aslanidou L, Piersigilli A, Fraga-Silva AR, Sordet-Dessimoz J, Villanueva-Perez P, Stampanoni M, Stergiopulos N, Segers P. Angiotensin II infusion into ApoE-/- mice: a model for aortic dissection rather than abdominal aortic aneurysm? *Cardiovascular Research*, 113: 1230-42, 2017.

[2] Yu X, Turcotte R, Seta F, Zhang Y. Micromechanics of elastic lamellae: unravelling the role of structural inhomogeneity in multi-scale arterial mechanics. *J. R. Soc. Interface,* 15: 20180492, 2018.

Predicting the healthy valve: relationships between the dimensions of the human mitral annulus

Charlotte Blake[1,2], Chirattikan Srisook[1,2], Rudolf Billeter-Clark[3], Donal McNally[2], Ricky Wildman[1], Ruth Goodridge[1]

[1]Centre for Additive Manufacturing, Faculty of Engineering, University of Nottingham, UK
[2]Bioengineering Research Group, Faculty of Engineering, University of Nottingham, UK
[3]Department of Anatomy, Faculty of Medicine and Health Sciences, University of Nottingham, UK

Introduction

Increased accuracy in valve sizing through presurgical prediction of valve dimensions holds the possibility of significantly improving patient care in cardiac valve surgery[1]. As such, a number of groups have looked into various methods to predict sizes of surgical implants using measurements of the intertrigonal distance and valve leaflet heights [2–4].

The mitral valve is commonly described as adhering to a 3:4 ratio between the anteroposterior and transverse diameters[5], and examples of surgical implants being designed according to this ratio can be found. However, limited evidence has been published to support this ratio. In this work, we investigated the relationship between these measurements using physical and digital measurements of human hearts.

Methods

Human hearts (n=16) were collected from cadavers donated for the purposes of anatomical teaching and study. Manual measurements were taken of the transverse and anteroposterior dimensions of the mitral annulus using digital callipers. In addition, 3D images were taken of the mitral valve from multiple angles and stitched together for digital measurement using MeshLab. To exclude hearts which deviated significantly from health in life, the mitral valve was scored visually out of 3 based on the visible damage to the heart as a whole from storage or disease. Following this, 10 hearts were included in statistical analysis which were viewed as showing no significant damage.

Results

Our data supports some relationship between the anteroposterior and transverse dimensions of the mitral annulus. A paired t-test shows there is no significant difference between the expected value (0.75) and ratios measured in this study (M=0.738, SD=0.086) (t(9)=0.460, p=0.656). Therefore whilst the data does not show an exact 3:4 ratio, we cannot exclude that possibility. Also of note is the wide individual variation of measurements around these relationships, shown in Figure 1.

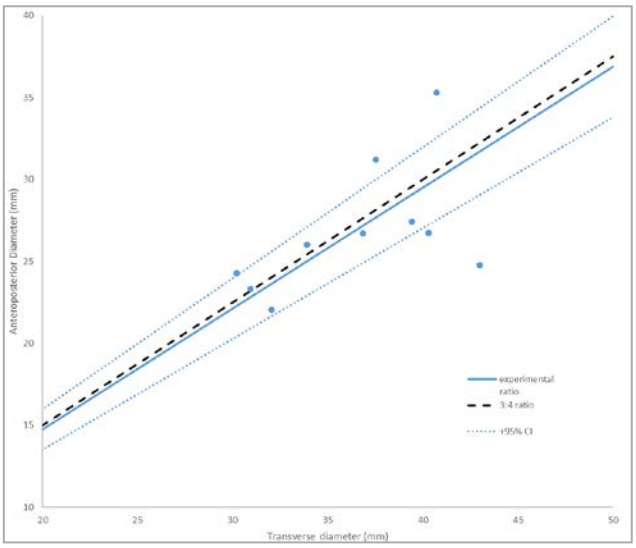

Figure 1: Plot of the anteroposterior and transverse diameters of each cadaver. The solid line represents a line of fit to the data presented *(y=0.62x+3.98)* and the dashed line represents the expected values of a 3:4 ratio *(y=0.75x)*.

Conclusions

This research shows that whilst there is a relationship between dimensions of the mitral valve, it is highly variable between individuals. It should be considered that treating mitral valve disease with a "one shape fits all" design of surgical implants may be improved upon with more bespoke approaches.

References

1. Al-Maisary, S. *et al.* Computer-based comparison of different methods for selecting mitral annuloplasty ring size. *J. Cardiothorac. Surg.* **12,** 8 (2017).
2. Cooray, S. D., Tutungi, E., Mezzatesta, J. P., Moshinsky, R. & Almeida, A. A. Echocardiographic measurement of mitral intertrigonal distance is an adjunct to annuloplasty ring sizing. *J. Heart Valve Dis.* **18,** 106–10 (2009).
3. Ender, J. *et al.* Prediction of the annuloplasty ring size in patients undergoing mitral valve repair using real-time three-dimensional transoesophageal echocardiography. *Eur. J. Echocardiogr.* **12,** 445–53 (2011).
4. Lecuyer, L., Berrebi, A., Florens, E., Huerre, C. & Fabiani, J. N. Height of the anterior leaflet (A2), measured by echocardiography predicts accurately the annuloplasty ring size used during mitral valve reconstruction using Carpentier's techniques. *Arch. Cardiovasc. Dis. Suppl.* **3,** (2011).
5. Carpentier, A., Adams, D. H. (David H. & Filsoufi, F. *Carpentier's reconstructive valve surgery : from valve analysis to valve reconstruction*. (Saunders/Elsevier, 2010).

On the Use of Circulating Osteogenic Blood Biomarkers to Determine Atherosclerotic Calcification Phenotype

Rachel Cahalane[1], Hilary Barrett[1,2], Aisling Ross[1], John Mulvihill[1], Helen Purtil[3], Julie O'Brien[4], Eamon Kavanagh[5], Michael Moloney[5], Michael Walsh[1] and Eibhlis O'Connor[6]

[1]BioSciBer, Biomaterials Cluster, Bernal Institute, Health Research Institute (HRI), School of Engineering, University of Limerick. [2]Biomechanics Lab, Department of Biomedical Engineering, Thoraxcenter, Erasmus Medical Center, Rotterdam, The Netherlands. [3]Department of Mathematics and Statistics, University of Limerick. [4]Department of Radiology, University Hospital Limerick. [5]Department of Vascular Surgery, University Hospital Limerick. [6]School of Natural Sciences and Department of Biological Sciences, University of Limerick.

Introduction

Calcification morphology plays a critical role in atherosclerotic plaque stability with high-density macrocalcifications providing a protective effect[1], while microcalcifications promote rupture[2]. Collectively, these findings indicate that calcified particle count could be pivotal in high-risk lesion identification. However, the current spatial resolution of clinical CT imaging is limited and cannot accurately distinguish areas of calcification[3]. In this regard, cardiovascular tissue is in immediate contact with blood circulation, therefore the development of a blood test to diagnose atherosclerotic calcification phenotype may be a worthwhile approach. Vascular calcification has a highly regulated formation process, similar to osteogenesis[4]. Consequently, the purpose of this study was to investigate whether the circulating levels of these osteogenic regulators could be indicative of atherosclerotic calcification phenotype.

Methods

39 patients undergoing standard endarterectomy procedures at the University Hospital Limerick were recruited for this study. Fasting venous bloods were collected pre-operatively. Circulating serum or plasma levels of fetuin-A, OPN, hs-CRP, BMP-2, OC, TNF-α, IL-6/8/18, FGF-23 and OPG were quantified using either commercially available Enzyme Linked ImmunoSorbent Assay or Magnetic Bead assay kits. High-resolution micro-Computed Tomography (15.68μm) was performed on the excised atherosclerotic specimens. ImageJ '3D Objects Counter' Plugin was employed to determine the total volume of calcification, calcified particle count and the microcalcification fraction (μCF) for each sample.

Results

Spearman's correlation coefficient (r_s) was used to assess the relationship between the calcification metrics and the circulating levels of osteogenic regulators. Results were analysed as total, carotid and peripheral lower limb datasets as presented in Figure 1. Levels of undercarboxylated osteocalcin (ucOC) are moderately negatively correlated with total volume of calcification in carotid lesions (rs = -0.521). However, total calcification volume is not a good marker of vulnerability[5]. Osteopontin is weakly negatively associated with total μCF (rs = -0.381) and Interleukin-18 is moderately positively associated with carotid μCF (rs = 0.516). The μCF of plaques might represent unstable morphologies; however, clinical studies are warranted to validate this hypothesis.

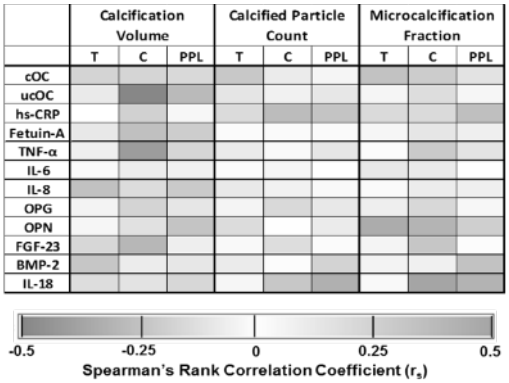

Figure 1: Heatmap of r_s for circulating protein levels versus calcification metrics

Conclusions

A blood-based biomarker capable of distinguishing between stable and unstable arterial disease would be imperative in cardiovascular patient management. The microcalcification fraction of plaques may be indicative of their stability. OPN is negatively associated with all μCF (rs = -0.521) and IL-18 is positively associated with carotid μCF (rs = 0.516). Future work will investigate Matrix-Gla Proteins.

References

[1] Criqui, M. (et al.) Calcium Density of Coronary Artery Plaque and Risk of Incident Cardiovascular Events, *The Journal of the American Medical Association*, 311: 271–278, 2014.

[2] Hutcheson, J. (et al.) Small entities with large impact, *Current Opinions in Lipidology*, 25: 327-332, 2014.

[3] Sarwar, A. (et al.) Calcified plaque: measurement of area at thin-section flat-panel CT and 64-section multidetector CT and comparison with histopathologic findings, *Radiology*, 249: 301-306, 2008.

[4] Doherty, T. (et al.) Calcification in atherosclerosis, *Proc Natl Acad Sci USA*, 100: 11201-11206, 2003.

[5] Nandalur, KR. (et al.) Composition of a stable carotid plaque, *Stroke*, 28: 935-940, 2007.

Computational Fluid Dynamics to predict thrombosis of a stentgraft inserted for peripheral artery occlusive disease

Lennart van de Velde, Erik Groot Jebbink, Michel Versluis, Michel Reijnen

Department of Surgery, Rijnstate Hospital, Arnhem & Physics of Fluids and Multi-Modality Imaging groups, TechMed Centre, University of Twente, The Netherlands

Introduction

Contemporary diagnostic modalities including CT and duplex-ultrasound have been insufficiently able to predict stentgraft complications. A likely mechanism that contributes to stentgraft complications are localized regions of flow stasis near the vessel wall, which can potentially be assessed with patient-specific computational fluid dynamics (CFD). By exemplification with a case report, we present an implementation of personalized CFD that has potential for predicting flow-related stentgraft complications in a clinical setting.

Methods

Unsteady CFD simulations were performed for a 63-year old female who was treated with a stentgraft in the femoral artery. The treatment was complicated by a proximal edge stenosis and stentgraft thrombosis, successfully treated with a drug-coated balloon and thrombolysis. CT-angiography and duplex ultrasound demonstrated no abnormalities after treatment and a good distal run-off, but stent occlusion re-occurred within half a year. CFD analysis, based on CT and ultrasound data of the patient, was performed retrospectively to investigate potential flow-related causes and levels of wall shear stress.

Results

The CFD simulations demonstrated focal regions of adverse, separating flow at the site of the edge stenosis and at the proximal edge of the stentgraft. These areas were associated with low flow velocities and time-averaged wall shear stress values below 0.05 Pa, substantially lower than physiological levels.

Conclusions

Personalized CFD simulations were able to predict the occurrence of stentgraft occlusion in a patient with otherwise normal anatomic and ultrasound assessment and a good distal run-off.

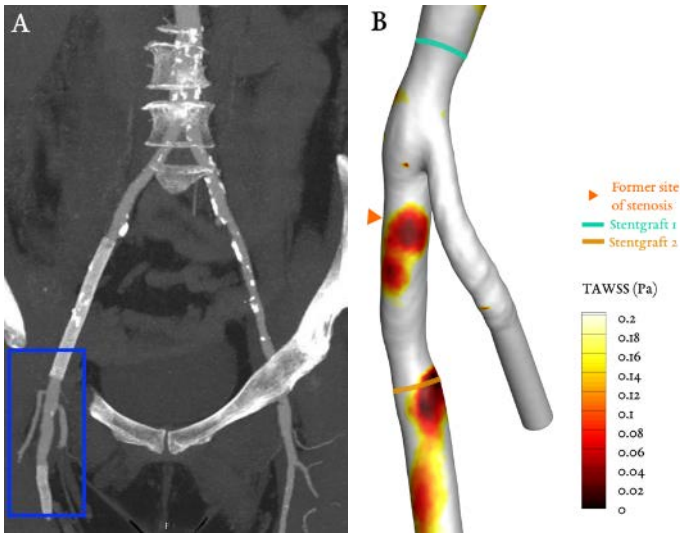

Figure 1 A CT-scan of the patient (A) after insertion of two stentgrafts in the external iliac and superficial femoral artery. Flow patterns in the blue area were investigated with CFD (B), showing minimal time-averaged wall shear stress (TAWSS) at the site of former stenotic lesion development and at the inflow section of the femoral artery stentgraft, where multiple thrombotic episodes occurred.

A novel method for more representative vessel model reconstruction and assessment of the local hemodynamic forces in coronary artery segments with metallic stent

Ryo Torii[1], Anantharaman Ramasamy[2, 3], Chongying Jin[2, 3], Hannah Safi[2, 3], Thomas Zanchin[2, 6], Daniel Jones[2, 3], Pieter Kitslaar[4], Jouke Dijkstra[4], Yoshinobu Onuma[5], Lorenz Raber[6], Muhiddin Ozkor[2], Rob Krams[3], Anthony Mathur[2, 3], Patrick W. Serruys[7], Andreas Baumbach[2], Christos V. Bourantas[1, 2, 3]

[1]University College London, UK; [2]Barts Heart Centre, UK; [3]Queen Mary University of London, UK; [4]Leiden University Medical Center, The Netherlands, [5]Erasmus Medical Center, The Netherlands, [6]Bern University Hospital, Switzerland; [7]Imperial College London, UK

Introduction
In vivo assessment of local hemodynamic forces using computational fluid dynamics (CFD) has become a common approach to study the implications of haemodynamic environment on coronary pathobiology in stented segments. However, studies incorporating full stent architecture, including malapposed struts, are still limited. We develop and verify a novel in vivo method that enables reliable coronary artery reconstruction of stented segments which relies on separate reconstruction of vessel and stent geometry.

Methods
Five coronary arteries implanted with Xience Alpine everolimus eluting stent that were assessed by optical coherence tomography (OCT) imaging immediately after stent implantation were included in this study. The stented segments were reconstructed from two angiographic projections and OCT images using two methodologies: (1) conventional method which assumes that stent struts are well apposed and generates a surface of the combined lumen and strut geometry and (2) novel method where the lumen and stent geometries are reconstructed separately, also utilising the known strut architecture, and then the two reconstructions are fused to generate the final geometry of the stented segment. Pulsatile blood flow simulation was performed to obtain the endothelial shear stress (ESS) as well as the shear rate, which were compared in the models obtained by the two reconstruction approaches.

Results
The conventional methodology was unable to reconstruct strut architecture in segments with strut malapposition and appeared to underestimate areas exposed to low ESS <1Pa (21±12% vs 27±13%, P<0.001) and lumen volume exposed to high shear rate >1000s^{-1} (0.72 mm^3 vs 1.17 mm^3, P=0.07) in these segments compared to the novel methodology. In cases of bifurcations, the novel methodology enabled a better assessment of flow dynamics and the flow disturbances caused by the protruded struts that resulted in a higher shear rate compared to the conventional method (1440 s^{-1} vs 1300 s^{-1}, P<0.001).

Conclusions
The new method allows more reliable reconstruction of stent struts and accurate estimation of local haemodynamic forces, especially at the bifurcations and when malapposed stent struts are present. This optimised novel method may provide invaluable information on predictors of stent failures and vascular response after stenting.

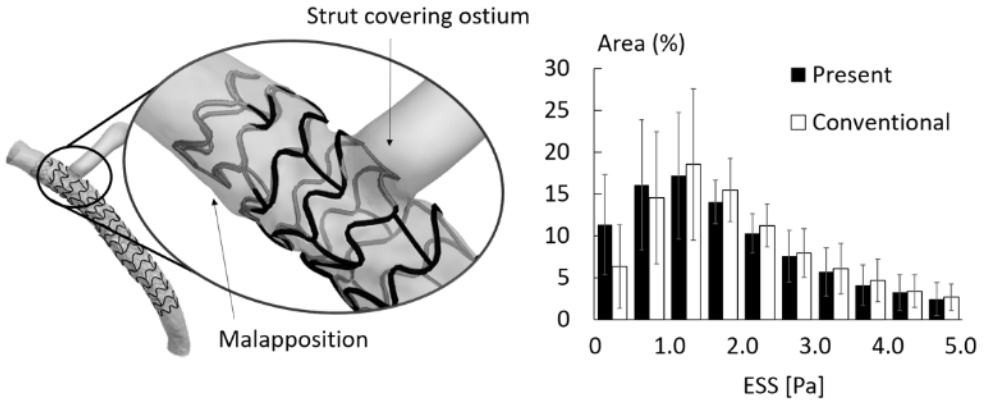

Figure: reconstructed model of stented segment (left) and comparsion of areas under different level of ESS between the two methods (right).

High-resolution mapping of flow dynamics in the zebrafish cardiovascular system

Jonathan M. Taylor[1], Vytautas Zickus[1,2]

[1]Glasgow University, Glasgow, UK [2]Now at: Edinburgh University, Edinburgh, UK

Introduction

Flow mapping *in vivo* presents numerous challenges: achieving high 3D resolution without bias, two-phase flow, limited tracer density, delicate live organs, and potential beat-to-beat variability. We will discuss these issues, and their implications for the accuracy of common *in vivo* flow imaging protocols. We will show how these issues can be overcome to build a clear and correct understanding of complex flow dynamics in the zebrafish cardiovascular system, suitable for reliable estimates of wall shear stress and other important biomechanical parameters.

Methods

Light sheet microscopy is an ideal tool for precision mapping of flow fields on a microscopic scale, due to its optical similarities with particle image velocimetry, which on a macroscopic scale is a mature technique in fields such as aerospace engineering. We will show how optical gating allows us to enhance the measurement quality dramatically, by applying statistically rigourous correlation-averaging techniques on the periodic flow within the beating heart[1]. This, however, in turn raises questions about the beat-to-beat repeatability of the underlying flow in healthy and in abnormal individuals.

Results

We show how our approach enables high-precision mapping of blood flow throughout the heartbeat, and quantification of actual pumped volumes in the presence of flow regurgitation. We explore the repeatability of the flow across heartbeats, as well as the distinction between blood plasma flow and transport of the red blood cells themselves. Finally, we present preliminary results showing recovery of the out-of-plane velocity component, permitting full 3-dimension, 3-component velocity mapping throughout the heartbeat.

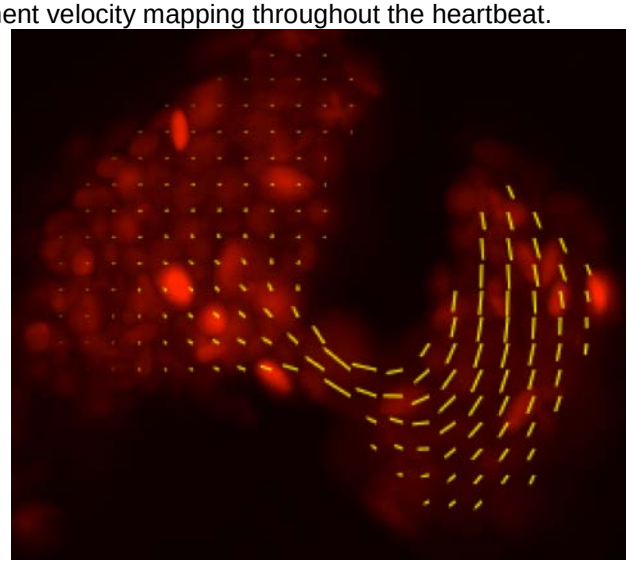

Figure 1: Computed flow vectors (yellow) determined from particle image velocimetry analysis of red blood cells (red – fluorescent reporter *gata1*:dsRed), showing flow field between atrium and ventricle mid-cycle in the embryonic zebrafish heart. A low-noise flow field was computed by exploiting the periodic nature of the flow and correlation-averaging across multiple heartbeats.

Conclusions

To understand *in vivo* flow dynamics on a microscopic scale in small-animal models demands careful consideration of both the imaging modality and the theory underpinning the analysis used. With a proper understanding of these, detailed mapping of flow dynamics hold great potential for improved understanding of shear stresses, fluid-structure interactions during development, and biomechanical aspects of heart disease models.

References

[1] V. Zickus and J. M. Taylor. “3D + time blood flow mapping using SPIM-microPIV in the developing zebrafish heart”, Biomedical Optics Express **9** 2418–2435 (2018).

Patient-specific Assessment of Stroke Risk in Pediatric Cerebrovascular Disease

Shaolie S. Hossain[1,2], Zbigniew Starosolski[3], Travis Sanders[1], Dianna Milewicz[4], and Ananth Annapragada[3]

[1]Institute for Computational Engineering and Sciences, The University of Texas at Austin, Austin, Texas, USA
[2]Department of Molecular Cardiology, Texas Heart Institute, Houston, Texas, USA
[3]Translational Imaging Group, Texas Children's Hospital, Houston, Texas, USA
[4]Department of Cardiology, University of Texas Health Science Centre, Houston, Texas, USA

Introduction

Moya**M**oya **D**isease (MMD) is a rare pediatric cerebrovascular disease characterized by progressive narrowing of the major arteries in the **C**ircle **o**f **W**illis (CoW), leading to rampant collateralization and recurring ischemic and hemorrhagic stroke. Clinical strategies to prevent or reverse vessel occlusion are not available. Instead, neurosurgical interventions are used to augment blood flow to the affected region and avert future stroke events; but carry the risk of perioperative infection, stroke, and intracranial hemorrhage. Treatment is an absolute necessity however, since a morbidity rate of > 70% in untreated patients is currently realized. While atypical vessel straightening, and collateralizations are commonly observed on the CT-angiograms, there is a lack of understanding how these vascular alterations affect local hemodynamics and disease progression, and there has been no study of the effect of surgical interventions on future stroke events. The main objective of this work is to develop a patient-specific analysis framework to assess stroke risk in patients with pediatric cerebrovascular disease and to evaluate scenarios affecting disease severity.

Methods

Using an in-house CAD-based vascular modeling pipeline, a hexahedral NURBS (Non-Uniform Rational B-Splines) mesh was generated from 3D CoW imaging data with boundary layer refinement [1]. Realistic blood flow simulations were carried out within the authentic CoW vasculatures using a Navier-Stokes solver within a finite-element based isogeometric analysis framework [2] subjected to appropriate boundary conditions, including a pulsatile inflow condition. Bulk and near wall flow features, such as wall shear rate were quantified. Vascular regions with critical wall shear rate values above the coagulation limit (> 5000 s^{-1}) were identified as having a higher probability of clot formation leading to stroke.

Results

ACTA2(-/-) knockout (KO) mouse model develops many of the phenotypic features of MMD including stenosis, and pathological straightening of cerebral arteries A pilot subject-specific CFD study in wild type and KO mouse CoW model revealed that characteristic vessel straightening alone may not lead to stroke. However, occlusions in one of the major arteries of the CoW results critical wall shear rate levels in vessels contralateral to the occlusion increasing stroke risk. An equivalent behavior in the human condition could have profound implications for patient care. A review of 50 pediatric MMD cases revealed that of the 28 patients that suffered a stroke, 10 (35.7%) went on to have a subsequent contralateral stroke. Patient-specific blood flow simulations were carried out on a CoW anatomy reconstructed from MRI and CTA images of a representative pediatric MMD patient that was presented with a severe stroke on the right side. Vascular regions at a higher risk for clot formation were identified and compared with corresponding clinical observations. Our analysis accurately predicted that an occlusion in the right supraclinoid artery resulted in critical wall shear stress levels in the contralateral side, which potentially led to a subsequent stroke two months later on the left side involving the middle cerebral artery.

Conclusions

Our patient-specific analysis framework could identify susceptible regions that could evolve into severe stenosis or vessel occlusion leading to stroke, facilitating early intervention in pediatric MMD patients.

References

[1] Urick B, Sanders TM, Hossain SS, et al., Review of Patient-Specific Vascular Modeling: Template-Based Isogeometric Framework and the Case for CAD, *Archives of Computational Methods in Engineering*, 1-24, 2017.
[2] Hossain SS, Zhang, Y, Liang, X, et al., In silico vascular modeling for personalized nanoparticle delivery, *Nanomedicine*, *8*(3): 343-357, 2013.

An animal-specific study investigating the association between helical flow and atherosclerotic plaque progression in coronary arteries

Giuseppe De Nisco[1], Ayla Hoogendoorn[2], Annette Kok[2], Claudio Chiastra[1], Diego Gallo[1], Jolanda Wentzel[2], Umberto Morbiducci[1]

[1] PoliTo[BIO]Med Lab, Departement of Mechanical and Aerospace Engineering, Politecnico di Torino, Turin, Italy
[2] Department of Biomedical Engineering, ErasmusMC, Rotterdam, The Netherlands

Introduction

Several previous studies suggest that helical flow plays an atheroprotective role by mitigating WSS disturbances in arteries [1][2][3] and it is inversely associated to atherosclerosis at the early stage [2]. In this work, we investigate the existence of a link between helical flow intensity and wall thickness (WT), a hallmark of atherosclerotic plaque growth, in pig coronary arteries.

Methods

Adult familial hypercholesterolemic pigs were put on a high fat diet and underwent computed tomography (CT) angiography and intravascular ultrasound (IVUS) imaging of the three main coronary arteries at two time points (baseline - after 3 months since start of the diet; T2 - after 6.4±1.9 months). The geometry of imaged coronary arteries (n=15) at baseline was reconstructed [4] and the finite volume method was used to numerically solve Navier-Stokes equations in properly discretized fluid domains by applying personalized boundary conditions obtained using individual velocity ComboWire Doppler measurements [5]. As for the analysis, each IVUS imaged arterial segment was divided into 3mm/45° sectors.

The intensity of helical flow structures (h_2, given by the integral value of the unsigned internal product of velocity and vorticity vectors [3]) in the near-wall region (10% of the local radius) was cycle- and volume-averaged over each 3mm/45° sector. Near-wall h_2 data were divided into artery-specific tertiles (low, mid and high). WT at the investigated time points was computed by subtracting the distance from the lumen center of the outer and inner semi-automatically segmented wall boundaries. The mean values of the difference between T2 and baseline WT measurements was evaluated for each sector (ΔWT) and normalized to follow-up time. Statistical analysis of helicity data was performed using a generalized-estimators equation model. Significance was assumed for $p<0.05$.

Results

For an explanatory case (Fig. 1A), the obtained 2D maps of the ΔWT per month and near-wall h_2 over 3mm/45° sectors values are reported in Fig. 1B. The 2D maps show an appreciable colocalization between high h_2 and low ΔWT/month. Coronary segments exposed to high baseline levels of near-wall h_2 exhibit a significantly larger plaque growth per month compared to regions with either mid or low h_2 (Fig.1 panel C).

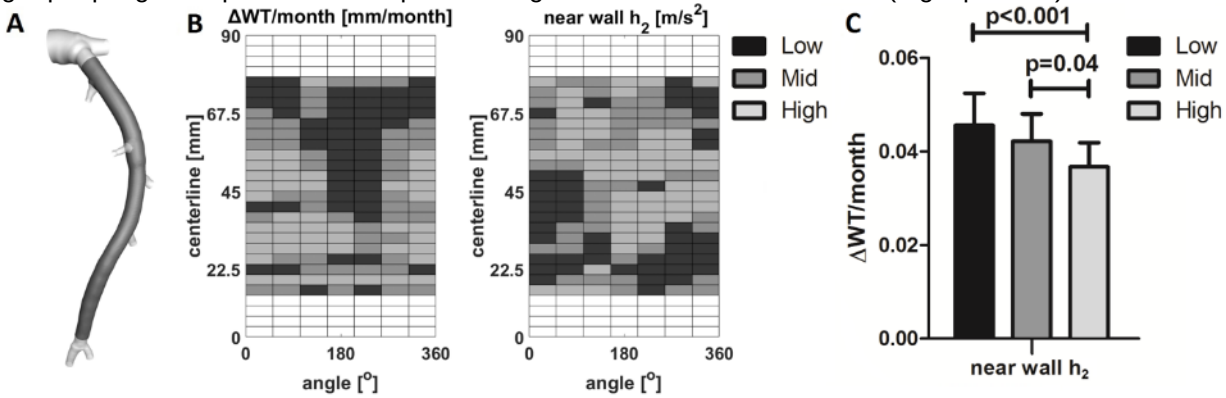

Figure.A) 3D artery model; **B)** 2D map of the plaque growth and h_2 levels; **C)** near-wall h2 vs. estimated ΔWT/month

Conclusions

Results from this study confirm the physiological significance of helical flow in coronary arteries [3], revealing its protective role against atherosclerotic plaque growth and its potential as WT predictor.

References

[1] Morbiducci, U et al., *J.Biomech*., 40:519-534, 2007
[2] Gallo, D et al., *J. R. Soc. Interface*, 15(147), 2018
[3] De Nisco, G et al., *Ann. Biomed. Eng.*, 2018 https://doi.org/10.1007/s10439-018-02169-x
[4] van der Giessen, AG et al., *Int. J. Cardiovasc. Imaging*, 26:781-796, 2010
[5] Huo, Y, Kassab, GS, *J. R. Soc. Interface*, 9:190-200, 2012

Ultrasound-image-based assessment of shear strain of the carotid artery in an intensive care unit

Spyretta Golemati[1], Demosthenes D. Cokkinos[2], Spyros Zakynthinos[1]

[1]First Intensive Care Unit, Medical School, National and Kapodistrian University of Athens, Athens, Greece

[2]Radiology Department, Evangelismos hospital, Athens, Greece

Introduction

Assessment of arterial mechanical properties in the Intensive Care Unit (ICU) has been investigated in a few studies, in particular in terms of feasibility and of the effect of drugs [1]. In this study, the feasibility of measuring shear strain using ultrasound imaging in the carotid artery of ICU patients was investigated. Shear strain, which is due to relative displacements of adjacent wall layers, remains challenging to assess, and many aspects of its implications for arterial wall pathophysiology are still unexplored [2].

Methods

B-mode ultrasound image sequences were acquired in 3 young (24-27 y.o.) and 3 elderly (49-66 y.o.) subjects in the ICU, who did not receive catecholamines. Image sequences depict longitudinal sections of the carotid artery wall, free from atheromatous plaque, and have a duration of 3 s and a frame rate of 41 Hz. Motion analysis was performed using adaptive block matching, and the derived radial and longitudinal displacement waveforms were used to calculate shear strain of the adventitial layer.

Results

Figure 1 shows examples of shear strains in a young and an elderly subject, which exhibit a periodic pattern following the periodic arterial distension. Maximum and pulse shear strain values (defined as the difference between maximum and minimum values) for each subject, as well as mean±standard deviation values, are presented in Table 1. As we can see, shear strain seems to be larger in elderly subjects, although there is high variability especially among younger individuals.

Conclusions

This pilot study shows that shear strain of the carotid artery wall, estimated from B-mode ultrasound, is feasible, and may provide valuable insight into arterial function.

References

[1] Golemati S, Cardiovascular computing in the intensive care unit, in *Cardiovascular Computing - Methodologies and Clinical Applications*, Springer 2019.

[2] Idzenga T, et al., Estimating cyclic shear strain in the common carotid artery using radiofrequency ultrasound, *Ultrasound Med Biol*, 38: 2229-2237, 2012.

Table 1. Maximum and pulse shear strain values in ICU patients.

	Max shear strain (deg)	***Pulse shear strain (deg)***
1 [male, 24 y.o.]	4.99	15.79
2 [male, 25 y.o.]	30.00	31.00
3 [male, 27 y.o.]	5.97	10.21
4 [female, 49 y.o.]	10.32	18.43
5 [male, 51 y.o.]	16.18	19.78
6 [male, 66 y.o.]	8.8	13.00

(a) (b)

Fig. 1. Waveforms showing shear strains in a young (a) and an elderly (b) subject.

In vivo function of flow-responsive *cis*-DNA elements in the endothelial nitric oxide synthase gene: a role for chromatin-based mechanisms

Kyung Ha (Kay) Ku[1,2], Britta J. Knight[1], Philip A. Marsden[1,2,3]

[1]Department of Laboratory Medicine and Pathobiology;

[2]Keenan Research Centre for Biomedical Science, St. Michael's Hospital;

[3]Division of Nephrology, Department of Medicine, University of Toronto, Toronto, ON, Canada

Introduction

Endothelial nitric oxide synthase (eNOS) is predominantly expressed in medium- to large-sized arteries where endothelial cells (ECs) are exposed to high frictional forces of blood flow or shear stress. Decreased shear stress due to Disturbed blood flow leads to reduced transcription of eNOS, which contributes to the development of atherosclerotic lesions preferentially at bifurcations, branch points, and curvatures of major arteries[1]. Two flow-responsive *cis*-regulatory DNA elements have been found within the eNOS promoter: a Shear Stress Response Element (SSRE) and a Krüppel-Like Factor (KLF) binding element. Both are argued to be functionally relevant to the positive effects of laminar shear on eNOS transcription *in vitro.* However, the functional role of these *cis*-elements *in vivo* remains unclear.

Methods

To investigate *in vivo* function of the SSRE and the KLF binding element, transgenic mice with a mutation at each flow-responsive *cis*-element were generated using a murine eNOS promoter-β-galactosidase reporter via linker-scanning mutagenesis. Murine ECs were isolated from the aortic arch (AA) and the descending thoracic aorta (DTA) to assess the levels of DNA methylation at the transgene and native eNOS proximal promoters by bisulfite sequencing and pyrosequencing.

Results

Wildtype mice with a functional murine eNOS promoter-reporter construct exhibited reduced endothelial staining in the lesser curvature of the AA as expected. Surprisingly, mutation of the SSRE completely abolished the reporter expression in murine aortic ECs. This was associated with aberrant hypermethylation at the transgene eNOS proximal promoter, indicating that the SSRE is necessary for eNOS transcription *in vivo*. Mutation of the KLF binding element evidenced reduced reporter expression in murine aortic ECs, manifesting an integration site-specific decrease in eNOS transcription. An inverse relationship between reporter expression and the transgene eNOS proximal promoter methylation was also observed. This indicated that the KLF binding element alone is not sufficient to induce eNOS transcription *in vivo*. Moreover, the proximal promoter of native eNOS in wildtype murine ECs from the AA demonstrated significant hypermethylation relative to those from the DTA, suggesting a functional role for flow-dependent DNA methylation in transcriptional regulation of eNOS *in vivo*.

Conclusions

Here, we demonstrate that the SSRE and the KLF binding element in the eNOS promoter are both necessary for flow-induced transcription of eNOS in arterial ECs *in vivo*. One element alone is not sufficient. This study is the first *in vivo* study to report the functional importance of a flow-responsive *cis*-DNA element. Furthermore, this work highlights an intimate relationship between the chromatin-based function of flow-responsive *cis*-DNA elements and epigenetic-based transcriptional processes.

References

[1] Won D, Zhu SN, Chen M, Teichert AM, Fish JE, Matouk CC, Bonert M, Ojha M, Marsden PA, Cybulsky, MI, Relative reduction of endothelial nitric-oxide synthase expression and transcription in atherosclerosis-prone regions of the mouse aorta and in an in vitro model of disturbed flow, *Am J Pathol*, 171(5): 1691-704, 2007.

Mechanosensitive Piezo1 channels mediate insulin release from pancreatic β-cells

Vijayalakshmi Deivasikamani[1], Savitha Dhayalan[1], Romana Mughal[1], Asjad Visnagri[1], Kevin Cuthbertson[2], Jason L Scragg[1], Nicola Blythe[1], Tim S Munsey[3], Hema Viswambharan[1], Richard Foster[2], Asipu Sivaprasadarao[3], Mark T Kearney[1], David J Beech[1] & Piruthivi Sukumar[1].

[1]Leeds Institute for Cardiovascular and Metabolic Medicine, Faculty of Medicine and Health, University of Leeds, Leeds, LS2 9JT, United Kingdom.
[2]School of Chemistry, Faculty of Mathematics and Physical Sciences, University of Leeds, Leeds, LS2 9JT, United Kingdom.
[3]School of Biomedical Sciences, Faculty of Biological Sciences, University of Leeds, Leeds, LS2 9JT, United Kingdom.

Introduction

Swelling of pancreatic β-cells induced by high glucose and hypotonicity has been shown to stimulate insulin release in K_{ATP} channel independent manner. While a role for stretch activated mechanisms/cationic channels has been proposed in this process, the exact identifity of such channels is not known. Recently, Piezo1 has been described as a mechanically-activated nonselective calcium permeable cationic channel in a range of mammalian cells. Hence, we hypothesised a role for Piezo1 in cell swelling-induced insulin release.

Methods

We used two rat β-cell lines (INS-1 and BRIN-BD11) and freshly-isolated mouse pancreatic islets as models for exploring Piezo1 activity and insulin release. We used cell permeable analogue of calcium sensitive ratiometric fluroscent dye (fura-2 AM) for intracellular calcium ion measurements. Piezo1 agonist Yoda1 and a competitive antagonist of Yoda1 (Dooku1) were used as chemical probes. Piezo1 mRNA and insulin secretion were measured by RT-PCR and ELISA respectively. As complete global deletion of Piezo1 ($Piezo^{-/-}$) is lethal in mice, we have generated and used heterozygous Piezo1 knockout ($Piezo1^{+/-}$) mice to confirm the role of Piezo1 stimulation in insulin secretion.

Results

Expression of Piezo1 was found in both β-cell lines and mouse islets. Yoda1, in dose depedent manner evoked Ca^{2+} entry in β-cell lines and it was inhibited by Yoda1 antagonist Dooku1 as well as generic Piezo1 inhibitors gadolinium and ruthenium red. Moreover, Yoda1 stimulated insulin release from β-cells and pancreatic islets which was blocked by Dooku1. Hypotonicity and high glucose increased basal and Yoda1-induced intracellular Ca^{2+} level. Pretreating the β-cells and islets with ruthenium red significantly reduced hypotonicity and also circular shear stress induced insulin release. Importantly, islets isolated from $Piezo^{+/-}$ mice showed significantly impaired Yoda1-induced insulin release compared to wild type islets.

Conclusions

The data show that Piezo1 channel agonist Yoda1 induces insulin release from β-cell lines and wild type mouse pancreatic islets. When Piezo1 is partially knockout, Yoda1 induced insulin release is significantly impaired. Thus the study suggest a role for Piezo1 in cell swelling induced insulin release. Hence we propose that Piezo1 agonists have a potential to be used as enhancers of insulin release.

Coronary Stent Fracture: Biological Consequence & Lifetime Prediction

Claire Conway[1,2], Elazer Edelman[2]

[1] Department of Biomedical Engineering, Aston University, Birmingham UK

[2] Biomedical Engineering Center, Massachussetts Institute of Technology, Cambridge, MA, USA

Introduction

Drug-eluting stent (DES) strut fracture (SF) is associated with higher incidence of in-stent restenosis (ISR) - return of blockage in a diseased artery post stenting - than seen with bare metal stents (BMS). It has been reported that the presence of both drug and SF play a key role in exascerbating neointimal formation [1]. Additionally, a recent review of stent fracture found that loadings, in particular, dictate device durability response in either phyiscial or computational experimentation [2]. This study aims to more accurately determine SF timelines taking into account realistic loading focusing on timelines where drug is stil present.

Methods

Finite element analysis (FEA) was used to investigate the implantation and in vivo deformations of three 316L stainless steel stent designs (Fig 1). A sensitivity analysis was also performed to examine response to 25% variation in complex loadings for one stent design. Each design was post-processed to extract cycles to failure predictions using the modified Smith-Watson-Topper fatigue life model [3].

Results

Following four cycles of representative multimodal loading the stress-strain states were analysed as per the methodology documented in Liu [3] to extract predicted number of cycles to failure. The sensitivity analysis found that the trend in deformations remained similar with the primary bending deformation in the plane normal to the applied bend. Finally, for each stent design, under the given loading conditions, failure was predicted with the fatigue methodology implemented.

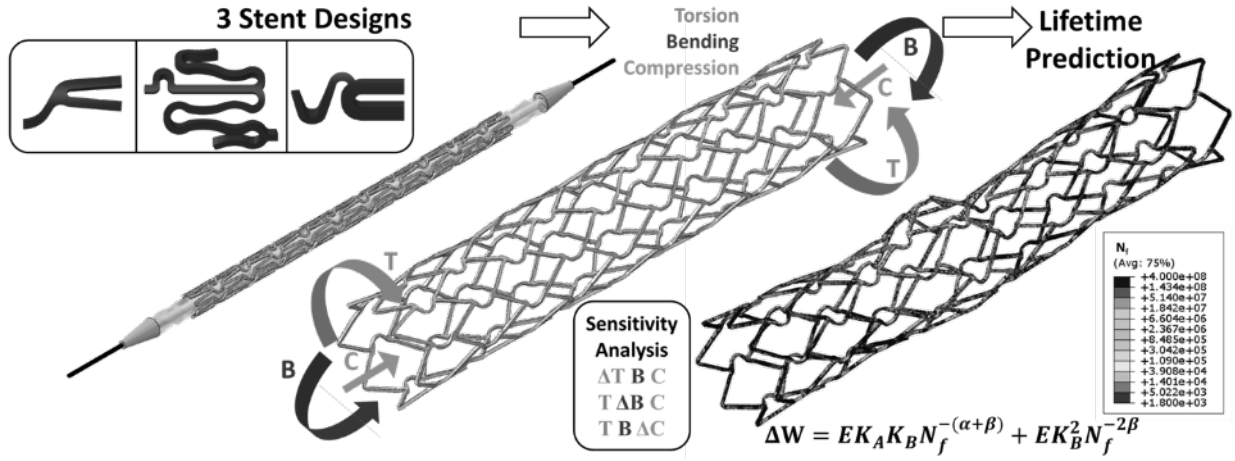

Fig 1 Predictive lifetime framework demonstrating number of cycles to failure, N_f, for a selected stent design.

Conclusions

Stents are tested for ten year survival using standardized methods before regulatory approval and yet clinical stent fracture is still evident, suggesting that such fatigue events are more complex than perhaps appreciated. This study not only demonstrates failure spatially but temporally, via an explicit calculation of number of cycles to failure based on an energy criterion. This highlights the crucial need for continued refinement of bench-top testing and in silico exploration as new device designs emerge and understanding of clinical use conditions evolve.

References

[1] Conway C, Desany GJ, Bailey LR, Keating JH, Baker BL, Edelman ER, Fracture in Drug-Eluting Stents Increases Focal Intimal Hyperplasia in the Atherosclerosed Rabbit Iliac Artery, *Catheterization & Cardiovascular Interventions* (2019 – in press).

[2] Conway C, Coronary Stent Fracture: Clinical Evidence Vs. the Testing Paradigm, *Cardiovascular Engineering & Technology*, 9(4): 752-760, 2018.

[3] Liu KC, *Advances in Multiaxial Fatigue ASTM STP 1191*, McDowell & Ellis, ASTM Philadelphia (1993), pp 67-84.

Substrate Regulation of Vascular Endothelial Cell Shape and Alignment

Abdul I. Barakat[1,2], Carlo Natale[1], Maria Gusseva[1], Julie Lafaurie-Janvore[1], Avin Babataheri[1]

[1]Hydrodynamics Laboratory, Ecole Polytechnique, Palaiseau, France

[2]School of Mechanical and Manufacturing Engineering, University of New South Wales Sydney, Australia

Introduction

In many cell types, shape and function are intricately intertwined. In the case of vascular endothelial cells (ECs), cell shape and alignment relative to blood flow have been correlated with the inflammatory state of the cells and with predisposition to the development of atherosclerosis. Therefore, understanding how EC shape and orientation are regulated is of importance. EC shape and orientation are known to be sensitive to the local flow environment to which the cells are subjected; however, recent studies have shown that EC shape is also regulated by the architecture of the substrate on which the cells reside. For instance, significant EC elongation can be induced by culturing the cells either on two-diemensional (2D) patterned surfaces with selectively-defined adhesive zones or on three-dimensional (3D) topographies consisting of series of micro-scale ridges and grooves. It remains unclear, however, how ECs perceive these different types of substrates and if the effect of the two types of substrates on ECs occurs *via* similar mechanisms. The goal of the present study is to quantitatively characterize EC elongation and alignment on both 2D patterned surfaces and 3D micrograting and to shed light onto the underlying mechanisms.

Methods

2D micropatterned (2DμP) substrates containing alternating 5 μm-wide adhesive (fibronectin) and non-adhesive (PLL-PEG) stripes were produced in PDMS using the deep UV light method. 3D micrograting (3DμG) substrates were fabricated by replica molding of PDMS on a silicon master containing straight channels with a groove/ridge width of 5 μm and a ridge height of 1 μm. The topographies and mechanical properties of the patterned surfaces were measured using atomic force microscopy (AFM). Because the AFM measurements indicated that the 3DμG substrate was significantly softer than the 2DμP surface, 3D microgrooved surfaces with the same dimensions as the 3DμG substrate but with comparable mechanical properties to the 2DμP substrates (3DμG*) were also produced. In other experiments, fibronectin was adsorbed selectively on the ridges (but not the grooves) of the 3D micrograting substrates by using microcontact printing to produce a 3D surface (3DFnR) with similar adhesive regions as the 2DμP substrate. Unpatterned PDMS substrates served as controls. Prior to cell seeding, all substrates were incubated with a 50 μg/mL fibronectin solution in PBS for 1 hr. Bovine aortic ECs (BAECs) were seeded on the different substrates, fixed and immunostained for both actin and vinculin (focal adhesions (FAs)) either 2 or 24 hrs after seeding. Quantification of cell elongation and alignment as well as FA distribution was performed using Fiji software.

Results

BAEC elongation and alignment were largely similar at the 2- and 24-hr time points, suggesting that cellular adaptation to the substrate architecture occurs rapidly. BAECs were highly aligned in the direction of the pattern on both 2DμP and 3DμG with average orientation angles relative to the pattern of 6.9±0.8° and 9.3±1.7°, respectively. Cells on the control unpatterned surfaces were randomly oriented as expected (43.0±3.1°). Interestingly, cells were considerably more elongated on 2DμP than on 3DμG (elongation indices of 18.9±3.1 and 5.9±0.5, respectively). Cell elongation on 3DμG*, which had the rigidity of 2DμP, was similar to that on 3DμG, suggesting that the difference in cell elongation between 2DμP and 3DμG is not attributable to differences in substrate stiffness. FAs on 2DμP were preferentially localized to pattern edges. On 3DμG surfaces, FAs were mostly detected on the ridge surfaces but those forming on the groove surfaces were preferentially distributed towards the center of the groove. Culturing cells on 3DFnR provided a FA organization that largely resembled that of 2DμP and led to ECs that were even more aligned (3.8±0.5°) and elongated (elongation index of 33.3±3.7) than on 2DμP.

Conclusions

The current results indicate that the manner by which a particular 2D or 3D patterned surface modulates EC elongation and alignment depends on the effect of the surface on FA organization. These findings enhance our understanding of EC shape regulation and promise to inform strategies aimed at optimizing the design of the surfaces of implantable endovascular devices to target specific cell shapes.

Intracranial aneurysm under high frequencies: can turbulent-like hemodynamic conditions translate to characteristic wall vibrations?

Alban Souche, Kristian Valen-Sendstad

Department of Computational Physiology, Simula Research Laboratory, Lysaker, Norway

Introduction

The presence of wall vibrations of relatively high frequencies (several hundreds of Hz) on the top of intracranial aneurysms have been reported in the 70's from open brain surgery measurements [1]. Later study [2], based on non-invasive recordings, provided additional evidences for charateristic high frequencie intracranial blood flow sounds associated with the presence of aneurysms. It is only recently that computational and experimental in-vitro studies modelled turbulent-like blood flow environments within intracranial vasculature, with characteristic fluctuations in the order of 100-300 Hz ([3, 4]). However, the link between unstable blood flow and arterial wall vibrations within intracranial aneurysms still remains speculative and is the focus of the present work.

Methods

We numerically assess fully coupled fluid-structure interactions (FSI) between the arterial wall deformation and the hemodynamic flow within patient-specific vascular geometries. The numerical tool is developed upon FEniCS Finite Element Model library and tailored to efficiently and accurately model the mechanical coupling at high temporal and spatial resolutions.

Results

Fig. 1 presents some preliminary results of aneurysm wall deformations under constant arterial blood flow (left panel). Only the aneurysm wall is subjected to FSI, whereas the rest of the vasculature is restricted to rigid walls. The right panel shows the temporal evolution of the displacement amplitude at selected locations, and illustrate the oscillatory mechanical response of the aneurysm sac.

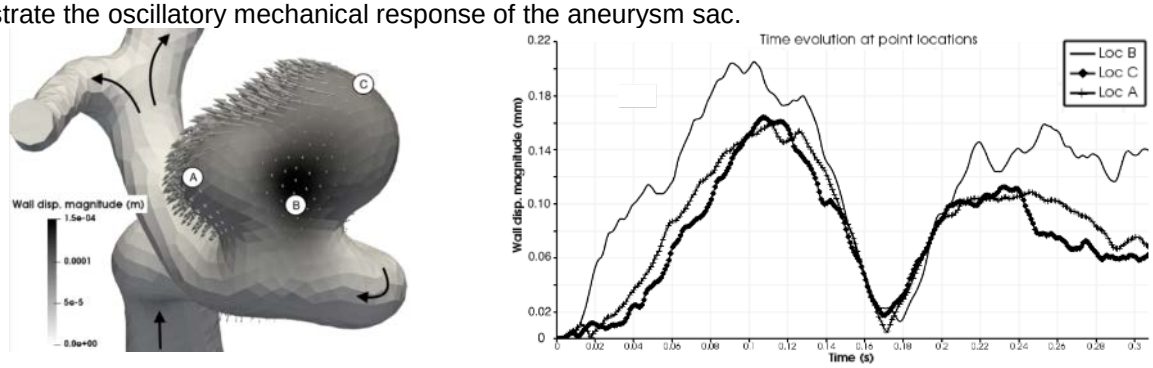

Fig. 1: Left: Wall displacement amplitude at 0.3 s. Right: Time evolution of the displacements at locations A/B/C.

Conclusions

At the moment, the interpretation of the results is restricted to a proof-of-concept of the link between hemodynamics and characteristic arterial wall deformation. However, the results already show a fundamental mechanical process unravelling the potential vibrating nature of aneurysms. More realistic studies will be performed to assess the importance of vibrations caused by turbulent-like flows on clinically relevant quantities, such as the wall shear stress, and how it could affect mechanotransduction and remodeling of the vasculature.

References

[1] Ferguson G.G., Turbulence in human intracranial saccular aneurysms, *J. Neurosurg.*, Vol. 33, 1970

[2] Kurokawa Y., Abiko S., Watanabe K., Noninvasive detection of intracranial vascular lesions by recording blood flow sounds, *Stroke*, Vol. 5, 397-402, 1994

[3] Valen-sendstad K., Piccinelli M., Steinman D.A., High-resolution computational fluid dynamics detects flow instabilities in the carotid siphon: Implications for aneurysm initiation and rupture?, *Journal of Biomechanics*, Vol. 47, 3210-3216, 2014

[4] Balasso A., Fritzche M., Liepsch D., etal., High-frequency wall vibrations in a cerebral patient-specific aneurysm model, *Biomed. Eng. - Biomed. Tech.*, 2018

An assessment of methods to estimate cardiovascular parameters from blood pressure and flow waveforms

Jorge Mariscal-Harana[1], Peter H Charlton[1], Spencer Sherwin[2], Jordi Alastruey[1]

1. School of Biomedical Engineering and Imaging Sciences, King's College London, King's Health Partners, UK
2. Department of Aeronautics, Imperial College London, London, UK

Introduction

Cardiovascular (CV) parameters can be used as markers of cardiovascular risk, and as inputs to computational models of arterial blood flow. However, they are difficult to measure directly. Several CV parameter estimation (CPE) methods have been proposed to estimate parameters from non-inasive blood pressure and flow waveforms, although it is not clear which perform best. The primary aim of this study was to assess the performance of CPE methods to estimate cardiac, arterial and microvascular parameters. The secondary aim was to use these methods with a model of the circulation to estimate central blood pressure (CBP) from waveforms which can be acquired non-invasively.

Methods

An extensive literature review of current CPE methods was performed: ten methods were identified for estimating characteristic impedance (Z); nine for both asymptotic outflow pressure (Pout) and peripheral compliance (C); six for left ventricular ejection time (LVET); and four for pulse wave velocity (PWV). These methods were implemented in a common framework. They were used to estimate the CV parameters of 258 simulated healthy subjects from an *in silico* pulse wave database (previously described in [2]). Imposed CV parameters and corresponding brachial pressure and central (aortic) flow waveforms from each subject were used as reference data. The performance of CPE methods was assessed individually using the mean percentage error (PE) between estimated and reference values. In addition, the estimated CV parameters were used as inputs to a 3-element Windkessel (0-D) model to estimate CBP. For each subject, CBP was estimated using the CV parameters estimated by every possible combination of CPE methods. The optimal combination of CPE methods was the one which resulted in the lowest mean root-mean-square error (RMSE) between the reference and estimated CBP waveforms for the entire dataset.

Results

The individual analysis indicated that the optimal CPE methods were: a 'first-derivative of pressure' analysis for LVET (PE: 8.1 %); 50 % of diastolic blood pressure (DBP) for Pout (8.4 %); an 'iterative DBP' method for C (29.7 %); and an 'early-systole PQ-loop' method for Z (68.6 %). The mean RMSE of CBP waveforms estimated using this combination of CPE methods was 2.4 mmHg. This was also the optimal combination of CPE methods, since remaining combinations resulted in larger mean RMSE values.

Conclusions

We have identified the best-performing CPE methods through comparison with known reference values in an *in silico* pulse wave database. When used as inputs to a 3-element Windkessel (0-D) model, these methods provided accurate estimation of CBP. The use of an *in silico* dataset has the advantage that the reference CV parameters were known precisely and were varied across a wide range of values. Future work will assess the performance of methods *in vivo*.

References

[1] McEniery et al. Central blood pressure: Current evidence and clinical importance. *European Heart Journal*, 35(26), 1719–1725, 2014.

[2] Charlton P.H. et al. Modelling arterial pulse wave propagation during healthy ageing, In *World Congress of Biomechanics 2018*, Dublin, Ireland, 2018.

Piezo1 channel coupling to endothelial nitric oxide synthase

Hannah J Gaunt[1], Marjolaine Debant[1], Melanie J Ludlow[1], Fiona Bartoli[1], David J Beech[1]

[1]School of Medicine, University of Leeds, Leeds, United-Kingdom

Introduction

The cation channel Piezo1 has emerged as a major determinant of vascular structure and response to shear stress [1]. It has been described as an activator of endothelial Nitric Oxyde Synthase (eNOS) in endothelial cells, through which mechanism it can trigger vessel relaxation. Multiple studies about shear-stress induced signaling have helped decipher the signalling pathway after a mechanical activation. But shear-stress activates numerous membrane proteins, such as TRPV4 or integrins [2]. Here we used a chemical activator of Piezo1 in order to activate Piezo1 channels and thus understand its specific signalling pathway.

Methods

Human Umbilical Vein Endothelial Cells were used in all experiments. The Piezo-1 activator, Yoda 1, was used at 2 µM and was compared to its vehicle DMSO. Western Blot (WB) was used to assess eNOS phosphorylation on its serine 1177, as well as AKT phosphorylation. Candidate proteins were knocked down using specific siRNA (transfecting agent: Lipofectamin) and experiments were conducted 48h later. Knock down efficiency was assessed by RT-qPCR or WB.

Results

Piezo1 chemical activation by Yoda1 caused eNOS S1177 phosphorylation in less than 1 minute, suggesting a priviledge relationship. We investigated the role of AKT, a well-known activator of shear stress-induced eNOS phosphorylation. Unexpectedly eNOS phosphorylation preceded AKT phosphorylation. Moreover, knockdown of Akt failed to affect the eNOS phosphorylation. In contrast, the Piezo1 channel blocker Gd^{3+} or reduced extracellular Ca^{2+} suppressed the phosphorylation, suggesting dependence on ion channel function of Piezo1 and Ca^{2+} entry. We therefore investigated the involvement of Ca^{2+}-dependent kinase CaMKII by the use of two inhibitors and found that eNOS phosphorylation was suppressed. However, knockdown of CaMKIIs failed to mimic the effect of pharmacological inhibition, suggesting involvement of other kinases which remain to be determined.

Conclusions

The data suggest a close signaling relationship between Piezo1 and eNOS which regulates nitric oxide production independently of Akt but dependently on Ca^{2+}.

Acknowledgements
Funded by the British Heart Foundation and Wellcome Trust.

References

[1] Li J, Hou B, Tumova S, Muraki K, Bruns A, Ludlow MJ, Sedo A, Hyman AJ, McKeown L, Young RS, Yuldasheva NY, Majeed Y, Wilson LA, Rode B, Bailey MA, Kim HR, Fu Z, Carter DA, Bilton J, Imrie H, Ajuh P, Dear TN, Cubbon RM, Kearney MT, Prasad RK, Evans PC, Ainscough JF, Beech DJ, Piezo1 integration of vascular architecture with physiological force, *Nature,* 13;515(7526):279-282, 2014

[2] Baratchi S, Khoshmanesh K, Woodman OL, Potocnik S, Peter K, McIntyre P, Molecular Sensors of Blood Flow in Endothelial Cells. *Trends Mol Med,* 23(9):850-868, 2017

Patient-specific hemodynamic analysis of CT-derived stented superficial femoral arteries

Monika Colombo[1], Marco Bologna[2], Marc Garbey[3,4], Scott Berceli[5,6], Yong He[6], Josè Felix Rodriguez Matas[1], Francesco Migliavacca[1], Claudio Chiastra[1,7]

1 LaBS, Dept. of Chemistry, Materials and Chemical Engineering "Giulio Natta", Politecnico di Milano, Milan, Italy
2 Dept. of Electronics, Information and Bioengineering, Politecnico di Milano, Milan, Italy
3 University of La Rochelle, LASIE UMR CNRS, La Rochelle, France
4 Houston Methodist Hospital Research Institute, Houston, TX, USA
5 Malcom Randall VAMC, Gainesville, FL, USA
6 Dept. of Surgery, University of Florida, Gainesville, FL, USA
7 PoliToBIOMed Lab, Dept. of Mechanical and Aerospace Engineering, Politecnico di Torino, Turin, Italy

Introduction

Abnormal hemodynamics seems to be one of the driven factors for in-stent restenosis at femoral artery level, as for other vascular districts [1]. In this study, the impact of altered hemodynamics on lumen variation at 1-year follow-up (1Y-FU) is analysed in patient-specific cases of diseased superficial femoral arteries (SFAs).

Methods

Five patients treated at Malcom Randall VAMC (Gainesville, FL, USA) were considered. Starting from the lumen geometry of SFAs reconstructed from computed tomography (CT) images at 1-week post-operative follow-up (1W-FU), computational fluid dynamics analyses were performed. Patient-speficic boundary conditions were derived from Doppler ultrasound data. The luminal model, reconstructed from 1Y-FU CT images, was used to quantify the arterial lumen variation due to neointimal regrowth and plaque development. To investigate the influence of abnormal hemodynamics on restenosis in SFA, both hemodynamic quantities (such as wall shear stress, oscillatory shear index and relative residence time) and lumen variation were computed, 3D mapped and visualized on the 1W-FU geometry.

Results

From the 3D post-processed maps of the hemodynamics quantities (Fig. 1), it is observable that the stent presence alters the hemodynamics and, consequently, may induce luminal remodeling (in terms of radial dilatation or restenosis). It is noticeable that values of wall shear stress are generally lower in the stented regions, where neointimal regrowth and plaque lesions are present. Moreover, areas of wide lumen variation lay in the zone of large variation in hemodynamic quantities.

Conclusions

Hemodynamics altered by stent presence is related to lumen variation, quantified after 1 year. Further investigation is required to find possible statistical correlation.

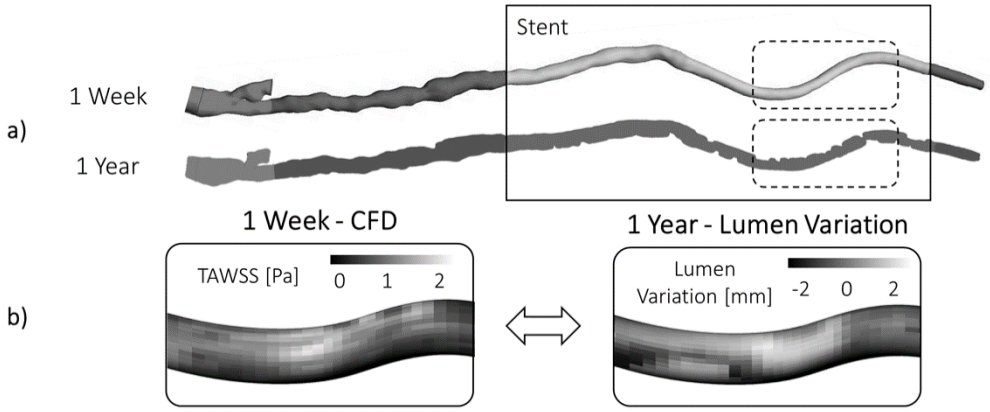

Figure 2 – a) Patient-specific stented SFA models, derived from 1W-FU (top) and 1Y-FU (bottom) CT images. b) Comparision between time-averaged wall shear stress (TAWSS) at 1W-FU and lumen variation at 1Y-FU.

References

[1] Schlager O et *al*. *Atherosclerosis*, 233: 76-82, 2014.

Acknoledgments

This work has been supported by Fondazione Cariplo, Italy (Grant number 2017-0792, TIME).

Numerical Investigation on the effect of Blood pressure on Wall Shear Stress and Vorticity.

Nitesh Kumar[1,2], Raghuvir Pai B[1], P A Kyriacou[2],S M Abdul Khader[1],S H Khan[2]

[1]Department of Mechanical and Manufacturing Engineering, Manipal Academy of higher Education, Manipal, India
[2]School of Mathematics, Computer Science and Engineering, Department of Electrical and Electronic Engineering, City, University of London, London, UK

Introduction

Numerical investigation of haemodynamics in the carotid artery using Fluid structure interaction tehcnique is an effective tool in understanding the flow dynamics and its effects on the arterial wall. The results from both structure and fluid are exchanged at the interface to obtain the desired results. In this study the behaviour of flow of blood through stenosed carotid artery is subjected to normal (120/80 mm Hg), prehypertension (120-139/80-89 mm Hg), hypertension stage 1(140-159/90-99 mm Hg), hypertension stage 2(≥ 160/ ≥ 100 mm Hg) and also hypotension (< 90/<60 mmHg) [1]. The purpose of this study was to compare the effects of different blood pressure ranges on the Wall Shear Stress (WSS) and vorticity and also in exploring the differences between Newtonian and non-Newtonian blood viscosity models.

Methods

A 3D model of a patient specific carotid artery was constructed by selecting CT angio data followed by converting 2D CT scan images into 3D CAD model using medical image processing software MIMICS 19 (Materialise, Leuven, Belgium). The FSI analysis was performed using Ansys CFX 19.0 and Ansys structural 19.0(ANSYS® Academic Research, Release 19.0). The artery was modelled as a linear elastic with Young's Modulus of 0.9 MPa, and Poison's ratio of 0.45. For the Newtonian viscosity model a density 1060 kg/m^3 and dynamic viscosity of 0.004 Pa-s was used and the non – Newtonian consideration, Carreau – Yasuda model [2] was chosen. The changes in WSS for different blood pressure ranges for both Newtonian and non – Newtonian models were considered and compared.

Results

Figure 1 shows the analysis of the difference in WSS between Newtonian and non – Newtonian models. Maximum Wall shear stress over the entire wall of the artery is noted with a clear observation that the Newtonian model underestimates the WSS compared to the Carreau Yasuda model. Vortex core regions were produced during the decelerating phase of the pulsatile flow. Flow diverged while approaching the bifurcation, and then showed helical motion representing vortex formation leading to low shear regions mainly near the carotid sinus and post stenosis in external carotid artery. During this helical flow the stagnation points appeared on the wall below the carotid sinus and at the inner wall immediately post stenosis. The region affected due to vortex formation was small during peak systole and higher during late and early diastole.

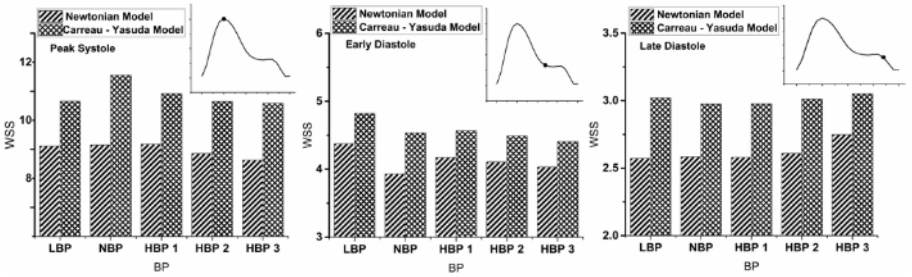

Figure 3: Comparision of WSS between different blood pressures and rheological models.

Conclusions

The bio-rheological characteristics of blood in arterial flow influences the quantitative behavior of the flow field. The results showed that the Newtonian model is not suitable for simulating the blood flow in the carotid artery with stenosis where the shear rate is less than 100 s^{-1}. The observations in the present study shows the differences in WSS and vorticity and their position was dependent on the flow distribution between the branches and the peripheral resistance due to pressure and also the blood rheology.

References

[1] Corrada, M.M., Hayden, K.M., Paganini-Hill, A., Bullain, S.S., DeMoss, J., Aguirre, C., Brookmeyer, R. and Kawas, C.H., 2017. Age of onset of hypertension and risk of dementia in the oldest-old: The 90+ Study. Alzheimer's & Dementia, 13(2), pp.103-110.

[2] Toloui, M., Firoozabadi, B. and Saidi, M.S., 2012. A numerical study of the effects of blood rheology and vessel deformability on the hemodynamics of carotid bifurcation. *Scientia Iranica*, *19*(1), pp.119-126.

The role of the mechanosensing endothelial glycocalyx in matrix stiffness-mediated vascular disease

Marwa Mahmoud, Mariya Mayer, Limary Cancel, John M. Tarbell

Department of Biomedical Engineering, The City College of New York, New York, USA

Introduction

With increased age and/or hypertension, arteries lose elasticity and thicken, giving rise to a stiffened arterial wall. Arterial stiffness is a key underlying risk factor and is a hallmark of cardiovascular diseases such as atherosclerosis. Endothelial cell (EC) dysfunction, characterized by increased proliferation and inflammation is at the heart of the mechanism driving vascular diseases. The glycocalyx (GCX) is a mechanosensor that is expressed on the surface of ECs and is a key player in EC homeostasis and vascular integrity. Interestingly, in hypertensive mice the expression of GCX genes are reduced, showing a correlation between the expression of GCX and hypertension. Hypertension causes vessel wall stiffness, and whilst stiffness-mediated tension is a mechanical force that promotes EC dysfunction and vascular disease, it is not known whether the effects of stiffness are translated into functional changes through the GCX. Consistent with this, the role of the GCX in hypertension has not been studied to date. We hypothesize that hypertension-related increases in arterial stiffness reduce glycocalyx expression from ECs, leading to EC dysfunction and vascular disease.

Methods

To study the effects of arterial stiffness directly on EC biology, ECs were cultured on polyacrylamide (PA) gels that were prepared to exhibit a stiffness of 10 kPa (mimicking physiological stiffness of aged/hypertensive arteries) vs. EC cultured on softer gels, with a stiffness of 2.5 kPa (mimicking physiological stiffness of young/normotensive arteries). As a control, cells were also cultured on PA gels at 5 kPa, 100 kPa and on glass. GCX expression was assessed by screening the expression of key glycocalyx genes (encoding GCX core proteins and GCX synthesis and degradation genes) at the protein & mRNA level using qPCR, Western blotting and immunostaining. The effects of stiffness on EC function was investigated by assessing inflammation (Inflammatory molecule expression & monocyte adhesion assay), proliferation (ki67 immunostaining), Endothelial to mesenchymal transition (EndMT) (qPCR), Nitric oxide production (Phospho-eNOS expression) and permeability (transwell assay). To assess the contribution of the GCX to stiffness-mediated EC dysfunction, the GCX was removed enzymatically using Heparinase, and for a more focused approach, key GCX candidate gene expression levels were manipulated using siRNA and overexpression plasmids, followed by assessment of EC function.

Results

The expression of the GCX (Heparan sulfate (HS) side chain by immunostaining) showed a dramatic reduction on the surface of EC cultured on stiff (10kPa) vs soft gels (2.5 kPa). The expression of the GCX showed a stiffness-level dependent reduction, as revelaed by EC cultured on a range of PA gels (2.5, 5, 10,100 kPa and on glass). These results revealed that stiffness inhibits GCX expression. The gene and protein expression screen revelaed that core protein, Glypican 1 (mRNA and protein level) showed a consistent and significant reduction in expression in EC cultured on stiff vs. soft gels. Stiffness promoted EC dysfunction, as shown by enhanced inflammation, proliferation, EndMT, permeability and reduced nitric oxide signaling in EC cultured on stiff vs soft gels. Removal of the GCX using heparinase treatment, reversed the protective effects of soft gels on EC dysfunction whilst having no effect on cells cultured on stiff gels. Consistent with this, Glypican-1 gene silencing also reversed the protective effects of soft gels on EC dysfunction. Taken together, these results reveal that stiffness inhibits the GCX and that the GCX, specifically core protein Glypican1 protects EC from stiffness-mediated EC dysfuntion and potentially vascular disease. All results were obtained from at least 4-8 individual experiments (N=4-8).

Conclusions

Hypertension-induced stiffness is a major contributor of EC dysfunction and vascular disease. Here we show for the first time, that hypertension-mediated stiffness triggers EC dysfunction through inhibiting the protective glycocalyx, by suppressing the expression of GCX core protein Glypican 1. Future studies will include assessing the expression of Glypican 1 in hypertensive mice and in human patient blood, along with overexpressing Glypican 1 using AAV (Adeno-associated virus) in hypertensive mice to assess its potential as a novel hypertension and vascular disease therapeutic.

Development and Testing of An Ultrasound Compatible Cardiac Phantom For Interventional Procedure Simulation Using Direct 3d Printing

Shu Wang, Yohan Noh, Jemma Brown, Shuangyi Wang, Richard Housden, Mar Casajuana Ester, Ronak Rajani, and Kawal Rhode

Biomedical Engineering & Imaging Sciences, King's College London, London, United Kindom

Introduction

Patient specific cardiac phantoms have been widely used for clinical simulation, pre-surgery planning, and medical training. To satisfy ultrasound imaging needs, a range of soft phantom materials have been well investigated[1]. In this paper, we explore how to fabricate the ultrasound cardiac phantom using direct 3D printing and report the finale ultrasound imaging evaluation results of both phantoms.

Methods

Before printing, the cardiac model should firstly be segmented from real patient chest CT scan using ITK-Snap[2] and further processed with smoothing, hole repairing, etc. Then Lay-fomm 40 was selected for its best flexibility and lowest attenuation among all the 3D printable materials using a mornal FDM desktop printer why TangoPlus was printed using Stratsys Object500 printer. Finally, both phantoms were validated by the IE33 2D Ultrasound (US) imaging machine with an ablation catheter inserted into the right ventricle of the phantom to simulate the interventional cardiology procedure[3].

Results

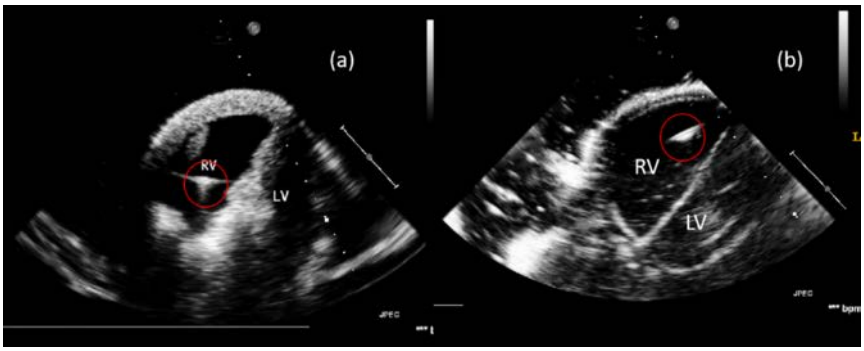

FIG.1. 2D echocardiography from TTE parasternal short axis view with a catheter inserted in the right ventricle (RV), labelled with the red circle. (a) Lay-fomm 40 phantom and (b) TangoPlus phantom

Figure 1 shows the 2D echocardiography of Lay-fomm 40 and TangoPlus cardiac phantoms from TTE (transthoracic echocardiography) parasternal short axis view respectively, the ablation catheter inside appeared as the bright spots labelled with the red circle. All the Poro-Lay series materials have significantly less attenuation compared to TangoPlus (24.0 dB/cm), while among them, Lay-fomm 40's is the smallest (6.8 dB/cm).

Conclusions

Both phantoms are demonstrated to be well ultrasound compatible, while Lay-fomm 40 can produce better ultrasound images with less artefacts and reflection on the phantom surface as well as less attenuation inside the material.

References

[1] Culjat M. O, Goldenberg D, Tewari P. Singh R S, A review of tissue substitutes for ultrasound imaging, *Ultrasound in Med. & Biol*,36: 861–873, 2010.

[2] Paul A. Yushkevich, Joseph Piven, Heather Cody Hazlett, et al, User-guided 3D active contour segmentation of anatomical structures: Significantly improved efficiency and reliability, *Neuroimage*, 31: 1116-1128, 2006.

[3] Camuglia. Anthony C, Randhawa. Varinder K, Lavi. Shahar, et al, Cardiac catheterization is associated with superior outcomes for survivors of out of hospital cardiac arrest, *Resuscitation*, 85 (11): 1533-1540, 2014.

Determinants of Peripheral Pulse Pressure and Pulse Pressure Amplification

Ye Li, Antoine Guilcher, Samuel Venin, Peter Chalton, Jordi Alastruey, Phil Chowienczyk

Department of Clinical Pharmacology, King's College London, London, UK

Introduction

Peripheral (e.g.brachial) pulse pressure (pPP) exceeds central pulse pressure (cPP) corresponding to the first (cPP1) or second (cPP2) peaks in the central waveform. This pulse pressure amplification, attributed to propagation of the pulse wave from aorta to periphery and influence of reflection in the periphery, is measured as pPP/cPP2 (when cPP2>cPP1). We examined whether the haemodynamic determinant of pPP relates more closely to cPP1 rather than cPP2.

Methods

We examined the theoretical influence of change in morphology of central aortic waveform on peripheral waveform when applying a reverse transfer function to the aortic waveform. Secondly, we examined the relationship between central and peripheral waveforms during modulation of central pressure with nitroglycerine (GTN). Central pressures were obtained during cardiac catheterisation with a Millar catheter placed in the proximal aortic root in patients with non-critical coronary artery disease (n=15) at baseline and after GTN. The digital arterial pulse was acquired simultaneously with a servo-controlled finger cuff.

Results

In theoretical analysis, pPP was sensitive only to the portion of the waveform up to the time of cPP1. Similar results were observed with GTN, which had no significant effect on cPP1 (38.7±2.0 and 37.1±2.5mmHg at baseline and after GTN respectively, P=0.36) nor on pPP (70.2±5.0 and 69.2±4.7mmHg at baseline and after GTN respectively, P=0.47) but reduced cPP2 by 17.0±1.8mmHg (P<0.001).

.

Conclusions

These results suggest that peripheral pulse pressure is determined by the early systolic portion of the central aortic pressure waveform up to the time of cPP1 and may be independent of cPP2.

Nitric Oxide Regulates Human Erythrocyte Deformability through regulating Band 3 Phosphorylation Status in Hypoxia

Yajin Zhao, Man Hou, Qinqin Yang, Xiang Wang*

Key Laboratory of Biorheological Science and Technology, Ministry of Education, College of Bioengineering, Chongqing University, Chongqing, PR China

Introduction

Hypoxia is an often seen problem in diverse conditions; systemic adaptations to hypoxia permit people to adjust to the hypoxic environment at high altitudes and to disease processes. In addition to the cardiopulmonary and hematologic adaptations that support systemic oxygen delivery in hypoxia, RBCs assist through newly described NO-based mechanisms, in line with their vital role in oxygen transport and delivery. Furthermore, to increase the local blood flow in proportion to metabolic demand, NO regulates membrane mechanical properties thereby modulating RBC deformability and oxygen carrying-releasing function. But the clear mechanisms of NO regulate RBC membrane mechanical properties remain unknown.

Methods

We have carried out a systematic study to find the mechanisms of NO regulate RBC deformability under hypoxia. NO levels, RBCs membrane elongation index (EI), band 3 and membrane bound haemachrome were determined with an NO donor (sodium nitroprusside) or an NO synthase inhibitor (l-nitro-arginine methylester) under hypoxia.

Results

Hypoxia increased NO metabolites from 25.65±1.95 μmol L−1 to 35.26±2.01 μmol L−1 compared with control. The elongation index decreased after hypoxia for 60 min from 0.567±0.019 to 0.409 ± 0.042, H+SNP group 0.59±0.031, H+L-NAME group 0.422±0.035 at a shear stress of 30 Pa. Hypoxia-stress induced band 3 clustering and tyrosine phosphorylation increased, and both decreased after hypoxia with SNP（Fig.1 and Fig.2）. The elongation index increased in the hypoxia group with SNP compared with the hypoxia group and L-NAME group after hypoxia. NO improved SHP-2 tyrosine phosphatase activity, and also inhibited the activity of Syk-induced by hypoxia stress (Fig.3).

Conclusions

In the present article, it is determined that NO plays a potential role in maintaining RBC deformability in hypoxia through altering band 3 tyrosine phosphorylation by maintaining the activity of SH-PTP2 and reducing band 3 crosslinking, which may occur during hypoxic ischaemia diseases, and at high altitudes. This study may provide insights into the molecular mechanisms of RBC adaptation to hypoxia.

Keywords: band 3; Deformability; Nitric oxide; Phosphorylation; Red blood cell

Acknowledgment

This work was supported by grants from the National Natural Science Foundation of China (No. 1010200620150034), Chinese National 863 High Tech Research and development program (No. 1010103920110136) and Chongqing University Postgraduates' Innovation Project (No.CYB15028).

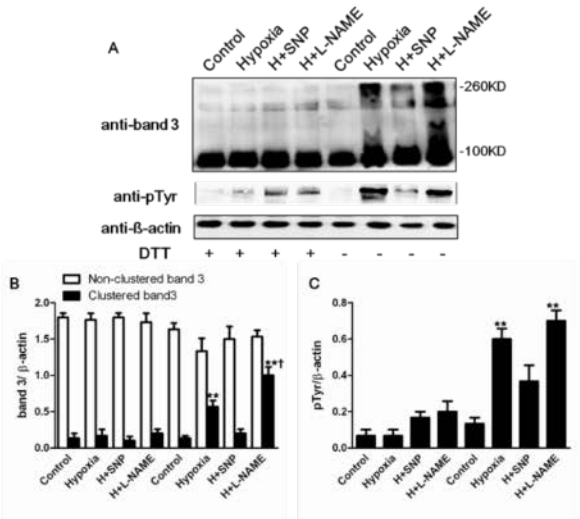

Fig.1. NO decreased the crosslinking of band 3 and the phosphorylation of tyrosine. (A) Erythrocytes were treated with 95% N_2 and 5% CO_2 for up to 120 min, and then ghosts were prepared. At the indicated times, Western blot analysis of band 3 (50 μg) per lane were probed with anti-band 3 antibodies or phosphor-tyrosine antibodies. (B) Densitometric analyses of immunoblots probed for band 3. (C) Densitometric analyses of immunoblots probed for phosphor-tyrosine. Values are means ±SEM. *P < 0.05 and **P<0.01 (n= 6 for each group).

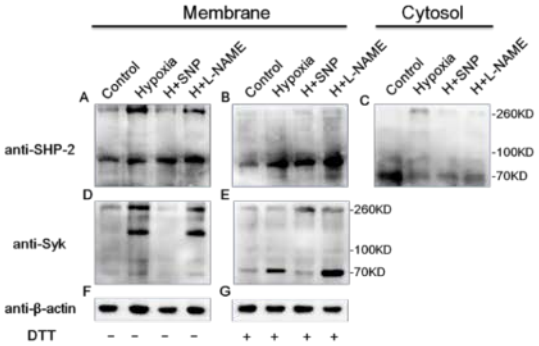

Fig.3. NO improve SHP-2 tyrosine phosphatase activity. (A) Western blot analysis of erythrocyte ghost(50 μg) per lane in each group were probed with the anti-SHP-2 antibody. NO inhibited SHP-2 crosslinking into Polymers. (B) Western blot analysis of erythrocyte ghost in each group incubated with DTT. The crosslinking of SHP-2 into polymers can be reduced by DTT. (C) Western blot analysis of cytosolic (1mg) per lane in each group. Hypoxia induced SHP-2 translocation from cytosol to membrane. (D)and (E) Western blot analysis of erythrocyte ghost in each group with or without DTT were probed with the anti-Syk antibody. NO inhibited the activity of Syk-induced by hypoxia stress.

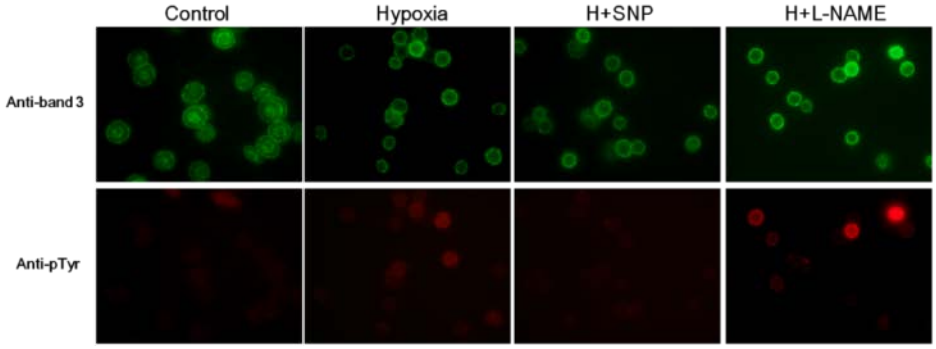

Fig.2. Immune-fluorescence of erythrocyte membrane protein band 3 clustering and phosporylation of tyrosine at hypoxia with SNP or L-NAME.

References

1. Bordin L, Brunati AM, Donella-Deana A, Baggio B, Toninello A. Band 3 is an anchor protein and a target for SHP-2 tyrosine phosphatase in human erythrocytes. BLOOD 2002,
2. Levett DZ, Fernandez BO, Riley HL, Martin DS, Mitchell K, Leckstrom CA, Ince C, et al.. The role of nitrogen oxides in human adaptation to hypoxia. Sci Rep 2011, 1: 109
3. Belanger AM, Keggi C, Kanias T, Gladwin MT, Kim-Shapiro DB. Effects of nitric oxide and its congeners on sickle red blood cell deformability. TRANSFUSION 2015, 55: 2464-2472
4. Ferru E, Giger K, Pantaleo A, Campanella E, Grey J, Ritchie K, Vono R, et al.. Regulation of membrane-cytoskeletal interactions by tyrosine phosphorylation of erythrocyte band 3. BLOOD 2011, 117: 5998-6006

Primary cilia affect the endothelial response to aneurysmal wall shear stress

Mannekomba R Diagbouga[1], Sandrine Morel[1], Beerend Hierck[2], Sylvain Lemeille[1], Brenda R Kwak[1]

[1] Department of Pathology and Immunology, University of Geneva, Switzerland

[2] Department of Anatomy and Embryology, Leiden University Medical Center, Netherlands

Introduction

Intracranial aneurysm (IA) is an arterial disease resulting in abnormal widening of the vessel lumen[1]. The pathogenesis is not completely understood; from their specific locations in the circle of Willis it is generally assumed that the initiation of IAs involves a high wall shear stress (WSS) gradient and growth of wide-neck IAs may be stimulated by low WSS[2]. Low WSS may be sensed by endothelial cells (ECs) via specialized structures called primary cilia[3]. People affected by polycystic kidney disease (PKD) have no or abnormal primary cilia and are more prone to develop IAs. Here, we test the hypothesis that defective primary cilia may alter EC behavior, which, in turn, may affect the pathogenesis of IA.

Methods

We used embryonic aortic ECs from wild-type (WT) and *Tg737*$^{orpk/orpk}$ mice, a transgenic model for PKD that lack primary cilia, and exposed them to physiological or aneurysmal levels of low WSS (30 and 2 dynes/cm^2) for 48h using a reciprocating syringe system (Ibidi). Total RNA was isolated and unbiased transcriptomic analysis was performed by RNAseq. Results were confirmed at protein level by immunofluorescent staining. Expression of ZO-1 was reduced with siRNA. Monolayers of ECs were cultured in Transwells to measure transendothelial electrical resistance and permeability for 4kDa FITC-dextran.

Results

The percentage of WT ECs with primary cilia was similar under physiological and aneurysmal flow, identifying that the WT and Tg737$^{orpk/orpk}$ ECs culture model is suited to decipher the role of primary cilia in WSS-mediated EC response. RNAseq transcriptome analysis (fold change≥3; p≤0.001) revealed 296 genes differentially expressed for *Tg737*$^{orpk/orpk}$ ECs against 58 genes in WT ECs when comparing physiological to aneurysmal flow. Further gene analysis revealed an enrichment of cell adhesion/tight junction pathways, which led us to test EC permeability. We found that monolayers of *Tg737*$^{orpk/orpk}$ ECs have a lower transendothelial resistance and higher permeability for large fluorescent molecules than WT ECs. In addition, we confirmed increased expression levels of ZO-1, ZO-2, Catenin-α1 and Claudin-3 in WT ECs. Interestingly, Catenin-α1 and Cx43 junctional location seemed perturbed in *Tg737*$^{orpk/orpk}$ ECs. Preliminary experiments with siRNA-mediated knock-down of ZO-1 in WT ECs also showed dispersion of junctional Catenin-α1 and Cx43 immunosignals.

Conclusion

The response to aneurysmal WSS in *Tg737*$^{orpk/orpk}$ ECs involved 5-to-6-fold more genes than in WT ECs, suggesting that an important role for primary cilia in ECs may be to dampen the pathological response to aneurysmal (low) WSS. Monolayers of *Tg737*$^{orpk/orpk}$ ECs display increased permeability compared to WT ECs, which may be due to a disturbed ZO-1 junctional interactome in these cells.

References

1. Diagbouga MR, Morel S, Bijlenga P, Kwak BR. Role of hemodynamics in initiation/growth of intracranial aneurysms. *Eur J Clin Invest.* 2018;48(9):e12992.
2. Meng H, Tutino VM, Xiang J, Siddiqui A. High WSS or low WSS? Complex interactions of hemodynamics with intracranial aneurysm initiation, growth, and rupture: toward a unifying hypothesis. *AJNR Am J Neuroradiol.* 2014;35(7):1254-1262.
3. Van der Heiden K, Egorova AD, Poelmann RE, Wentzel JJ, Hierck BP. Role for primary cilia as flow detectors in the cardiovascular system. *Int Rev Cell Mol Biol.* 2011;290:87-119.

A Novel Method to Predict Risk in Coronary Artery Bypass Graft Patients

Arron Peace[12] Andrew Muir[3] Robyn Lotto[1] Ian Jones[1] Dick Thijssen[2]

1: Faculty of Education, Health and Community, Liverpool John Moores University
2: Research Institute for Sport and Exercise Science, Liverpool John Moores University
3: Liverpool Heart and Chest Hospital NHS Foundation Trust

Background: Risk factors known to increase the risk of CAD also affects the endothelium. The endothelium lines arteries and is crucial in vascular homeostasis and health. Endothelial dysfunction precedes development of atherosclerosis, whilst measures of endothelial function independently predict cardiovascular disease, cardiovascular events and survival. Current methods to investigate endothelial (dys)function are invasive or prohibitively expensive. The carotid artery shares structural and function similarities to the coronary arteries and is uniquely placed to offer a unique insight into coronary artery endothelial function. Our group has shown carotid artery endothelial function correlates with coronary artery endothelial function and carotid artery response (CAR) predicts disease progression and event risk in peripheral arterial disease patients.

Method: Carotid artery endothelial function is assessed by measuring carotid artery diameter change in response to sympathetic stimulation (using the cold pressor test) using ultrasound in CABG patients pre-surgery. Patients are then followed-up for incidence of heart attack, stroke and survival. To investigate if CAR predicts risk in this high-risk population.

Results: To date 60 patients have undergone testing and surgery and recruitment is ongoing.

Conclusion and clinical relevance: Recruitment is on-going and is expected to reach ~150 patients. This may identify high-risk patients and inform clinical management.

RGD-functionalized superparamagnetic γ-Fe_2O_3 nanoparticles enhance the cell migration of osteoblasts *in vitro*

LIU Xue#, YANG Xiao-ling#, HU Qiao, LIU Mao-shi, XU Wen-feng, HUANG Qiu-hong, LIAO Xiao-ling*

Institute of Biomedical Engineering, Chongqing Engineering Laboratory of Nano/Micro Biological Medicine Detection Technology, Chongqing University of Science and Technology, Chongqing 401331, China # These authors contributed equally to this work

Abstract

Directional migration of bone-related cells to reach the defect site by superparamagnetic γ-Fe_2O_3 nanoparticles (Fe_2O_3 NPs) is a promising method of cell-based therapy for hard tissue regeneration. However, the efficiency and selectivity of cellular uptake of Fe_2O_3 NPs still needs to be improved. It is known that Arg-Gly-Asp (RGD) peptide-functionalized magnetic nanoparticles have better performance in cell differentiation control and targeted drug delivery, but it remained unclear if this method can be used to facilitate the migration process of osteoblasts in bone repair. Here we prepared RGD-modified Fe_2O_3 NPs (RGD-Fe_2O_3 NPs) using the convenient 1-Ethyl-3-(3-dimethylaminopropyl) carbodiimide hydrochloride (EDC)/N-hydroxysuccinimide (NHS) method. The obtained RGD-Fe_2O_3 NPs had a grafting ratio of 33.3-37.4% and a size of 5-6 nm with a good water dispersibility and low cytotoxicity. MC3T3-E1 osteoblast cells treated with RGD-Fe_2O_3 NPs showed a better migration response to the magnetic field than those treated with pure Fe_2O_3 NPs reflected by higher migration speed. In addition, cells treated with RGD-Fe_2O_3 NPs also showed higher Fe uptake indicated better specific cellular binding. Therefore, our results suggest that the RGD-functionalized Fe_2O_3 NPs can promote osteoblast cell migration in a magnetic field, which is potentially useful for improving hard tissue repair in the field of targeted therapy.

Keywords: Superparamagnetic iron oxide nanoparticles; RGD; Osteoblast cells; Cell migration; Bone tissue regeneration

Gender differences in the resolution of intraluminal thrombosis in a rat aneurysm model

Sandrine Morel[1,2], Agnieszka Karol[3], Vanessa Graf[3], Graziano Pelli[1], Henning Richter[4], Esther Sutter[1], Vincent Braunersreuther[1], Juhana Frösen[5], Philippe Bijlenga[2], Brenda R. Kwak[1], Katja M. Nuss[3]

[1]Department of Pathology and Immunology, Faculty of Medicine, University of Geneva, Geneva, Switzerland
[2]Department of Clinical Neurosciences, Faculty of Medicine, Geneva University Hospitals, Geneva, Switzerland
[3]Musculoskeletal Research Unit, Vetsuisse Faculty, University of Zürich, Zurich, Switzerland
[4]Diagnostic Imaging Research Unit, Vetsuisse Faculty, University of Zurich, Zurich, Switzerland
[5]Department of Neurosurgery, Kuopio University Hospital, Kuopio, Finland

Introduction

Intracranial aneurysms which are the result of an arterial wall deformation affect mostly women [1]. Two hypotheses to explain this female predominance have been proposed, i.e. hormonal effects or hemodynamic causes, but no convincing evidence supports one or the other hypothesis. In the present study, we have investigated differences and similarities in aneurysmal thrombus resolution between female, male and ovariectomised female rats over the time.

Methods

The Helsinki surgical model of side-wall aneurysm [2] was used in this study. A total of 204 female, male and ovariectomized female Wistar rats (10-12 weeks old) were used. Parental artery and aneurysm size was followed by Magnetic Resonance Imaging at implant and at 1, 2 and 4 weeks after surgery. No aneurysm rupture occurred. Aneurysmal sections were stained with Hematoxylin-Eosin, Martius Scarlet blue (for red blood cells and fibrin), Masson-Trichrome (for total collagen) and Victoria blue (for elastin) or immunolabelled with antibodies recognising α-smooth muscle actin, CD68 or CD31 using previously described protocols [3]. Twenty-six unruptured human saccular intracranial aneurysm samples were obtained during microsurgery by resecting the aneurysmal dome after clipping of the aneurysmal neck and stored in the Swiss AneuX biobank [3].

Results

In female rats, until 2 weeks after aneurysm creation, the thrombus was mainly composed of red blood cells and fibrin. Around 14 days post-surgery, macrophages and smooth muscle cells started to invade the thrombus leading to the removal of red blood cells and deposition of collagen and elastin. Similar profiles of thrombus re-organisation were observed in male and ovariectomised female rats. However, collagen content was higher in thrombi of male rats than in female rats ($46\pm6\%$ vs $23\pm2\%$, $P<0.05$), and vessel wall inflammation was higher in aneurysms of male rats. More aneurysm growth was observed in ovariectomised female rats compared with female or male rats (20%(12/31) vs 1%(-3/6) and -6%(-13/11) respectively, $P<0.05$). Thrombus coverage by endothelial cells was lower in ovariectomised female than in female or male rats (33% vs 83% and 60% respectively, $P<0.0001$). Finally, analysis of human intracranial aneurysm domes showed that endothelial cell coverage was lower in men and post-menopausal women in comparison to younger women ($P<0.0001$).

Conclusions

Aneurysm growth and intraluminal thrombus resolution show important gender-dependent differences. While certain processes (endothelial cell coverage and collagen deposition) point to a strong hormonal dependence, others (wall inflammation and aneurysm growth) seem to be influenced by both hormones and parental artery size.

References

[1] Diagbouga MR, Morel S, Bijlenga P, Kwak BR. Role of hemodynamics in initiation/growth of intracranial aneurysms. Eur J Clin Invest, 48: e12992, 2018,

[2] Marbacher S, Marjamaa J, Abdelhameed E, Hernesniemi J, Niemela M, Frosen J. The Helsinki rat microsurgical sidewall aneurysm model. J Vis Exp: e51071, 2014

[3] Morel S, Diagbouga MR, Dupuy N, Sutter E, Braunersreuther V, Pelli G, Corniola M, Gondar R, Jagersberg M, Isidor N et al. Correlating Clinical Risk Factors and Histological Features in Ruptured and Unruptured Human Intracranial Aneurysms: The Swiss AneuX Study. J Neuropathol Exp Neurol 77: 555-566, 2018

Modeling of Vascular Delivery of Targeted Nanoparticles to Detect Vulnerable Plaques

Shaolie S. Hossain, Thomas J.R. Hughes

Oden Institute for Computational Engineering and Sciences, The University of Texas at Austin, Texas, USA

Introduction

Roughly 70% of heart attacks occur due to blockages caused by rupture of vulnerable plaques. Vulnerable plaques often go undetected by standard imaging modalities such as CT, MRI and ultrasound, as they generally do not create significant narrowing of the coronary arteries unlike stable plaques. Detection and treatment of vulnerable plaques present a huge unmet clinical need. The extent and location of plaque inflammation is one of the key factors in determining plaque instability as it contributes to the loss of collagen in the fibrous cap, a precursor to cap rupture. Inflammation is also known to induce differential surface expression of specific vascular molecules, such as vascular cell adhesion molecules (VCAM-1). Blood-borne nanoparticles, conjugated with targeting components (ligands) and loaded with imaging and/or therapeutic agents, can recognize and use these molecules (receptors) as vascular docking sites, allowing us to detect activated vulnerable plaques and/or deliver site-specific acute therapy [1]. A patient's individual characteristics such as local blood flow features and disease state; as well as nanoparticle properties including size, shape and surface characteristics (e.g., ligand density, type) influence nanoparticle vascular deposition pattern, and thus, therapeutic efficacy. Mathematical models can be utilized to manipulate nanoparticle design parameters in conjunction with patient-specific attributes to maximize nanoparticle targeting efficiency.

Methods

A hexahedral NURBS (Non-uniform Rational B-splines) model for a portion of the left coronary artery tree was generated from CT imaging data using an in-house CAD-integrated vascular modeling pipeline [2]. A 3D Navier-Stokes solver coupled to the unsteady scalar advection-diffusion equation was used to describe blood flow and mass transport of nanoparticles within the authentic vasculature. A special Robyn type boundary condition coupled to a probablilty of adhesion model was implemented to account for particle adhesion the vessel wall [1]. Parallel plate flow chamber experiments were carried out to validate the model for a range of particle size and physiological wall shear stress (WSS) levels. Patient-specific blood flow simulations were performed for several cardiac cycles and near wall quantities (e.g., WSS) were quantified. Vascular inflammation was estimated as a function of local WSS employing an experimentally derived phenomenological model [1]. A cylindrical catheter was placed at the left coronary artery inlet through which spherical nanoparticles of different sizes were injected *in silico*. Vascular distribution pattern of firmly adhered particles was quantified in terms of particle surface density.

Results

Experiments showed that particle adhesion was modulated by the balance between adhesive interactions and the dislodging hydrodynamic forces, resulting in a bi-phasic relationship with respect to particle size. Inflammation-targeted nanoparticles preferentially accumulated near the plaque located in the left circumflex branch, and the larger particles (2.0 um) fared better than smaller (0.5 um) ones. The complex interplay between local WSS, surface receptor density and particle availability dictated particle adhesion pattern. As a result, nanoparticles deposition was particularly affected by vascular architecture, plaque shape and location. Realistic patient specific 3D geometry is therefore an essential ingredient in creating physiological flow and transport features necessary for developing targeted nanoparticle delivery procedures.

Conclusions

The methodology developed in this work can aid the rational design of nanoparticles to personalize, thus optimize, therapeutic intervention. This can ultimately lead to the development of a non-invasive clinical procedure for imaging and treatment of vulnerable plaques.

References

[1] Hossain SS, Hughes, TJR, Decuzzi, P., Vascular Deposition Patterns for Catheter-Injected Nanoparticles in an Inflamed Patient-specific Arterial Tree, *Biomechanics and Modeling in Mechanobiology*, 13: 585-597, 2014.

[2] Urick B, Sanders TM, Hossain SS, et al., Review of Patient-Specific Vascular Modeling: Template-Based Isogeometric Framework and the Case for CAD, *Archives of Computational Methods in Engineering*, 1-24, 2017.

Developing an indicator of rupture in abdominal aortic aneurysm using XFEM approach

Wisam Al-obaidi[1,3], Alistair Revell[1], Christopher Lowe[2], Parthasarathi Mandal[1]

[1]School of Mechanical, Aerospace and Civil Engineering, University of Manchester, Manchester, M13 9PL, UK,
[2]Institute of Cardiovascular Sciences, University of Manchester, Manchester, UK,
[3]Department of Mechanical Engineering, College of Engineering, University of Al Qadisiyah: Qadisiyah, Iraq.

Introduction

Abdominal aortic aneurysm (AAA) is a life-threatening cardio-vascular condition. Current NHS recommendation for surgical interventions to avoid potential rupture is based on the maximum diameter threshold of 5.5 cm. However, in some cases aneurysms smaller than the threshold value have been observed to rupture(1). Over the past years, two indicators to predict potential rupture, Rupture Potential Index (RPI) and Finite Element Analysis Rupture Index (FEARI), had been developed using finite element analysis (FEA), based on the predicted maximum wall stress and statistical or local wall strength. The purpose of this study is to develop a numerical model using extended finite element method (XFEM) to understand the initiation/growth of potential rupture and predict its location in abdominal aortic aneurysm wall by involving the parameters of failure: the wall stress, wall strength and strain, as well as, investigating the use of 3D-US AAA models instead of CT models.

Methods

Failure analyses were conducted on numerical models of AAA derived from 3D-US and CT images for four elected patients to examine the initiation and growth of potential rupture under three different pressures of 120, 140 and 160 mmHg and three different wall strengths of 0.33, 1.34 and 2.36 MPa respectively.

Results

The majority of AAAs showed insignificant differences in stress distributions between 3D-US and CT models, except one patient where the 3D-US model remarkably showed higher stress compared to the CT model. The location of rupture initiation was predicted reliably for both the models of AAA which have been independently verfied with visual predictions by cardio-vascular surgeons. However, the predicted length of rupture and the potential penetration (full damage of the wall) varied between the models depending upon the applied pressure and the strength of the wall.

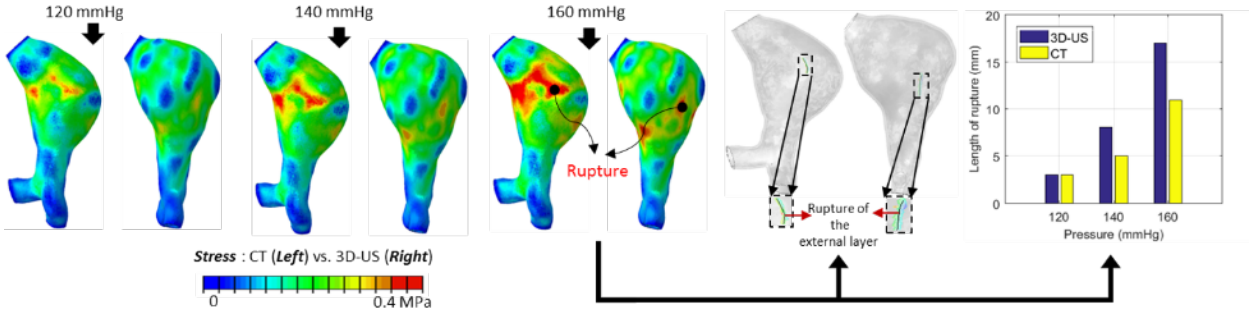

Figure (1- 1): illustrates comparisons of wall stress distribution, rupture shape and locations between 3D-US and CT models of AAA for three different pressures (wall strength: 0.33 MPa).

Conclusions

XFEM being based on the principles of fracture mechanics is shown to be also suitable for AAA rupture risk assessment. This approach provides detailed information about the rupture location, length and stress distribution. Moreover, it was found that the 3D-US models of AAA show good agreement with CT based model in predicting the rupture site; although US image-based models predict relatively higher risk of rupture.

References:

1. Nicholls SC, Gardner JB, Meissner MH, Johansen KH. Rupture in small abdominal aortic aneurysms. Journal of Vascular Surgery. 1998;28(5):884-8.

Spatially Resolved Distensibility of Healthy, Diseased, and Aneurysmal Aortic Walls Determined from Temporally Resolved 3D Ultrasound Measurements

Andreas Wittek[1], Wojciech Derwich[2], Thomas Schmitz-Rixen[2], Armin Huß[1], Christopher Blase[1]

1 Personalized Biomedical Engineering Laboratory, Frankfurt University of Applied Sciences, Frankfurt, Germany
2 Vascular and Endovascular Surgery, Goethe University Hospital, Frankfurt, Germany

Introduction

Abdominal aortic aneurysms (AAA) are a degenerative disease of the human aortic wall that may lead to weakening and eventually rupture of the wall with high mortality rates. Since the currently established criterion for surgical or endovascular treatment of the disease is imprecise in the individual case and treatment is not free of complications, the need for additional patient-individual biomarkers for short-term AAA rupture risk as basis for improved clinical decision making is widely acknowledged. Time resolved 3D ultrasound combined with speckle tracking algorithms is a novel non-invasive medical imaging technique that provides full-field displacement and strain measurements of aortic and aneurysmal wall motion [1]. This is patient-individual information that has not been used so far to assess wall strength and rupture risk. In the current study we have used 4D ultrasound strain imaging to compute the spatially resolved distensibility distribution in three patient groups: young volunteers <60 y. o. without known cardiovascular diseases, aged arteriosclerotic patients >60 y. o. without AAA, and AAA patients. We have correlated the observed changes in the distribution of local elastic properties with the aortic diamater within each group.

Methods

Local distensibilities were determined for wall areas of 2 - 10 mm² based on local circumferential strains and pulse pressure. Mean and maximum distensibilities as well as indices for the local variations of the distensibility distribution (local distensibility ratio, heterogeneity index) have been determined.

Results

Mean distensibility is significantly decreasing from young (3.83 [2.82, 5.87] 10^{-3} $mmHg^{-1}$) to elderly (0.67 [0.39, 0.87] 10^{-3} $mmHg^{-1}$) and AAA (0.27 [0.20, 0.54] 10^{-3} $mmHg^{-1}$). Mean and maximum distensibility are inversely correlated and the heterogeneity of the elastic properties is correlated positively with the aortic diameter in the young group. In contrast, no correlation between any distensibility distribution index with diameter is observed in the aged or diseased group. Both indices characterising the heterogeneous elastic properties are significantly increasing from young through elderly to AAA.

Conclusions

The size and distribution of local distensibilities provides information on the mechanical properties of the aortic and aneurysmal wall. Since it depends on geometrical information (local diameter), local distensibility is not a ‘proper’ material parameter. However, in the case of aged and pathologic aortic walls this dependency is neglibible compared to the changes in the aortic stiffness. We propose that the heterogeneous distribution is indicative of microstructural changes in the aortic wall. Therefore, the variable distribution of distensibilities might be a candidate biomarker to classify aneurysms with respect to their rupture risk. Since it is not correlated with the maximum aneurysm diameter, it could provide additional individual information to the established criterion for treatment.

References

[1] Karatolios K, Wittek A, Nwe TH, Bihari P, Shelke A, Josef D, Schmitz-Rixen T, Geks J, Maisch B, Blase C, Moosdorf R, Vogt S, Method for Aortic Wall Strain Measurement With Three-Dimensional Ultrasound Speckle Tracking and Fitted Finite Element Analysis, *Annals of Thoracic Surgery,* 96(5):1664–71, 2013.

Quantifying orientation of endothelial cells under uniaxial and multidirectional flow by swirling normal and modified cell culture plates with and without raised viscosity of the medium

Mehwish Arshad[1,2], Mean Ghim[1], Spencer J. Sherwin[2] and Peter D. Weinberg[1]

Departments of [1]Biomedical Engineering and [2]Aeronautics Imperial College London, London, UK

Introduction

The non-uniform distribution of atherosclerosis within the arterial tree has been attributed to low wall shear stress (WSS) and to highly multidirectional flow, amongst other mechanical factors (reviewed in [1]). Effects of shear on cultured endothelial cells are being investigated by swirling the culture dishes on an orbital shaker. Computational fluid dynamics can be used to simulate flows in the wells and the extracted WSS metrics are compared to cell properties [2]. It is widely assumed that cells have no net alignment under multidirectional flow whereas under uniaxial flow they elongate and align to the mean WSS direction [1]. To further test this, we adapted the geometry of a 12-well and the viscosity of the medium to disrupt WSS patterns, and investigated whether the cells did align to the mean WSS direction.

Methods

The geometry of the 12-well model was varied by suspending PDMS cylinders of radius 8mm from the culture plate lid, leaving a 2 mm gap from the base of the well. The viscosity of the medium was varied by adding 3% dextran and measured using a glass capillary viscometer. Human aortic endothelial cells were seeded in all the adapted wells and the plates were either swirled or kept stationary (control) for 4 days under 95% air/5% CO_2 at 37°C. Cells were then fixed, their nuclei stained with DRAQ5, and imaged en face using a confocal microscope. Post-processing in MATLAB was performed to extract nuclear properties. Flow in the adapted wells was simulated using the volume of fluid method in STAR-CCM+ (CD-Adapco). WSS metrics were extracted and plotted across the radius of the well.

Results

Adding 3% dextran to the cell culture medium increased the viscosity from 0.7 mPa.s to 3.1 mPa.s and increased the average WSS magnitude by 0.26Pa; this made the cells align so as to reduce flow across their long axis, rather than with the mean WSS direction. Adding a suspended cylinder flattened the wave and produced purely multidirectional flow over most of the well; the further addition of 3% dextran to the fluid increased the average WSS magnitude by 0.14Pa. Cells had no net alignment with the suspended cylinders, as in all static cases.

Conclusions

Under static conditions or purely multidirectional flow, there was no alignment of endothelial cells at normal or increased viscosity, as expected. However, when viscosity was increased in swirled conventional wells, the orientation moved away from that of the mean WSS direction and towards that which minimised transverse WSS. This result suggests that transverse WSS is deleterious to endothelial cells and, when it has a sufficiently high value, they attempt to reduce it. *(This study was funded by the BHF).*

References

[1] Levesque MJ, Nerem RM.. J Biomech Eng 1985;107:341–347
[2] Ghim, M. et al.. Am J Physiol 2017;313:H959–H973.

A Comparison Between Invasive and Non-invasive Wave Intensity Analysis Using 1D Computational Modelling of Arterial Haemodynamics

Ryan Reavette[1], Mengxing Tang[1], Spencer Sherwin[2], Peter Weinberg[1]

[1]Department of Bioengineering, Imperial College London
[2]Department of Aeronautics, Imperial College London

Introduction

Information propagates away from the heart the form of pulse waves; these travel through the vascular system and are reflected back towards the heart at bifurcations, other changes in arterial geometry and changes in material properties, including at distal resistance vessels. They carry information about pressure and velocity changes from the heart. Wave Intensity (WI) has been defined as the product of these changes in blood velocity and pressure occurring over a small sampling interval [1]:

$$dI = dU\,dP.$$

It has the useful property that it is positive when forward travelling wavefronts are dominant, and negative when backward travelling wavefronts are dominant. If wave speed is known, then we may additionally separate the waves into their forward and backward travelling components. WI is a clinically relevant parameter; for example, it provides information about the contraction and relaxation of the heart. Its clinical utility is restricted, however, as pressure may only be accurately measured with adequate temporal resolution through invasive catheterisation; non-invasive estimates tend to be inaccurate. This restriction is obviated through employing a non-invasive formulation of WI based on the product of blood velocity and arterial diameter [2]:

$$_{n}dI = dU\,dD,$$

In our implementation, both quantities are measured from the same B-mode ultrasound images. While blood pressure and arterial diameter are intrinsically related, the relationship between the two in the physiological range is non-linear: the arterial wall has a complex structure and exhibits properties such as viscoelasticity and strain-stiffening. Here, we show that these non-linearities do not have a significant impact on the key quantities which may be derived from the different WIs.

Methods

Using 1D reduced modelling of the arterial tree, we may simulate arterial haemodynamics to good accuracy with reasonable computational complexity. Simulations of a 55 artery model of the human arterial tree, which incorporated a non-linear relationship between pressure and diameter, were conducted using Nektar++ - an open-source framework based on *hp*/spectral element methods. Both WIs were calculated for the mid-points of the thoracic aorta, and the common carotid, brachial, and radial arteries; the latter three were chosen as they are easily accessible to ultrasound. The WIs were then separated into their forward and backward travelling components, from which we calculated ratios of wave heights, reflection coefficients for reflected waves, the timing of the different peaks and the relative differences in peak heights.

Results

While magnitudes of each WI differed as expected, there were no significant differences between the ratios and the other quantities derived for either WI formulation.

Conclusions

The non-invasive formulation of WI has been shown to accurately mimic the key behaviour of the established invasive WI. Thus, non-invasive WI may be integrated into the clinic for routine use in assessing cardiac function and dysfunction.

Acknowledgements

The authors gratefully acknowledge advice from Professor Kim Parker[1] and funding from the EPSRC.

References

[1] Parker, K. *An introduction to wave intensity analysis*. Med Biol Eng Comput (2009) 47:175-188.
[2] Feng, J; Khir, A.W. *Determination of wave speed and wave separation in the arteries using diameter and velocity.* Journal of Biomechanics (2010) 43:455-462.

A systematic investigation into the measurement of skin microcirculation in the foot

Gayathri Balasubramanian, Nachiappan Chockalingam, Roozbeh Naemi

Centre for Biomechanics and Rehabilitation Technologies, Staffordshire University, UK

Introduction

The role of microcirculatory dysfunction has been implicated in the development of foot complications such as peripheral arterial diseases, diabetic foot complications, impaired tissue response to injury or trauma, and poor wound healing. Moreover, an association between the presence of peripheral sensory neuropathy and altered microvascular reactivity in the lower limb has been established in people with diabetes.[1] One of the measures to assess microcirculatory function is reactive hyperaemia which is an indicator of the intrinsic ability of an organ or tissue to locally autoregulate its blood supply. Post Occlusive Reactive Hyperaemia (PORH) has been used to assess the microvascular function with/without the temperature control, while occlusion time for PORH based on previous studies ranged from 3 to 10 minutes.[2–5] However, with an increase in the occlusion time there will be an increase in pain at the site and risk of complications, especially in people with diabetic foot disease. Despite this, there is no standard protocol to test PORH.[3,6,7] The aim of this study is to investigate the effect of systematically controlled changes in temperature and occlusion time on PORH measurements.

Methods

12 healthy adults age range 18 to 50 years took part in this study after obtaining ethical approval. The participants laid in supine position and testing commenced following 15 minutes acclimatisation to room temperature. PORH was measured using Perimed PeriFlux system with the probes placed at the distal/plantar aspect of the hallux. The occlusion was at the ankle and hallux levels (one followed by other), while the cuffs were inflated to a suprasystolic pressure (200 mmHg). The occlusion times were 10, 30, and 60 seconds. Additionally, the same set of tests were performed with and without temperature control at 33°C at the probe site. For each participant, the PORH was measured in 12 different conditions (3 occlusion times with/without temperature control).

Results

The initial data analysis indicated the role of temperature and occlusion time on the hyperaemic response namely: maximum hyperaemic response, hyperaemic repayment, time to recovery and time to peak.

Conclusions

In developing protocols for reliable measurements of PORH, it is vital that the variation in temperature and occlusion time should be taken into account.

References

[1]. Barwick AL, Tessier JW, Janse de Jonge X, Ivers JR, Chuter VH. Peripheral sensory neuropathy is associated with altered postocclusive reactive hyperemia in the diabetic foot. *BMJ Open Diabetes Res Care*. 2016;4(1):e000235-e000235. doi:10.1136/bmjdrc-2016-000235

[2]. Lanting SM, Barwick AL, Twigg SM, et al. Post-occlusive reactive hyperaemia of skin microvasculature and foot complications in type 2 diabetes. *J Diabetes Complications*. 2017;31(8):1305-1310. doi:10.1016/j.jdiacomp.2017.05.005

[3]. Morales F, Graaff R, Smit AJ, et al. How to assess post-occlusive reactive hyperaemia by means of laser Doppler perfusion monitoring: Application of a standardised protocol to patients with peripheral arterial obstructive disease. *Microvasc Res*. 2005;69(1-2):17-23. doi:10.1016/j.mvr.2005.01.006

[4]. de Mul FFMM, Morales F, Smit AJ, Graaff R. A model for post-occlusive reactive hyperemia as measured with laser-Doppler perfusion monitoring. *IEEE Trans Biomed Eng*. 2005;52(2):184-190. doi:10.1109/TBME.2004.840507

[5]. Clough G, Chipperfield A, Byrne C, de Mul F, Gush R. Evaluation of a new high power, wide separation laser Doppler probe: potential measurement of deeper tissue blood flow. *Microvasc Res*. 2009;78(2):155-161. doi:10.1016/j.mvr.2009.05.003

[6]. Babos L, Járai Z, Nemcsik J. Evaluation of microvascular reactivity with laser Doppler flowmetry in chronic kidney disease. *World J Nephrol*. 2013;2(3):77-83. doi:10.5527/wjn.v2.i3.77

[7]. Lanting SM, Johnson NA, Baker MK, Caterson ID, Chuter VH. The effect of exercise training on cutaneous microvascular reactivity: A systematic review and meta-analysis. *J Sci Med Sport*. 2017;20(2):170-177. doi:10.1016/j.jsams.2016.04.002

Suppression of endothelial activation depends on the type and duration of applied shear stress in vitro

Kuin Tian Pang[1,2], Mean Ghim[1], Xiaomeng Wang[2,3,4,5,] Peter D. Weinberg[1]

[1]Department of Bioengineering, Imperial College London, UK.
[2]Institute of Molecular and Cell Biology, Agency for Science, Technology and Research (A*STAR), Singapore.
[3]Lee Kong Chian School of Medicine, Nanyang Technological University, Singapore.
[4]Department of Cell Biology, Institute of Ophthalmology, University College London, UK.
[5]Singapore Eye Research Institute, Singapore.

Introduction

Endothelial cells (EC) sense the shear stress generated by the flow of blood over them and respond by altering their stiffness, morphology, and junctions with neighboring cells. A swirling well system has gained increasing attention in the study of the effect of shear stress on EC because it can induce complex flow with spatial variation in flow characteristics [1]. However, the effect of the duration of such shear stresses on endothelial activation is still poorly characterised. This study aims to investigate the role of prolonged shear stress on endothelial activation using the orbital shaker.

Methods

Flow in a swirling 6-well plate was simulated in STARCCM+ and post-processed using MATLAB, to produce maps of shear stress. Human Umbilical Vein Endothelial Cells (HUVEC) were grown in a specific region of the well by coating the region with fibronectin and passivating the remainder with Pluronic F-127. HUVEC were scaped off for Western Blot analysis after 15min, 6h, and 1, 3, and 4 days on the orbital shaker to study the effect of shear stress duration on VCAM-1, ICAM-1, Ikbα, and eNOS expression. Calcein-AM-labelled THP-1 monocytes were incubated under static condition for 1h with previously-sheared HUVEC, prior to fixation and immunofluorescence imaging. On a separate plate, HUVEC were fixed and stained with DRAQ5 to quantify the number of cells in the different regions.

Results

The centre of the swirling 6-well plate experienced Low Magnitude Multidirectional Flow (LMMF) whereas the edge experienced High Magnitude Uniaxial Flow (HMUF). VCAM-1 was suppressed in HUVEC exposed to HMUF for 1, 3, and 4 days, as compared to LMMF. Longer exposure to HMUF resulted in greater suppression. ICAM-1 and IkBα were significantly suppressed at 3 days and 1 day, respectively. eNOS was activated in HUVEC exposed to HMUF for 3 days, as compared to LMMF. Both untreated and TNF-α-treated HUVEC exposed to HMUF for 3 days and 7 days had lower monocyte adhesion, compared to HUVEC exposed to LMMF, the effect being larger at 7 days.

Conclusions

A swirling well system allows shear stress to be applied chronically for up to 7 days. This study has demonstrated that endothelial activation in response to shear stress is time-dependent, and prolonged exposure to HMUF suppressed endothelial activation. (Funded by BHF and A*STAR)

References

[1] Ghim, M., Pang, K.T., Arshad, M., Wang, X., & Weinberg, P.D. A novel method for segmenting growth of cells in sheared endothelial culture reveals the secretion of an anti-inflammatory mediator. *Journal of biological engineering*, 12:15, 2018.

Can turbulent-like flow cause high frequency vibrations of intracranial aneurysm walls?

Alban Souche, Kristian Valen-Sendstad

Department of Computational Physiology, Simula Research Laboratory, Lysaker, Norway

Introduction

Acoustic signals at relatively high frequencies (several hundreds of Hz) have been measured at exposed aneurysm sacs during open head surgery [1], and also later non-invasively [2], providing correlations between bruits and aneurysms. More recently, in-silico and in-vitro studies found turbulent-like flows within intracranial vasculature, with similar characteristic flow phenotypes, and fluctuations at the order of 100-300 Hz ([3, 4]). However, the link between turbulent-like blood flow and high-frequency aneurysmal wall vibrations has not been addressed and is the focus of the present work.

Methods

A physiologically plausible sidewall aneurysm model located at the C6 segment of the internal carotid artery, previously shown to harbour a turbulent-like flow, was meshed with a resolution shown to adequately resolve the major features. A fully coupled and monolithic 2nd order accurate fluid-structure interaction (FSI) solver was used; taking 2k time steps per second. We applied a steady state inflow of 6.7ml/s corresponding to peak systolic flow rates, and solved the full transient 3D Navier-Stokes equations. The arterial segments were assumed rigid while the aneurysm sac was modelled as a hyperelastic material.

Results

Fig. 1 (left panel) shows the aneurysm wall deformation at t=0.13s, as indicated by the surface vectors. The right panel shows the temporal evolution of the displacement magnitude from a collection of points located at the top of the aneurysm and illustrates the pseudorandom mechanical response of the aneurysm sac to the turbulent-like flow.

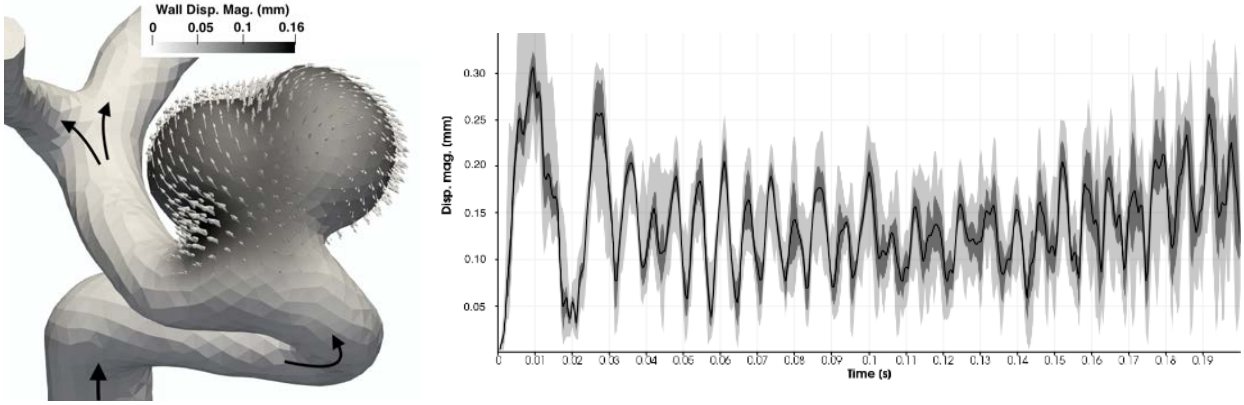

Fig. 1: Left: Wall displacement magnitude at 0.13 s. Right: Temporal evolution of the displacement magnitude of a collection of points located on the top of the aneurysm sac.

Conclusions

These preliminary results demonstrate a proof-of-concept between turbulent-like hemodynamics and high-frequency aneurysm wall vibrations, with amplitudes approaching the thickness of the aneurysm wall thickness. Consequently, the wall (shear) stresses might be more complex than previously thought or even described, and could potentially affect mechanotransduction and vascular remodelling [5]. That being said, there are as many limitations as there are novel results; most notably disregarding the perianeurysmal environment and constant flow rate. The former might dampen wall vibrations while the latter is just a pragmatic way of identifying flow instabilities. Nevertheless, there are still no clinical observations, laboratory experiments, or numerical results in conflict with the current observations.

References

[1] Ferguson, *J.Neurosurg*, 1970; [2] Kurokawa et al., *Stroke*, 1994; [3] Valen-sendstad et al., *Biomech*, 2014; [4] Balasso et al., *BiomedEng*, 2018; [5] Chien, *Am J Physiol Heart Circ Physiol*, 2007

Should aortic dilated bicuspid aortic valve patients be treated like other aneurysms?

Ya Hua Chim[1], Hannah Davies[2], Mark Field[3], Jill Madine[2], Riaz Akhtar[1]

[1] Department of Biomedical Engineering, University of Liverpool, Liverpool, UK
[2] Divison of Integrated Biology, University of Liverpool, Liverpool, UK
[3] Liverpool Heart and Chest Hospital, Liverpool, UK

Introduction

Patient with biscusid aortic valve (BAV) are known to get dilations at the root and/ or the ascending aorta due to the structural weakening of the wall [1]. Therefore early elective surgeries are performed to repair the aorta on these patients, to limit the likihood of a dissection and/ or rupture to occur. Elastin microstructure is an important factor in aortic aneurysms [2]. However, it is unclear whether elastin microstructure varies in different ascending aneurysm aetiologies, thus explaining the need for early interventions on BAV patients. Here, we measured the micromechanical properties, biochemical properties and the elastin microstructural properties within the aortic tissue of two specific aneurysmal groups; bicuspid aortic valve with associated aneurysm (BAV-A) and idiopathic degenerative aneurysm (DA). Aneurysmal tissues were also compared against non-aneurysmal tissues.

Methods

Aortic biopsies were taken from 39 patients (mean age=62.8±11.8 years) undergoing either coronary by-pass graft (CABG), BAV-A or DA aneurysmal repair. Dynamic nanoindentation with 100µm flat probe was applied to the medial layer, as reported previously [3]. The same tissues were enzymatically or chemically digested and measured for collagen using hydroxyproline, for elastin using fastin elastin kit, and for glycosaminoglycan (GAG) levels using 1-9 dimethylmethylene blue. To analyse the elastin microstructure, all the tissues were formalin fixed and paraffin embedded, then stained for elastin using Verhoeff Van Gieson. The entire tissue cross-section (n=4 for each patient) was portioned into 10 sections, and was quantified for elastin content, number of elastin segments and their lengths.

Results

The elastic modulus of CABG tissues were found to be significantly lower ($p=0.005$) than BAV-A tissues. However, from the biochemical data, only collagen levels from DA appeared to have significantly elevated compared to CABG tissues. BAV-A tissues were found to be significantly ($p=0.048$) stiffer than DA tissues, while their biochemical levels were the same. CABG and BAV-A tissues had significantly more elastin content for majority of the sections ($p<0.02$) relative to DA tissues. DA tissues had low number of segments, and each segment was shorter in comparison to CABG and BAV-A tissues. Although CABG and BAV-A tissues had similar elastin content for majority of the cross-section, from the outer media to adventitia, both BAV-A and DA tissues had a significant reduction in content ($p<0.04$). Also, it was noted that there were more elastin segments in BAV-A tissues in comparison to CABG tissues.

Conclusions

The elastin microstructure for both aneurysm groups differ enormously. Our data show that BAV-A tissues are more structurally intact than DA tissues. As current patients with DA have surgical interventions later than patients with BAV-A, we have shown that proposed early surgical interventions may not be required for patients with BAV-A.

References

[1] Nardi P, Ruvolo G, Current indications to surgical repair of the aneurysms of ascending aorta, *J.Vasc. Endovasc. Surg.*, 1, 2016.

[2]Tsamis A, Krawiec JT, Vorp DA, Elastin and collagen fibre microstructure of the human aorta in ageing and disease: a review, *J R Soc. Interface*, 10: 20121004, 2013.

[3] Peters AE, Comerford EJ, Macaulay S, Bates KT, Akhtar R, Micromechanical properties of canine femoral articular cartilage following multiple freeze-thaw cycles, *J Mech Behav Biomed Mater*, 71: 114-121, 2017.

Imaging of blood flow dynamics using engineered point-spread functions

Yongzhuang Zhou, Vytautas Zickus, Jonathan M. Taylor, Andrew R. Harvey

School of Physics and Astronomy, University of Glasgow, Glasgow, UK

Introduction

Imaging of blood flow dynamics in living organisms is crucial for understanding the development and function of cardiovascular systems [1], the challenge remains in high-speed imaging of large volumes with high resolution. We utilized engineered point-spread functions (PSFs, i.e. the image of a point source) to track fluorescent beads that are injected to 3 days post-fertilization (dpf) zebrafish. The spatial trajectories of the tracer beads within flowing blood were recorded during transit through both cardinal and intersegmental vessels. Sub-100nm precision can be achieved through the whole thickness of the zebrafish which provides the potential for real-time assessment of wall shear stress in three dimensions.

In this abstract, we first describe briefly encoding 3D tracer locations using Airy-beam-based PSFs, then we show our results of *in vivo* blood flow tracking within a 3dpf zebrafish.

Methods

Pupil engineering is widely used to alter the 'shape' of the PSF for encoding the 3D coordinates of emitters in single-molecule microscopy. For example, by placing a cubic phase mask at the Fourier plane of the microscope, we get the Airy-beam PSF which yields the following desired properties: (1) it translates as the defocus changes, encoding the emitter's 3D coordinates in a 2D image as shown in Fig. 1. (2) it maintains good signal-to-noise ratio at large defocus, enabling imaging through thick biological samples such as the zebrafish[2]. We also utilized other Airy-beam-based PSFs for this purpose [3].

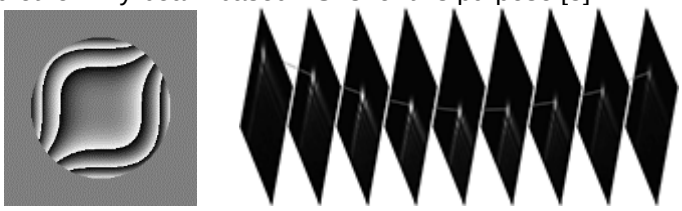

Figure 1. Cubic phase mask and depth-dependent translation of the Airy-beam PSF.

Results

One-micron fluorescent tracer beads are injected in the common cardinal vein of a 3dpf zebrafish and the injected tracers can be tracked at video-rate limited only by the camera performance. In our experiment, we imaged at 50 frames per second. Each tracer's 3D coordinates and thus their trajectories can be deduced. As shown in Fig. 2, the 3D structure of both the cardinal vessels and the intersegmental vessels can be clearly observed.

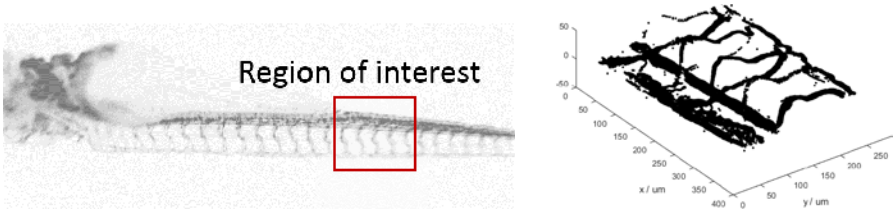

Figure 2. Blood flow tracking in a 3dpf zebrafish.

Conclusions

We conclude that the engineered PSFs have potential for precise measurement of blood flow dynamics at video rate over extended volumes, we demonstrate especially the Airy-beam-based techniques. This method provides sufficient spatial and temporal resolution for the measurement of 3D blood flow and has the potential for directly probing biomechanical quantities such as wall shear stress, as well as exploring the fluidic repercussions of cardiovascular diseases.

References

[1] Hove JR, Köster RW, Forouhar AS, Acevedo-Bolton G, Fraser SE, Gharib M, "Intracardiac fluid forces are an essential epigenetic factor for embryonic cardiogenesis," *Nature* 421, 172–177 (2003)

[2] Zhou Y, Zickus V, Zammit P, Taylor JM, Harvey AR, "High-speed extended-volume blood flow measurement using engineered point-spread function," Biomed. Opt. Express 9, 6444-6454 (2018)

[3] Zhou Y, Zickus V, Harvey AR, Pammit P, "Double-Cubic Point Spread Function for 3D Extended-Depth Localization Microscopy," in Imaging and Applied Optics 2018, OSA Technical Digest, paper CM3E.4.

Distal Pressure Measurement Location and Its Impact on Virtual Fractional Flow Reserve

Eric KW Poon[1], Shuang J Zhu[1], Andrew SH Ooi[1], Peter Barlis[2,3,4]

[1] Department of Mechanical Engineering, The University of Melbourne, Parkville, Australia; [2] Department of Medicine and Radiology, Faculty of Medicine, Dentistry and Health Sciences, The University of Melbourne, Parkville, Australia; [3] Department of Cardiology, Northern Hospital, Epping, Australia; [4] St Vicent's Heart Centre, Fitzroy, Australia;

Introduction

Fractional flow reserve, which measures the ratio of distal coronary pressure (Pd) to aortic pressure (Pa), is an invasive procedure that demonstrates high accuracy, sensitivity and specificity in assessing the physiological importance coronary lesions. Virtual fractional flow reserve (vFFR), which can be derived from either non-invasive [1] or invasive imaging data [2], represents the cutting edge of clinical research utilising computational fluid dynamics (CFD). Despite recent advancements in vFFR methodologies, the complexity of human coronary system presents a challenge for CFD modelling. In particular, the location of the distal pressure measurement (Pd) on the calculated vFFR remains unclear.

Methods

A patient-specific coronary arterial model with a 50% diameter stenosis was reconstructed from two angiographic projections >35° apart. Pulsatile blood flow through the coronary artery model was numerically simulated by directly solving the incompressible Navier–Stokes equations [3]. Hyperaemic flow based on the coronary artery diameter was simulated to mimic the effect of induced adenosine during invasive FFR measurement.

Results

The existence of flow recirculation has a major effect on the local haemodynamics. To elucidate the effect of flow reversal on the local blood pressure, we employed the λ_2 vortex identification method [4]. The λ_2 vortex identification method identifies regions of local pressure minimum. The variations in λ_2 distal to the coronary lesion are presented over multiple cross-sectional slices (Panel A). Panels B and C show the location and size of the vortex core (eye of the vortex) and the variation in blood pressure, respectively, at a selected cross-section. The vortex cores (identified by the bright red λ_2 contours) are pushed away from the bottom left of the figure. As a result, there is a substantially difference in blood pressure (>5 mmHg) across the bottom left of the cross-section and other regions.

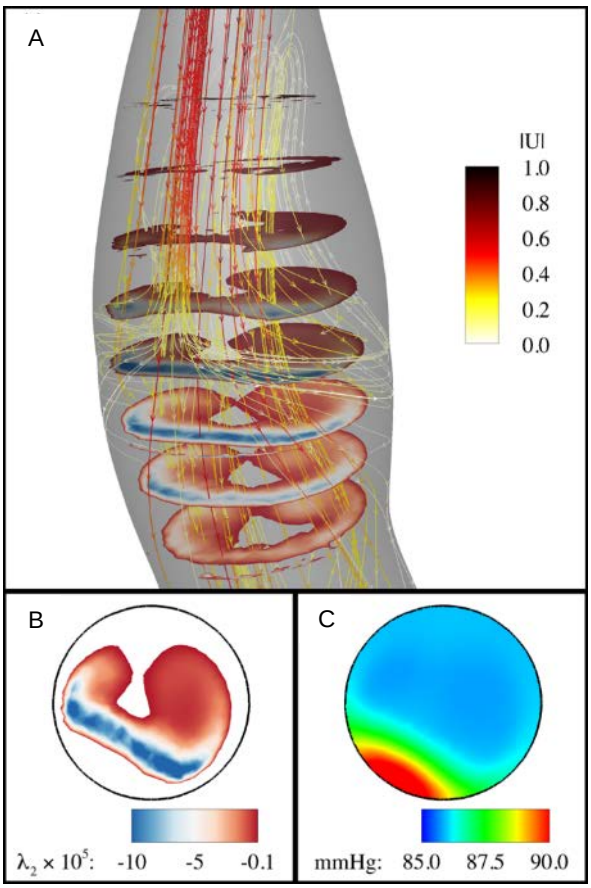

Conclusions

The existence of distal flow reversal significantly impacts the pressure difference (>5 mmHg) laterally. Distal pressure measurement should be performed away from the narrowing, guided by λ_2, to avoid flow reversal affecting the calculated vFFR.

References

[1] Min JK, Berman DS, et al., Rationale and design of the DeFACTO (Determination of Fractional Flow Reserve by Anatomic Computed Tomographic AngiOgraphy) study, *J Cardiovasc Comput Tomogr*, 5: 301–309, 2011.

[2] Poon EKW, Thondapu V, et al., Coronary optical coherence tomography-derived virtual fractional flow reserve (FFR): Anatomy and physiology all-in-one. *Eur Heart J*, 38(48): 3604-3605, 2017.

[3] Poon EKW, Thondapu V, et al., Elevated blood viscosity and micro-recirculation resulting from coronary stent malapposition, *J Biomech Eng*, 140: 051006-1, 2018.

[4] Jeong J, Hussain F, On the identification of a vortex, *J Fluid Mech*, 285: 69–94, 1995.

The mechanical properties of the ovine aorta at the macro- and micro- scale correlation with regional variations in collagen, elastin and glycosominoglycan levels

Phakakorn Panpho[1,4], Mark Field[2], Jillian Madine[3], Riaz Akhtar[1]

[1]Department of Mechanical, School of Engineering, University of Liverpool, U.K.
[2]Department of Cardiac Surgery, Liverpool Heart and Chest Hospital, Liverpool, U.K.
[3]Institute of Integrative Biology, University of Liverpool, Biosciences Building, Liverpool, U.K.
[4]Faculty of Science and technology, Pibulsongkram Rajabhat University, Phitsanulok, Thailand

Introduction

Aortic diseases are a significant cardiovascular health problem and occurs in different ways across the vascular tree. Investigation of the mechanical properties of the aorta is important for better understanding of aortic diseases. While there have been previous studies examining the alterations in the macroscopic biomechanical behaviour and how they correlate well with regional microstructural changes, little is known about how these properties vary across its entire length [1,2]. Our study presents maps the biomechanical properties (at the macro-scale via tensile testing and micro- scale via oscillatory nanoindentation and biochemical properties (Collagen, Elastin and GAG) along its entire length of the ovine aorta.

Methods

Three ovine aortas were used for nanoindentation testing and three for uniaxial tensile testing. For nanoindentation, the entire aorta was split into nine transverse sections. The aorta was divided into sections separated by 2 cm in length from the aortic root to the celiac artery region. Each of these sections were used to create three 5-millimeter circle biopsy punches for nanoindentation (a total of 81 biopsies). For uniaxial testing, a total of 27 strips of aortic specimens were collected from three animals with three strips for each of the following regions: ascending, upper thoracic, upper abdominal aorta. Each strip had a testing length of 4x12 mm after clamping. Subsequently, the same samples were used to determine elastin, collagen and glycosaminoglycan (GAG) levels using established biochemical assays.

Results

Overall, our study found that although the testing approach and loading orientation and rates differed with the two methods, reasonable agreement was found that the elastic modulus via tensile and nanoindentation increased with increasing distance from heart. The elastic modulus determined from nanoindentation testing was in the range of 0.04-0.12 MPa and from uniaxial tensile testing at physiological elastic modulus about 0.08-0.20 MPa. One interesting finding in our study is that there was a significant correlation between an increase in G' ($P<0.0001$) and collagen ($P=0.001$) with distance from the aortic root whilst elastin ($P=0.001$) and GAG ($P=0.01$) levels were significantly decreased. Our results seem to be consistent with with previous studies [2, 3], which also showed that the mechanical properties of the aortic tissue increased from proximal to distal locations of the aorta. The collagen GAG and elastin distribution in the proximal and distal regions is also agreeable with those of previous studies [2,4].

Conclusions

In conclusion, there is a significant increase in macroscopic and micromechanical properties from the ascending aorta to the abdominal aorta. It implys that the biomechnical changes were correlated with increased collagen, decreased elastin and GAGs as the distance from the heart increases. The findings of this study shows the relationship between the mechanical and biochemical properties across the entire aorta. The findings can aid the development of a better understanding of the mechanisms of aneurysm and dissection development in different regions of the aorta.

References

[1] Haskett, Darren, et al. *Biomechanics and modeling in mechanobiology* 9.6 (2010): 725-736.
[2] Sokolis, DIMITRIOS P., Harisios Boudoulas, and Panayotis E. Karayannacos. *Hellenic J Cardiol* 49.3 (2008): 145-54.
[3] Kermani, Golriz, et al. *Journal of the mechanical behavior of biomedical materials* 69 (2017): 50-56.
[4] Harkness, Margaret LR, R. D. Harkness, and D. A. McDonald. *Proc. R. Soc. Lond. B* 146.925 (1957): 541-551.

FSI modeling of an atherosclerotic murine carotid artery instrumented with a blood flow-modifying cuff!

Miten B. Patel[1], Fotios Savvopoulos[1], Ranil de Silva[1,4], Ryan M. Pedrigi[2], Rob Krams[3]

[1]National Heart & Lung Institute, Imperial College London, London, UK; [2]Mechanical and Materials Engineering, University of Nebraska-Lincoln, Lincoln, USA; [3]School of Engineering and Materials Science, Queen Mary University of London, London, UK; [4]Harefield NHS Foundation Trust, London, UK

Introduction

Rupture of an advanced atherosclerotic plaque is the most common cause of a heart attack, which is a leading cause of death globally. Atherosclerotic plaques form in regions of the vasculature that experience disturbed blood flow [1]. We previously showed that imposing disturbed flow in the carotid arteries of hypercholesterolemic mice caused the development of advanced plaques [1]. Quantification of the disturbed biomechanical environment, both fluid and solid, is needed to identify the specific biomechanical signatures that promote advanced plaque formation in this animal model.

Methods

One female ApoE-/- mouse was placed on a high-fat diet and instrumented with a blood flow-modifying cuff around the left carotid artery. Nine weeks after cuff placement, the mouse was scanned with micro-CT to obtain a 3-D reconstruction of each carotid artery in vivo. These geometries were used to create FSI models by adding an outlet boundary extension to each that simulated the resistance and compliance of the downstream vasculature [2]. Simulations were performed using Abaqus v6.14. The vessel wall was modeled as a hyperelastic solid (Ogden) and the blood as a non- Newtonian fluid (Carreau-Yasuda). Two wall thickness models were formulated; one with nominal 50um thickness (TNOM) and the other with wall thickness and material property heterogeneity based on histology (THIST) at end-point. The residual circumferential stress present in the artery *in vivo* along with stress due to axial stretch and diastolic pressure estimated and incorporated into each FSI model as a pre-load. FSI simulations were then run over three cardiac cycles.

Results

FSI simulations of the cuffed and control carotid arteries exhibited pressure waveforms that ranged from approximately 82 to 114 mmHg. These pressure pulsations resulted in a maximum nominal vessel wall dilatation that aligned with our ultrasound measurements. The range of time averaged wall shear stress (TAWSS) was 15% lower than that observed in the corresponding CFD model. Notably, the TAWSS variation between the TNOM model and THISTmodel was minimal. Cuff model displayed similar TAWSS results vs CFD and between the two wall thickness variants.

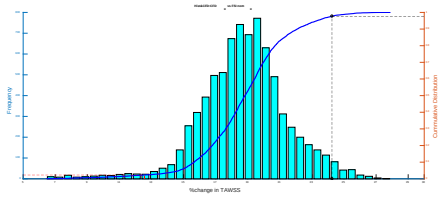

Comparison	95.5% conffidence level
Control: CFD vs nominal FSI	12.5% - 24.2%
Cuff: CFD vs nominal FSI	2.1% - 31%
Cuff FSI: nominal vs histology	-0.2% - 0.75%

Time average cyclic strain was observed to be primarily in the circumferential direction in the control vessel. More over, the time average angle between strain and wall shear was chiefly 90degs. TISTcuff model demonstrates material variation in the plaques areas as compares to the TNOM model.

Conclusions

The FSI model developed provides a physiological relevant simulation of the murine instrumented animal model. The model suggests a nominal wall thickness implementation is sufficient to study the interplay between shear stress and plaque development and morphology. Strain metrics developed enable the evaluation of changes in angle between strain and wall shear and its correlation with plaque formation.

References

[1] Pedrigi, R.M., et al., (2016). R Soc Open Sci, 3(10) p160588.
[2] Pahlevan, N.M., et al., (2011). Ann Biomed Eng, 39(5) p1470-81.

An *in vitro* tissue-based model of vascular remodeling in the descending aorta at intercostal artery branch points

Mairi E. Sandison

Department of Biomedical Engineering, University of Strathclyde, Glasgow, United Kingdom

Introduction

Phenotypic modulation of smooth muscle cells (SMCs) is thought to be central to the remodelling that underlies cardiovascular disease. Although there is a wealth of evidence to support this, there has been a lack of any direct obervations. Therefore, we recently employed a range of time-lapse and fluorescence microscopy techniques to track the fate of freshly isolated SMCs [1]. This demonstrated unambiguously that mature, fully contractile SMCs can rapidly transform into not only a migratory and proliferative but also a phagocytic phenotype. However, standard culture conditions (e.g. rigid glass/plastic dishes) are far removed from the *in vivo* environment. Therefore, a new tissue-based, *in vitro* model has been developed to investigate the fate of SMCs as their phenotype changes in a physiologically relevant environment, an approach that could also be exploited as an experimental model for studying the effects of fluid flow.

Methods

An open PDMS fluidic channel (0.8mm thick) was plasma bonded to a coverslip-bottomed 35mm dish. Freshly isolated, *en face* tissue was then either placed directly over the channel and secured by pinning into the PDMS or was attached to an upper PDMS support (produced by casting into a 3D printed mould) that was then pinned to the lower channel. This upper part comprised a central fluidic channel, over which tissue could be stretched, surrounded by a trench to accommodate pins for securing the tissue. Freshly isolated thoracic aortas were obtained from male, Sprague Dawleys rats (275-325g). Surrounding connective tissue was carefully removed under a dissection microscope. To ensure the tissue used was comprised of only SMCs, the adventitia was removed by enzymatic stripping [1], the tissue was cut open and the endothelium was removed by gentle scraping. The stripping process cleanly removed the attached intercostal arteries leaving a clear opening at the branch point. The tissue was then washed several times in sterile MOPS buffer to remove any loosely adhered material and pinned into the device, with the branch point suspended over the centre of the channel. The tissue was then cultured in 1:1 Waymouth's:Ham's F-12 media containing 10% FBS with 1% penicillin–streptomycin and 1% L-glutamine. A combination of fixed-time point and time-lapse imaging was employed to track the remodelling of the branch region, using both brightfield and fluorescence imaging (with a x20, 0.75NA objective). Cell nuclei were fluorescently labelled using the FUCCI Cell Cycle Sensor (Geminin-GFP and Cdt1-RFP, ThermoFisher) which enabled tracking of the migration of individual cells (as well as indicating cell cycle phase). Calcium imaging was performed using the fluorescent indicator Cal520-AM (Stratech).

Results

Remodelling of the suspended *tunica media* tissue was readily observable by live-cell imaging of branch regions, around which single cells can be more easily identified and tracked as compared to bulk tissue. Clear evidence of SMC proliferation and migration was observed. In all cases (5 regions from 3 animals), substantial narrowing of the branch opening occurred within 7 days through a combination of migration and proliferation. Division of individual cells was directly observed at the edges of the branch opening. When maintained in culture for 21 days, almost complete closure of the opening occurred. Preliminary results from nuclei tracking suggest similar rates of cell migration ($0.2\mu m\ min^{-1}$) to that observed on glass occurred in this tissue-based model, whilst preliminary calcium imaging showed clear responses of sub-populations of individual cells to common SMC agonists (phenylephrine and endothelin-1).

Conclusions

Results show that phenotypic modulation can be directly observed within tissue, where SMC become migratory and proliferative over time-scales similar to that observed in standard culture. This tissue-based approach provides a useful model of vascular remodelling that could be exploited to study the effects of fluid-flow through branch regions in tissue, including with and without the initima/adventitia.

References

[1] Sandison ME, Dempster J, McCarron JG, The transition of smooth muscle cells from a contractile to a migratory, phagocytic phenotype: direct demonstration of phenotypic modulation, *J Physiol*, 594: 6189–6209, 2016.

Manipulation of angiogenesis: controlling sprouting with patterns of notch ligands

Laura Tiemeijer[1,2], JP Frimat[3], Oscar Stassen[2], Carlijn Bouten[2], Cecilia Sahlgren[1,2]

[1]Department of Cell Biology, Åbo Akademi University, Finland
[2]Department of Biomedical Engineering, Eindhoven University of Technology, The Netherlands
[3]Department of Mechanical Engineering, Eindhoven University of Technology, The Netherlands

Introduction

Control over vascularization and the creation of vasculature, are important challenges in the field of regenerative medicine and tissue engineering [1,2]. Angiogenesis, the development of new blood vessels out of existing ones, is imperative for tissue growth, development and regeneration [3]. During Angiogenesis, the Notch cell-cell signaling pathway plays a central role in endothelial cell phenotype specification [4,5]. The Notch signalling pathway, specifically Dll4 – Notch1 signaling, directs endothelial cells into migrating tip or proliferative stalk cells, during endothelial sprouting in the first stage of angiogenesis [4,5]. Recently, we showed that lines of immobilized Dll4 could control endothelial sprouting location and direction [6].

Methods

The patterns of immobilized Dll4 were created via micro contact printing, using stamps with 100 µm wide lines and 100 µm wide spacing (fig. 1). On top of the printed Dll4 lines, reversible microfluidic channels were placed and used for the perpendicular seeding of Human Umbilical Vein Endothelial Cells (HUVEC) in 300 µm wide channels. After removal of the channels, the HUVECs were left to sprout 24h in the presence of Matrigel. Afterwards they were stained with DAPI (nuclei) and Phalloidin (actin) and imaged for sprouting behaviour/ efficiency of controlled sprouting.

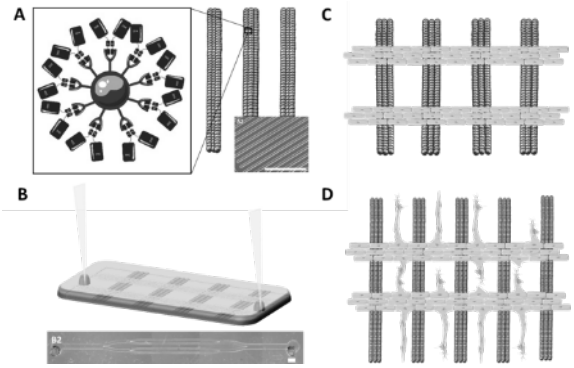

Results

We found that the immobilized Dll4 as used in our micro contact printing ink was able to induce expression of Dll4 – Notch1 endothelial target gene Ephrin B2. Moreover, the Dll4 pattern indeed induced a change in sprout direction from random to unidirectional. Finally, we demonstrated an increase of the efficiency of controlled sprouting from 54.5±3.1% for the control, to an average of 84.7±1.86% on the Dll4 patterned surface.

Figure 4. Micro contact printing of immobilized Dll4 (A) and microfluidic seeding of HUVECs (B, C) to hypothesized controlled sprouting (D) after 24h.

Conclusions

We showed that patterns of immobilized Dll4 can control sprouting angiogenesis by increasing the directionality and dictating the location of sprouting. More insights in the mechanism of this control by means of patterns of Dll4 or other Notch signalling ligands will be needed to properly design biomaterials for the manipulation and control of angiogenesis in tissue engineering and regenerative applications.

References

[1] Rouwkema J & Khademhosseini A, Vascularization and Angiogenesis in Tissue Engineering: Beyond Creating Static Networks 2016, *Trends Biotechnol*. 34: 733–745, 2016
[2] Malheiro A, Wieringa P, Mota C, Baker M & Moroni L, Patterning Vasculature: The Role of Biofabrication to Achieve an Integrated Multicellular Ecosystem 2016, *ACS Biomater. Sci. Eng*. 2: 1694–1709, 2016.
[3] Carmeliet P, Angiogenesis in life, disease and medicine 2005, *Nature* 438: 932–936, 2005.
[4] Hellström M, et al. Dll4 signalling through Notch1 regulates formation of tip cells during angiogenesis 2007, *Nature* 445: 776–780, 2007.
[5] Phng LK & Gerhardt H, Angiogenesis: A Team Effort Coordinated by Notch 2009. *Dev. Cell* 16: 196–208, 2009.
[6] Tiemeijer LA, Frimat J, Stassen OMJA, Bouten CVC & Sahlgren CM, Spatial patterning of the Notch ligand Dll4 controls endothelial sprouting in vitro 2018, *Sci. Rep.* 8, 2018.

Piezo1 ion channels are required for shear stress sensing in placental blood vessels

[1,2]Lara Morley, [1]Sara Ibrahem, [1]Jian Shi, [1]Hannah Gaunt, [2]James Walker, [2]Nigel Simpson, [2]David Beech

Leeds Institute of Cardiovascular and Metabolic Medicine, University of Leeds, UK, Academic Department of Obstetrics and Gynaecology, Leeds Teaching Hospitals Trust, UK

Introduction

A key element of normal vascular adaptation in pregnancy is vasodilatation through nitric oxide (NO) production from the endothelium of fetoplacental blood vessels[1]. Failure of this adaptation can lead to pregnancies complicated by gestational disorders including fetal growth restriction (FGR), the pathogenesis of which centres upon high vascular resistance and hypoperfusion[1]. FGR affects 3-8% of pregnancies, with consequences including stillbirth, neurodevelopmental delay and increased risk of cardiovascular disease[1]. Shear stress (SS) generated by blood flow is an important stimulus for NO production but the mechanisms by which the force is detected and transduced in the placenta are unclear. We have demonstrated that the mechanosensitive ion channel, Piezo1, is present in fetoplacental endothelial cells (FPECs)[2]. Depletion of Piezo1 has been shown to reduce endothelial NO phosphorylation[3]. The aim of this study is to determine whether Piezo1 is required for SS sensing in FPECs.

Methods

Patients were consented at Leeds Teaching Hospitals Trust. Primary FpECs were used immediately for patch-clamp electrophysiology studies, or cultured to passage 6 after isolation using CD31 MicroBeads (Miltenyi). FpECs were exposed to the synthetic Piezo1 channel agonist Yoda1 and/or Piezo1 specific short interfering RNA (siRNA). SS was generated using an orbital shaker and cell alignment quantified using image analysis. Intracellular Ca^{2+} concentration, cell viability and endothelial nitric oxide synthase (eNOS) phosphorylation were assessed using a FlexStation fluorometer, membrane integrity assay and western blotting, respectively. All experiments were performed on a minimum of 3 independent patient samples. This research was supported by the MRC and RCOG.

Results

Application of SS led to striking alignment of FpECs to the direction of flow and significantly increased eNOS phosphorylation (3 fold change). Patch-clamp recordings showed single channels characteristic of Piezo1, which were SS-activated. The alignment of cells in response to shear was suppressed by Piezo1 knockdown ($p < 0.05$) without losing cell viability. Chemical activation with Yoda1 caused strong elevation of the intracellular Ca^{2+} concentration, in a dose-dependent manner. The Yoda1 Ca^{2+} response was suppressed following Piezo1 knockdown ($p<0.01$) demonstrating that the effect of Yoda1 was Piezo1 mediated. The application of Yoda1 significantly increased eNOS phosphorylation ($p<0.01$).

Conclusions

Piezo1 is present and functionally active in human FpECs. Disrupting Piezo1 prevents the normal response to SS. Our data suggest that Piezo1 stimulation activates signaling pathways leading to production of the potent placental vasodilator, NO. Understanding the mechanisms through which FpECs sense and respond to SS will provide novel insights into the regulation of blood flow, both in healthy pregnancy and those complicated by placental vascular dysfunction.

References

[1] Jones S, Bischof H, Lang I *et al*, Dysregulated flow-mediated vasodilatation in the human placenta in fetal growth restriction. *J Physiol*, 593: 3077-92, 2015.

[2] Morley LC, Shi J, Gaunt HJ *et al*, Piezo1 Channels Are Mechanosensors in Human Fetoplacental Endothelial Cells, *Mol Hum Reprod*, 24: 510-520, 2018.

[3] Li J, Hou B, Tumova S *et al*, Piezo1 integration of vascular architecture with physiological force, *Nature*, 515: 279-82, 2014.

Atorvastatin effect on homing of MSCs and EPCs on a 3D blood vessel model

Njoroge W[1], Harper A[1], Butler R[1,2], Sandhu K[2], Yang Y[1]

[1]Institute of Science and Technology in Medicine, School of Medicine, Keele University, Stoke-on-Trent, ST4 7QB

[2]Cardiology Department, University Hospitals of North Midlands, Stoke-on-Trent, ST4 6QG

Introduction

Statins are the standard prescription for lowering levels of circulating low density lipoprotein (LDL). A number of studies have shown that they are effective, safe and have become a cornerstone of risk modification for ischaemic heart disease patients. This has led to recommendation of statin therapy in both national and international guidelines. Studies have also shown that they have pleiotropic effects beyond lowering cholesterol. These pleiotropic effects are believed to be an augmentation of endothelial progenitor cells and damaged endothelial cells within blood vessels [1]. This study aims to evaluate the effect of atorvastatin on the homing of endothelial progenitor cells to a vascular injury site, as well as characterizing changes in chemokine expression, specifically SDF-1 (CXCL-12).

Methods

To evaluate atorvastatin effect on cell homing, a 3D tissue engineered blood vessel model (TEBV) was made by seeding commercially obtained human cardiac artery smooth muscle cells (HCASMC) into a collagen gel, followed by the addition of human umbilical vein endothelial cells (HUVEC) seeded on top of an aligned PLA nanofiber mesh [2]. The TEBV was then lesioned with ferric chloride ($FeCl_3$), and incubated for 3 and 5 hours with 60μg/ml atorvastatin. Using a parallel plate flow chamber, the model was then perfused for 45 minutes, at 15 dyne/cm^2, with fluorescently labelled (CFSE) human MSCs (hMSCs) and human endothelial progenitor cells (EPCs). The perfused cells were also inoculated with 60μg/ml atorvastatin. Attachment of cells was observed using fluorescence microscopy and quantified using imageJ. The expression of SDF-1 with and without the inclusion of atorvastatin at these time points was also evaluated. EPCs were obtained from healthy volunteers following ethical approval.

Results

hEPCs and hMSCs were both found to congregate at a higher density on the surface of the lesioned TEBV construct when treated with atorvastatin, compared to a vehicle-treated control. This suggests atorvastatin enhances homing of cells to sites of injury. Analysis of SDF-1 production found that atorvastatin incubation accelerated the release of the chemokine, which allowed a higher maximum concentration to be released compared to a vehicle-treated control sample. The highest concentration was observed after 3 hours of incubation with atorvastatin, after which the levels of the drug sharply decreased to almost nil after 5 hours. On the control samples, the maximum concentration was achieved at 5 hours and this value was far lower than that observed at 3 hours with atorvastatin.

Conclusions

The incubation and perfusion data suggested that statins have a time dependent effect on the SDF-1/ CXCR4 axis, and the lesioned biomimetic blood vessel model was able to simulate the EPC and hMSC homing process under physiologically relevant conditions. This study also demonstrated that atorvastatin greatly accelerated the rate of SDF-1 production, and subsequently increased the density of cell recruitment upon vascular injury. The 3D model used provides a realistic tool to reveal the interactions between statins and circulating progenitor cells.

References

[1] K. Sandhu, M. Mamas and R. Butler, "Endothelial progenitor cells: Exploring the pleiotropic effects of statins", *World Journal of Cardiology*, vol. 9, no. 1, p. 1, 2017. Available: 10.4330/wjc. v9. i1.1.

[2] F. Musa, A. Harper and Y. Yang, "A Real-Time Monitoring System to Assess the Platelet Aggregatory Capacity of Components of a Tissue-Engineered Blood Vessel Wall", *Tissue Engineering Part C: Methods*, vol. 22, no. 7, pp. 691-699, 2016. Available: 10.1089/ten.tec.2015.0582

Anthropomorphic Cardiac Valve Fabrication Based on Two-part Water Soluble PVA Mould

Shu Wang*, Harminder Gill*, Yohan Noh, Nio Amanda, Joao Filipe Fernandes, Ronak Rajani, Pablo Lamata, and Kawal Rhode

Biomedical Engineering & Imaging Sciences, King's College London, London, United Kingdom. * Joint first authors

Introduction

Valvular heart disease affects 27 million patients worldwide[1] and is associated with significant morbidity and mortality. In-vitro study of valve disease and pre-procedural interventional planning can benefit from advances in 3D printing[2]. In this work we present the feasibility of low-cost fabrication of anthropomorphic cardiac valve phantoms and an early demonstration of functional capability.

Methods

The aortic valve geometries were segmented from volumetric CT scan with a post-processing smoothing step. Based on the positive valve model, a two-part negative mould was developed in Solidworks. The internal mould part was printed with water-soluble PVA (polyvinyl alcohol) to ease the mould removal procedure, while the external part was printed with rigid PLA (polylactic acid) for reuse. After printing and assembling the mould, liquid silicone was injected to form the anthropomorphic valve. Silicone was chosen because it is a room temperature-vulcanized material with a stiffness similar to soft tissue[3]. After extraction from the mould, valve function was evaluated using 2D colour Doppler ultrasound (Philips IE33).

Results

The manufacturing process has been successfully used to generate 3 aortic valves with different types of silicone, which have tested to be robust in different flow conditions. Valves showed a physiologically plausible behaviour when imaged using echocardiography (see Fig.1).

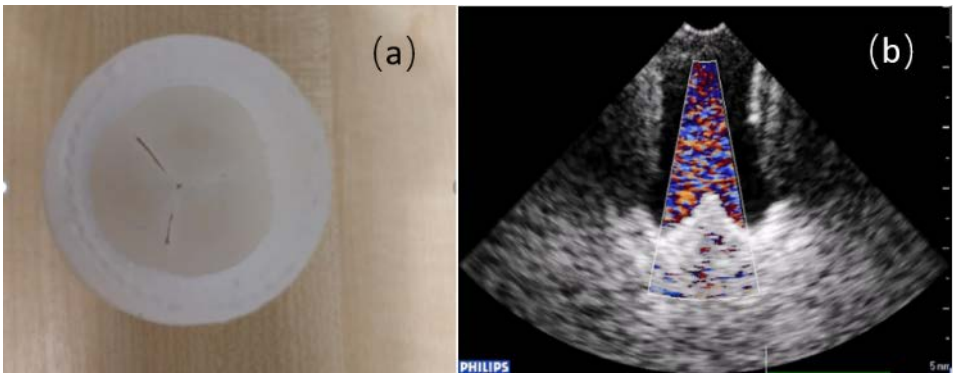

FIG.1. (a) Top view of the silicone valve (b) Corresponding 2D Valve Echo from Long Axis View (LAX)

Conclusions

Water soluble mould-based techniques bring the feasibility to fabricate anthropomorphic cardiac valve phantoms with a low-cost fusion deposition modelling 3D printer.

References

[1] Laura Ann Hockaday, Bin Duan, Kevin Heeyong Kang, 3D Printed Hydrogel Technologies for Tissue-Engineered Heart Valves, *3D Printing and Additive Manufacturing*, 1(3): 122-136, 2014

[2] Qian Z, Wang K, Liu S, et al. Quantitative Prediction of Paravalvular Leak in Transcatheter Aortic Valve Replacement Based on Tissue-Mimicking 3D Printing. *JACC Cardiovasc Imaging*. 2017;10(7):719-731. doi:10.1016/j.jcmg.2017.04.005

[3] Yancheng Wang, Bruce l. Tai, Hongwei Yu, et al, Silicone-based tissue-mimicking phantom for needle insertion simulation, *Transaction of the ASME*, 8: 021001-1–021001-7, 2014

Developing new machine learning tools to interrogate the epigenome of endothelial cells during plaque development in vivo

Yean Kok Chooi[2], Roza Nikolopoulou[2], C.A. Mein[3], Eva Wozniak[3], Alex Delahunty[2], Nasar Jarka[1,2], Miten B. Patel[1,2], Fotios Savvopoulos[1,2], Pan Jang[1,2], Ranil de Silva[1], and Rob Krams[2].

[1]NHLI, Imperial College, and [2]Bioengineering and [3]Genomics Centre, Queen Mary's and the Genome Centre, Queen Mary University

Introduction. Endothelial cells (EC's) are continuously exposed to mechanical factors (stress/strain) and disturbances in these factors play an important role in disease, including atherosclerosis. These biomechanical factors, activate about 10-20% of the genome (3,000-5,000 genes) distributed over >100 signaling pathways. The sheer complexity of this process has warranted us to do a systematic study into the regulation of the mechanotransductive pathways by microRNA.

Methods and results. Six female ApoE-/- mouse were instrumented with a blood flow-modifying cuff around the left carotid artery, inducing low shear stress upstream of the cuff. One week after cuff placement, laser capture microdissection was performed on endothelial cells (PALM, Zeiss). Total RNA was isolated from endothelial cells only using Qiagen kits, medium laser power, glass slides and 20 um cross sections and split into two vials for mRNA and miRNA using an Illumina HiSeq 4000.
The endothelial mRNA's were first analyzed with an extensive quality control (FASTQ), followed by alignment (STAR), read and differential gene expression are performed using the PARTEK Genome Suite at the Bart's and the London Genome Centre. In total, 2300 differentially expressed mRNA were identified encompassing known (MAPK) and unknown signaling (Insulin, WnT, TGF, Notch) pathways.
In a parallel sample, 1,500 microRNA were identified using a novel method correcting for bias by UMI's (Qiagen miRNA kit). We applied Sparse Principal Components (sPCA) to reduce the high dimensionality of features (e.g. miRNA's) space with respect to number of samples (n=8). The first three principal components (n=600 miR's) accounted for ~90% of variation in the dataset. A further combined Lasso and Ridge regression using Elastic Net from R, after cross validation, identified ~500 miR's affecting ~40% of the differentially expressed genes. Current work is focused on which signaling pathways is dominantly regulated by the mechanosensitive miRNA's

In conclusion, we have developed a novel analysis pipeline to identify regulators of mechanotransduction and identified many novel microRNA families which might be used in the future for drug treatment.

Acknowledgements
Thanks to the British Heart Foundation for financial support (RG/11/13/29055 and PG/15/49/31595).

Exploring the interaction between age, sex and differing types of exercise upon exercise-induced shear stress and subsequent markers of vascular health.

Gemma K. Lyall, Karen E. Porter, Karen M. Birch

School of Biomedical Sciences, University of Leeds, Leeds, UK

Introduction

Traditional cardiovascular disease (CVD) risk factors account for only 60% of CVD risk, with the remaining 40% thought to be directly related to the vasculature, particularly endothelial dysfunction and arterial stiffness [1]. CVD risk increases with age, however the rate of CVD progression differs between males and females [2]. Exercise-induced modification of traditional risk factors only explains 40-60% of CVD risk reduction [1]. Beyond these traditional risk factors, exercise directly impacts the vasculature via increases in shear stress (SS). The greater work rates undertaken in interval exercise training provide greater SS and this has been suggested to be more effective in improving markers of vascular health compared to continuous exercise training. However, differing exercise-induced SS patterns may interact with age and sex, negating positive effects. Thus, the aim of the study was to evaluate the effect of age and sex upon exercise induced vascular SS during interval and continuous exercise training and the subsequent impact upon markers of vascular health.

Methods

35 healthy males and females aged 20-35 (8 m; 9 f) or 45-60 years (5 m; 13 f) were randomly assigned to 4 weeks of either: aerobic interval cycling (AIT: 4min at 85-90% heart rate peak (HR_{peak}) with 4min active recovery at 60-65% HR_{peak} repeated 4 times) or 32min continuous cycling (CON: 65-70% HR_{peak}). Doppler ultrasound was used to characterise brachial artery anterograde and retrograde SS during the first and final exercise training sessions. The acute and chronic effect of exercise upon FMD was assessed by recording FMD pre and post exercise at baseline and after exercise training. Data were assessed for group and time effects.

Results

Anterograde and retrograde SS mirrored the pattern of the exercise protocols. Volumes of exercise-induced anterograde SS were comparable between protocols ($P>0.05$). However, volumes of retrograde SS were higher in the AIT exercise protocol compared to CON (201.7±100.3 vs. 115.6±65.9 s^{-1}; $P<0.05$). Whilst, age and sex had no impact upon volumes of in-exercise anterograde and retrograde SS ($P>0.05$), in-exercise anterograde SS was higher in older females, although this did not reach statistical significance (older females vs older males: mean 824±367 vs. 584±220 s^{-1}, $P>0.05$). At baseline acute FMD increased following exercise (6.02±4.42 to 11.03±5.33 %, $P<0.05$), regardless of exercise protocol, age or sex ($P>0.05$). However, following exercise training this acute FMD response was blunted in all groups ($P>0.05$). Pre-exercise FMD increased from 6.02±4.42 to 8.86±4.57 % over the training period ($P<0.05$), irrespective of exercise protocol, age or sex ($P>0.05$).

Conclusions

Age and sex did not influence patterns of exercise-induced anterograde and retrograde SS. However, type of exercise, i.e. CON v AIT, determined both pattern and volume of exercise-induced SS. Older females appear to receive a greater anterograde SS compared to older males, with volumes of mean anterograde SS consistent with those in younger males and females. By contrast older males may require a greater exercise stimulus to see comparable volumes of anterograde SS. Importantly, greater volumes of exercise-induced retrograde SS during AIT exercise did not detrimentally impact markers of vascular health. This suggests that both CON and AIT type exercise are beneficial for improving vascular health in young and middle aged populations, irrespective of sex. The volume of exercise-induced SS, rather than the pattern, is potentially the greatest factor in determining SS mediated improvements in markers of vascular health.

References

1. Joyner, M.J. and D.J. Green, *Exercise protects the cardiovascular system: effects beyond traditional risk factors.* The Journal of Physiology, 2009. **587**(23): p. 5551-5558.
2. Celermajer, D.S., et al., *Aging is associated with endothelial dysfunction in healthy men years before the age-related decline in women.* Journal of the American College of Cardiology, 1994. **24**(2): p. 471-476.

The influence of bending on coronary arteries bio-mechanics assessed by fluid-structure interaction modelling

Pan Yang[1], Naser Jarka[1], Miten Patel[1], Fotios Savvopoulos[1], Ryan M. Pedrigi[2], Rob Krams[3], Ranil de Silva[1,4]

[1]National Heart & Lung Institute, Imperial College London, Guy Scadding Building, Cale Street, London, SW3 6LY, United Kingdom; [2]Mechanical and Materials Engineering, University of Nebraska-Lincoln, Lincoln, NE 68588-0526, United States; [3]School of Engineering and Materials Science, Queen Mary University of London, Mile End Road, London, E1 4NS, United Kingdom; [4]Harefield NHS Foundation Trust, Level 2 Chelsea Wing, Sydney Street, London, SW3 6NP, United Kingdom

Introduction

Atherosclerotic plaques are not evenly distributed over the arterial tree, and ample evidence has indicated that biomechanical forces play an essential role in its distribution of the two important mechanical forces, shear stress (the force imposed by the blood flow on the wall) and blood pressure derived strain, shear stress has received the most attention. Endothelial strain has been mentioned but has hardly been measured in coronary arteries in vivo. This work aims to develop subject-specific physiological relevant comprehensive modelling using measured clinical source data.

Methods

The fluid-structure interaction (FSI) model was built in ABAQUS. We developed two models: Model 1 - FSI model without bending; and Model 2 - FSI model with bending. The workflow is as follows: (1) a 270-slice in vivo OCT dataset of vessel lumen was acquired for the left circumflex artery (LCx); (2) segment OCT and bi-plane angiograms; (3) calculate the centreline of the OCT catheter (VMTK Lab) and smooth the catheter path; (4) reconstruct the 3D coronary geometry using in-house MATLAB code which assumes rotation on basis of a "stress-free" state of the catheter; (5) smooth the reconstructed vessel lumen; (6) reconstruct vessel lumen to generate the solid mesh and input file for the ABAQUS\Standard; (7) the stress due to diastolic pressure estimated and incorporated into each FSI model as a pre-load; (8) multi-timeframe bi-plane angiograms reconstructions are used to model the bending procedure in the FSI model; (9) reconstruct the vessel lumen to generate the fluid mesh and input file for the ABAQUS\CFD solver; (10) smooth Combowire blood pressure and velocity time series and insert in the ABAQUS\CFD input file as the fluid boundary conditions; (11) run the FSI simulations; (12) quantify shear and strain metrics are generated.

Results

The simulated pressure and velocity waves along the entire vessel are similar to match the measured Combowire wave patterns applied to the inlet and outlet boundaries. Preliminary results of vessel wall dilatation from the FSI model matched the measured pressure wave pattern obtained from the Combowire. The FSI model with bending (M2) exhibited TAWSS that was three-fold larger than the model without bending (M1) and the distribution is different. For strain metrics, there is 3 times difference between model with and without bending.

Summary and Conclusions

We have developed a comprehensive FSI model framework using angiography, in vivo optical coherence tomography (OCT), in vivo blood velocity and pressure for subject-specific modelling of coronary arterial biomechanics using measured clinical source data. Our first results indicate that bending of the coronary artery might be relevant as it affects both the distribution and pattern of the shear stress and strain maps. FSI models based on measured intracoronary imaging and physiology source data that incorporate bending have the potential to improve subject and vessel specific quantification of shear and strain metrics.

Acknowledgements

This work is carried out under funding from the British Heart Foundation (SP/17/1/32702). Authors are grateful for the support provided by the British Heart Foundation.

References

[1] A. Version, 6.14 Documentation (Abaqus), 2014, Abaqus User's Manual.

The synergistic effect of NIRS-detected lipid-rich plaque and five different wall shear stress metrics on human coronary plaque growth

Eline M.J. Hartman, Annette M. Kok, Ayla Hoogendoorn, Giuseppe De Nisco, Antonius F.W. van der Steen, Frank J.H. Gijsen, Joost Daemen, Jolanda J. Wentzel

Department of Cardiology, Biomedical Engineering, Erasmus MC, Rotterdam, The Netherlands

Introduction

Local wall shear stress (WSS) metrics, high local lipid content (as detected by near-infrared spectroscopy (NIRS)), as well as systemic lipid levels, have been individually associated with atherosclerotic plaque progression. However, a possible synergistic effect remains to be elucidated. This study is the first study that combines five different WSS metrics with local lipid content to investigate this synergistic effect in human coronary arteries.

Methods

The IMPACT study is a prospective, single centre study investigating the relation between atherosclerotic plaque progression and WSS in human coronary arteries. Patients with acute coronary syndrome treated with percutaneous coronary intervention were included. At baseline and after 1 year follow-up, patients underwent near-infrared spectroscopy intravascular ultrasound (NIRS-IVUS) imaging and intravascular doppler flow measurements of at least one non-culprit coronary artery. One month after baseline imaging, a CT scan was made. Combining the IVUS derived lumen contours, the CT derived vessel centreline and side branch segmentation, resulted in a 3D reconstruction of the coronary artery including the side branches. The following WSS metrics were computed using CFD applying the vessel specific invasive flow measurements: time-average wall shear stress (TAWSS), oscillatory shear index, relative residence time (RRT), cross-flow index and transverse wall shear stress (transWSS). The arteries were divided into 1.5mm/45° sectors. Based on baseline and follow-up IVUS segmentation of lumen and vessel wall, average wall thickness change was determined at each sector. Furthermore, each arterial sector was classified for the presence of lipid-rich plaque as NIRS-positive or NIRS-negative and for each WSS metric as low, mid or high WSS dependent on the average value (tertiles per vessel).

Results

15 non-culprit coronary arteries from the first 14 patients were analyzed (age 62±10 years old and 92.9% male). A total of 2219 sectors were analyzed for wall thickness changes. After studying all five WSS metrics, plaque growth was clearly related to all WSS metrics except for transWSS (Fig A). Furthermore, we found an amplified effect of shear stress on plaque progression after splitting the sectors based on NIRS content (Fig B/C). Sectors presenting with baseline NIRS-detected lipid-rich plaque showed more progression when they were colocalized with low TAWSS (p=0.07) or high RRT (p=0.012) and more regression in sectors additionally exposed to high TAWSS (p=0.10) or low RRT (p=0.06) compared to NIRS-negative sectors (Fig. B/C).

Conclusions

Hereby we presented the first preliminary results of the IMPACT study, showing that intravascular lipid-rich plaque (NIRS) assessment and local shear stress metric values synergistically influence plaque progression or regression in human coronary arteries. This finding suggests that combining local biomechanical assessment with knowledge on local plaque composition could improve patient risk assessment.

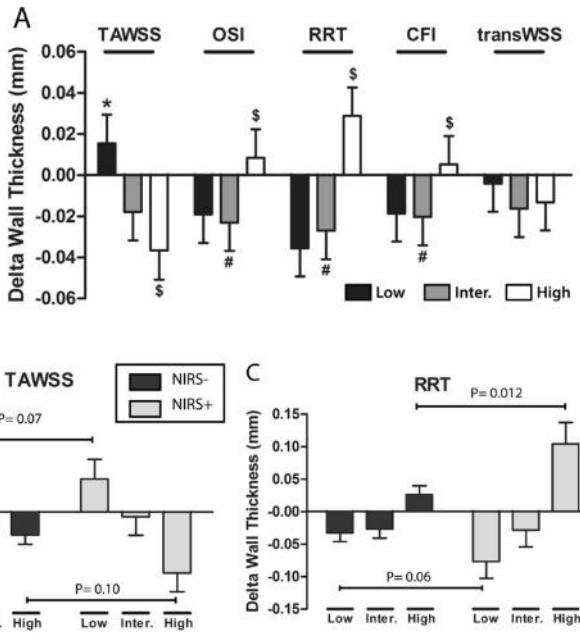

A: 5 different shear stress metrics change in wall thickness after 1 year for low, intermediate and high shear stress. *p<0.05:* low versus intermediate, # intermediate versus high or $ low versus high* **B/C:** Effect of local lipid detection on shear stress (TAWSS or RRT) related change in wall thickness after 1 year.

Cuffless BP Estimation Using Single Channel PPG: Evaluation of Machine Learning Approaches on MIMIC II database

Syed Ghufran Khalid, Jufen Zheng, Dingchang Zhang

Faculty of Health, Education, Medicine, and Social Care, Anglia Ruskin University, United Kingdom

Introduction

Blood pressure (BP) is a vital sign parameter recommended to monitor cardiovascular health. Frequent BP measurements with a cuff-based BP monitor provides discomfort and inconvenience to the users during the measurements. To overcome these limitations, cuffless BP using PTT-based technologies has been proposed. However, these technologies face frequent calibration and wearability issues. Thus, single channel PPG-based BP estimation has been attempted which eliminate these limitations, but the standard BP estimation accuracy has not been achieved. Therefore, an improved single channel PPG-based BP estimation algorithm with standard accuracy is required.

Methods

In this study, PPG waveforms and corresponding BP data were obtained from the MIMIC II database. Each PPG signal recordings present in the database were segmented into 5-second signal segments from which 9877 good quality signal segments with their corresponding BP were extracted. In total, 17 PPG signal features were extracted from each signal segment out of which three significant features (total area, rising time and width 25%) were selected using the multicollinearity test. Three machine learning approaches (Multiple Linear Regression (MLR), Support Vector Machine (SVM) and Regression Tree) were trained and tested from the dataset consists of 9877 sets of three significant PPG signal features along with corresponding BP using 10-fold cross-validation. The cross-validated data were also separated into two BP categories (Normotensive and Hypertensive) present in the dataset to calculate categorical BP accuracies according to AAMI/ISO standard criteria (mean difference no greater than ±5mmHg and standard deviation (SD) of difference no greater than ±8mmHg) for BP measurement device validation.

Results

The Regression Tree algorithm achieved the least mean difference and SD of difference for SBP (-0.03±13.4) mmHg and DBP (-0.1±9.3) mmHg as compared to the MLR (SBP 0.09±18.6, DBP 1.1±10.9) mmHg and SVM (SBP -0.8±19.7, DBP 1.2±11.1) mmHg. However, only the mean differences of all the algorithms matched with AAMI/ISO standard criteria. The Regression Tree algorithm also achieved least mean difference and SD of difference in Normotensive (SBP -4.7±12.9, DBP -1.5±7.7) mmHg and Hypertensive (SBP 3.9±12.9, DBP 1.1±10.3) mmHg BP categories as compared to the MLR and SVM. The Bland-Altman plots also showed the agreement of Regression Tree algorithm and the reference BP method with small percentage of outliers (<3%).

Conclusions

This study revealed that the Regression Tree algorithm is the best cuffless BP estimating algorithm that meets the AAMI/ISO standard criteria in terms of overall mean difference with the least SD of difference when applies to the MIMIC II database. Moreover, it showed that Regression Tree algorithm also estimate categorical BP (Normotensive and Hypertensive) with the least mean difference.

References

[1] Khalid, S.G, Zhang, J, Chen, F, & Zheng, D 2018, 'BP estimation using photoplethysmography only: comparison between different machine learning approaches', Journal of Healthcare Engineering, vol. 2018, pp. 1-13.

A numerical analysis of the stress distributions in an idealised, three-dimensional model of an atherosclerotic plaque

César Alegre Martínez, Kwing-So Choi, Outi Tammisola, Donal McNally

Faculty of Engineering, University of Nottingham, Nottingham, United Kingdom

Introduction

Numerical simulations of incompressible flow through idealised, stenosed geometries have been performed in order to model the blood flow through a partially blocked vessel due to an atherosclerotic plaque. Previously published studies have suggested that a plaque may rupture where the wall stresses are high [1-3]. Therefore, in this work we investigate the stress distributions along the wall in order to shed light on the initiation of the rupture process. The main goal is to identify what mechanical features may affect those stress distributions and, according to the literature, the location of the rupture. In particular, we first study the effects of the geometry by considering different models of the lipid core, including both eccentric and axisymmetric configurations. In addition, a parametric analysis of the lipid core length and the lipid core stiffness is also performed.

Methods

The numerical simulations are performed using COMSOL Multiphysics. A fluid-structure interaction configuration is considered: the flow is modelled as steady, incompressible and Newtonian, whereas the artery wall is modelled as a hyperelastic material. An idealised, three-dimensional plaque with an eccentric lipid core is analysed. Other variants are included in the study as well, such as the positive remodelling of the artery or axisymmetric geometries with concentric lipid cores.

Results

First, the effect of the different geometries was studied, along with a comparison to axisymmetric models. In this case, the positive remodelling had the largest effect on the stress distributions along the axial direction, increasing the maximum stress levels significantly. The axisymmetric models presented a stress distribution similar to that of the three-dimensional cases (except the positive remodelling one), suggesting that the axisymmetric geometry could provide important information with a lower computational cost. Secondly, the analysis of the lipid core stiffness showed that, overall, the stress on the fibrous cap increased when the stiffness of the lipid core decreased. In addition, the stress distribution changed depending on the stiffness of the core, varying from a two-peak distribution for low stiffness values to a one-peak distribution for a stiffer core. Finally, it was found that short lipid cores may present higher risk of rupture if there was an abrupt change of wall thickness.

Conclusions

The study has shown that some features of the stress distributions along the artery wall remained stable for both the three-dimensional models and the axisymmetric geometries considered. Common findings were: the positive remodelling presenting the highest stress levels, the change of the stress distribution when the lipid core stiffness decreased and the effect of the length of the core shifting the location of the peak stresses. The maximum stresses and, therefore, the potential location of the rupture, were usually located at the midpoints of the upstream and downstream sections of the stenosis, except for the cases when the stiffness of the core was increased.

References

[1] Tang D, Teng Z, Canton G, Yang C, Ferguson M, Huang X, Zheng J, Woodard P, Yuan C, Sites of Rupture in Human Atherosclerotic Carotid Plaques Are Associated With High Structural Stresses: An In Vivo MRI-Based 3D Fluid-Structure Interaction Study, *Stroke*, 40: 3258-3263, 2009.

[2] Canton G, 3D Critical Plaque Wall Stress Is a Better Predictor of Carotid Plaque Rupture Sites Than Flow Shear Stress: An In Vivo MRI-Based 3D FSI Study, *Journal of Biomechanical Engineering*, 132: 031007, 2010.

[3] Gao H, Long Q, Das S, Sadat U, Graves M, Gillard J, Li Z, Stress analysis of carotid atheroma in transient ischemic attack patients: Evidence for extreme stress-induced plaque rupture, *Annals of Biomedical Engineering*, 39: 2203-2212, 2011.

Stabilisation of Vessel Bifurcations during Flow-Regulated Vascular Remodelling

Lowell T. Edgar, Miguel O. Bernabeu

Usher Institute of Population Health Sciences and Informatics, University of Edinburgh, Edinburgh, United Kingdom

Introduction

Angiogenesis occurs as two phases: an early sprouting phase, and a late remodelling phase which involves the pruning of superfluous connections. Recent experiments show that this remodelling phase is driven by vascular endothelial cells (ECs) responding to shear stress by polarising/migrating against blood flow [1-3]. Flow-migration coupling results in the regression/loss of certain vessel connections and the stabilization/maintenance of others, as well as vessel diameter control. These hypotheses present a paradigm shift through which we can now view quiescent vascular structures as nonlinear dynamic systems of migrating cells which have reached stability at a fixed point, and shifts between healthy vascular tissue and diseased now as transitions between stable fixed points which may be reversible. However, questions arise as to how vascular integrity is preserved: for any vessel segment to remain stable, a net flux of zero should be achieved between incoming/outgoing/proliferating/apoptotic cells. How do vessel networks preserve their branched structure and satisfy this zero flux condition within this highly dynamic migratory environment?

Methods

Towards answering this, we have implemented an agent-based model (ABM) of flow-regulated migration in a simplified model of the mouse retina consisting of a high-pressure artery connected to a low-pressure vein by proximal and distal branches. Individual ECs are modelled as independent agents. During each time step, ECs migrate against the direction of flow. Vessel diameter is calculated using 3D approximations of the lumen based on the number of cells in the vessel, directly linking flow to migration.

Results

With this model we have determined that cells must make a decision upon reaching a bifurcation (see Figure). Cells that choose to migrate along either the path of highest flow or continuing along polarity alignment result in a loss of either the distal or proximal branch, respectively, as these choices do not satisfy the zero flux condition in both branches. However, if cells randomly choose one of the two paths upon encountering a bifurcation, the incoming cells are split evenly and both branches remain. Alternatively, if cells slightly prefer one branch over the other, both branches remain but with unequal diameter, effectively implementing a form of diameter control: a key outcome of vascular remodelling.

Conclusions

Thus, any persistent bifurcation within a vessel network must include a mechanism to split the flux of incoming cells between its two branches. ECs in vessels are joined by dynamic adherens junctions [4], and ECs must migrate with these junctions intact in order to maintain the epithelium [1]. Force is transmitted amongst neighbouring cells which coordinate and migrate as a supracellular unit, known as collective cell migration (CCM). We hypothesise that at stable vessel bifurcations, cells within each branch transmit force to incoming cells and “pull” them inside, ensuring a constant supply of new cells and satisfying the zero flux condition within each branch. Larger diameter vessels will transmit more force to incoming cells and pull more cells than smaller branches. Thus, collective cell migration and diameter control work together to stabilize vessel bifurcations. Currently, we are expanding our ABM with representations of adherens junctions to fully demonstrate that force transmission during CCM stabilizes vessel bifurcations and preserves branched networks during vascular remodelling.

References

[1] Franco CA et. al, Dynamic endothelial cell rearrangements drive developmental vessel regression, *PLoS Biol*, 13(4) 2015.

[2] Franco CA et. al., Non-canonical Wnt signalling modulates the endothelial shear stress flow sensor in vascular remodelling *eLife* 5, 2016.

[3] Vion AC et. al., Primary cilia sensitize endothelial cells to BMP and prevent excessive vascular regression, *J Cell Biol* 217(5) 2018.

[4] Bentley K et. al., The role of differential VE-cadherin dynamics in cell rearrangement during angiogenesis, *Nat Cell Biol* 16(4) 2014.

Effect of Patient-Specific Values of Coronary Flow Reserve (CFR) on the Accuracy of Non-Invasive Fractional Flow Reserve (FFR) Estimates

John Oshinski (1,2), Jackson Hair (2), David Molony (3), Lucas Timmins (4), Habib Samady (3)

Department of Radiology & Imaging Sciences (1), Biomedical Engineering (2), Medicine-Cardiology (3), Emory School of Medicine, Atlanta, GA USA, and (4) Biomedical Engineering, University of Utah, Salt Lake City, UT, USA

Introduction

Guiding percutaneous coronary intervention (PCI) and stent placement based on the functional severity of stenoses has been shown to be far more beneficial in optimizing patient outcomes than simply using anatomic stenosis severity [1-2]. Fractional Flow Reserve (FFR) is the clinical standard for determining functional severity of stenosis. FFR has traditionally required a coronary catheterization, administration of adenosine to induce hyperemic flow, and measurement of pressures across the stenosis. Non-invasive angiography techniques, such as computed tomography (CT), can determine patient-specific coronary anatomy, enabling estimation of *simulated FFR* through computational fluid dynamics (CFD) modeling. Most simulated FFR techniques, however, do not use patient-specific flow information. Instead they rely on allometric scaling to determine basal flow conditions and population-averaged measurements to predict hyperemic flow. The clinical parameter used to characterize hyperemic flow response to adensosine is the coronary flow reserve (CFR), defined as the ratio of hyperemic flow to baseline flow. Recent studies have shown a discordance between CFR and FFR values in patients, as well as a wide range of CFR values in patients with the same FFR values [3]. We conducted a study to examine how assuming different values of CFR affects the accuracy of *simulated FFR*.

Methods

Nine subjects undergoing cardiac catheterization had basal and hyperemic flow measured in their left anterior descending (LAD) artery by intracoronary Doppler ultrasound, enabling calculation of patient-specific CFR values. A separate patient presenting with moderate CAD was imaged with magnetic resonance angiography (MRA), and the images were used to construct a geometric model of the coronary arteries. FFR values were determined by conducting CFD simulations using: 1) each patients' time-dependent basal and hyperemic flow waveforms as the input flow boundary conditions for the model (*True FFR)*, 2) hyperemic flow simulated by scaling the basal flow by the patients' CFR (*patient specific FFR*), and 3) hyperemic flow simulated by scaling the basal flow by the patient-cohort average CFR value (*patient average FFR*). True FFR values were compared to the two CFR-scaled FFR values in both steady and transient simulations.

Results

Scaling basal flow by the patinet specific CFR resulted in a correlation value of 0.98 with True FFR. The correlation between patient average FFR and the True FFR was only 0.76, indicating that using a population average CFR for scaling will ***not*** provide accurate results for individuals whose CFR deviates from the average. We also found that that steady-state CFD estimates of FFR are equivalent to transient CFD estimates for a given CFR value. The impact of these results is that a *population-average* CFR value will not yield accurate simulations of FFR on a patient-specific basis. However, since the time-dependent hyperemic flow patterns are not needed to the accurately simulate FFR, CFR could be determined by another modality (PET, MRI) and applied to coronary anatomy determined by CT or MRI.

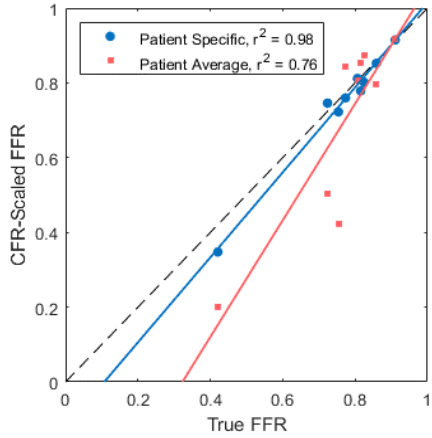

True FFR versus CFR-scaled FFR using patient specific CFR and patient cohort average CFR. Patient specific values have a much higher correlation than patient cohort averge (0.98 vs 0.76).

Conclusions

Patient-specific CFR is required to accurately predict FFR using non-invasive imaging and CFD, but time-dependent hyperemic flow waveforms are not needed.

References

1. Tonino, P.A., et al. New England Journal of Medicine, 2009. 2. De Bruyne, B., et al. N Engl J Med, 2012. 3. Ahn, S.G., et al. JACC Cardiovasc Interv, 2017.

Manipulating shear rate patterns in the common femoral artery using acute continuous and interval exercise

Abigail L. Cook [1], Gemma K. Lyall [1], Paul C. Evans [2], Karen M. Birch [1]

[1] School of Biomedical Sciences, University of Leeds, UK. [2] University of Sheffield, UK.

Introduction

Cardiovascular disease (CVD) is one of the leading causes of mortality in the Western world, responsible for 25% of all deaths in the UK alone [1]. Atherosclerosis is the underlying pathology to CVD, an early indicator of which is endothelial dysfunction. Shear stress (SS) regulates endothelial function and endothelial cell phenotype and can be assessed via ultrasound as vascular shear rate (SR). SR represents the frictional force of blood flowing over the endothelium, with retrograde SR being associated with proatherogenic effects on the endothelium [2]. Exercise increases SR and thus can influence endothelial function and phenoptype, however, the impact of continuous (CON) and interval (INT) exercise upon patterns of anterograde (ANT) and retrograde (RET) SR is unknown. The purpose of this study was to examine SR patterns during CON and INT exercise in the common femoral artery (CFA) and determine the subsequent effect upon acute endothelial function.

Methods

10 young healthy individuals (25±3 years; 5 male, 5 female) completed a ramp incremental exercise test on a supine cycle ergometer to determine lactate threshold. Following this test, on separate days, two intensity-matched exercise sessions at 125% lactate threshold (1 CON [12 mins, 116 ±24 W], 1 INT [1 min exercise,1 min rest for 24 mins at 164 ±37 W) on a supine cycle ergometer. ANT and RET SR were measured in the CFA by Doppler ultrasound at regular intervals during a brief (30 s) cessation in exercise in both training sessions. CFA flow-mediated dilation (FMD) was measured pre- and 10 minutes post-exercise to assess the acute effect of the two protocols upon endothelial function.

Results

ANT SR and RET SR increased from rest to exercise, reached a plateau and did not change further throughout either CON or INT exercise (P>0.05). Peak and mean ANT SR were higher in the INT than CON, however this did not reach statistical significance (peak: 1480±510 s^{-1} *vs* 1258±403; mean: 1358±469 *vs* 1171±372 s^{-1}, respectively; P>0.05). RET SR peak and mean did not differ between protocols (peak: 108±75 *vs* 107±123 s^{-1}, mean: 54±55 *vs* 61±81 s^{-1} P>0.05). Total ANT SR was higher in the INT than CON protocol (INT: $1.95x10^6$ $\pm6.74x10^5$ *vs* CON: $8.61x10^5$ $\pm2.91x10^5$ s^{-1}: P<0.05), whilst total RET SR did not differ (INT: $7.81x10^4$ $\pm7.86x10^4$ *vs* CON: $7.66x10^4$ $\pm8.93x10^4$ s^{-1} P>0.05). No time was spent in pure oscillatory shear (>0.5 AU) in either exercise protocol. FMD did not differ pre- to post-exercise in either CON or INT protocol (CON: 9.9±8.1% *vs* 8.4±6.2%; INT: 9.1±5.9% *vs* 6.6±3.4%: P>0.05).

Conclusions

During exercise matched for intensity and duration of muscular work, INT exercise produced a greater volume of ANT SR than CON, however this did not translate to an acute improvement in FMD post-exercise. Importantly, exercise in an interval fashion using one minute intervals did not enhance oscillatory shear, and thus no acute impairment in endothelial function was seen.

References

1. BritishHeartFoundation. *BHF Statistics Factsheet - UK*. 2018 [cited 2019 12/02/2019]; Available from: https://www.bhf.org.uk/what-we-do/our-research/heart-statistics/heart-statistics-publications.
2. Thijssen, D.H., et al., *Retrograde flow and shear rate acutely impair endothelial function in humans.* Hypertension, 2009. **53**(6): p. 986-92.

Shear-induced maturation of human pluripotent stem cell-derived endothelial cells towards an arterial subtype[1]

Jing Ying Adele Lam[1,2], Seep Arora[1,3], Christine Cheung[6,7], Evelyn KF Yim[8], Yi-Chin Toh[1,,3,4,5]

1. Department of Biomedical Engineering, National University of Singapore, Singapore
2. Department of Bioengineering, Imperial College London, London, United Kingdom
3. Singapore Institute for Neurotechnology (SINAPSE), National University of Singapore, Singapore
4. Biomedical Institute for Global Health Research and Technology (BIGHEART), National University of Singapore, Singapore
5. NUS Tissue Engineering Program, National University of Singapore, Singapore
6. Lee Kong Chian School of Medicine, Nanyang Technical University, Singapore
7. Institute of Molecular and Cell Biology, Agency for Science, Technology and Research, Singapore, Proteos, Singapore
8. Department of Chemical Engineering, University of Waterloo, Waterloo, ON, Canada

Introduction

Human pluripotent stem cell-derived endothelial cells (hPSC-ECs) present an attractive alternative to primary endothelial cell sources for clinical vascular grafting applications. However, hPSC-ECs are functionally heterogeneous and thus require additional factors to mature towards either an arterial or venous subtype [2]. Although the arterio-venous specification of ECs during early embryonic development is largely genetically predetermined, the maintenance and further development of the ECs' arterial/venous identity is regulated by shear stress after the onset of flow. There have been a few attempts to employ adult arterial shear stress conditions to induce vascular maturation of hPSC-ECs. However, hPSC-ECs are naïve to shear stress and their shear-induced responses are still not well understood. Therefore, this study aimed to investigate the shear-induced responses of ECs over a wider range of shear stress magnitudes coincidental with physiological levels of embryonic and adult vasculatures.

Methods

A six-channel microfluidic system was developed and used to systematically investigate the dose-time shear responses on hPSC-ECs morphology and arterial/venous phenotypes, over a shear stress range of 0.4-15 dyne/cm^2.

Results

It was found that hPSC-ECs required up to 40 hours of shear stress exposure to elicit a stable phenotypic change. Cell alignment was visible at shear stress <1 dyne/cm^2 and was independent of the magnitude and duration of exposure, which is indicative of the naivety of the hPSC-ECs to shear stress. The arterial markers NOTCH1 and EphrinB2 exhibited a dose-dependent increase in a similar manner beyond a threshold level of 3.8 dyne/cm^2, whereas the expression of venous markers COUP-TFII and EphB4 displayed no statistically significant variations across different magnitudes.

Conclusions

The results suggest that hPSC-ECs were sensitive to relatively low magnitudes of shear stress but required at least 40 hours of culture under flow conditions to initiate phenotypic changes indicative of vascular maturation. Although shear stress had no apparent effect on the expression of venous EC markers of hPSC-ECs, it may be that a critical level of ~4 dyne/cm^2 could be used in future vascular tissue engineering applications to preferentially enhance maturation of these cells into an arterial phenotype.

References

1. Arora, S., et al., *Determination of critical shear stress for maturation of human pluripotent stem cell derived endothelial cells towards an arterial subtype.* Biotechnology and Bioengineering, 2018. **0**(ja).
2. Rufaihah, A.J., et al., *Human induced pluripotent stem cell-derived endothelial cells exhibit functional heterogeneity.* American Journal of Translational Research, 2013. **5**(1): p. 21-35.

Vimentin regulates Notch signaling strength and arterial remodeling in response to hemodynamic forces

Adolfo Rivero-Müller, Nicole C.A. van Engeland, Tommaso Ristori, Camille L. Duran, Marika Sjöqvist, Oscar M.J.A. Stassen, Daniel Antfolk, Saku Ruohonen, Suvi T. Ruohonen, Salla Nuutinen, Eriika Savontaus, Sandra Loerakker, Kayla J. Bayless, John Eriksson, Carlijn V. Bouten, Cecilia M. Sahlgren

Department of Biomedical Engineering, Eindhoven University of Technology, Eindhoven, the Netherlands

Åbo Akademi University, Faculty of Science and Engineering, Biosciences, Turku, Finland

Introduction

The arterial vessel wall is a multicellular structure with an endothelial cell (EC) sheet surrounded by a layered contractile structure of vascular smooth muscle cells (VSMCs), interlayered with extracellular matrix. The vascular wall is subjected to hemodynamic forces like shear stress and strain, and arteries form and adapt their structure depending on the hemodynamic environment. In response to changes in blood flow, ECs lining the vessel lumen communicate with VSMCs via Notch signalling pathways to regulate the formation and remodelling of the wall architecture, which is required to maintain mechanical homeostasis. However, the underlining mechanisms linking mechanics to Notch signalling are mostly unknown. Intermediate filament (IF) proteins are critical mechanical cellular components that maintain cell and tissue integrity and are involved in transferring mechanical forces from the cell membrane to the nucleus. Vimentin, a mesenchymal IF, regulates actin stress fibre assembly and contractility and is found in high content in larger arteries such as the aorta and carotid artery. The vimentin network in ECs reorganizes in response to shear stress and is important for vascular integrity and flow induced arterial dilation and remodelling. Given the known role of IFs as signaling scaffolds and regulators of the morphogenic processes, here we raised the question if vimentin could serve as hub integrating mechanics and Notch signaling in vascular remodeling.

Methods

To assess if vimentin plays a role in arterial remodeling, we ligated the left carotid artery of wildtype (VimWT) and vimentin knock out (VimKO) mice *in vivo*, and analyzed the arterial structure, and expression of VSMC markers in the contralateral artery after 4 weeks. We next analyzed the effect of vimentin deletion on the expression of Notch ligands, receptors and target genes in the remodeling artery via experimental and computational techniques. To further assess the importance of vimentin in regulating the VSMC phenotype, we used an *ex vivo* aortic ring assay. Aortae from VimWT and VimKO mice were harvested, cut into rings, embedded into collagen, and fed medium supplemented with VEGF to induce endothelial sprouting. Furthermore, to assess how vimentin affects Jagged1 signaling we exposed ECs to shear stress and VSMCs to uniaxial strain *in vitro.*

Results

In this study we show that vimentin is essential for Notch mechanotransduction and arterial remodelling. Vimentin interacts with the Notch ligand Jagged and is important for transactivation of Notch under mechanical stimuli and for Notch-mediated mechanoresponses. Loss of vimentin leads to disrupted Notch mechanotransduction and deregulated expression of Notch ligands and receptors. VimKO mice display disorganized and stiffer arteries with disrupted responses to contractile and relaxation stimuli and adverse remodelling with reduced VSMC coverage. We show that dedifferentiation of VSMCs and tissue homeostasis can be explained by reduced Jagged-Notch transactivation as demonstrated by a computational model of Notch signalling in the arterial wall and by experimental data. Notch re-activation by recombinant Jagged1 ligands rescues VSMC coverage and differentiation in VimKO aortic outgrowths.

Conclusions

Our findings identify vimentin as a central part of a mechanochemical transduction pathway and suggest that targeting mechanosensitive Notch regulators may lead to new strategies to control structural homeostasis of cardiovascular tissues.

c-Rel drives atherosclerosis at sites of disturbed blood flow by activating inflammatory and proliferative transcriptional programmes in endothelium.

Blanca Tardajos Ayllón[1], Fiona Oakley[2], Paul C. Evans[1]

[1]Department of Infection, Immunity and Cardiovascular disease/ INSIGNEO Institute for In Silico Medicine/ the Bateson Centre, University of Sheffield, Sheffield, UK. [2]Medical School, Newcastle University, Newcastle, UK

Introduction
Atherosclerosis is an inflammatory disease that develops preferentially at bends and branches of the vasculature exposed to disturbed flow and low shear stress (LSS). Shear stress modifies endothelial cell (EC) function by regulating proliferation, inflammation and other fundamental processes. Shear stress alters multiple transcriptional programs, including those regulated by the NF-κB family of transcription factors. Although some members of the NF-κB pathway are known to respond to shear, the influence of haemodynamics on the c-Rel NF-κB subunit and its role in atherogenesis are unknown, and are a focus of the current study.

Methods
C57BL/6 wildtype and c-Rel knockout mice were used to quantify the expression of c-Rel, the proportion of proliferating EC (using anti-Ki67 antibodies) and the inflammatory adhesion protein E-Selectin at LSS and high shear stress (HSS) regions of the murine aortic arch. To establish the role of c-Rel in atherosclerosis, C57BL/6 wildtype and c-Rel knockout mice were treated with AAV-PCSK9, exposed to a western diet for 6 weeks, and stained with Oil Red O to quantify lesions. *In vitro* studies were performed using human umbilical vein EC (HUVEC) or human coronary artery EC (HCAEC), which were exposed to flow for 72 hours and c-Rel protein was measured by Western blotting. The expression of c-Rel was silenced in HUVEC under LSS using siRNA and effects on EC proliferation and expression of inflammatory markers were measured by staining of PCNA and qRT-PCR, respectively. To elucidate the mechanism by which c-Rel regulates these processes, gene expression was studied using a microarray in HUVEC treated with a c-Rel siRNA to silence c-Rel or with a scrambled control siRNA. Differentially expressed genes under LSS were annotated using DAVID.

Results
En face staining of murine aortas revealed that c-Rel was enriched at LSS regions compared to HSS regions ($P<0.01$). c-Rel genetic deletion in mice resulted in decreased proliferation and reduced expression of E-Selectin in EC exposed to LSS ($P<0.05$), indicating that c-Rel promotes EC proliferation and inflammation under LSS. c-Rel genetic deletion also reduced lesion area in AAV-PCSK9-treated mice, indicating that c-Rel promotes atherosclerosis ($P<0.05$). These observations were recapitulated in cultured HUVEC and HCAEC, which showed enrichment of c-Rel under LSS compared to HSS by Western blotting ($P<0.05$). Moreover, depletion of c-Rel by siRNA in HUVEC resulted in decreased proliferation and expression of inflammatory markers in EC exposed to LSS ($P<0.05$). Microarray studies and subsequent validation experiments revealed that c-Rel positively regulates multiple genes implicated in inflammation and proliferation, including components of the MAPK (e.g. p38, TXNIP; $P<0.05$) and non-canonical (e.g. RANK; $P<0.05$) NF-κB signalling pathways, among others.

Conclusions
Our data demonstrate that c-Rel promotes EC pathophysiological changes at LSS regions and is a driver of atherosclerosis. Studies in cultured EC revealed that c-Rel activates numerous genes including components of MAPK and non-canonical NF-κB pathways, thereby providing a potential mechanism for its proinflammatory and proproliferative effects.

A pivotal role for Nrf2 in endothelial detachment– implications for endothelial erosion of stenotic plaques

Sandro Satta[1], Michael McElroy[2], Alex Langford Smith[1], Glenn R Ferris[1], Jack Teasdale[3], Yongcheol Kim[4], Giampaolo Niccoli[5], Tom Tanjeko Ajime[6], Jef Serré[6], Georgina Hazell[3], Graciela Sala Newby[3], Ping Wang[7], Jason L Johnson[3], Martin J Humphries[8], Ghislaine Gayan-Ramirez[6], Peter Libby[9], Filippo Crea[5], Hans Degens[1], Frank Gijsen[10], Thomas Johnson[11], Amir Keshmiri[2], Yvonne Alexander[1], Andrew C Newby[3], Stephen J White[1]

[1] Department of Life Sciences, Manchester Metropolitan University, Manchester M1 5GD UK
[2] School of Mechanical, Aerospace and Civil Engineering (MACE), The University of Manchester, Manchester, M13 9PL, UK
[3] Bristol Heart Institute, University of Bristol, Bristol BS2 8HW, UK
[4] Department of Cardiovascular Medicine, Chonnam National University Hospital, Dong-gu, Gwangju, 61469 Republic of Korea
[5] Fondazione Policlinico Universitario A. Gemelli IRCCS, Roma, Italia; Universita' Cattolica del Sacro Cuore, Roma, Italia
[6] Laboratory of Pneumology, Department of Chronic Diseases, Metabolism and Ageing, KULeuven, Leuven, Belgium
[7] Bioinformatics Core Facility, Faculty of Biology, Medical and Health, University of Manchester
[8] Wellcome Centre for Cell-Matrix Research, Faculty of Biology, Medicine & Health, University of Manchester, Manchester, M13 9PT, UK
[9] Brigham and Women's Hospital, Harvard Medical School, Boston, MA 02115 USA
[10] Department of Cardiology, Biomedical Engineering, Erasmus MC, Rotterdam, The Netherlands
[11] Department of Cardiology, Bristol Heart Institute Upper Maudlin St. Bristol BS2 8HW

Introduction

Endothelial erosion of atherosclerotic plaques and resulting thrombosis causes approximately 30% of acute coronary syndromes (ACS). Plaque erosion is most frequently observed in smokers, which exacerbates endothelial dysfunction, partially through elevated circulating mediators of inflammation, such as tumour necrosis factor-alpha (TNFα), as well as free radical, oxidative and chemically induced damage. For example, we have previously demonstrated that fresh aqueous cigarette smoke extract (CSE) increases the expression of Nrf2-target genes in human coronary artery endothelial cells, which was further increased by TNFα in a shear stress-dependent manner.

Methods

The haemodynamic environment significantly regulates both plaque development and endothelial function; therefore, we determined the haemodynamic environment permissive for plaque erosion. We reconstructed the coronary artery geometries from 17 heart attack patients with thrombi overlying intact fibrous caps (OCT-defined erosion) and performed computational fluid dynamic analysis. We created an in vitro model of erosion by culturing human coronary artery endothelial cells under elevated flow and exposing them to aqueous cigarette smoke extract and TNFα.

Results

We identified that in 14 cases of OCT-defined erosion occurred in areas of stenosis, with the preeminent flow feature being elevated flow. Exposing human coronary artery endothelial cells to elevated flow, CSE and TNFα induced significant endothelial detachment, which was enhanced by pharmacological activation of the antioxidant system controlled by transcription factor Nrf2. The Oxidative Stress Growth INhibitor genes OSGIN1 and OSGIN2 were both maximally upregulated under these conditions and also in the aortas of mice exposed to cigarette smoke. Adenoviral overexpression of OSGIN1+2 in static culture resulted in cell cycle arrest in S-phase (5.5-fold increase, p= 0.003), with a significant increase in the number of multinucleated cells (4.5-fold, p= <0.001). Immunocytochemical analysis indicated loss of focal adhesions and stress fibres, dysregulation of autophagy and induction of senescence in HCAEC, with a significant increase in senescence-associated β-galactosidase staining (6.7-fold, p= <0.001) and P16 expression (3.2-fold, p= 0.035). Importantly, overexpression of either Nrf2, or OSGIN1+2 induced cell detachment, which was independent of apoptosis, and could be rescued by inhibition of HSP70 nucleotide binding site using VER-155008, or AMPK activation using Metformin.

Conclusions

In summary, we have defined the haemodynamic environment in which endothelial erosion occurs and identified that smoking-induced hyperactivation of Nrf2 may promote endothelial cell detachment, contributing to plaque erosion overlying stenotic plaques, through the combined upregulation of OSGIN1 and OSGIN2. This highlights a completely novel mechanism potentially contributing to 30% of acute coronary syndromes and suggests possible therapeutic avenues for further investigation. (https://www.biorxiv.org/content/10.1101/537852v1)

A numerical study of smooth muscle cell sensitivity in vascular remodeling

Lauranne Maes[1], Julie Vastmans[1], Stéphane Avril[2], Nele Famaey[1]

[1]KU Leuven, Belgium; [2]Ecole des Mines de Saint-Etienne, France

Introduction

The mechanosensitive responses of smooth muscle cells (SMC) play an essential role in vascular remodeling. SMC in their contractile phenotype respond by contracting or relaxing to restore the homeostatic wall (shear) stress. On a longer time scale, contractile SMC change to a synthetic state under sustained nonphysiological loading. These SMC produce extracellular matrix, allowing for a continuous turnover of collagen content. The balance between degradation and production determines the vascular remodeling process. In this study, the response rate of SMC to an altered loading condition is tested numerically.

Methods

As described in [1], sheep underwent a surgery in which the pulmonary artery (PA), under pulmonary arterial pressure (P_P), is placed in aortic position, under systemic pressure (P_S). Six months later, samples of the graft were extracted and tested mechanically and histologically. An inhomogeneous loading pattern resulted in a significantly thickened section on one side and a section that had not increased in thickness on the other side. This experiment was simulated in Abaqus 2017, in which a virtual artery was pressurized up to the homeostatic P_P. Next, the artery was brought to P_S and allowed to remodel. The numerical implementation of the growth and remodeling algorithm, described in [2], was modified to allow for a variation in the amount and sensitivity of the synthetic SMC. Two extreme cases were considered. In the low sensitivity case (LSC), the SMC are made completely insensitive to the ambient stress state, and produce collagen as usual. In the high sensitivity case (HSC), an increased stress state triggers a switch in phenotype and an increased collagen production rate to the physical maximum of the SMC. In parallel, an analytic experiment was performed, in which two questions were investigated: for an artery with a given content of elastin, SMC and collagen, and when the pressure rises from P_P to P_S, (1) what would be the resulting diameter increase of the artery for a fixed tissue composition, and (2) what would be the required increase in collagen to maintain the original diameter? The first question relates to the low response case and the second to the high response case.

Results

Figure 1 shows the evolution in time of the arterial diameter (top right) and of the total collagen content (bottom right) for 4 cases, namely the high and low sensitivity cases that were tested numerically (nHSC and nLSC), and the corresponding two analytical cases (aHSC and aLSC). The left images show histological slices with H&E staining of baseline PA (A) and the two different types of remodeled PA after six months under systemic pressure (B and C).

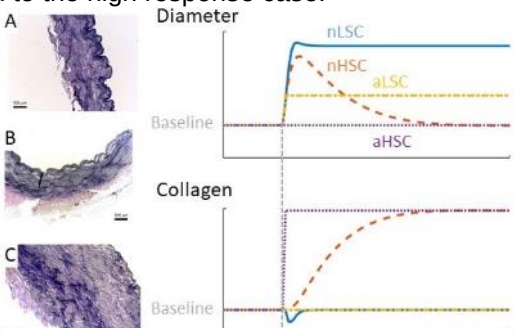

Figure 5: Evolution of arterial diameter and collagen content during remodeling [1]

Conclusions

Tuning the sensitivity of the SMC will yield a different remodeling response of the artery, whereby both extremes were also noticed experimentally in [1].

References

[1] Vanderveken E, Vastmans J, Verbelen T, Verbrugghe P, Famaey N, Verbeken E, Treasure T, Rega F, Reinforcing the pulmonary artery autograft in the aortic position with a textile mesh: a histological evaluation, *Interactive CardioVascular and Thoracic Surgery*, 27(4), 566-573, 2018.

[2] Famaey N, Vastmans J, Fehervary H, Maes L, Vanderveken E, Rega F, Mousavi SJ, Avril S, Numerical simulation of arterial remodeling in pulmonary autografts, *Mathematical and Computational Modeling in Biomechanics*, 98(12), 2239-2257, 2018.

Acknowledgements

This work was supported by the Research Foundation Flanders (SB1S35316N, 11A6519N, PDO/012) and by a KU Leuven project (C2-ADAPT).

Multidirectional wall shear stress promotes development of coronary plaques with vulnerable characteristics – a pre-clinical imaging and histopathological study

Ayla Hoogendoorn[1], Annette M. Kok[1], Eline M.J. Hartman[1], Claudio Chiastra[2], Lorena Casadonte[3], Adriaan Coenen[1], Suze-Anne Korteland[1], Kim van der Heiden[1], Frank J. H. Gijsen[1], Dirk J. Duncker[1], Antonius F.W. van der Steen[1], Jolanda J. Wentzel[1]

[1] Departments of Cardiology and Radiology, Erasmus MC, Rotterdam, The Netherlands
[2] Laboratory of Biological Structure Mechanics, Department of Chemistry, Materials and Chemical Engineering "Giulio Natta", Politecnico di Milano, Milan, Italy
[3] Department of Biomedical Engineering and Physics, Amsterdam UMC, Amsterdam, The Netherlands

Introduction

Wall shear stress (WSS) has been widely associated with plaque development and destabilization. However, the multidirectionality of WSS, induced by the pulsatile nature of blood flow in combination with the arterial geometry, is rarely taken into account. The purpose of this study was to investigate the influence and predictive value of five (multidirectional) WSS parameters on coronary plaque progression and composition.

Methods

Familial hypercholesterolemic pigs (n=10, castrated male, 3 years old) were put on a high-fat diet and underwent imaging of the three main coronary arteries at 3, 9 and 12 months follow-up. Local flow velocity measurements were combined with a 3D-geometry of the arterial lumen to calculate baseline WSS. For the analysis, arteries were divided into 3mm/45° sectors (n=3627) and WSS metric values were divided in vessel-specific tertiles. Changes in wall thickness (WT) and plaque composition were assessed with NIRS-IVUS and OCT imaging, and histology.

Results

Half of the pigs developed lumen intruding, complex, lipid-rich plaques. Plaque growth and the presence of lipids (detected by NIRS, OCT or histology) and necrotic core (histology) at the last time point were associated with baseline low and multidirectional WSS ($p<0.05$) (Fig. 1). All multidirectional WSS metrics, except the transverse WSS, had a good predictive value for the development of plaque (WT>0.5mm) (43-50%) and this value was even higher for the development of advanced fibrous cap atheroma: 49-61%.

Conclusions

This study demonstrates that both low and multidirectional WSS promote the development of large and complex coronary atherosclerotic plaques with vulnerable characteristics. The high predictive values for fibrous cap atheroma development demonstrate the potential of multidirectional WSS metrics as a predictive clinical marker for vulnerable disease.

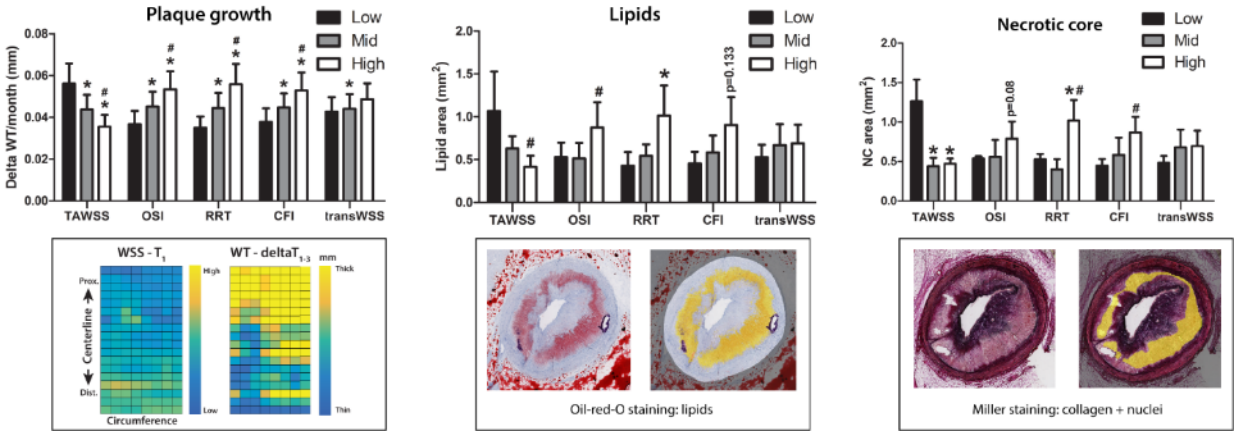

Fig. 1: Association between (multidirectional) WSS metrics and plaque growth, and histological plaque composition (lipid and necrotic core (NC) area). Time-averaged WSS (TAWSS); oscillatory shear index (OSI); relative residence time (RRT); cross-flow index (CFI); transverse WSS (transWSS). *p<0.05 compared to 'low', #p<0.05 compared to 'mid'.

Endothelial Sox17 is critical for maintaining adult artery phenotype and enhances arterial response to hemodynamic flow

Diana Kim, Guohao Dai

Department of Bioengineering, Northeastern University, Boston, MA, USA

Introduction

Arterial and venous endothelial cells (ECs) exhibit distinct molecular profiles, which contribute to their structural and functional differences and ultimately disease processes[1]. The establishment of such molecular distinction is orchestrated by series of transcriptional programs during early vascular development and further regulated by extracellular matrix (ECM) and hemodynamic environment throughout the life. The transcriptional regulation of arterial venous differentiation has been well studied in developmental biology. However, how these transcriptional programs control adult blood vessel function and their roles in vascular diseases remain elusive.

Methods

To address this question, we examined the transcription profile of arterial *vs*. venous ECs in adult blood vessels and have identified several key transcription factors that are most differentially expressed in arterial *vs*. venous ECs. Among them, Sox17 are highly expressed in adult arterial ECs but not in venous ECs. We then generated Tet-on lentiviral system to precisely induce the expression of Sox17 in ECs, and then investigated Sox17-dependant EC phenotypes, EC-SMC crosstalk as well as SMC phenotypes.

Results

Over-expressing Sox17 reprograms venous ECs toward arterial ECs by reconstitutes all the known arterial markers and downregulating venous markers (**Fig. 1**). Sox17 also significanly enhances arterial markers in response to arterial flow (**Fig. 2**). Importantly, Sox17 induces the expression of multiple families of molecules (Notch, Ephrin, Connexins, PDGF) that may confer signals from ECs to smooth muscle cells (SMCs) to regulate SMC phenotypes in blood vessels. To confirm this, in EC-SMC co-culture, EC-Sox17 significantly enhances the SMC contractile phenotype by upregulating α-SMA, SM22-α, calponin 1 and PDGFR-β, as well as elastin and decorin (**Fig. 3**), the critical ECM components of artery.

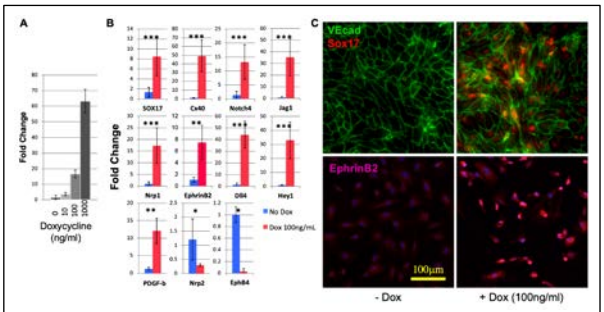

Figure 1. Sox17 reprograms venous ECs toward arterial ECs. (A) Sox17 gene expression at increasing doxycycline doses; (B) Gene expression levels of HSVECs transduced with Tet-On Sox17 lentivirus and treated with or without 100ng/mL doxycycline for 2 days. Rn18s served as endogenous control. n=3, Student's *t*-test, **p*<0.05, ***p*<0.01, ****p*<0.001; (C) Immunofluorescent staining of Sox17 and EphrinB2 in Sox17-HSVECs treated with or without doxcycyline for 2 days.

Conclusions

Our data suggests that EC Sox17 is a key regulator of arterial function by maintaining arterial EC phenotype, enabling response to arterial flow and engaging EC-SMC crosstalk. This study has broad implications in vascular diseases where homeostatic regulation of arterial remodeling is impaired, such as stenosis, aneurysm and pulmonary arterial hypertension. In addition, because Sox17 is missing in vein graft, re-introducing Sox17 may help to improve the arterialization of vein graft, as well as to design better tissue engineered vascular graft.

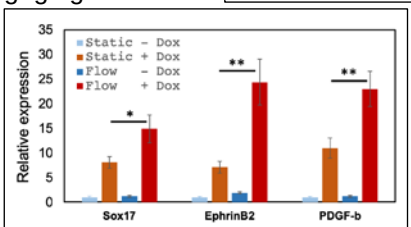

Figure 2. Sox17 enhances EC's response to hemodynamic flow. HSVECs with the Tet-on Sox17 were cultured under static or arterial flow for 72 hours, with or without Dox. Gene expression was analyzed by RT-PCR, n=3, **p*<0.05, ***p*<0.01.

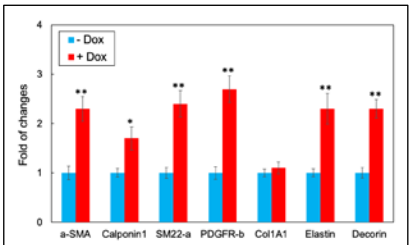

Figure 3. EC Sox17 enhances SMC contractile phenotypes in EC-SMC co-culture. HSVECs with Tet-on Sox17 were co-cultured with aortic SMCs in transwell, SMC gene expression was analyzed by RT-PCR. n=3, **p*<0.05, ***p*<0.01.

Reference:

1. Niklason L and Dai G. Arterial Venous Differentiation for Vascular Bioengineering. *Annu Rev Biomed Eng*. 2018;20:431-447.

Increasing Membrane Tension Transiently Reduces Syndecan-1 Expression through Actin Remodelling

Weiqi Li and Wen Wang

Institute of Bioengineering, School of Engineering and Materials Science, Queen Mary University of London, London UK

Introduction

The endothelial glycocalyx, located at the interface of vascular lumen, is a carbohydrate-rich complex that controls vascular functions such as solute permeation, neutrophil extravasation and mechanotransduction. It anchors to the cell membrane through core proteins, e.g. syndecan-1, which closely couple to the actin cytoskeleton. Membrane tension plays an important role in the reorganisation of membrane-bound proteins, however, little is known on the effect of the membrane tension on the various components of the glycocalyx. In the current study, we aim to investigate how membrane tension affects syndecan-1 expression.

Methods

Membrane tension is manipulated using hypo-osmotic shock (standard medium: 313 mOsm, hypo-osmotic medium: 283 mOsm, 255 mOsm and 167 mOsm). Syndecan-1 is visualised using immunostaining and determined by reading fluorescence intensity in confocal images. Actomyosin dynamics is examined using phalloidin staining in combination with cytoskeletal drugs including cyotochalasin D, jasplakinolide and blebbistain.

Results

Our results show that following 20 min exposure to the hypo-osmotic medium, the expression of syndecan-1 become 103.8 ± 2.9% (285 mOsm), 84.7 ± 3.6 % (255 mOsm) and 64.7 ± 2.1 % (167 mOsm). This reduction, however, is transient and partial recovery is observed at the end of 2 h exposure to the hypo-osmotic medium. The transient reduction of syndecan-1 is associated with depolymerisation of the actin cytoskeleton. Further examination of the effect of actin manipulation reveals that actin depolymerisation by cytochalasin D results in sustained syndecan-1 reduction. In contrast, stabilising actin using jasplakinolide abolishes the transient reduction of syndecan-1 completely. In addition, we find that the transient response is not affected when actomyosin contractility is inhibited by blebbistatin.

Conclusions

Taken together, we demonstrate, for the first time, that membrane tension plays an important role in the regulation of syndecan-1 expression and this effect is through controlling the reorganisation of the actin cytoskeleton. Our findings suggest a new venue of research to better understand the protective role of the glycocalyx in vascular pathophysiology and diseases.

Uniaxially sheared endothelial cells secrete mediators that reduce inflammation and endothelial permeability

Mean Ghim, Kuin T Pang, Peter D Weinberg

Department of Bioengineering, Imperial College London, London, UK

Introduction

Endothelial permeability to circulating macromolecules and patterns of haemodynamic wall shear stress (WSS) vary from site to site within the arterial system. Influences of local blood flow on macromolecule transport across the endothelium may account for the patchy nature of atherosclerosis. To investigate this relation, endothelial cells grown in multiwell plates can be swirled on an orbital shaker, thus inducing chronic WSS that varies depending on location within the well[1]. Ghim et al. suggested cells in one region of the well may release mediators into the medium which affect the behaviour of all cells and confound results[2]. We developed a method that allows culture and shearing of endothelial cells only in specific regions to obtain conditioned medium (CM), and subsequently investigated the effects of CM on paracellular and transcellular permeability to macromolecules and inflammation of endothelial cells.

Methods

PDMS masks were used to confine gelatin to specific areas within the wells and achieve region-specific gelatin coating. The mask was removed, the uncoated surface was passivated with a pluronic solution and porcine aortic endothelial cells (PAECs) were cultured and swirled. To study permeability, CM was collected and applied to static cultures of PAECs grown on biotinylated gelatin and either FITC-conjugated avidin (FITC-A) or Quantum dot 800 conjugated streptavidin (Qdot800) was applied above the monolayer for a short duration and removed. Tracer accumulation under cells was quantified using a plate reader. To study inflammation, static cultures of PAECs were preconditioned with CM and challenged with TNF-α for 24h. Translocation of NF-κB p65 in the nuclei was quantified by immunofluorescence, expression of VCAM-1, IκBα and phospho-IκBα were quantified by western blots and finally monocyte adhesion assays were performed.

Results

CM from PAECs confined to the edges of the well, exposed to uniaxial WSS, reduced Qdot800 but not FITC-A permeability of PAEC monolayers compared to monolayers treated with CM from PAECs grown at the centre of the well, exposed to multidirectional WSS. Nuclear NF-κB p65, expression of VCAM-1 and phospho-IκBα/IκBα and the number of adhered monocytes were lower for PAECs preconditioned with CM collected from sheared cells grown at the edge of wells and treated with TNF-α compared to monolayers preconditioned with CM collected from sheared cells grown at the centre of the well.

Conclusions

Our study suggests CM from endothelial cells exposed to uniaxial WSS contain a mediator(s) which decreases transcellular transport and inflammatory effects of TNF-α on endothelial cells, giving mechanistic insight into the role of shear stress in atherosclerosis and suggesting treatment strategies. This study was funded by the British Heart Foundation.

References

1. Warboys CM, Eric Berson R, Mann GE, Pearson JD, Weinberg PD. Acute and chronic exposure to shear stress have opposite effects on endothelial permeability to macromolecules. *Am J Physiol Heart Circ Physiol*. 2010;298:H1850-6.
2. Ghim M, Alpresa P, Yang S, Braakman ST, Gray SG, Sherwin SJ, van Reeuwijk M, Weinberg PD. Visualisation of three pathways for macromolecule transport across cultured endothelium and their modification by flow. *Am J Physiol Heart Circ Physiol*. 2017;ajpheart.00218.2017.

On the role played by wall shear stress in the alteration of biomechanical properties of ascending thoracic aortic aneurysms

Francesca Condemi, Salvatore Campisi, Magalie Viallon, Pierre Croisille and Stéphane Avril

Mines Saint-Etienne, Univ Lyon, Univ Jean Monnet, INSERM, U 1059 Sainbiose, Centre CIS, F - 42023 Saint-Etienne, France

Introduction

Ascending thoracic aortic aneurysm (aTAA) is a major cause of human deaths. Despite important recent progress to better understand its pathogenesis and development [1], the role played by deranged hemodynamics on aTAA risk of rupture is still partially unknown [2]. The aim of this study is to obtain crucial indications about this role by combining for the first time all together *in vivo*, *in vitro* and *in silico* analyses.

Methods

Computational fluid dynamic (CFD) analyses were performed and validated on 10 patients using patient-specific data derived from CT scan and 4D MRI. The systolic wall shear stress (WSS), the time-averaged wall shear stress (TAWSS), the flow eccentricity and the helicity intensity were assessed [3]. A bulge inflation test was carried out *in vitro* on the 10 aTAA samples resected during surgical repair. The biomechanical and rupture properties of these samples were derived: the burst pressure, the physiological tangent elastic modulus, the Cauchy stress at rupture, the rupture stretch ($\lambda rupt$) and the rupture stretch criterion [4]. Parametric and non-parametric statistical analyses were performed to determine correlation between all variables.

Results

Statistically highly significant ($p<0.01$) positive correlation between $\lambda rupt$ and the TAWSS ($r=0.867$ and $p=0.001$) was found.

Conclusions

Understanding the pathogenesis of aTAA remains crucial to reduce the morbidity and mortality, therefore deriving relevant biomarkers will permit to plan elective surgery repairs as timely as possible. This study showed that large TAWSS may have globally a protective effect in aTAA as they are related to larger rupture properties.

References

[1] Michel J-B, Jondeau G, Milewicz DM, From genetics to response to injury: vascular smooth muscle cells in aneurysms and dissections of the ascending aorta, *Cardiovascular Research*, 114:578-589, 2018.

[2] Guzzardi DG, Barker AJ, Van Ooij P, Malaisrie SC, Puthumana JJ, Belke DD, Collins, J. Valve-related hemodynamics mediate human bicuspid aortopathy: insights from wall shear stress mapping. *Journal of the American College of Cardiology*, 66(8):892-900, 2015.

[3] Condemi F, Campisi S, Viallon M, Troalen T, Xuexin G, Barker AJ, Duprey A, Avril S. Fluid-and biomechanical analysis of ascending thoracic aorta aneurysm with concomitant aortic insufficiency. *Annals of biomedical engineering*, 45(12), 2921-2932, 2017.

[4] Duprey A, Trabelsi O, Vola M, Favre J-P, Avril S. Biaxial rupture properties of ascending thoracic aortic aneurysms. *Acta biomaterialia*, 42:273-285, 2016.

Towards the Establishment of Lesion-specific Stenting Strategies: Correction of Curvature Induced OCT Image Distortion is Required for Accurate 3D Reconstructions of Deployed Coronary Stents

Mark R. Elliott[1], David S. Molony[2], Brigham R. Smith[3], Sarang Joshi[1,4], Habib Samady[2], Lucas H. Timmins[1,4]

1 Department of Biomedical Engineering, University of Utah, Salt Lake City, UT, USA
2 Division of Cardiology, Emory University School of Medicine, Atlanta, GA, USA
3 Division of Cardiovascular Medicine, University of Utah School of Medicine, Salt Lake City, UT, USA
4 Scientific Computing and Imaging Institute, University of Utah, Salt Lake City, UT, USA

Introduction

Vascular stent implantation leads to alterations in the mechanical environment that provoke pathobiological responses and contribute to device failure [1,2]. The extension of previous computational efforts to the clinical setting are limited by a lack of understanding of the *in vivo* deployed stent geometry. To advance efforts in establishing lesion-specific stenting strategies, the aim of this investigation was to extend our recently developed reconstruction framework [3] and reconstruct the *in vivo* 3D post-deployed stent geometry through the fusion of angiographic and optical coherence tomography (OCT) image data.

Methods

Biplane coronary angiography and OCT image data from patients (n=2) undergoing percutaneous coronary intervention were analyzed. Stent struts were automatically identified in the OCT images utilizing a classifier based on unique signal characteristics, resulting in a 3D point cloud of the deployed stent (OCT_{PC}). Examination of the OCT_{PC} revealed an angular (circumferential) distortion of image orientation that appeared to depend on vessel curvature. To determine the relationship between angular distortion and curvature, a torsion-free experimental test bed with machined channels of constant curvature was manufactured. OCT image data were acquired in each channel, and linear regression analysis performed to identify a relationship between curvature and angular distortion per mm (i.e., *correction factor*). The *correction factor* was applied to the *in vivo* derived OCT_{PC} prior to fusion with angiography data. MicroCT derived wireframe models of identical stent designs to those deployed *in vivo*, but rather deployed in open-air, were created. Each wireframe was spatially co-registered to the corresponding OCT_{PC}, and the wireframe was deformed to the OCT_{PC} through a constrained iterative deformation process directed by diffeomorphic metric mapping [3].

Results

A positive correlation was observed between curvature and the magnitude of angular distortion. For curvature values of 0, 1/60, 1/30, and 1/20 mm^{-1}, the average angular distortion per mm of pullback was 0.10º ± 0.06º, -0.05º ± 0.02º, -0.24º ± 0.05º, and -1.0º ± 0.05º, respectively ($p<0.05$). Linear regression demonstrated the relationship between curvature (κ) and angular drift per mm (Δdeg) as $\Delta deg = -21\kappa + 0.23$. Implementation of the angular distortion *correction factor* into the stent reconstruction algorithm had an observable effect on the OCT_{PC}. The angular distortion in the two implanted stent designs were -0.75º ± 0.41º and -0.95º ± 0.57º per mm that resulted in accumulated angular distortions of -29.6º and -18.2º, respectively, at the proximal end of the stents. Strong agreement between the deformed wireframe and OCT_{PC} was identified, which demonstrated the importance in accounting for angular distortion, and the resulting geometry was a continuous, high-resolution geometry of an *in vivo* deployed vascular stent.

Conclusions

This investigation highlights the influence that vessel curvature has on OCT image angular (circumferential) distortion, and the requirement for distortion correction when reconstructing a deployed vascular stent from OCT image data. Future computational studies that integrate this reconstruction framework hold tremendous potential in establishing lesion-specific stenting strategies.

References

[1] Timmins, LH et al., *Lab. Invest.*, 91:955-967, 2011; [2] Duraiswamy, N et al., *J. Biomech. Eng.*, 131:061006, 2009; [3] Elliott, MR et al., *IEEE Trans. Med. Imaging*, (in press)

A Novel Approach for Heterogenous Material Characterization of Atherosclerotic Plaques

Ronald D. van den Berg[1], Stephane Avril[2], Frank J.H. Gijsen[1], Ali C. Akyildiz[1]

[1] Department of Biomedical Engineering, Erasmus MC, Rotterdam, the Netherlands

[2] Centre for Biomedical and Healthcare Engineering, Mines Saint-Etienne, Saint-Etienne, France

Introduction

Atherosclerotic plaque rupture, a major cause of fatal cardiovascular events, is demonstrated to correlate with high structural plaque stresses [1]. Hence, plaque stress analyses are of great value and can support clinical rupture risk assessment in the future. Accuracy of the computational stress analyses depend on the correct representation of heterogenous plaque material properties in the models [2]. Current techniques for material parameter estimation, such as inverse FE modelling [3], have large computational costs (hours or days). This study aims to develop and validate a novel approach based on virtual fields method (VFM) [4] to much faster obtain heterogenous plaque properties.

Methods

VFM is a mechanical energy balance approach that employs the virtual work principle and utilizes 2D or 3D full-field deformation measurements of the investigated structure [4]. The analytical equations, obtained by prescribing multiple kinematically admissible virtual deformation fields for the energy balance equation, are solved for unknown material stiffness parameters. The prescription of the virtual fields is a key point in VFM as it depends on the particular loading and deformation of the investigated structure.

In this study, firstly a set of appropriate virtual displacement fields that allows application of the VFM approach for component-wise stiffness characterization in atherosclerotic arteries were identified. As VFM is used for plaque characterization for the first time, we then performed a validation study where synthetic experimental full-field plaque deformation maps were computed with finite element (FE) plaque models of ten realistic human carotid plaque geometries. Computed deformation maps were then used as input for the developed VFM approach. VFM-estimated plaque stiffness values were finally compared against the ground truth stiffness prescribed in the FE models.

Results

Appropriate virtual deformation fields were identified and the VFM approach was successfully developed for this particular application of heterogeneous plaque tissue characterization. VFM very successfully estimated the stiffness values of all plaque components for all ten plaque geometries. The VFM- estimated stiffness values with the highest average error were 732 kPa (vs ground truth: 720 kPa) for fibrous tissue, 1548 kPa (vs. 1500 kPa) for wall, 42 kPa (vs. 30 kPa) for lipid and 2704 kPa (vs. 2500 kPa) for calcified tissue. The highest absolute error was obtained for the calcified tissue (204 kPa) with a relative error of 8%. The VFM evaluations took <5 min using a custom-developed MATLAB code in a decent PC (Intel i7, single core, memory=16 GB).

Conclusions

In this study, VFM was used for the first time for atherosclerotic plaque mechanical characterization. The validation analysis showed high accuracy of the VFM approach for this particular application. The computational time required for the VFM approach was in the order of minutes, much shorter than the alternatives such as inverse FE approach, which might take hours or days. These findings demonstrate the great potential of the developed VFM technique for heterogeneous plaque characterization in-vivo, where full-field plaque deformation measurements can be obtained with MRI or ultrasound.

References

[1] Cheng G C et al., *Circulation*, 87.4: 1179-1187, 1993. [2] Akyildiz, A et al., *Biomed Eng Online*, 10:25, 2011. [3] Akyildiz, A et al., *Annals Biomed Eng*, 44(4):968, 2016. [4] Pierron, F; Grediac,M, *Springer*, ”The virtual fields method”, 2012.

High LDL filtration rate and plaque development in intracranial arteries: a computational study

Haipeng Liu[1,2], Dingchang Zheng[1], Xinyi Leng[2], Linfang Lan[2], Hing Lung Ip[2], Thomas Wai Hong Leung[2]

[1]Faculty of Health, Education, Medicine and Social Care, Anglia Ruskin University, Chelmsford, Essex, UK
[2] Department of Medicine and Therapeutics, The Chinese University of Hong Kong, Shatin, Hong Kong, China

Introduction
Low-density lipoprotein (LDL) plays an important role in the growth of atherosclerotic plaques. LDL filtration rate could be estimated by the 3-pore model based on computational fluid dynamics (CFD). The coronary studies indicated the relationship between the high LDL filtration rate (LDLfr) and atherosclerotic plaque growth [1]. However, there is a scarcity of the studies on the relationship between LDLfr and intracranial atherosclerotic plaque growth.

Methods
Three-dimensional geometric models were rebuilt from the CTA imaging of 39 intracranial arteries with symptomatic stenosis due to atherosclerotic plaques. The CFD simulations and the calculation of LDLfr were performed on the baseline models, based on our former study with parameters of the 3-pore model adjusted as the cerebrovascular ones [1]. The high LDLfr areas were compared with corresponding areas in follow-up geometric models. Observable changes in radius larger than 0.2mm or 1/4 of the radius of the former geometry were viewed as reduction or enlargement of existing plaques or newly-developed atherosclerotic stenoses.

Results
In the 39 cases, we observed reduction and enlargement of existing plaques in 10 and 7 cases respectively. In other 22 cases, there were only mild changes of existing plaques. In the cases with reduction and mild changes of existing plaques, high LDLfr appeared in 59 areas of which 4 were colocalized with newly developed plaques. In the cases with enlargement of existing plaques, there were 20 areas with high LDLfr, in which 8 and 3 colocalized respectively with enlargement of existing plaques and newly-developed stenoses. In some cases, the colocalization between areas with high LDLfr and the plaque growth could be observed in detail

Conclusions
The accordance between high LDLfr and plaque growth existed in some intracranial arteries, especially those with the growth of existing plaques. Although promising, this relationship is limited to a few cases and needs large-scale validation.

References
[1] Liu H, Gong Y, Leng X, et al. Estimating current and long-term risks of coronary artery in silico by fractional flow reserve, wall shear stress and low-density lipoprotein filtration rate[J]. *Biomedical Physics & Engineering Express*, 2018, 4(2): 025006.

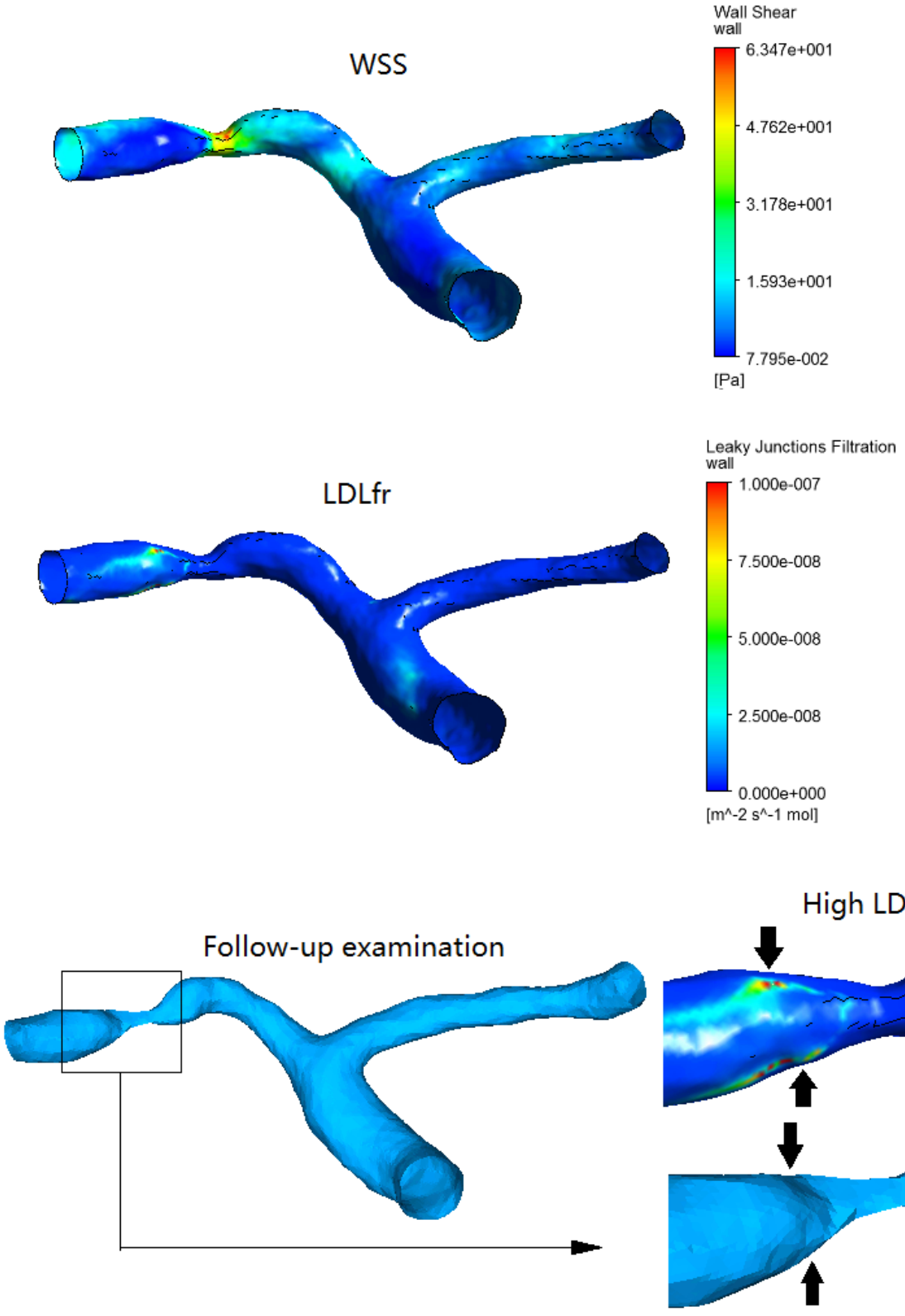

Figure 1. The WSS and LDLfr distributions of an intracranial arterial model. In the middle cerebral artery, the areas with high LDLfr colocalize with plaque growth areas.

Mechanical Predictors of Atherosclerotic Plaque Rupture

Beyond "Where Stress, There Rupture"

Daniel M.A. Rutten[1], Marina S. Ferguson[2], Thomas S. Hatsukami[3], Frank J.H. Gijsen[1], Ali C. Akyildiz[1]

[1] Department of Biomedical Engineering, Erasmus MC, Rotterdam, the Netherlands

[2] Department of Radiology & [3] Department of Surgery, University of Washington, Seattle, USA

Introduction

Majority of acute cardiovascular events are precipitated by atherosclerotic plaque rupture[1]. Plaque rupture occurs when the structural integrity of plaque tissue is compromised by an overwhelming mechanical load. Hence, plaque biomechanics are key to predicting rupture. Seminal biomechanical modelling studies demonstrated colocalisation of rupture and the concentration of a mechanical metric, the circumferential stress[2,3]. Subsequent research has mostly focused on improving modelling techniques and the acquisition of (imaging-)data. However, there has been little-to-no investigation into the rupture-predictive power of alternative mechanical metrics. This study performs colocalisation-analyses for a comprehensive selection of mechanical metrics to identify their predictive power for rupture risk and improve our fundamental understanding of rupture mechanisms.

Methods

A total of ten mechanical stress, strain, and energy metrics were selected for computational finite element modelling, based on a unique histopathological dataset of ruptured carotid plaques (n=30)[4], with a minimal morphological change. This allowed replication of pre-rupture geometry, a hard-to-find feature for such analyses. Segmentation of the histology images for the structural components (i.e calcification, necrotic core, fibrous tissue, intraplaque haemorrhage, and arterial wall) produced plaque geometries for the models. In addition, the histology images were processed through a custom-made image-processing tool for detecting intra-plaque collagen fibres. This enabled implementation of local fibre orientation and dispersion for anisotropic plaque material behaviour for the first time. In the end, colocalisation analyses of rupture sites with the mechanical metrics obtained from the computational models were performed.

Results

Ten of the twelve ruptures (83%) analysed so far showed colocalisation with at least one mechanical metric. Two metrics had sensitivity below 50% and the average sensitivity of the metrics was 58% (64% without the two <50% metrics). Not a stress metric, but a strain metric, the "fibre-shear strain" had the highest sensitivity (75%). Furthermore, "fibre-shear strain" was the only predictor for one rupture case.

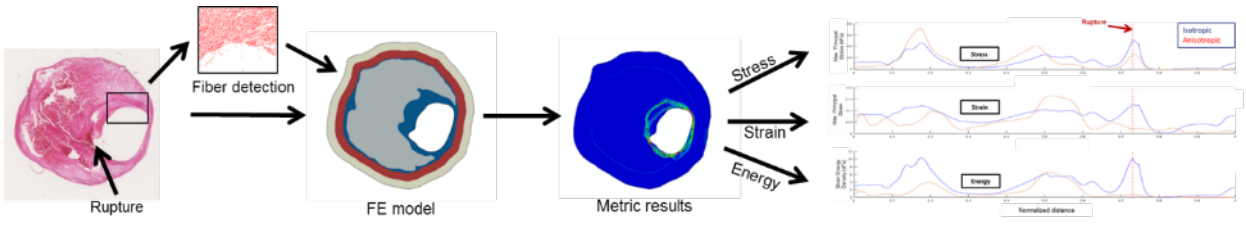

Figure: Workflow from histology to colocalization analyses

Conclusions

The overall success of the mechanical metrics for rupture colocalization highlights once more the great role of local mechanics in plaque rupture. The high sensitivity of the anisotropic fibre-shear strain supports the previously-posited delamination-based damage mode[4]. Furthermore, reliable strain-based predictors may promote the application of biomechanical results in clinical settings, since strain measurements are possible with recent advancements in ultrasound and MR imaging. Analysis of the remainder of the dataset planned as the next step is expected to strengthen these results.

References

[1] Falk et al. 2013, *European Heart Journal*, 34(10): 719-728. [2] Cheng et al. 1993, *Circulation*, 87(4):1179-1187. [3] Richardson et al. 1989, *The Lancet*, 334(8669):941-944. [4] Daemen et al. 2016, *Atherosclerosis*, 254:102-108.

Effect of Calcification & Fibrous Tissue Features on Atherosclerotic Plaque Rupture Risk

Bas Vis, Hilary Barrett, Astrid Moerman, Frank J.H. Gijsen, Ali C. Akyildiz

Department of Biomedical Engineering, Erasmus MC, Rotterdam, the Netherlands

Introduction

Atherosclerotic plaque rupture is demonstrated to correlate with high mechanical plaque stresses[1]. A highly prevalent structural component in plaques is calcification. Recent histopathological examinations[2] demonstrated plaque ruptures spanning from calcification-fibrous tissue interface, a potential stress concentration location[3]. However, the calcification-fibrous tissue interface mechanics has not been studied in detail before. The current study investigates stresses at the calcification-fibrous tissue interface, their dependency on local fibrous tissue anisotropy and the calcification geometry.

Methods

First, morphometric analyses were conducted to identify the calcification geometric features regarding its shape, size and location and the fiber alignment around the calcifications from H&E histology images (n=65) of carotid endarterectomy samples (n=16). Normalized radial location, D_{norm} (distance to lumen/plaque thickness); normalized width, W_{norm} (radial width/plaque thickness) and aspect ratio, *AR* (circumferential length/radial width) of the calcifications were measured. Subsequently, computational stress analyses for an intraluminal pressure of 140 mmHg were performed, with the local fibrous tissue anisotropy[4] and measured calcification morphometry incorporated. Maximum plaque tissue stresses at the calcification-fibrous tissue interface were computed and analyzed for potential correlations to the three morphometric features (D_{norm}, W_{norm}, and *AR*) and fiber orientation.

Results

In the 65 histology cross-sections 145 calcifications were examined. Four distinct fiber patterns in the fibrous plaque tissue surrounding calcifications were identified (Figure): 1) "a*ttached*" pattern (40% prevalence), 2) "encircling" pattern (25% prevalence), 3) "p*ushed aside*" fiber pattern (15% prevalence), and 4) "*random*" pattern (10% prevalence). The radial location of the calcifications showed great variation for all fiber patterns but the "*random*" pattern, which was located more abluminally (high D_{norm}). "A*ttached*" pattern clearly showed presence around larger (high W_{norm}) and more slender (high *AR*) calcifications than the other patterns. The computational stress analyses demonstrated that the "*attached"* pattern has significantly greater maximum tissue stress (median [Q1:Q3] = 274 [155:535] kPa) than the other patterns (median for "*pushed aside*" = 85 kPa, and <5 kPa for "*encircling*" and "*random*"), which is about the previously-reported plaque strength level[1]. Multivariate regression analyses revealed that W_{norm} and *AR* correlate significantly and positively and D_{norm} negatively with stress, implying that larger and/or slender calcifications located juxtaluminally have higher interface stresses.

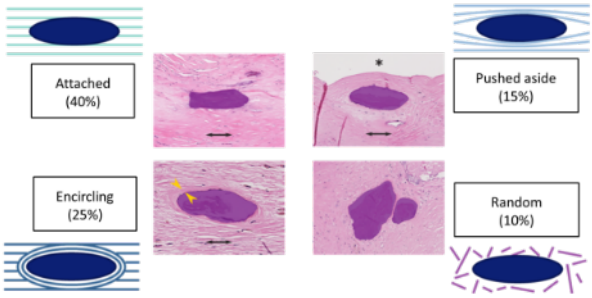

Figure: Four distinct fiber patterns of the plaque tissue surrounding calcifications

Conclusions

This first comprehensive morphometric and stress analyses showed that calcification-tissue interface stresses can reach levels considered as high risk for rupture[1], providing mechanistic explanation for the histopathological rupture observations at calcification interfaces[2]. Large and slender calcifications with "a*ttached*" fiber pattern located juxtaluminally showed the highest risk for high stresses.

References

[1] Cheng, G et al, *Circulation*, 87:4, 1993. [2] Daemen, M et al., *Atherosclerosis*, 254:102, 2016. [3] Buffinton C et al, *CVET*, 5:244, 2014. [4] Douglas, G et al., *Annals of Biomed Eng*, 45:1462, 2017.

Prognostic implications of endothelial shear stress distribution estimated in three-dimensional quantitative coronary angiography models: A combined analysis of the PROSPECT and IBIS 4 studies

Christos V. Bourantas,[1,2,3] MD, PhD; Thomas Zanchin,[1,4,5] MD; Ryo Torii,[5] PhD; Patrick W. Serruys,[6] MD, PhD; Alexios Karagiannis,[7] PhD; Anantharaman Ramasamy,[1,3] MBChB, MRCP; Ahmet Umit Coskun,[8] PhD; Gerhard Koning,[9] MSc; Yoshinobu Onuma,[10] MD, PhD; Rob Krams,[11] MD, PhD; Anthony Mathur,[1,3] MD, PhD; Andreas Baumbach,[1,3] MD, FRCP; Stephan Windecker,[4] MD; Alexandra Lansky,[2,13] MD; Akiko Maehara,[12] MD; Peter H. Stone, MD; Lorenz Raber,[4] MD, PhD; Gregg W. Stone,[12] MD

[1] Department of Cardiology, Barts Heart Centre, Barts Health NHS Trust, London, UK
[2] Institute of Cardiovascular Sciences, University College London, London, UK
[3] William Harvey Research Institute, Queen Mary University London, UK
[4] Department of Cardiology, Bern University Hospital, Bern, Switzerland
[5] Department of Mechanical Engineering, University College London, London, UK
[6] Faculty of Medicine, National Heart & Lung Institute, Imperial College London, UK
[7] CTU Bern, Institute of Social and Preventive Medicine, Bern University, Bern, Switzerland
[8] Mechanical and Industrial Engineering, Northeastern University, Boston, MA, USA
[9] Medis Medical Imaging Systems bv, Leiden, The Netherlands
[10] Department of Interventional Cardiology, Thoraxcenter, Erasmus Medical Center, Rotterdam, The Netherlands
[11] Department pf Molecular Bioengineering, Engineering and Material Sciences, Queen Mary University London, London, UK
[12] Department of Cardiology, Columbia University Medical Center and the Cardiovascular Research Foundation, New York, NY
[13] Division of Cardiovascular Medicine, Department of Internal Medicine, Yale School of Medicine, New Haven, CT
[14] Cardiovascular Division, Brigham & Women's Hospital, Harvard Medical School, Boston, MA

Aims: To evaluate the potential value of endothelial shear stress (ESS) distribution estimated in three-dimensional quantitative coronary angiography (3D-QCA) models in detecting high-risk plaques.

Methods: In this post hoc analysis of the PROSPECT and IBIS 4 trials we analysed the baseline intravascular ultrasound virtual histology (IVUS-VH) and angiographic data from 28 non-culprit lesions with a vulnerable phenotype (i.e., fibroatheroma or thin cap fibroatheroma) that caused major adverse cardiac events or required revascularization (nc-MACE-R) at 5-year follow-up and from a control group of 119 vulnerable plaques that remained quiescent. The segments in interest that was assessed by IVUS-VH at baseline was identified in coronary angiography and reconstructed using a well validated 3D-QCA software. In the obtained geometries blood flow simulation was performed and the resting Pd/Pa across the vulnerable plaque and the mean ESS values in 3mm sub-segments were estimated. A propensity score was built by the baseline plaque characteristics and the hemodynamic indices and its efficacy in detecting nc-MACE-R lesions was examined.

Results: Lesions that required revascularization or cause events were longer, had smaller minimum lumen area (MLA), increased plaque burden (PB), were exposed to higher ESS, and exhibited a lower resting Pd/Pa. In multivariable analysis the maximum 3mm ESS value (hazard ratio: 1.08, P=0.016) was the only independent predictor of nc-MACE-R. The revascularization and the event rate was higher in lesions exposed to high ESS (>4.95Pa) with a high-risk anatomy (MLA<4mm^2 and PB>70%) (53.8%) than those with a low-risk anatomy exposed to high ESS (31.6%) or those exposed to low ESS that had high (20.0%) or low-risk anatomy (7.1%, P<0.001).

Conclusions: 3D-QCA-derived local hemodynamic variables appear to provide useful prognostic information and in combination with lesion anatomy enable more accurate identification of nc-MACE-R lesions.

Impaired ALK1 mechanotransduction and inflammation converge on Connexin37 (Cx37) to permits high-flow arteriovenous shunting

Hanna M Peacock [1], Nathan Criem [1], Ashkan Tabibian[1] Vincenza Caolo [2], Lauriane Hamard [3], Jacques-Antoine Haefliger [3], Brenda R Kwak [4], An Zwijsen [1], Elizabeth AV Jones [1*]

[1] Department of Cardiovascular Sciences, Centre for Molecular and Vascular Biology, KU Leuven, Belgium.
[2]Leeds Institute of Cardiovascular and Metabolic Medicine, School of Medicine, University of Leeds, UK.
[3]Department of Medicine, Centre Hospitalier Universitaire Vaudois, University of Lausanne, Switzerland. [4] Department of Pathology and Immunology, University of Geneva, Switzerland

Introduction
High-flow shunts between arteries and veins, known as arteriovenous malformations (AVMs), are caused by disruptions of the ALK1/Endoglin/SMAD1/4/5 signaling pathway. This pathway is activated by BMP9/10 as well as by shear stress. Given the incomplete penetrance of AVMs in HHT, a "second hit" has been proposed to be necessary in AVM development, though the exact nature of this stimuli is unknown.

Methods
Endothelial cells were exposed to flow with and without active BMP signalling and shear-specific targets of BMP signalling were identified by RNASeq. Formation of AVMs in response to various stimuli was evaluated using en embryo culture model with mice that had an endothelial-specific deficiency in Smad signalling.

Results
We identify *GJA4* (Connexin37; Cx37) as a mechanotransduced target of ALK1 signaling. Cx37 expression is induced by BMP9 but repressed by the addition of shear stress. In developing embryos, Cx37 is present in non-remodeling yolk sac vasculature. We examined whether inflammation might act as a "second hit" to disrupt Cx37 expression. Indeed, low concentrations of TNFα abolished BMP9-induced Cx37 expression in vitro. TNFα treatment resulted in Cx37-negative regions between the forming arterial and venous trees in the yolk sac vasculature of cultured mouse embryos with reduced ALK1 or endothelial SMAD1/5 signaling. TNFα also robustly induced AVM formation in these embryos. In inflammation, Cx37 is upstream of Cox2 regulation and Cox2 expression is known to be elevated in AVMs. We found that COX2 inhibitor celecoxib was able to prevent embryos from developing TNFα-induced AVMs.

Conclusions
Our data demonstrate that Cx37 expression is regulated by a combination of shear stress and ALK1 signaling. We further demonstrate that inflammation causes a localized loss of Cx37 and is a "second hit" to permit AVM development. These data suggest that localized disruption of Cx37 is permissive to capillary dilation and AVM formation in HHT, and that COX2 inhibitors may prevent or even treatment of AVMs.

An MRI-based pipeline to register patient-specific wall shear stress data to histology

Astrid M. Moerman, Kristine Dilba, Suze-Anne Korteland, Dirk H.J. Poot, Stefan Klein, Jolanda J. Wentzel, Kim van Gaalen, Ellen V. Rouwet, Aad van der Lugt, Antonius F.W. van der Steen, Frank J.H. Gijsen and Kim van der Heiden

Department of Biomedical Engineering, Erasmus MC, Rotterdam, The Netherlands

Introduction

Atherosclerosis is characterised by the accumulation of lipid and inflammatory cells in the arterial wall, resulting in plaque formation. Although risk factors for atherosclerosis are systemic in nature, plaques develop at specific sites in the arterial tree. At these predilection sites the blood-exerted wall shear stress (WSS) is low, resulting in activation of pro-inflammatory pathways in endothelial cells, which initiates plaque formation. At more advanced stages of the disease, the plaque intrudes into the lumen, affecting local WSS patterns. WSS increases on the upstream side and throat of the lumen-intruding plaque, while WSS remains low on the downstream side. We hypothesise that alterations in the WSS patterns during plaque growth influence plaque composition and play a role in plaque destabilisation. To investigate the relation between WSS and atherosclerotic plaque composition, we developed a pipeline to register wall shear stress data to the corresponding 2D histological cross sections of human carotid plaques.

Methods

As input parameters for the WSS map we obtained in vivo lumen geometry by MR imaging using a black blood stabilised 3D FSE sequence, as well as patient-specific time-dependent in- and outlet flow profiles, measured by 3D PC-MRI. A mesh was generated after manual lumen segmentation. CFD simulations were performed according to standard numerical procedures and 3D wall WSS maps were generated.
Of that same patient, the carotid plaque was surgically removed after *in vivo* MRI. The excised plaque was imaged *ex vivo* by MRI and was cut into 1 mm segments, which were each histologically processed and cut into 5 µm sections. We visualised plaque components using histochemical staining procedures (haematoxylin-eosin and resorcin-fuchsin) and also identified markers of plaque vulnerability, i.e. cap thickness, necrotic core size and macrophage infiltration.
The image registration method required four types of plaque images: (1) *in vivo* MRI, (2) *ex vivo* MRI, (3) photographs of transversally sectioned 1mm plaque tissue segments and (4) histology images. These images are transformed to a shared 3D image domain by applying a combination of rigid and non-rigid registration algorithms. Transformation matrices obtained from registration of these images are used to transform subject-specific WSS data to the shared 3D image domain as well. WSS values originating from the 3D WSS map are visualised in 2D on the corresponding lumen locations in the histological sections and divided into eight radial segments. In each radial segment, the correlation between WSS values and plaque composition based on histological parameters can be assessed.

Results and Conclusions

We successfully implemented this registration pipeline on carotid endarterectomy samples of two patients. We are currently applying this method to a larger dataset in order to investigate the correlation between WSS and plaque composition.

Inflammatory Activation of Endothelial Cells Induced by Disturbed Flow is Regulated by Frizzled-4 and β-catenin via a Non-Canonical Pathway

Matthew Rickman, Mean Ghim, Maciã Sureda-Vives, Ana Cristina Rocha, Elena Drudi, Kuin Pang, Peter Weinberg, Christina Warboys

Department of Bioengineering, Imperial College London, London, UK

Introduction
The development of cardiovascular disease is strongly influenced by local mechanical forces. Endothelial cells are sensitive to haemodynamic stresses, and in particular to perturbations of flow direction. Atherosclerotic plaques develop in regions of arteries where flow is multi-directional or 'disturbed'; such flow is known to promote endothelial dysfunction, although the signalling mechanisms responsible are not fully understood. The Wnt/β-catenin pathway plays an important role in mechanosignalling in non-vascular cells; in this study, its role in mediating the effects of disturbed flow on human aortic endothelial cells was explored.

Methods
Cells seeded into 6-well plates were exposed to flow for 72h using an orbital shaker housed inside an incubator. The swirling of the medium with each rotation of the platform creates two distinct flow environments within each well: an area in the centre exposed to disturbed flow (DF) and a region around the edge exposed to undisturbed flow (UF). Flow metrics within each region were determined by computational fluid dynamics using STAR-CCM+. Following exposure to flow, cells were harvested from each region and either RNA or protein was prepared for qRT-PCR or western blot, respectively. For immunofluorescence studies, cells were fixed directly in glass-bottomed wells and imaged by confocal microscopy.

Results
The expression of Frizzled-4 was significantly increased in cells exposed to DF for 72h, as was the expression and transcriptional activity of β-catenin. Interestingly, this was not associated with activation (phosphorylation) of Lrp-6, suggesting that β-catenin is activated by a non-canonical pathway. Increased expression of Frizzled-4 protein was associated with increased expression of R-spondin-3 that protects Frizzled receptors from ubiquitin-mediated degradation. Knockdown of either Frizzled-4 or β-catenin significantly reduced the expression of pro-inflammatory transcripts (E-sel, MCP-1, VCAM-1) in cells exposed to DF, and this was associated with reduced activation and nuclear localisation of NF-κB. Similar effects were observed when cells were treated with iCRT5, an inhibitor of β-catenin transcriptional activity. Treatment with iCRT5 also reduced the adhesion of THP-1 monocytes to endothelial cells exposed to DF, confirming the importance of β-catenin activation in mediating inflammatory responses to DF. Treatment with DKK-1, an inhibitor of canonical Wnt signalling, had no effect on the expression of pro-inflammatory genes, NF-κB activity or monocyte adhesion under DF conditions, suggesting that the canonical Wnt-Fzd pathway is not involved in these responses.

Conclusions
These data suggest the involvement of a novel Frizzled-4-β-catenin mechanosignalling pathway in endothelium exposed to DF that promotes a pro-inflammatory phenotype.

This work was supported by The British Heart Foundation

The effect of confounding factors on flow mediated dilation: a novel computational study using one-dimentioanal blood flow modelling

Weiwei Jin[1], Phil Chowienczyk[2], Jordi Alastruey[1]

[1]Department of Biomedical Engineering, [2]Department of Clinical Pharmacology, King's College London, London, UK

Introduction

Dysfunction of endothelial cells lining the inner part of blood vessels is a major cause of blood vessel degeneration leading to cardiovascular diseases such as diabetes, hypertension, and hypovolemia. A common test for endothelial function assessment is flow-mediated dilation (FMD), which measures the increase in arterial diameter in response to an increase in wall shear stress (WSS) produced by a surge in blood flow, triggered by deflation of a sphygmomanometer cuff around the forearm [1]. The current FMD test assumes that diameter changes are entirely due to WSS changes. However, a recent study showed that diameter changes cannot only be attributed to WSS but are also affected by other confounding factors, such as blood pressure and arterial wall stiffness [2]. The aim of this study is to study the effects of several confounding factors on the results of FMD using computational modelling.

Methods

We used a one-dimensional (1-D) solver [3] to simulate blood flow in the 116 larger arteries of the systemic circulation coupled with a model of vessel-wall motion. The latter was driven by variations in arterial wall Young's Modulus calculated from the change in WSS and blood pressure in the right-arm vasculature. Haemodynamics during cuff inflation and deflation were simulated by prescribing a pressure drop across the right radial and ulnar arteries, and a decrease in the peripheral resistance of the right hand 1-D model arterial segements. The simulated results were ualitatively vertified by comparison against *in-vivo* data acquired in 8 subjects [2].

Results

According to our results, the FMD index is considerably affected by vascular stiffness, peripheral vascular dilation during cuff deflation, mean blood pressure, and the measurement location. FMD increased by 1.8% (i.e. from 8.6% to 10.4%) and decreased by 1.0% when arterial wall stiffness decreased and increased by 25%, respectively. Increasing and decreasing the peripheral vascular dilation by 10% increased and decreased the FMD by 2.8% and 1.9%, respectively. Increasing the central mean blood pressure by 15 mmHg and 30 mmHg, increased the FMD by 2.5% and 3.9%, respectively. We also found that the FMD index is measurement-location dependent within the brachial artery. The FMD result first increased (by 1.9% at the mid-point compared to the inlet), and then decreased (by 1.9% at the outlet compared to the mid-point).

Conclusions

We have successfully developed a distributed-tree numerical model that describes FMD haemodynamcis and investigated 4 confounding factors (vascular stiffness, peripheral vascular resistance, mean blood pressure, and measurement location) that can influence the FMD index. We are currently using our novel model to develop a modified FMD index that is less affected by those confounding factors.

References

[1] J. E. Deanfield, J. P. Halcox, and T. J. Rabelink, "Endothelial function and dysfunction: Testing and clinical relevance," *Circulation*, vol. 115, no. 10, pp. 1285–1295, 2007.

[2] B. Jiang, M. Seddon, H. Fok, A. Donald, and P. Chowienczyk, "Flow-mediated dilation of the radial artery is offset by flow-induced reduction in transmural pressure," *Hypertension*, vol. 57, no. 6, pp. 1145–1150, 2011.

[3] J. Alastruey, K. H. Parker, and S. J. Sherwin, "Arterial pulse wave haemodynamics," *Anderson S 11th Int. Conf. Press. Surges, Virtual PiE Led t/a BHR Group, Chapter 7*, pp. 401–442, 2012.

Flow-dependent regulation of caspase-3 in endothelial cells

Virginia Tajadura*, Marie Haugsten-Hansen*, Vasco Claro*, Julian Evans*, Christina Warboys± and Albert Ferro*

*School of Cardiovascular Medicine & Sciences, British Heart Foundation Centre of Research Excellence, King's College London.
±Department of Bioengineering, Imperial College London.

Introduction
Endothelial cell (EC) apoptosis is associated with the development of atherosclerotic plaques that develop predominantly at sites exposed to low magnitude, multidirectional (disturbed) flow. Therefore, strategies to promote cell survival and prevent apoptosis may be important in reducing cardiovascular disease. In this study, we investigated the regulation of caspase-3, the executor protease, in EC exposed to physiological or atheroprone flow.

Methods
Human umbilical vein endothelial cells (HUVEC) or Human Aortic endothelial cells (HAoEC) were grown in 6-well plates and subjected to flow for 72h on an orbital shaker. Cells were fixed and stained to monitor apoptosis or samples collected from the centre of the well (disturbed flow; DF) or from the edge of the well (undisturbed flow; UF) for mRNA, miRNA and western blot analysis. When necessary, EC were transfected with 50 nM Scr control or β-catenin siRNA at the onset of flow or treated with DMSO or 50 µM iCRT5 (a β-catenin/TCF-LEF inhibitor) for the last 24h under flow.

Results
We performed a transcriptome array to study the expression of apoptosis related genes in human umbilical vein endothelial cells (HUVEC) exposed to undisturbed (UF) or disturbed (DF) flow. A major difference observed was a significant downregulation in the expression of inhibitors of apoptosis in cells exposed to DF compared to those exposed to UF (including several members of the IAP family: NIAP (BIRC1), cIAP-1 (BIRC2), Survivin (BIRC5) and BIRC6 (3.6, 2.0, 1.6 and 2.5 fold change respectively; n=3, $p<0.05$) suggesting that downregulation of anti-apoptotic regulators might be an important mechanism predisposing EC to apoptosis at atheroprone sites. Indeed, HUVEC and HAoEC challenged with inhibitors of β-catenin, a known pro-survival gene in EC, promoted apoptosis in EC exposed to DF, (1.1% DMSO vs 1.7% iCRT5-HUVEC and 1.0% to 1.96%-HAoEC; n=4, $p<0.05$), meanwhile interference with this pro-survival pathway had no effect on apoptosis in EC exposed to UF. In agreement with the higher level of apoptosis observed in EC exposed to DF (1.1% DF vs 0.12% UF; n=6, $p<0.01$), higher levels of cleaved caspase-3 were detected by western blotting in lysates from HUVEC subjected to DF compared to UF (n=3, $p<0.05$). Furthermore we found that the expression of pro-caspase-3 (not cleaved) was 80% lower in EC exposed to UF compared to DF (n=4, $p<0.01$) though caspase-3 mRNA expression showed only a 20% reduction (n=4, $p<0.05$). These data suggest that a post-translational mechanism may regulate the protein expression of caspase-3 to prevent or limit apoptosis and maintain viability under adverse conditions in EC exposed to UF. Interestingly one of the inhibitors of apoptosis upregulated by UF (compared to DF) in HUVEC and HAoEC is the E3 ubiquitin ligase cIAP1 (BIRC2) suggesting that high levels of IAP in EC exposed to UF (in comparison with EC exposed to DF) could be contributing to the degradation of caspase-3 and conferring protection against apoptotic stimuli. Since the mRNA expression of caspase-3 is reduced in UF exposed HUVEC, we also studied the expression of previously described flow-dependent miRNAs that could potentially target the caspase-3 mRNA in EC samples. We found that none of the miRNAs tested was differentially regulated between UF and DF conditions.

Conclusion
Down-regulation of caspase-3 expression and/or activity by increased expression of inhibitors of apoptosis might contribute to maintenance of cell viability in EC exposed to UF.

This work was supported by The British Heart Foundation

GenEPi: Piezo1-based fluorescent reporter for visualizing mechanical stimuli with high spatiotemporal resolution

Sine Yaganoglu[1], Nordine Helassa[2,3], Benjamin M. Gaub[1], Maaike Welling[1,4], Jian Shi[5], Daniel J. Müller[1], Katalin Török[2], Periklis Pantazis[1,4*]

[1]Department of Biosystems Science and Engineering, Eidgenössische Technische Hochschule (ETH) Zurich, 4058 Basel, Switzerland
[2]Molecular and Clinical Sciences Research Institute, St. George's, University of London, UK
[3]Department of Cellular and Molecular Physiology, Institute of Translational Medicine, University of Liverpool, UK
[4]Department of Bioengineering, Imperial College London, South Kensington Campus, London SW7 2AZ, UK
[5]Leeds Institute of Cardiovascular and Metabolic Medicine, LIGHT Laboratories, University of Leeds, Leeds, LS2 9JT, UK
*Correspondence to: Periklis Pantazis, p.pantazis@imperial.ac.uk

Introduction

Mechanosensing is a ubiquitous process to translate external mechanical stimuli into biological responses during development, homeostasis, and disease. However, non-invasive investigation of cellular mechanosensing in complex and intact live tissue remains challenging.

Methods

In order to develop a non-invasive, genetically-encoded fluorescent reporter for mechanical stimuli that is applicable to a wide variety of cells and types of mechanical stimuli, we set out to generate a reporter of Piezo1 activity. In a systematic screen, we generated a library of reporters by fusing five different low-affinity GCaMPs [1,2] (with Kd-s in the 0.6 to 6 µM range) to the C-terminus of human Piezo1. The generated variants were evaluated based on their response to both mechanical stimuli and cytosolic Ca2+ fluctuations that were independent of Piezo1 activity.

Results

Among the candidates tested, we identified one GCaMP-Piezo1 fusion variant that satisfied our requirements, hereby referred to as GenEPi. We show that GenEPi has high specificity and spatiotemporal resolution for Piezo1-dependent mechanical stimuli (incl. including shear stress and compressive forces), exemplified by resolving repetitive mechanical stimuli of spontaneously contracting cardiomyocytes within microtissues, in a non-invasive manner.

Conclusions

In summary, we introduced GenEPi as an intensiometric, genetically-encoded reporter for mechanical stimuli. GenEPi provides a specific and non-invasive functional readout of Piezo1 activity in response to mechanical stimuli. This was achieved by successfully targeting a low-affinity GCaMP to the Ca2+ microdomain near the Piezo1 channel, which resulted in specificity for only Piezo1-dependent Ca2+ signals. GenEPi has a significantly broader applicability as compared to other genetically-encoded mechanical reporters, since Piezo1 has been identified to play a central role for mechanosensation in an increasing number of cell types and contexts[3,4].

References

1 Sun, X. R. *et al.* Fast GCaMPs for improved tracking of neuronal activity. *Nature communications* **4**, 2170, doi:10.1038/ncomms3170 (2013).
2 Helassa, N., Podor, B., Fine, A. & Torok, K. Design and mechanistic insight into ultrafast calcium indicators for monitoring intracellular calcium dynamics. *Scientific reports* **6**, 38276, doi:10.1038/srep38276 (2016).
3 Pathak, M. M. *et al.* Stretch-activated ion channel Piezo1 directs lineage choice in human neural stem cells. *Proc Natl Acad Sci U S A* **111**, 16148-16153, doi:10.1073/pnas.1409802111 (2014).
4 Faucherre, A., Kissa, K., Nargeot, J., Mangoni, M. E. & Jopling, C. Piezo1 plays a role in erythrocyte volume homeostasis. *Haematologica* **99**, 70-75, doi:10.3324/haematol.2013.086090 (2014).

Hemodynamics in the HeartMate 3 under dynamic operating conditions: Of the need to understand the biologic effects of turbulence on blood

Lena Wiegmann[1], Bente Thamsen[2], Diane de Zélicourt[1], Marcus Granegger[2,3], Stefan Boës[4], Marianne Schmid Daners[4], Mirko Meboldt[4], Vartan Kurtcuoglu[1]

[1]The Interface Group, Institute of Physiology, University of Zurich, Zurich, Switzerland, [2]Pediatric Heart Centre, University Children's Hospital Zurich, Zurich, Switzerland, [3]Biofluid Mechanics Lab, Institute for Imaging Science and Computational Modelling in Cardiovascular Medicine, Charité University of Medicine, Berlin, Germany, [4]Product Development Group Zurich, Department of Mechanical and Process Engineering, ETH Zurich, Zurich, Switzerland

Introduction

Ventricular assist devices (VADs), among which the HeartMate 3 (HM3) is the latest clinically approved representative, are often the therapy of choice for patients with end-stage heart failure. Despite reduced occurrence of pump thrombi, rates of stroke and bleeding in HM3 patients remain high. These complications are attributed to the flow field within the VAD, among other factors. One of the HM3's characteristic features is an 'artificial pulse' that changes the rotor speed periodically by 4000 rpm, which is meant to reduce zones of recirculation and stasis. Yet, the hemodynamic consequences of this sudden change in rotor speed remain unexplored.

Methods

Using computational fluid dynamics (CFD), we compared Eulerian and Lagrangian features of the flow fields during constant pump operation, during operation with the 'artificial pulse' and with the effect of the residual native cardiac cycle. CFD simulations employed high spatial and temporal resolution and one-way coupling to a lumped parameter model of the cardiovascular system for physiologic pressure boundary conditions. Pump speed was adjusted to mean cardiac output of 5L/min in all investigated cases. Lagrangian particle tracking and passive scalar advection were implemented to probe blood cell paths and overall pump washout. CFD results were validated against experimental measurements.

Results

Overall, viscous stresses in the HM3 were lower than in other current VADs and we observed good washout in all investigated situations. Compared to a constant pump operation, the 'artificial pulse' had no additional benefit on washout performance, but induced rapid variations in the flow velocity and its gradients. It also substantially increased turbulence and thereby the total stresses (Fig. B2).

Conclusions

The observed good washout appears to reflect a favorable design (e.g. large gap sizes) and fits clinical experience. Although stresses were lower than in other current VADs, they were frequently higher than levels suspected to lead to von Willebrand factor damage and platelet activation. Additionally, the artificial pulse substantially increased total stress, which might contribute to hemocompatibility-related problems observed clinically. While the exact biological consequences of turbulence on cells are yet unclear, the increased turbulence content during dynamic operation might be of clinical relevance.

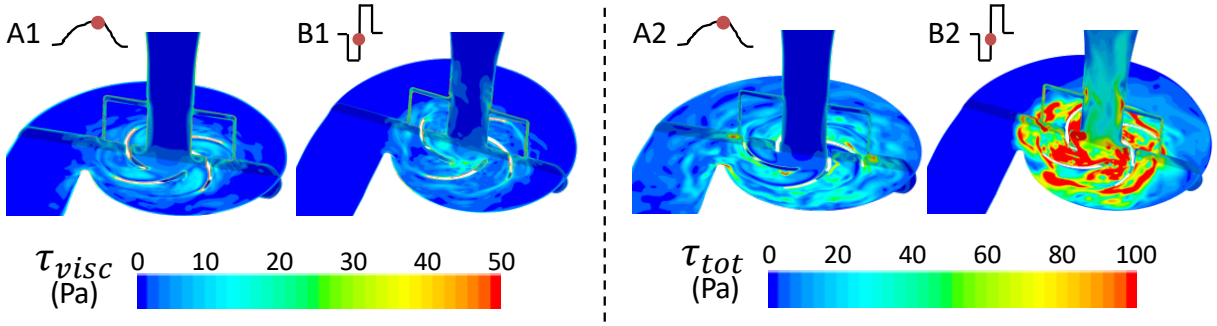

Figure: Comparison of the viscous (Left) and total (Right) stresses in the HeartMate 3 at peak systole of the remaining native cardiac function (A1-2), or during the acceleration phase of the artificial pulse (B1-2).

Flow-responsive Notch signaling modulates EFNB2/EphB4 Axis to promote vascular regeneration

Kyung In Baek[1], Meyrdad Roustaei[1], Chih-Chiang Chang[1], Shyr-shea Chang[2], Marcus Roper[2], Rongsong Li[3], Tzung K. Hsiai[1,4]

[1]Department of Bioengineering, University of California, Los Angeles, Los Angeles, CA 90095
[2]Department of Mathematics, University of California, Los Angeles, Los Angeles, CA 90095
[3]College of Health Science and Environmental Engineering, Shenzhen Technology University, Guangdong, China
[4]School of Medicine, Division of Cardiology, University of California, Los Angeles, Los Angeles, CA 90095

Introduction

Vascular disease characterized by ischemic reperfusion and myocardial infarction are significant causes of morbidity and mortality [1]. A plethora of studies highlighted pathologic blood flow is one of the central risk factors of vascular injury subsequently after initial ischemic insult. However, molecular events underlying vascular injury and regeneration remains elusive. Zebrafish is an emerging model organism in biomedical research due to constructive cardiovascular regenerations and a genome that bears the similarity to human's. [2, 3] The Notch signaling involves in a series of cellular proliferation and angiogenic sprouting. [4] Notch activation in the endothelium further plays a pivotal role in cell-fate determination by promoting the expression of arterial endothelial marker, ephrinB2 (EFNB2) in the endothelial cells (EC). [5] In this context, we seek to investigate whether hemodynamic shear forces facilitate vascular regeneration post injury and whether Notch activation determines vascular fate in regenerating vessel by modulating EFNB2-EphB4 axis.

Methods

To investigate whether hemodynamic shear force is implicated in Notch signaling-mediated vascular regeneration, the transgenic *Tg(tp1:eGFP; flk1:mCherry)* line was utilized to assess spatiotemporal variations of endothelial Notch activation during vascular regeneration. After the initial collection of the embryos, viscosity and consequent endothelial wall shear stress in zebrafish embryos were genetically manipulated by micro-injecting control *p53* morpholino oligonucleotide (MO), *Gata1a* MO, or erythropoietin (*epo*) mRNA. At 3 days post fertilization (dpf), embryos from each group were randomly chosen and immobilized in 0.02% tricaine solution (Sigma-Aldrich, MO) for mechanical tail amputation. Vascular regeneration in conjunction with Notch activity were z-scanned for 4 days under confocal microscope (Leica, Gemany). Variations of time-average velocity of the blood flow and the level of hematocrit above the threshold were evaluated *in silico* by using both customized MATLAB code. Immunofluorescence against collagen type 4 (Ab6586, Abcam, UK) was performed as a marker of vessel dialation and wound healing. To further investigate whether Notch signaling is implicated in vascular regeneration, the level of Notch signalling was genetically manipulated by micro-injecting Notch Intracellular Cytoplasmic Domain (NICD) mRNA, Dominant Negative (DN)-Notch1b mRNA, or by using pharmacological ADAM 10 inhibitor (GI254023X, Sigma-Aldrich, MO) to reduce proteolytic cleavage of the receptor. Similarly, EFNB2/EphB4 axis was modulated by using corresponding MOs or mRNAs. In addition, Human Aortic Endothelial Cells (HAEC, Cell applications) with and without exposure to Pulsatile shear stress (PSS, 23±8 dyne·cm^{-2} at 1 Hz) was utilized to assess differential expression patterns of Notch signaling related genes including EFNB2 and EphB4, distribution of EFNB2/EphB4 proximity ligation, and EFNB2-mediated EphB4 pull down.

Results

The control *Tg(tp1:eGFP; flk1: mCherry)* zebrafish embryos underwent mechanical amputation exhibited a complete vascular regeneration by forming a loop between the dorsal aorta (DA) and the dorsal longitudinal anastomotic vessel (DLAV) at 4 dpa. In response to the tail injury, segmental vessels (SV) adjacent to the injured site developed 2-fold and 5-fold increase in the time average velocity and the hematocrit above threshold accompanied with a gradual progression of endothelial Notch acitivity and depositions of collagen type 4. Genetic manipulations of viscosity-mediated shear stress via *Gata1a* MO injection or *epo* mRNA revealed a linear relationship the between endothelial wall shear stress and Notch-mediated vascular regeneration. Micro-injection of *NICD* mRNA as a means to over-express Notch activiation promoted vascular regeneration, and restored *DN-Notch1b* mRNA- and GI254023X- impaired vascular regeneration. *NICD* mRNA further rescued impaired vascular regeneration in the presence of *Gata1a* MO. *In vitro* model of HAEC monolayer further demonstrated exposure to PSS up-regulate the expression level of Notch ligands DLL4, JAG1 and JAG2, the Notch receptor Notch1b, and the downstream target Hes1, Hey2 and EFNB2. Zebrafish embryos injected with *EFNB2* or *EphB4* MO developed disrupted vascular network in conjunction with impaired vascular repair, whereas silencing EFNB2/EphB4 with MOs completely mitigated vascular regeneration post injury. In contrast, *EFNB2* mRNA rescued impaired vascular regeneration in the absence of endothelial Notch signaling suggesting flow-dependent Notch signaling is a critical regulator of vascular regeneration by promoting EFNB2. Proximity ligation assay and immunoprecipitation revealed PSS increases the level of EFNB2 mediated EphB4 pull down.

Conclusions

Our present data supported the notion that vascular injury perturbs blood flow and constructively induces hemodynamic shear forces on the vascular endothelium which drives Notch-EFNB2/EphB4 pathway to promote vascular regeneration.

References

[1] K. De Bock, M. Georgiadou, and P. Carmeliet, “Role of endothelial cell metabolism in vessel sprouting,” *Cell Metab,* vol. 18, no. 5, pp. 634-47, Nov 5, 2013.

[2] R. Li, T. Beebe, N. Jen, F. Yu, W. Takabe, M. Harrison, H. Cao, J. Lee, H. Yang, P. Han, K. Wang, H. Shimizu, J. Chen, C. L. Lien, N. C. Chi, and T. K. Hsiai, “Shear stress-activated Wnt-angiopoietin-2 signaling recapitulates vascular repair in zebrafish embryos,” *Arterioscler Thromb Vasc Biol,* vol. 34, no. 10, pp. 2268-75, Oct, 2014.

[3] K. I. Baek, R. R. S. Packard, J. J. Hsu, A. Saffari, Z. Ma, A. P. Luu, A. Pietersen, H. Yen, B. Ren, and Y. Ding, “Ultrafine Particle Exposure Reveals the Importance of FOXO1/Notch Activation Complex for Vascular Regeneration,” *Antioxidants & redox signaling,* vol. 28, no. 13, pp. 1209-1223, 2018.

[4] S. J. Bray, “Notch signalling in context,” *Nat Rev Mol Cell Biol,* vol. 17, no. 11, pp. 722-735, Nov, 2016.

[5] T. Masumura, K. Yamamoto, N. Shimizu, S. Obi, and J. Ando, “Shear stress increases expression of the arterial endothelial marker ephrinB2 in murine ES cells via the VEGF-Notch signaling pathways,” *Arterioscler Thromb Vasc Biol,* vol. 29, no. 12, pp. 2125-31, Dec, 2009.

Ex Vivo Organotypic Model for the Study of the Epicardium

Davide Maselli, Patrizia Camelliti, Robert D Johnson, Rolando S Matos, Ciro Chiappini, Paola Campagnolo

Department of Biochemical Sciences, University of Surrey, Guildford, UK and Centre for Craniofacial and Regenerative Biology Kings College London, London, UK

Introduction

The epicardium is the most external layer of the myocardium, composed of an epithelial layer and an underlying mesenchyme. The epicardium contributes to post- myocardial infarction repair by providing a source of progenitors that support cardiac and vascular regeneration by releasing pro-angiogenic and pro-survival factors, and by differentiating towards multiple cell lineages [1]-[4]. During this process, activated epicardial cells migrate to the site of injury where they contribute to post-ischemic remodelling and fibrosis [5] .There is a limited knowledge of the cellular and molecular processes that regulate the epicardial contribution to the loss of mechanical function of the cardiac wall, associated with tissue fibrosis. This lack of knowledge is in part due to the lack of inexpensive, robust and representative models to study the remodelling in large animal heart and limits the development of pharmacological interventions. In this project, we develop an *ex vivo* 3D organotypic model derived from porcine hearts, amenable to culture which enables structural, molecular and cellular studies.

Methods

Thin epicardial/cardiac tissue slices (EpCardio-TS) are obtained by cutting the first layer from the epicardial side of tissue blocks from porcine hearts, using a vibratome. Slices are cultured for up to 72h in a bioreactor system based on a 3D printed chamber connected to a peristaltic pump and a feedback control system, ensuring stable and controllable culture conditions. Epicardial cells are tracked by the local intracellular delivery of fluorescent quantum-dots (Qdots), performed using a nanoneedle chip[ciro]. Cell fate is visualised in 3D by immunofluorescence on decolourised slices[cubic].

Results

EpCardio tissue slices can be obtained reproducibly and present both of a heathy epicardium, expressing the typical markers (wt-1, mesothelin, uroplakin) and a live and electrically connected myocardium. The optimized culture conditions preserve the viability of the epicardium (70%) and myocardium (40%); TUNEL assay confirms low levels of apoptosis. The morphology of epicardial cells and their marker expression is also preserved during culture. Interestingly, the presence of proliferating epicardial cells (PCNA+) and the increase in wt1+ cells and epicardial gene expression suggest a healthy and activated epicardium. Nanoinjection of fluorescent Qdots to EpCardio-TS localizes them to the wt-1 cells on the slice surface, in a simple strategy to selectively mark the epicardial layer. This, combined with the successful decolourisation of the slices, provides the ideal platform to track the role of epicardial cells in cardiac remodeling and fibrosis.

Conclusions

EpCardio-TS represents a robust *ex vivo* model merging the complexity of a 3D, organotypic culture from large animals with the simplicity and reproducibility of the *in vitro* culture. EpCardio-TS is amenable to culture, cell tracking and experimental challenge (i.e. hypoxia) and finds application in drug/gene therapy screening for the modulation of the epicardium/myocardium interactions and tissue remodeling.

References

[1] J. M. González-Rosa, M. Peralta, and N. Mercader, “Pan-epicardial lineage tracing reveals that epicardium derived cells give rise to myofibroblasts and perivascular cells during zebrafish heart regeneration,” *Dev Biol*, vol. 370, no. 2, pp. 173–186, 2012.

[2] B. van Wijk, Q. D. Gunst, A. F. M. Moorman, and M. J. B. van den Hoff, “Cardiac Regeneration from Activated Epicardium,” *PLoS ONE*, vol. 7, no. 9, 2012.

[3] N. Smart, C. A. Risebro, A. A. D. Melville, K. Moses, R. J. Schwartz, K. R. Chien, and P. R. Riley, “Thymosin β4 induces adult epicardial progenitor mobilization and neovascularization,” *Nature*, vol. 445, no. 7124, pp. 177–182, 2006.

[4] N. Smart, S. Bollini, K. N. Dubé, J. M. Vieira, B. Zhou, S. Davidson, D. Yellon, J. Riegler, A. N. Price, M. F. Lythgoe, W. T. Pu, and P. R. Riley, “De novo cardiomyocytes from within the activated adult heart after injury,” *Nature*, vol. 474, no. 7353, pp. 640–644, 2011.

[5] C. M. Braitsch, O. Kanisicak, J. H. van Berlo, J. D. Molkentin, and K. E. Yutzey, “Differential expression of embryonic epicardial progenitor markers and localization of cardiac fibrosis in adult ischemic injury and hypertensive heart disease,” *J Mol Cell Cardiol*, vol. 65, no. 0, pp. 108–119, 2013.

Vascular constructs using human pluripotent stem cells in the therapy of peripheral arterial disease

Eleonora Zucchelli[1], Qasim Majid[1], Thomas J Owen[1], Edit Gara[2], Sian Harding[1], Gábor Földes[1,2]

[1] National Heart and Lung Institute, Imperial College London, London, United Kingdom; [2] Heart and Vascular Center, Semmelweis University, Budapest, Hungary

Introduction

Tissue engineering has emerged as a promising alternative for vascular grafts. The aim of this study was to determine the feasibility and safety of tissue-engineered vascular grafts, obtained using canine decellularized aortae reseeded with human induced pluripotent stem cell-derived endothelial cells (hiPSC-EC) in a large animal model.

Methods

In the present work, we compared the expression of endothelial markers in 2D hiPSC-EC cultures maintained under either static or continuos dynamic cell culture conditions, using the Alvetex multi-welled system. Human iPSC-EC were used to reseed decellularised canine aortic tissues. Generated tissue-engineered grafts were implanted in a clinically relevant large animal model of abdominal aortic replacement for 1 week ($n = 4$). To demonstrate cell retention *in vivo*, we performed endoscopic analysis, and evaluated size and patency of the constructs by colour Doppler ultrasound and CT angiography. Finally, vascular grafts were collected for gene expression analyses and histological / immunohistochemical examinations *ex vivo*.

Results

Our results demonstrated that hiPSC-EC cultures responded to dynamic circulation and continuos perfusion of medium for 1 week in 2D*,* by increasing the expression of endothelial markers, such as *CD31* and *VE-cadherin* (6 and 5 times upregulated, respectively; $p \leq 0.05$), and YAP (downstream effector of the Hippo pathway, 9 times upregulated; $p \leq 0.001$), as compared to cells maintained in static conditions. Human iPSC-EC was able to recellularise 3D vascular decellularised biomatrices and thereby it developed a mature, functional phenotype (e.g. antiplatelet and vasoactive effects) *in vitro*. hiPSC-EC cultured on 3D decellularised vascular biomatrices showed increased expression of arterial, venous, common endothelial marker genes and angiogenesis-related proteins (e.g. *angiopoietins, endoglin, FGFs*), compared to 2D hiPSC-EC cultures grown on collagen-coated dishes. Cell-matrix adhesion proteins (e.g. collagen XVIII, MMP8 and 9, TIMP1) were also upregulated, suggesting the increased adhesive capacity of cells upon reseeding. *In vivo*, ultrasonographic and CT angiography confirmed that implanted vascular constructs displayed good patency with no obvious thrombi. No adverse immunoreactions were reported in any of the treated animals. Post-implantation analysis of the grafts showed that hiPSC-EC responded to shear stress and dynamic flow *in vivo,* by upregulating Notch signalling (*Notch 1* and *Notch 2*; 3 and 5 times upregulated, respectively) and mechanosensitive YAP (2 times upregulated) / TAZ (5 times upregulated) compared to 3D static cultures.

Conclusions

Our results showed that hiPSC-EC can be used to repopulate decellularised aortic walls. Optimising dynamic cell culture conditions is necessary to obtain functional vascular tissue-engineered grafts for therapeutic applications.

Systematic evaluation of the influence of wall shear stress features on endothelial cell phenotypes in-vitro with correlation to ex-vivo bovine Arteriovenous tissue

David T. O'Connor, Marco Franzoni, Michael T. Walsh

Biomaterials Cluster, Bernal Institute, University of Limerick, Limerick, Ireland

Introduction

The wall shear stress (WSS) is the frictional force per unit area exerted at the interface of the flowing blood and the endothelium. WSS is a potent stimulus capable of evoking variable phenotypes in endothelial cells (EC)[1,2]. In-vivo and in-vitro observations demonstrated the existence of two major pathways that may activate EC as a response to different WSS waveforms. In adults, these two pathways are alternatively involved in inducing EC quiescence conferring a protective effect on endothelium or EC activation and pro-inflammatory signalling inducing endothelium dysfunction and pro-inflammatory and pro-thrombotic effects[3]. Physiological WSS patterns were decomposed correlating to imperative features such as time-averaged WSS (TAWSS), peak magnitude or maximum WSS, temporal WSS gradient and OSI (in the presence of a reverse phase). Flow-induced morphological adaptations alongside gene and protein expression, known to be involved in vascular lesion development have been analysed. The overarching aim is to systematically evaluate the features as mediators of venous EC activation and signalling.

Methods

The study encompasses two sectors which analyse the in vitro and ex-vivo WSS exposure using a real time-controlled Cone and Plate device along with a custom designed ex-vivo perfusion system.

In-vitro experiments: To adequately decompose the critical driving factors correlated to WSS in-vivo, 10 idealised waveforms were created ranging for WSS peak magnitude of 0.5 to 2.5 Pa, t-WSSG from 2 to 20 Pa/s and from 0 to 0.5 of oscillatory shear index (OSI) value. Experiments were performed for a duration of 24 hours and evaluation of differential protein and gene expression was completed using RT-PCR, Western Blot and Immunoflourescence staining. Preferential analysis was completed on NF-kB, PECAM-1, a-SMA and KLF-2 due to previously decribed relationship with vascular disease.

Ex-vivo experiments: Using a custom designed perfusion system with aid of labview software controlled peristaltic pump, idealised physiological waveforms were used to exposed surgically created bovine AVF tissue samples for up to 2 weeks to correlate the tissue response to hemodynamics presented in in-vitro model. H&E and immunofluorescent staining techniques were used to compare the tissue's structural remodelling and differential protein response to specified hemodynamics.

Results

Our results indicate that WSS waveforms with a peak magnitude of 1.5 or 2.5 Pa can induce a protective phenotype in ECs in culture in terms of KLF-2, KLF-4, IL-8 and VCAM-1 expression. By presenting a reverse phase or decreasing TAWSS of the waveforms with a peak of 1.5 or 2.5 Pa, the flow-induced protective effect is maintained. A WSS peak of 1.5 Pa show to be sufficient to induce protective pathways. Pro-inflammatory gene expression showed no differences in the expression of two subunits of NFkB (NFkb-1, NFkB-3). Differential expression of protective and pro-inflammatory proteins colocalising with areas of disturbed hemodynamics in the ex-vivo model.

Conclusions

In conclusion, when assessing the effects of unsteady WSS profiles, atherogenic time-averaged WSS threshold should be reconsidered and reduced significantly, at least for venous EC. Similarly, preliminary results from ex-vivo tests suggest differential protein expression at the sites of disturbed WSS patterns within the tissue samples correlating with previous flow studies.

References

1. Nakajima, H. & Mochizuki, N. Flow pattern-dependent endothelial cell responses through transcriptional regulation. *Cell Cycle* **16,** 1893–1901 (2017).
2. Chatterjee, S. Endothelial Mechanotransduction, Redox Signaling and the Regulation of Vascular Inflammatory Pathways. *Front. Physiol.* **9,** 524 (2018).
3. Chang, E., Nayak, L. & Jain, M. K. Krüppel-like factors in endothelial cell biology. *Curr. Opin. Hematol.* **24,** 224–229 (2017).

A Novel High-throughput loss-of-fundtion Microarray Platform for Targeting Gene Networks in Primary Cells

Aliah Abuammah [2, 3, 4], Nataly Maimari [1], Sean Herault [1], Jacques Behmoaras 2, Rob Krams 3, Christina Warboys 1 and Leila Towhidi 1

Department of Bioengineering [1] and Medicine [2], Imperial College London, London, United Kingdom.
Queen Mary University, Departement of bioengeneerign, London, United Kingdom [3]
King Saud University, College of Medicine, Riyadh, Saudi Arabia [4]

Introduction

The endothelial cell responds to mechanical stimulation by activation of ~2500 genes, which are organised in a network of 10,000 interactions. In aiddition, this gene network adapts over time and during disease progression. This sheer number of genes, necessitates the development of novel tools to study this. Here we describe the design, fabrication and evaluation of a high-throughput platform for evaluation of gene networks, and applied to mechanotransduction studies in primary mammalian cells.

Methods

Here we developed a High-throughput screening (HTS) reverse-transfection validation platform using CRISPR-Cas9 gene-editing technology and High-throughput imaging (HTS) to capture functional and morphometric information from single cells, in combination with high content analysis (HCA) to extract and understand the multi-parametric data obtained from HTS. In a first series, we supplied the same 4 gRNA's to all spots which were loaded with CAS9+ fibriblasts and evaluated the supernatant and gene expression with qPCR after merging all spots. In a second series, we evaluated single CAS9+ GFP+ HEK cells and evaluated the dose-dependently on a single cell level.

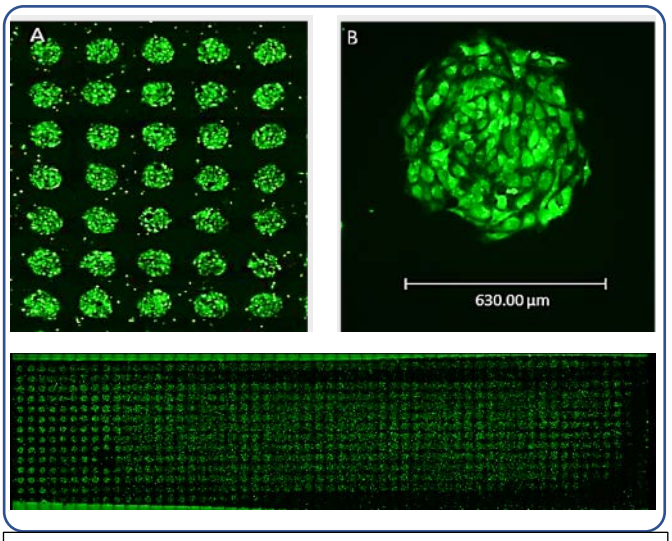

Figure 1: A **stitching of a tile scan microscope image** using Zeiss Axiovert 200 inverted widefield fluorescent microscope in GFP channel at 10x objective of an ITO slide printed with 840 siRNA spots and seeded with copGFP HUVECs at the first day. A: Tile scan of spots. B: A random spot.

Results

Overall inhibtion caused by gRNA directed against the purinergic receptor in fibrobalsts was 65% at its highest dosage. On a single cell level we measured a dose dependent decrease of GFP upto 85%

Conclusions

This study introduced a novel high throughput platform for mammalian cells, which was developed for studies on mechanobiology. Using a novel protocol, we were able to have stable spots and seed living cells only on the spots to eliminate cross contamination (Figure 1). Using this protocol, up to 86% gene knockout was achieved and further optimization can be conducted to achieve higher efficiency.All components are compatible with standard microscopes enabling to perform automatic screening and high resolution imaging at a single cell level.

Coronary artery inflammation compared to wall shear stress, plaque composition and pericoronary adipose tissue using PET-CT

Jason M Tarkin,[1,2] Yuan Huang,[3] Roido Manavaki,[4] Adam J Brown,[5] Martin R Bennett,[1] Damini Dey,[6] Piotr Slomka,[6] Frank Gijsen,[7] Jolanda Wentzel,[7] James HF Rudd[1]

[1]Division of Cardiology, University of Cambridge, UK; [2]National Heart & Lung Institute, Imperial College London, UK; [3]Cambridge Centre for Mathematics in Healthcare, University of Cambridge, UK; [4]Department of Radiology, University of Cambridge, UK; [5]Monash Cardiovascular Research Centre and MonashHeart, Melbourne, Australia; [6]Department of Imaging, Cedars-Sinai Medical Center, Los Angeles, USA; [7]Department of Biomedical Engineering, ErasmusMC, Rotterdam, The Netherlands

Introduction

The pathophysiology of atherosclerotic plaque rupture triggering most acute coronary events is complex and multi-factorial. Vascular inflammation is a common mechanistic link connecting many of these factors, which can be measured using positron emission tomography (PET) with tracers targeted to macrophage activity, including ^{68}Ga-DOTATATE and ^{18}F-FDG.[1] We aimed to examine patterns of coronary artery inflammation to wall shear stress (WSS), plaque composition and pericoronary adipose tissue using PET-CT in patients with stable atherosclerosis.

Methods

ECG-gated PET imaging and CT coronary angiography (CTCA) were performed as previously described.[1] CTCA-based vessel segmentation using level set principles in MeVisLab resulted in 3D coronary reconstruction including the side branches. Coronary arteries with dense calcification, stents, or image artefacts precluding accurate vessel segmentation were excluded. PET and CTCA images were coregistered using FusionQuant. PET standardized uptake values (SUV) were interpolated onto the luminal surface using cubic splines and visualized in Paraview. The time-average wall shear stress was computed using computational fluid dynamics applying as input flow the empirical relations as previously described,[2] using the diameter as the most important input parameter and Kassab's law for the flow distribution. Semi-automated plaque analysis was perfomed using Autoplaque.

Results

Coronary arteries from 8 patients (median age 59 [IQR 57-73] years, 88% men) were included. A representative example demonstrating patterns of vascular inflammation compared to WSS distribution in the left anterior descending (LAD) artery (arrow) is shown in the Figure: (**A**) CTCA; (**B-C**) PET images (units, SUV); (**E**) WSS map (units, Pa); (**F-G**) PET color maps (units, SUV). In this case, the left main stem/LAD (**D**) plaque volume was 0.95 mL (plaque composition: 1.9% calcified [yellow], 98.1% non-calcified [red], 29.5% low density non-calcified) and (**H**) pericoronary fat volume (defined as -130 to -30 HU) was 94.4 mL. Data analysis is ongoing.

Conclusions

Based on our initial observations, we hypothesize there will be a significant relationship between PET markers of vascular inflammation and low WSS in areas of predominately non-calcified plaque associated with high pericoronary fat volume. Further analysis is needed to test this hypothesis.

References

[1] Tarkin JM, Joshi FR, Evans NR, et al. Detection of Atherosclerotic Inflammation by (68)Ga-DOTATATE PET Compared to [(18)F]FDG PET Imaging, *J Am Coll Cardiol*, 69(14):1774-1791, 2017.

[2] van der Giessen AG, Groen HC, Doriot P-A, et al. The influence of boundary conditions on wall shear stress distribution in patients specific coronary trees. *J Biomechanics*, 44(6):1089-1095, 2011.

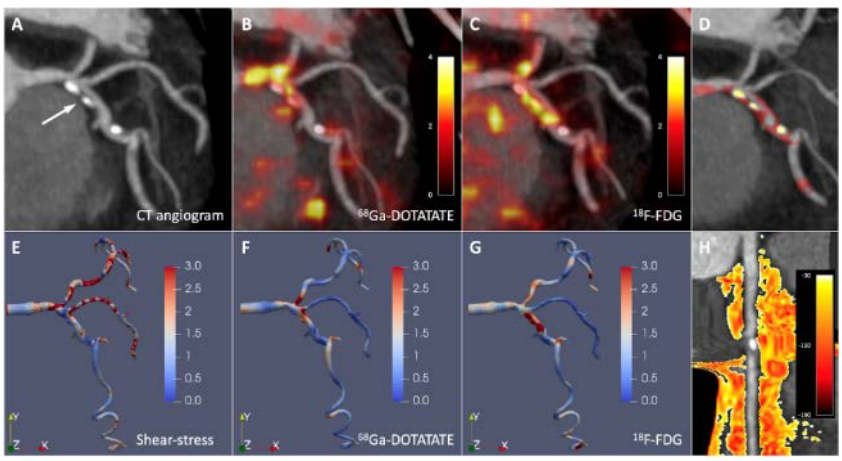

Piezo1 channels are expressed and functional in cardiac fibroblasts

Nicola M Blythe, Mark J. Drinkhill, David J. Beech, Neil A. Turner

Leeds Institute of Cardiovascular and Metabolic Medicine, University of Leeds, UK

Introduction
Piezo1 is a mechanosensitive cation channel with widespread physiological importance, however its role in the heart is poorly understood. Cardiac fibroblasts are mechanosensitive cells responsible for preserving the structural integrity of the myocardium and play a key role in regulating its repair and remodeling following stress or injury [1]. We investigated expression and function of Piezo1 in cultured cardiac fibroblasts.

Methods
We used RT-PCR analysis, intracellular calcium (Ca^{2+}) measurements and small interfering RNA (siRNA) in order to investigate Piezo1 in cardiac fibroblasts. Yoda1, a synthetic molecule, was used to activate the Piezo1 channel [2].

Results
RT-PCR studies confirmed expression of Piezo1 mRNA in human and mouse cardiac fibroblasts at similar levels to endothelial cells. Fura-2 intracellular Ca^{2+} measurements validated Piezo1 as a functional ion channel which could be activated by the Piezo1 agonist, Yoda1. Yoda1-induced Ca^{2+} entry was inhibited by Piezo1 blockers (gadolinium, ruthenium red) [3] and the Ca^{2+} response was reduced proportionally by Piezo1 siRNA knockdown or in cells from $Piezo1^{+/-}$ mice. Investigation of Yoda1 effects on selected remodeling genes indicated that Piezo1 activation opposed cardiac fibroblast differentiation; data confirmed by immunocytochemistry and functional assays (collagen gel contraction).

Conclusions
In summary, this study reveals that cardiac fibroblasts express functional Piezo1 mechanosensitive cation channels and that their activation is coupled to reduced myofibroblast activation.

References
[1] Porter KE, Turner NA, Cardiac fibroblasts: At the heart of myocardial remodelling, *Pharmacology & Therapeutics*, v.123:2, p. 255–278, 2009.
[2] Syeda R, Xu J, Dubin AE, Coste B, Mathur J, Huynh T, Matzen J, Lao J, Tully DC, Engels IH, Petrassi HM, Schumacher AM, Montal M, Bandell M, Patapoutian A, Chemical activation of the mechanotransduction channel Piezo1, *eLife*, 4, 2015.
[3] Coste B, Mathur J, Schmidt M, Earley TJ, Ranade S, Petrus MJ, Dubin AE, Patapoutian A, Piezo1 and Piezo2 are essential components of distinct mechanically-activated cation channels, *Science*, 330, 55-60, 2010.

This research was funded by The British Heart Foundation.

Contractile and Hemodynamic Forces Promote Cardiac Valve Development via Notch1b-mediated Endothelial-to-Mesenchymal Transition

Jeffrey J. Hsu[1], Vijay Vedula[2], Kyung In Baek[3], Cynthia Chen[3], Junjie Chen[3], Man In Chou[3], Jeffrey Lam[3], Shivani Subhedar[3], Jennifer Wang[3], Yichen Ding[3], Chih-Chiang Chang[3], Juhyun Lee[4], Linda L. Demer[1,3,5], Yin Tintut[1,5], Alison L. Marsden[2], Tzung K. Hsiai[1,3]*

[1]Division of Cardiology, Department of Medicine, University of California, Los Angeles, Los Angeles, CA. [2]Departments of Pediatrics and Bioengineering, Stanford University, Stanford, CA. [3]Department of Bioengineering, University of California Los Angeles, Los Angeles, CA. [4]Department of Bioengineering, University of Texas - Arlington, Arlington, TX. [5]Department of Physiology, University of California Los Angeles, Los Angeles, CA.

Introduction: Myocardial contractile and hemodynamic shear forces modulate cardiac valve formation. While endothelial-to-mesenchymal transition (EndoMT) mediates valve development, the mechanotransduction mechanisms underlying EndoMT in embryonic valve development remain poorly understood.

Hypothesis: We hypothesized that increased myocardial contractility and wall shear stress (WSS) promote valve formation in the outflow tract (OFT) by inducing Notch-mediated EndoMT.

Methods and Results: Integrating 4-D light-sheet imaging with moving fluid-solid-interface computational fluid dynamic modeling, we assessed the effects of hemodynamic modulation on ventriculobulbar (VB) valve formation in the OFT of transgenic *Tg(fli1:GFP)* zebrafish embryos. Increasing WSS in the OFT via *EPO* mRNA injection to increase viscosity or treatment with the beta-agonist isoproterenol resulted in hyperplastic VB valve leaflets, accompanied by an increase in *Notch1b* activity in the OFT of transgenic *Tg(tp1:GFP)* embryos. While upregulation of Notch activity with *NICD* mRNA injection supports *Notch1b*-mediated hyperplastic VB valve development, reduction of myocardial contractility and WSS with 2,3-butanedione monoxime (BDM) treatment or complete arrest of contractility with *Tnnt2a* morpholino oligonucleotide injection resulted in decreased *Notch1b* activity and absence of VB valve leaflets. Immunofluorescence analysis of the EndoMT marker, DM-GRASP, showed increased EndoMT in the OFT of isoproterenol-treated embryos, and absence of EndoMT in BDM-treated embryos. *In vitro* flow experiments confirmed that increased WSS promotes the upregulation of mesenchymal genes (*COL1A1*, *ACTA2, FSP1*) in human umbilical vein endothelial cells.

Conclusions: Myocardial contractility and hemodynamic forces activate endocardial *Notch1b* signaling in the OFT, accompanied by VB valve development. Increases in contractility and WSS results in *Notch1b* activity-mediated VB valve hyperplasia via EndoMT, whereas decreased contractility and WSS results in decreased *Notch1b* activity and VB valve underdevelopment in the absence of EndoMT. Thus, we provide developmental mechanotransduction mechanisms underlying *Notch1b*-mediated EndoMT in VB valve development.

The Impact of Strut Design on the Hemodynamic Behaviour of Various Bioresorbable Scaffolds

Imane Tarrahi[1], Eline Hartman[1], Monika Colombo[2], Claudio Chiastra[2,3], Ryo Torii[1], Natalia Tovar[1], Jolanda Wentzel[1], Joost Daemen[1], Frank Gijsen[1]

[1]Department of Biomedical Engineering, ErasmusMC, Rotterdam, The Netherlands
[2] LaBS, Dept. of Chemistry, Materials and Chemical Engineering "Giulio Natta", Politecnico di Milano, Milan, Italy
[3] PoliToBIOMed Lab, Dept. of Mechanical and Aerospace Engineering, Politecnico di Torino, Turin, Italy

Introduction

The hemodynamic environment after BioResorbable Scaffolds (BRS) deployment plays an important role in the mid- to long-term efficacy of these devices. Scaffolded regions exposed to flow recirculation, low Time Averaged Wall Shear Stress (TAWSS) and high Oscillatory Shear Index (OSI) are prone to develop increased neo-intima formation. We aimed to compare the hemodynamic behaviour of 3 different BRS with rectangular struts of varying height, namely the Fantom (125µm), Fantom Encore (98µm), and Absorb (157µm) and one BRS with rounded struts, the Magmaris (150µm). We performed in vitro scaffold deployment to study the TAWSS, the OSI and recirculation zones in 2D and 3D.

Methods

BRSs were deployed in plastic tubes and were imaged with high resolution microCT. From the microCT data, both 2D and 3D geometrical models of the deployed scaffolds in the tube were reconstructed. For the 3D models, the centreline of the scaffolds was extracted (Mimics software) and the surface models (Rhinoceros software) were reconstructed by lofting the 2D cross-sectional strut shape along the centerline. Computational fluid dynamics was performed on the 2D and 3D geometrical models with FLUENT to compute TAWSS and OSI (Figure 1).

Results

The 2D simulations showed that the size of the recirculation zone and the minimal TAWSS were largest for the Absorb (240 µm and -0.18 Pa), followed by the Magmaris (170 µm and -0.15 Pa), the Fantom (140 µm and -0.14 Pa) and the Fantom Encore (100 µm and -0.13 Pa). For the rectangular scaffolds, the 2D models showed that a larger strut height was almost linearly correlated with a larger size of the recirculation zone and lower values of minimal TAWSS. The Magmaris had a smaller recirculation zone than expected based on the strut thickness, due to the rounded strut edges. Whilst the hemodynamic behaviour in 2D depended on strut size and shape, stent design and strut lay-out played a role as well in the 3D simulations. For the BRS with rectangular struts, the percentage area with adverse TAWSS (<0.5 Pa) and OSI (>0.2) was highest for the Fantom (56% and 30%) and lowest for the Fantom Encore (30% and 25%). The Absorb had a more open strut design with reduced coverage of the stented region compared to the Fantom scaffold, resulting in a smaller region with adverse TAWSS and OSI (53% and 33%). Lastly, the Magmaris had both less coverage of the stented region as well as rounded strut edges, leading to the smallest region of adverse TAWSS and OSI (25% and 20%).

Conclusions

In BRS with rectangular shaped struts, Fantom Encore showed the smallest recirculation zone and lowest value of minimal TAWSS in 2D. Due to the impact of stent design and strut lay-out both the Fantom Encore and the Magmaris showed smaller TAWSS and OSI in 3D as compared to the thicker strut Fantom and Absorb BRS. This study shows the benefit of CFD to disentangle the effect of strut height and layout on the hemodynamic performance of coronary stents.

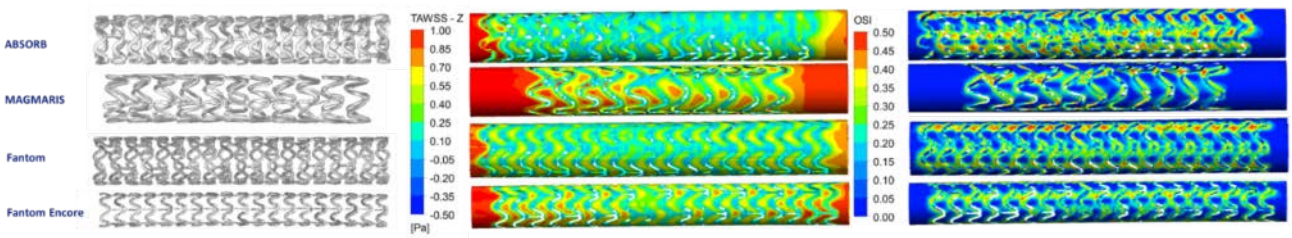

Figure 6 CFD was performed in the 4 scaffolds shown. The results show the low TAWSS regions and the high OSI regions per scaffold.

Imaging the Depostion of Nanocarriers in Patient Reconstructed Blood Vessels

Maria Khoury, Mark Epshtein and Netanel Korin

Department of Biomedical Engineering, Technion - IIT, Haifa, Israel

Introduction

Drug targeting to sites of disease is a multistep process, which is based on the transport of drug carriers to the target region followed by deposition of drug carriers at the desired destination. Important flow and mass transport parameters including Reynolds number and flow characteristics are highly dependent on vessel geometry and blood flow pattern. Here we study particle deposition in endothelialized models of human arterial bifurcations under physiological hemodyamic conditions.

Methods

We have designed and fabricated 3D artery models of the carotid bifurcation cultured with human umbilical vein endothelial cells. The models were connected to a programmable perfusion system which was used to replicate the physiological blood flow pulse. Fluorescent nano-particles (200nm and 2 microns) were resuspended in blood, introduced to the system and their deposition within the model was monitored via real-time high resultion microscopy. Based on time-lapse movies the kinetic was particle adhesion in different locations within the models was analysed.

Results

Our results show that the particles tend to localize at specific sites within the bifurcation based on hemodynamics and particles properties. These findings highlight the key role of hemodynamics in the development of vascular targeting of nano-carriers.

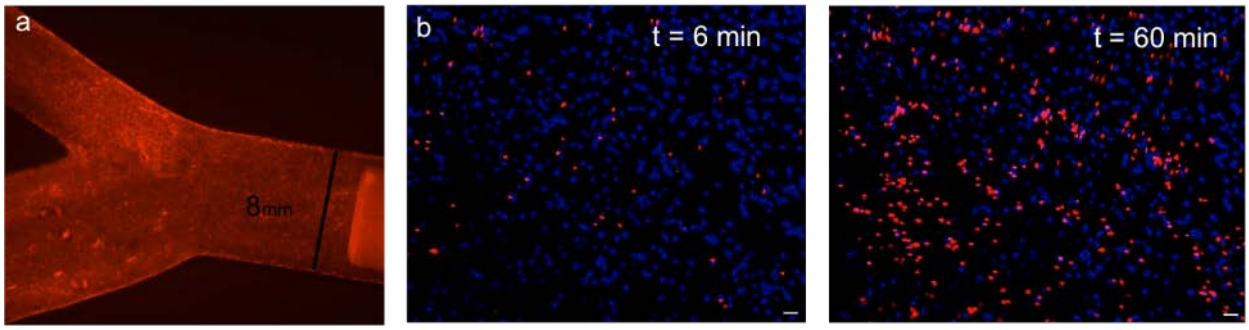

Figure 1: Monitoring of particle deposition in endothelialized models of human arterial bifurcations under physiological hemodynamic conditions. (a) HUVEC seeded in a 3D carotid bifurcation model, Actin is stained with Phalloidin conjugates, (b) Deposition of 2µm Particles (red) in the 3D cultured model, cells stained with Dapi (blue)

Conclusions

Studying the dynamic of particle adhesion in patient recomstructed bllod vessel models may provide valuable information for the design of efficient cardiovascular nanomedicines.

Contribution of endothelial Piezo1 channels to whole body physical activity

Fiona Bartoli[1], Lee D Roberts[1], T Simon Futers[1], David J Beech[1]

[1]School of Medicine, University of Leeds, Leeds LS2 9JT, UK

Introduction

Regular physical activity confers significant beneficial effects against multiple diseases and preserve quality of life. Beneficial effects of exercise involve an improvement of endothelial function, meaning endothelial cells have a key role in physical performance, especially via their role as shear stress sensors, a frictional force which arises because of blood flow. It has been suggested that the sensing of this mechanical force depends on Piezo1 channels [1]. The deletion of Piezo1 is lethal during embryonic stages due to a disruption of vascular network maturation and its role in adults are emerging through conditional genetic techniques. Previous work identified a role for endothelial Piezo1 in whole physical activity [2] with a Piezo1-dependence of elevated blood pressure during exercise and modest but significant decrease in exercise performance when mice had voluntary access to a running wheel. Surprisigly, the effect on exercise performance was lost after 2 days of training. Here, using the same mouse model, we assessed the impact of a longer deletion of endothelial Piezo1 on physical performance.

Methods

Piezo1-modified mice: We used a mouse model with conditional Cre-Lox-mediated disruption of Piezo1 in the endothelium (Piezo1$^{\Delta EC}$ mice). Mice were injected with Tamoxifen at 10 weeks to induce the deletion of Piezo1 and the experiments were performed on male mice aged 20 weeks.
Analysis of muscle mass: Mice aged 20 weeks were sacrified and different hind limb muscles (Rectus Femoris, Vastus Lateralis, Gastrocnemius and soleus) were collected and weighted.
Analysis of exercise performance: Mice were housed individually into Comprehensive Laboratory Animal Monitoring System (CLAMS) cages (Columbus Instruments, Columbus, OH, USA). For 4 days, energy expenditures (O_2 consumption, CO_2 production, respiratory exchange ratio), heat production, food intake and physical activity were monitored. Each CLAMS cage was equipped with optical beams to measure home cage activity and an instrumented running wheel (diameter, 9.4 cm) to measure voluntary exercise. The first day was considered as an acclimatization period and data were not included in the analyses.

Results

Piezo1$^{\Delta EC}$ mice showed less global locomotor or vertical exploratory activity throughout the 3 days of the experiment, associated with decreased running wheel rotations and running speed compared to the control mice. Interestingly, there is no compensation with the training, which had been seen previously when Piezo1 was deleted for 2 weeks. The interest in undertaking exercise was preserved in the Piezo1$^{\Delta EC}$ mice with a similar number of bouts of exercise than the control mice. Moreover, the mice showed no difference in energy expenditure or food intake, nor in the weight of their hind limb muscles.

Conclusions

Our results suggest that after 10 weeks of endothelial Piezo1 deletion, murine physical performance is strongly compromised and training does not compensate. Investigations are in process to determine underlying mechanisms.

Acknowledgements

Funded by the British Heart Foundation.

References

[1] Li J, Hou B, Tumova S, Muraki K, Bruns A, Ludlow MJ, Sedo A, Hyman AJ, McKeown L, Young RS, Yuldasheva NY, Majeed Y, Wilson LA, Rode B, Bailey MA, Kim HR, Fu Z, Carter DA, Bilton J, Imrie H, Ajuh P, Dear TN, Cubbon RM, Kearney MT, Prasad RK, Evans PC, Ainscough JF and Beech DJ, Piezo1 integration of vascular architecture with physiological force, 2014. *Nature* **515**, 279-282

[2] Rode B, Shi J, Endesh N, Drinkhill MJ, Webster PJ, Lotteau SJ, Bailey MA, Yuldasheva NY, Ludlow ML, Cubbon RM, Li J, Futers TS, Morley L, Gaunt HJ, Marszalek K, Viswambharan H, Cuthbertson K, Baxter PD, Foster R, Sukumar P, Weightman A, Calaghan SC, Wheatcroft SB, Kearney MT and Beech DJ, Piezo1 channels sense whole body physical activity to reset cardiovascular homeostasis and enhance performance, 2017. *Nat Commun* **8**, 350.

A Microfluidic Model of Ischemia/Reperfusion Injury

Danielle Nemcovsky Amar and Netanel Korin

Department of Biomedical Engineering, Technion - IIT, Haifa, Israel

Introduction

Ischemia is associated with a variety of cardiovascular diseases including myocardial infraction and thrombotic stroke, among others. Although restoring blood flow is critical to prevent cellular damage, rapid reperfusion increases tissue damage, even in tissues that were not directly affected by the ischemia. A variety of *in vivo* models have been developed to investigate Ischemia/Reperfusion (IR) injury. However, they often do not mimic properly human physiology. Here, we propose to develop a microfluidic cell culture device that offers an alternative *in vitro* system for recapitulating certain features of human IR injury.

Methods

Microfluidic device were prepared from polydimethylsiloxane (PDMS) via replica molding based on a 3D printed mold. The channels were precoated with fibronectin and then Human Umbilical Vein Endothelial cells (HUVEC) were cultured in them. Blood clots were fabricated by mixing fibrinogen and thrombin with rat's whole blood. Two hours after cell seeding clots were injected into the channel to create an emboli obstructed channel. We then added tissue plasminogen activator (tPA) to a plasminogen solution, and introdcued the solution to dissolve the embolus, under a constant physiological pressure gradient. Cells morphology and inflammation factor were monitored after 5 hours post restoration of flow.

Results

We were able replicate a blood clot obstruction of flow in an endothlized compartment as well as the restoration of flow via treatment with a thromblytic drug, within a microfluidic device (see Fig. 1). The system allows to simulate IR under defined and controlled conditions which can aloow system study of IR injury and possible therapeutics for IR.

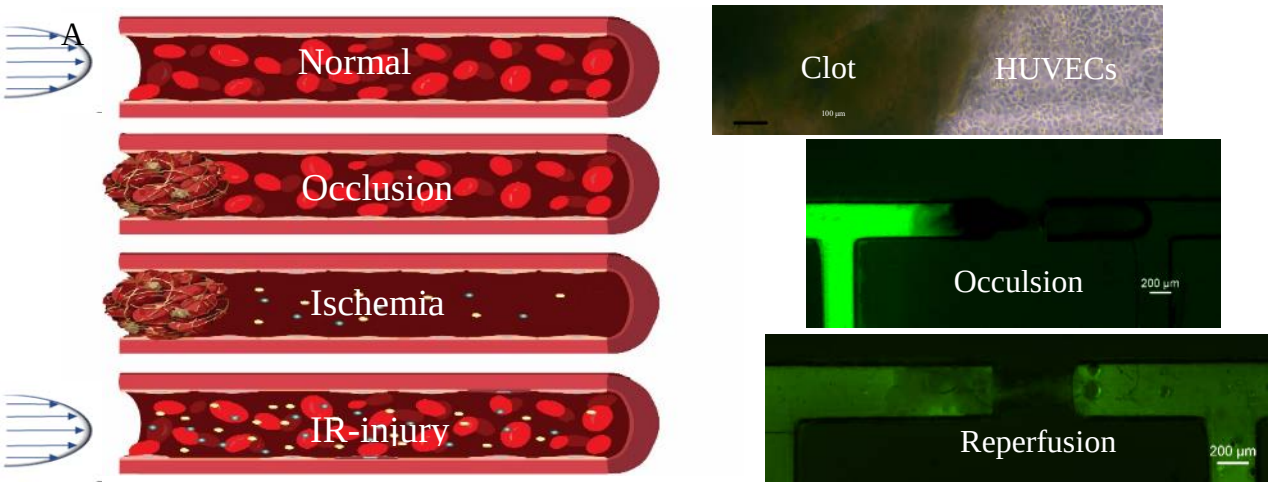

Fig.1: *Schematic illustrating IR (A) and images of IR injury induced in microfluidic device (B).*

Conclusions

By proper design, microfluidic models can be developed to replicate important feature of IR injury. These devices may also serve a replacement modality for animal testing and allow the study of IR injury under defined conditions on using human cells.

The Influence of Mechanical Factors on Occludin Expression of HUVECs

Junyang Huang, Shuang Ge, Desha Luo, Yang Wang, Ruolin Du, Tieying Yin, Guixue Wang*

Key Laboratory for Biorheological Science and Technology of Ministry of Education, State and Local Joint Engineering Laboratory for Vascular Implants, Bioengineering College of Chongqing University, Chongqing 400030, China
* Corresponding author. E-mail: wanggx@cqu.edu.cn

Introduction

Tight junctions are the most apical intercellular junctions of the lateral membrane in endothelial cells, regulating the paracellular material and energy exchange and maintain plasma membrane polarity. Occludin protein is one of the important proteins involved in endothelial tight junctions, and also closely related to the occurrence of atherosclerosis. Therefore, the study of occludin is valuable[1]. The present study tried to explore the impact of mechanical stimulation after stent implantation on the expression of occludin by cell and animal experiment.

Methods

HUVECs were exposed to 40 Kpa static pressure, 5 dyn/cm^2 (low shear stress, LSS) and 12 dyn/cm^2 (high shear stress, HSS) fluid shear stress for 6 hours and 12 hours respectively. After loading, cell lysate were collected to gene analysis and Western blotting. In addition, the loaded cell were immunofluorescence stained. In animal model, ApoE$^{-/-}$ mice were given carotid ligation for 48 hours and analyzed expression level of occludin by qPCR.Male SD rats were applied PLLA stents implantation.Sample sections were taken at one week, one month, three months and one year, respectively. The sample sections were stained with immunofluorescence.

Results

Compared to control, the expression of *occludin* in endothelial cells extremely significantly increased after loading for 6 hours at static pressure, LSS and HSS. After loading at 40 Kpa static pressure for 12 hours, occludin protein contents in endothelial cells significantly increased. At the same time, we observed that occludin fluorescence intensity increased significantly. In animal model, the expression of *occludin* extremely significantly increased, compared to control. Three months after stent implantation, the fluorescence intensity of the sample was the strongest.

Conclusions

In the present study, we tried to explore the impact of mechanical stimulation after stent implantation on the expression of occludin. We observed that the expression of occludin and the intercellular junction increased in endothelial cells after loading 40 Kpa static pressure, LSS and HSS for 6 and 12 hours. Moreover, the expression of occludin was significantly higher in LSS than HSS. So LSS has greater effect on the intercellular junction in endothelial cells, compared with HSS. In animal models, the results were consistent with those of cell experiments. Therefore, we speculate that the permeability of endothelial cells will change accordingly under these conditions.

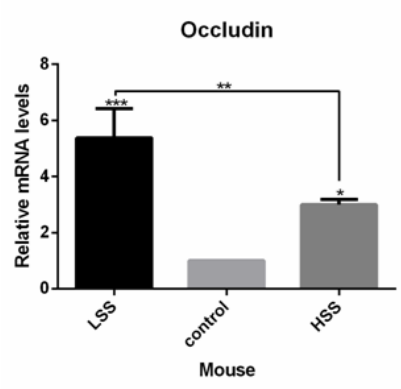

Fig1. quantitative analysis of *occludin* in ApoE-/- mice was given carotid ligation for 48 hours.

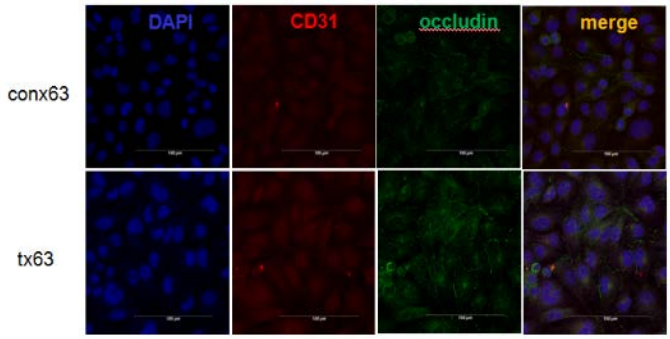

Fig2. Immunofluorescence staining of HUVECs after loading 40 Kpa for 12 hours.

References

[1]Chen L , Chen Z , Ge M , et al. Monocytic cell junction proteins serve important roles in atherosclerosis via the endoglin pathway, *Molecular Medicine Reports*, 16: 6750-6756, 2017.

Changes in tight junction-associated proteins after PLLA stent implantation

Shuang Ge, Yang Wang, Ruolin Du, Junyang Huang, Tieying Yin*, Yazhou Wang, Guixue Wang

Key Laboratory for Biorheological Science and Technology of Ministry of Education, State and Local Joint Engineering Laboratory for Vascular Implants, Bioengineering College of Chongqing University, Chongqing 400030, China
* Corresponding author. E-mail: ilyyty28@126.com

Introduction

After implantation of the poly-L-lactic acid (PLLA) stent, hemodynamic was changed, and the stent filament also swelled, which exacerbated the low shear stress characteristics of the stent implantation segment. Low wall shear stress and local disturbing flow caused endothelial cell dysfunction that enhanced vascular endothelial cell permeability [1]. While the permeability of blood vessel was maintained by tight junction protein (TJP) cross-linking to the cytoskeleton. So TJP involved in the barrier of the blood vessel. Once the integrity of the intima was destroyed, blood cells and harmful substances invaded the wall, and lipid deposition promoted the formation of restenosis [2].

Methods

The PLLA stents implanted into the abdominal aorta of SD male rats. Three days prior to surgery, 2 mg/kg aspirin and 1.5 mg/kg clopidogrel were added to the normal diet. The paraffin slices of the blood vessel with PLLA stent segment were stained with immunofluorescence for VE-cadherin, CD31, Occludin, ZO-1, Piezo1, Tricellulin, Claudin-5 at various time points (1 week, 1 month, 3 months, 1 year) accordingly.

Results

The results showed that the expression of ZO-1 at was higher and exhibited at stents implantation site , compared to other groups.. The silk site was not expressed at the same time and the cross-sectional area of the lumen was reduced. And the expression of Piezo1 was lowest in control , and highest at 1 year. Additionally, Tricellulin and Claudin-5 were higher in 1 month and 3 months, compared to other groups.

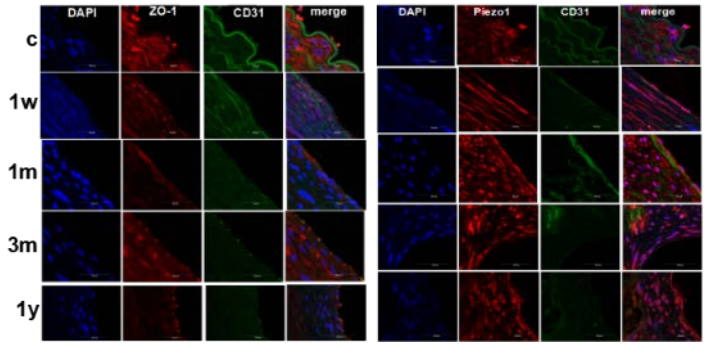

Figure: CD31/ZO-1 and CD31/Piezo1 after PLLA stents implantation at different time points..

Conclusions

In this study, the PLLA stents implanted with an expanded state within 3 months, indicating that vascular endothelial cells were disfunction. And expression levels of ZO-1, Piezo1, Occludin, Tricellulin and Claudin-5 were changed after stents implantation. Additionally, intimal hyperplasia were severe in 1 month and 3 months, and up-regulated at indicated time. Overall, ZO-1, Piezo 1, Occludin, Tricellulin and Claudin-5 response to injury caused by stents implantation.

References

[1] Vahl T P, Gasior P, Gongora C A, et al. Four-year polymer biocompatibility and vascular healing profile of a novel ultrahigh molecular weight amorphous PLLA bioresorbable vascular scaffold: an OCT study in healthy porcine coronary arteries[J]. EuroIntervention, 2016,12(12): 1510-1518.

[2] Cheng X , Wang X , Wan Y , et al. Myosin light chain kinase inhibitor ML7 improves vascular endothelial dysfunction via tight junction regulation in a rabbit model of atherosclerosis[J]. Molecular Medicine Reports, 2015.

Endothelial Tight Junction Protein Zo-1 Response to Multiple-Mechanical Stimulations

Yang Wang, Shuang Ge, Desha Luo, Ruolin Du, Yazhou Wang, and Guixue Wang*

Key Laboratory for Biorheological Science and Technology of Ministry of Education, State and Local Joint Engineering Laboratory for Vascular Implants, Bioengineering College of Chongqing University, Chongqing 400030, China
* Corresponding author. E-mail: wanggx@cqu.edu.cn

Introduction

Zonula occludens-1 (ZO-1) is a peripheral membrane protein belongs to the family of zona occludens proteins and plays a role as a scaffold protein which cross-links and anchors tight junction (TJ) strand proteins, within the lipid bilayer, to the actin cytoskeleton [1-2]. Stent implantation is the most effective method in the treatment of cardiovascular disease but always destroy junctions of endothelial cells. Endothelial cells that lack the ZO-1 gene showed relatively low content of tight junction related proteins [3], the functions of the tight junction were also affected. However, the role of ZO-1 before and after stent implantation has not been fully understood.

Methods

In vitro, HUVECs were exposed to fluid shear stress and static pressure respectively. Namely, shear stress at 5 dyn/cm^2 (low shear stress, LSS) and 12 dyn/cm^2 (high shear stress) for 6 h, and 40 KPa static pressure for 6 h and 12 h. The expression level of ZO-1 was analyzed by qPCR, western blot and immunofluorescence. In vivo, ApoE$^{-/-}$ mice and male SD rats were applied carotid ligation for 48 h and PLLA stents implantation for indicated time (1 week, 1 month , 3 month and 1 year), expression level of ZO-1 analyzed by qPCR in ApoE$^{-/-}$ mice and immunofluorescence in SD rats, respectively.

Results

In vitro, the expression level of ZO-1 showed higher at indicated shear stress, no statistical difference under static pressure at 6 h but significantly higher at 12 h, compared to control. Fluorescent staining showed more loose connection between cells and surrounding edges of the cells presented a gear shape with many small forks, compared to control. In vivo, expression of ZO-1 showed interestingly lower, compared to control in ApoE$^{-/-}$ mice and SD rats, except stents implantation at 3 month.

Conclusions

In the present study, we tried to indicate the role of ZO-1 before and after stent implantation by applying different mechanical stimulations respectively to imitate the mechanical environment endothelial cells might confront in vitro and in vivo. Interestingly, we found that expression of ZO-1 was diametrically opposed in vitro and in vivo except stents implantation for 3 month in rats. Since endothelial cells confront different mechanical stimulations at the same time and environment in vivo is complex, and ZO-1 might be inhibited or degraded in RNA level in vivo, therefore, our findings still make some sense.

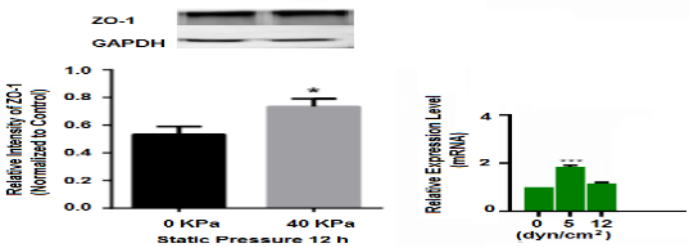

Fig. Western blot (HUVECs) and qPCR analysis of ZO-1(ApoE$^{-/-}$ mice)

References

[1] Walsh D R, Nolin T D, Friedman P A, Drug Transporters and Na+/H+ Exchange Regulatory Factor PSD-95/Drosophila Discs Large/ZO-1 Proteins 2015, *Pharmacological Reviews*, 67(3):656-680, 2015.
[2] Duan C Y, Zhang J, Wu H L, et al, Regulatory mechanisms, prophylaxis and treatment of vascular leakage following severe trauma and shock, *Military Medical Research*, 4(1):11, 2017
[3] Gonzalez-Mariscal L, Quiros M, Diaz-Coranguez M. Zo proteins and redox-dependent processes. *Antioxid Redox Signal*,15:1235-1253,2011.

Local Disturbing Flow Induced by Stent Implantation Affects Endothelial Cell Rearrangement and Endothelialization

Ruolin Du, Yuzhen Ren, Shicheng He, Shuang Ge, Yang Wang, Junyang Huang, Yazhou Wang, Guixue Wang, Tieying Yin*

Key Laboratory for Biorheological Science and Technology of Ministry of Education, State and Local Joint Engineering Laboratory for Vascular Implants, Bioengineering College of Chongqing University, Chongqing 400030, China
* Corresponding author. E-mail: wanggx@cqu.edu.cn

Introduction

With the implantation of coronary stents, the integrity of the vascular endothelium was damaged and the local mechanical environment at the stent segment was changed too. At the juncture of the stent and blood vessel, the fluid reversed sharply, and the disturbing blood flow was formed. Local disturbing flow may impel platelet aggregation and activation at the injured site and affects the endothelial repair process at the same time.

Methods

In this study, 316L stents were implanted to the coronary arteries of pigs and target segments were picked out after 1, 3, 6, 12 and 24 months. The local cell morphology of neointima with stents was observed by scanning electron microscopy. the shear stress distribution of "S-shaped" stent was simulated and analyzed in detail via ANSYS cfx software. In-vitro cell experiment was down according to the simulation, HUVECs were cultured and analyzed under different scrambling conditions.

Results

in vivo experiments in mini pigs confirmed that the surface of all stent groups was partially covered with cobblestone-like endothelial cells at 1, 3 and 6 months, the morphology of cells adhered seemed to become oval from the initial roundness. The vascular endothelial cells responded to the change of shear stress distribution by particular cell rearrangement: on the straight segment of the stent, ECs were arranged closely along with the direction of blood flow and the stent body; close to the “S” shape (Link), the rearrangement of ECs became more disorderly and multi-shaped in accordance with the direction of the blood flow. The simulation showed that region at the “S” shape of the stent is a low shear stress area and blood flow through formed local disturb flow, while the bare area of the vessel between stent struct had high shear stress. In-vitro cell experiments found the cytokines related to the arrangement and intercellular connection and obtained similar results related to the simulation results.

Conclusions

Our in-vivo an in-vitro experiment demonstrated that the local disturbing flow caused by the stents affected the endothelial cell rearrangement and endothelialization, which in turn affect the morphology and function of ECs. This study will be helpful to further understand the rules of vascular remodeling and re-endothelialization after stent implantation.

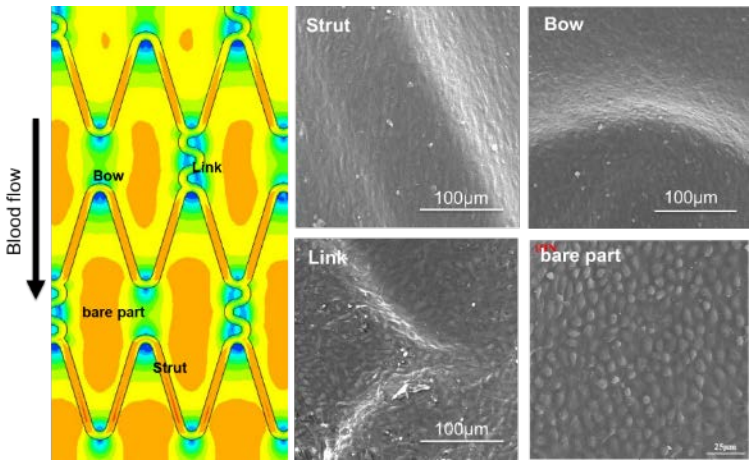

Fig. Simulation of stress after stent implantation and arrangement of vascular endothelial cells in vivo

Integrating Light-Sheet Imaging with Advanced Computation to Recapitulate Developmental Cardiac Mechanics

Yichen Ding[1,2], Varun Gudapati[1], Junjie Chen[2], Arash Abiri[3], René R. Sevag Packard[1], Tzung K. Hsiai[1,2,4]

[1] Department of Medicine, University of California, Los Angeles, CA 90095, USA
[2] Department of Bioengineering, University of California, Los Angeles, CA 90095, USA
[3] Department of Biomedical Engineering, University of California, Irvine, CA 92697, USA
[4] Medical Engineering, California Institute of Technology, Pasadena, CA 91125, USA

Introduction

Light-sheet fluorescence microscopy (LSFM) is revolutionizing multi-scale imaging from live zebrafish embryos to adult rodent. LSFM imaging enables high spatiotemporal resolution in the 4-dimensional (4-D) domain with minimal photobleaching and phototoxicity. We hereby integrate LSFM and post-imaging computation to study chemo-induced myocardic injury and repair. To acquire the periodical cardiac cycle, we have built an in-house LSFM with the sub-voxel spatial resolution, interactive quantification, and machine learning-based post-image segmentation. To localize regional ventricular myocardium and subsequent contractile function, we have developed the displacement analysis of myocardial mechanical deformation (DIAMOND) to assess 4-D cardiac structure and function. We hypothesize that the basal ventricular segments adjacent to the atrioventricular (AV) canal displays the highest 3-D displacement and also the most susceptible region to chemo-induced injury.

Methods

We have developed the DIAMOND to quantify local and global displacement of mass centroids of different segmented myocardium. This newly developed method enables the precise determination of the displacement of mass centroids in 3-D space as a segmental metric of micro-cardiac mechanics, providing an opportunity to localize segmental myocardial deformation in response to chemo-induced cardiac injury. We established the subspace approximation with augmented kernels (SAAK) transform to enhance efficiency and accuracy of post-image processing for 4-D DIAMOND. Our virtual reality (VR) based LSFM platform further enables to interactively compute segmented myocardial displacement and strain with a user-directed perspective.

Results

The critical produres of the multi-scale LSFM imaging are indicated for both embryonic zebrafish and mouse studies (Fig 1). We provided SAAK transform based image segmentation of adult zebrafish heart with only 18 training images (Figs 1 A-D), and quantified the 4-D ventricular contractility occurring between consecutive frames as the user operates on the 4-D contracting heart in a transgenic *Tg(cmlc2:gfp)* zebrafish embryo at 5 dpf (Figs 1E-G). We analyzed 3-D myocardial displacements of a single segment illustrated from end-systole to end-diastole in the myocardium, and illustrated 3-D displacement vectors of sequential consecutive deformations (Figs 1H-I). We applied this hybrid platform to track end-to-end displacement of six myocardial segments from end-systole to end-diastole in the chemo-induced cardiac injury in zebrafish embryos (Fig 1G).

Conclusions

Our integrated LSFM and computation reveal that the basal myocardium contributes to the most myocardial contractile function and that this segment is also most-suceptible to chemo-inudced myocardiac injury.

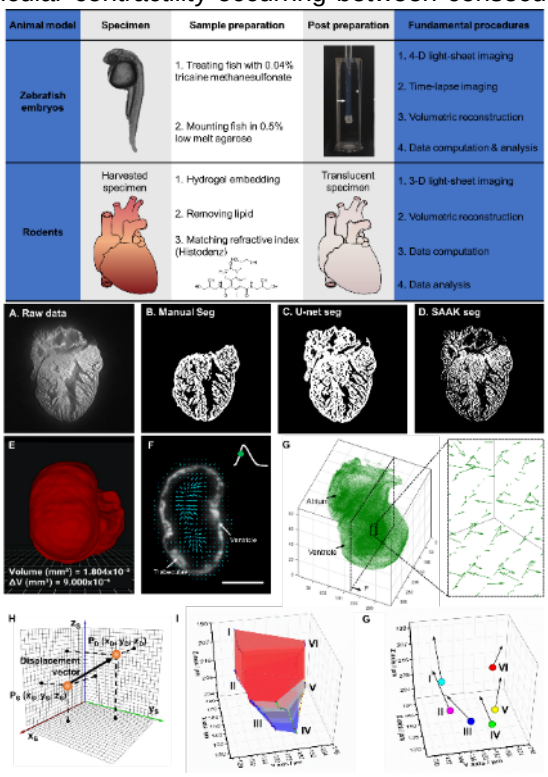

Figure 1. Fundamental concept of the LSFM strategy and computational analysis.

Predicting False Lumen Thrombosis after TEVAR in Type B Aortic Dissection

C.H. Armour [1]⊥, C. Menichini [1]⊥, K. Milinis [2], R.G.J. Gibbs [3], X.Y. Xu [1]

[1] Department of Chemical Engineering, Imperial College London, London, United Kingdom; [2] Imperial College NHS Trust, London, United Kingdom; [3] Regional Vascular Unit, St Mary's Hospital, Imperial College Healthcare National Health Service Trust, Imperial College London, London, United Kingdom.
⊥ Co-first author.

Introduction

TEVAR has been shown to be an effective treatment method for type B aortic dissection, with higher levels of false lumen thrombosis (FLT) compared to patients treated with medical therapy alone [1,2]. A number of morphological features have been identified to influence FLT after TEVAR [3,4], but the underlying reasons why these parameters affect FLT are unclear. Therefore, the objective of this study is to investigate how morphological features may influence FLT after TEVAR through computational modelling of flow and thrombus formation in patient-specific geometries.

Methods

Three patients from the ADSORB trial [2] were included in this study. The first post-TEVAR CT scans were used to build patient-specific models and their computational mesh, with each mesh containing 5-10 million elements depending on the geometry and mesh sensitivity tests. Additional models were created to study the role of specific morphological parameters. For patient 1 the first post-stent entry tear (FET) was artificially moved upwards by 30 mm to study the influence of tear location relative to the end of the stent graft (SG). In patient 2 two post-stent tears close to the distal end of the SG were occluded to simulate an extension of the SG by 30 mm.

In all models (3 original and 2 modified) a flat pulsatile velocity profile was specified at the inlet and 3-element Windkessel models were applied at all outlets. Simulations of flow were performed for 4 cycles first, before being coupled with the thrombosis model developed by Menichini et al. [5,6].

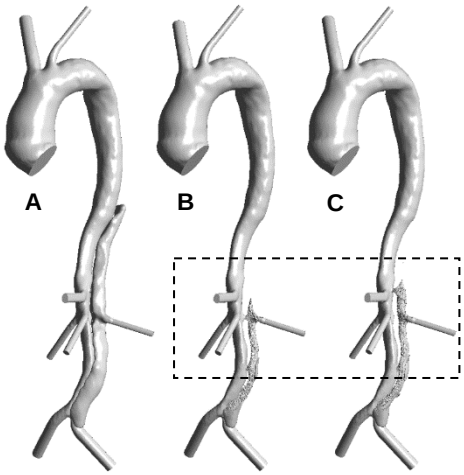

Figure 1: A) Reconstructed post-TEVAR geometry of patient 1. Predicted thrombus formation for patient 1 in B) original geometry and C) modified geometry. Difference in predictions due to modified FET is highlighted.

Results

Flow results showed reduced flow and low time-averaged wall shear stress (TAWSS) in the false lumen of patients 1 and 3, who notably presented large SG-FET distances. Thrombus predictions for each patient were consistent with observed FLT from follow-up CT scans, demonstrating the validity of our predictive model. Modification of patient 1 by moving the FET reduced the SG-FET distance, which resulted in increased flow in the upper abdominal FL, elevated TAWSS and reduced FLT (Figure 1). Modification of patient 2 by occluding the proximal tears increased the SG-FLT distance, resulting in quicker thoracic FLT and varied abdominal FLT patterns.

Conclusions

These results show that the location of post-stent entry tears has a strong influence on the progression of FLT by affecting FL flow and TAWSS. Increasing the SG-FET distance favours thrombus formation in the false lumen, and this can be achieved through extending the length of SG coverage in some aortic dissection patients.

References

[1] Nienaber, C.A., et al. (2014). *Heart,* 100:1491-1497
[2] Brunkwall, J., et al. (2014). *Eur J Vasc Endovasc*, 48(3):285-291
[3] Qin, Y-L., et al. (2012). *J Vasc Surg*, 56:1232-1238
[4] Tolenaar, J.L., et al. (2014). *Ann Cardiothorac Surg*, 3(3):225-263
[5] Menichini, C. and Xu, X.Y. (2016) *J Math Biol,* 73(5):1205-1226
[6] Menichini, C., et al. (2018). *J Biomech,* 66:36-43

Ventricular dynamics is a main determinant of the augmentation index: An in *in vivo* and *in silico* study

Sam Vennin[1,2], Ye Li[1], Jorge Mariscal-Harana[2], Peter Charlton[2], Jordi Alastruey[2], Phil Chowienczyk[1]

[1]Department of Clinical Pharmacology, King's College London, UK [2]Department of Biomedical Engineering, King's College London, UK

Introduction

The role of pulse wave reflections in the increase of the augmentation pressure and, in turn, pulse pressure (PP) with ageing has been recently challenged as recent studies have highlighted the potential importance of ventricular ejection properties in determining blood pressure pulsatile components [1,2]. The first systolic shoulder (P1) of the pressure waveform is proportional to the product between the aortic pulse wave velocity (PWV) and aortic flow at time of P1 (U1) [3], and the usual peak pressure (P2) to the product between PWV and the volume of blood (V2) ejected at the time of P2 [4]. Assuming proportionality between proximal and distal PWV and noticing the close relationship between the augementation index (AIx) and the ratio P2/P1, we investigate the relationship between AIx and a new index based entirely on ventricular mechanics, QIx, defined as V2/U1.

Methods

The study involved patients from a normotensive (n=164, 126 men, age 49±8 years, blood pressure 110±16/69±10 mmHg, means±SD) and hypertensive (n=156, 83 men, age 46±17 years, blood pressure 130±23/83±13 mmHg) cohort. Reflected waves were quantified using the reflection coefficient Γ, *i.e.* the ratio of backward to forward pressure component. A Least Absolute Shrinkage and Selector Operator (LASSO) analysis was performed to statistically identify the main contributors to AIx among a set of cardiac and arterial parameters (Age, PWV, Γ, QIx, MBP, PP). To determine the relative contribution to AIx of arterial (Γ) and cardiac (QIx) properties, variations of AIx with QIx for an approximately fixed Γwere assessed, and *vice versa*. A sensitivity analysis of changes in AIx to QIx and $\Gamma$was also performed using an *in silico* model of blood flow in the larger arteries of the upper thoracic aorta.

Results

The LASSO analysis identified QIx and Γ as the main determinants of AIx with standardised coefficients of 0.24 and 0.49, respectively ($p>0.001$ in each case). AIx was found to increase with increasing QIx and Γ. *In silico* and *in vivo* studies were consistent as the coefficient of % increase in AIx per ml.s.m^{-1} increase in QIx was 0.18, for both normotensive and hypertensive subjects, compared with a theoretical value derived from the sensitivity analysis of 0.16 % change in AIx per change ml.s.m^{-1} in QIx. Change in AIx per change in Γ was 35% and 28% for normotensive and hypertensive cohorts, respectively, compared with a theoretical value derived from the sensitivity analysis of 30 % change in AIx per change in Γ. The sensitivity analysis also confirmed QIx had a greater impact on AIx since a 30% change in QIx from baseline resulted in a 35% increase in Aix, while the same increase in baseline Γyielded a 27% increase in AIx.

Conclusions

We have proposed a new index based entirely on ventricular ejection dynamics and studied its relationship with AIx. The results of this part-*in-silico*/part-*in-vivo* study further challenge the role of reflection waves in the increase of AIx, as our new index was as correlated, if not more, to AIx than Γ.

References

[1] Torjessen AA, Wang N, Larson MGn Hamburg NM, Vita JA, Levy D, Benjamin EJ, Vasan RS, Mitchell GF, Forward and backward wave morphology and central pressure augmentation in men and women in the Framingham Heart Study, *Hypertension*, 64(2):259-265, 2014

[2] Fok H, Guilcher A, Li Y, Brett S, Shah A, Clapp B, Chowienczyk P, Augmentation Pressure Is Influenced by Ventricular Contractility/Relaxation Dynamics, *Hypertension*, 63(5):1050-1055, 2014

[3] Vennin S, Mayer A, Li Y, Fok H, Clapp B, Alastruey J, Chowienczyk P. Noninvasive calculation of the aortic blood pressure waveform from the flow velocity waveform: a proof of concept, *Am J Physiol Heart Circ Physiol*, 309(5):H969-76, 2015

[4] Vennin S, Li Y, Willemet M, Fok H, Gu H, Charlton P, Alastruey J, Chowienczyk P. Identifying hemodynamic determinants of pulse pressure. A combined numerical and physiological approach, *Hypertension*, 70(6):1176-1182, 2017

Mechanical Regulation of Autonomously Forming Endothelial Gaps and Cancer Extravasation

Jorge Escribano[1,2], Michelle B. Chen[2,3], Emad Moeendarbary[2,4], Xuan Cao[5], Vivek Shenoy[5], Jose Manuel Garcia-Aznar[1,*], Roger D. Kamm[2,6,7,*], Fabian Spill[6,8,*]

1Department of Mechanical Engineering, University of Zaragoza, Zaragoza, Spain
2Department of Biological Engineering, Massachusetts Institute of Technology, Cambridge, MA 02139, USA
3Department of Bioengineering, Stanford University, Stanford, CA 94305, USA
4Department of Mechanical Engineering, University College London, London WC1E 6BT, United Kingdom
5Department of Materials Science and Engineering, University of Pennsylvania, Philadelphia, PA 19104, USA
6Department of Mechanical Engineering, Massachusetts Institute of Technology, Cambridge, MA 02139, USA
7BioSystems and Micromechanics (BioSyM), Singapore-MIT Alliance for Research and Technology, Singapore, Singapore
8School of Mathematics, University of Birmingham, Birmingham, B15 2TT, UK
* Corresponding authors, jmgaraz@unizar.es, rdkamm@mit.edu, f.spill@bham.ac.uk

Introduction
Endothelial cells constantly push and pull on neighbouring cells, leading to forces on VE-cadherin mediated cell-cell junctions. These junctions are highly dynamic, and their rupture may lead to the autonomous formation of gaps in the endothelium. We present a novel mathematical model that predicts the frequency, lifetime and size of these gaps, and validate the predictions with experiments of HUVEC monolayers.

Methods
Our major new method is a stochastic-mechanical multiscale model of endothelial cells. It captures different intracellular forces, and the force-dependent, mechanical regulation of cell-cell adhesions. The computational model predictions are validated by monocultures of HUVECs. Moreover, co-cultures of HUVEC monolayers with MDA-MB-231 cancer cells are used for the extravasation studies.

Results
We find that gaps occur more often at the vertices of three or more cells, as opposed to the borders between two cells. Interestingly, cancer cells follow this trend and primarily extravasate at the vertices. Notably, they do so even when they first arrest on the two cell border, where they subsequently typically migrate towards the endothelial vertices

Conclusions
Our findings indicate that the cancer cells exploit the autonomously forming gaps, and do not necessarily rely on signaling to the endothelium to initiate gap formation. The highly dynamic nature of the endothelium consequently plays a fundamental role in the regulation of gaps and in controlling cancer and immune cell extravasation.

References
[1] Escribano J, Chen M, Moeendarbary E, Cao X, Shenoy V, Garcia-Aznar JM, Kamm R, Spill F. Balance of Mechanical Forces Drives Endothelial Gap Formation and May Facilitate Cancer and Immune-Cell Extravasation. bioRxiv. 2018 Jan 1:375931.

High Coronary Shear Stress in Patients With Coronary Artery Disease Predicts Myocardial Infarction.

Kumar A[1], Thompson EW[2], Lefieux A[3], Molony DS[2], Davis EL[2], Chand N[2], Fournier S[4], Lee HS[2], Suh J[2], Sato K[5], Ko YA[6], Molloy D[2], Chandran K[2], Hosseini H[2], Gupta S[2], Milkas A[4], Gogas B[2], Chang HJ[7], Min JK[7], Fearon WF[8], Veneziani A[9], Giddens DP[10], King SB 3rd[2], De Bruyne B[4], Samady H[11].

Emory University, Atlanta and Emory University Hospital, Atlanta

Introduction
Coronary lesions with low fractional flow reserve (FFR) that are treated medically are associated with higher revascularization rates. High wall shear stress (WSS) has been linked with increased plaque vulnerability.

Objectives:
This study investigated the prognostic value of WSS measured in the proximal segments of lesions (WSS_{prox}) to predict myocardial infarction (MI) in patients with stable coronary artery disease (CAD) and hemodynamically significant lesions. The authors hypothesized that in patients with low FFR and stable CAD, higher WSS_{prox} would predict MI.

Methods:
Among 441 patients in the FAME II (Fractional Flow Reserve Versus Angiography for Multivessel Evaluation II) trial with FFR ≤0.80 who were randomized to medical therapy alone, 34 (8%) had subsequent MI within 3 years. Patients with vessel-related MI and adequate angiograms for 3-dimensional reconstruction (n = 29) were propensity matched to a control group with no MI (n = 29) by using demographic and clinical variables. Coronary lesions were divided into proximal, middle, and distal, along with 5-mm upstream and downstream segments. WSS was calculated for each segment.

Results:
Median age was 62 years, and 46 (79%) were male. In the marginal Cox model, whereas lower FFR showed a trend (hazard ratio: 0.084; p = 0.064), higher WSS_{prox} (hazard ratio: 1.234; p = 0.002, C-index = 0.65) predicted MI. Adding WSS_{prox} to FFR resulted in a significant increase in global chi-square for predicting MI (p = 0.045), a net reclassification improvement of 0.69 (p = 0.005), and an integrated discrimination index of 0.11 (p = 0.010).

Conclusions:
In patients with stable CAD and hemodynamically significant lesions, higher WSS in the proximal segments of atherosclerotic lesions is predictive of MI and has incremental prognostic value over FFR.

Endothelial Stat5a is enriched at atheroprone regions of the aorta and drives inflammation in response to low shear stress.

Hannah Roddie, Maria Fragiadaki* and Paul Evans*
(* joint senior authors)

Department of Infection, Immunity and Cardiovascular Disease, The Medical School, University of Sheffield, UK.

Introduction

Atherosclerosis is an inflammatory disease that develops at bends and branches of the arteries that are exposed to disturbed blood flow which generates low wall shear stress (WSS). These haemodynamic conditions lead to altered endothelial function and promote proliferation, apoptosis and inflammatory activation of endothelial cells (ECs), as well as other fundamental processes that drive disease. The Janus Kinase and Signal Transducer and Activators of Transcription (JAK/STAT) is an evolutionarily conserved pathway with key roles in the control of proliferation, apoptosis and inflammatory activation, yet its role in atherosclerosis is poorly understood despite the fact that these processes drive atherogenesis.

Methods

Microarrays were performed on ECs from the porcine aorta to quantify stat5a expression in low WSS (atheroprone) and high WSS (atheroprotected) regions, and data were validated by qRT-PCR. *En face* immunostaining of the murine aortic arch was carried out to quantify Stat5a expression at low and high WSS. *In vitro* studies were performed using human coronary artery endothelial cells (HCAECs) and human umbilical vein endothelial cells (HUVECs) which were subjected to either retroviral-mediated shRNA (HCAECs) or siRNA (HUVECs) silencing of Stat5a. These cells were then exposed to low (5 dynes/cm^2) or high (10 dynes/cm^2) WSS for 72 hours on the orbital system and inflammatory molecule (ICAM-1, VCAM-1, E-Selectin and MCP-1) expression was studied by qRT-PCR.

Results

qRT-PCR analysis of the porcine aorta identified that Stat5a was enriched at low WSS regions compared to high WSS regions ($P<0.05$). *En face* staining of the murine aorta also revealed that endothelial Stat5a expression was enhanced at regions of low WSS compared to high WSS ($P<0.05$). Similarly, Stat5a mRNA expression was enhanced in cultured HCAEC exposed to low compared to high WSS. Functional studies showed that silencing of Stat5a led to a reduction of ICAM-1 ($P<0.05$), VCAM-1 ($P<0.05$), E-Selectin ($P<0.05$) and MCP-1 ($P<0.05$), indicating that Stat5a is a positive regulator of EC inflammatory activation.

Conclusions

Our data demonstrate that Stat5a is upregulated by low WSS both *in vivo* and *in vitro*, and that its silencing reduces inflammatory gene expression. These data therefore suggest that Stat5a may regulate the focal nature of atherogenesis by promoting inflammation.

Disturbed flow induces aortic valve calcification by activating the HIF-1α Pathway triggered by loss of miR-483-3p, leading to increased UBE2C and degradation of pVHL.

Joan Fernandez Esmerats[1], Nicolas Villa-Roel[1], Sandeep Kumar[1], Lina Gu[1], Md Tausif Salim[2], Michael Ohh[3], W. Robert Taylor[4], Robert M. Nerem[5], Ajit P. Yoganathan[1,2], and Hanjoong Jo[1,2]

[1]Wallace H. Coulter Department of Biomedical Engineering, Georgia Institute of Technology and Emory University; [2]School of Chemical and Biomolecular Engineering, Georgia Institute of Technology; [3]Department of Biochemistry, University of Toronto, Canada; [4]Division of Cardiology, Department of Medicine, Emory University; [5]Parker H. Petit Institute for Bioengineering and Bioscience, Georgia Institute of Technology, Atlanta, GA, USA

Objective—Calcific aortic valve (AV) disease, characterized by AV sclerosis and calcification, is a major cause of death in the aging population; however, there are no effective medical therapies other than valve replacement. AV calcification preferentially occurs on the fibrosa side, exposed to disturbed flow (d-flow), whereas the ventricularis side exposed to predominantly stable flow remains protected by unclear mechanisms. Here, we tested the role of novel flow-sensitive UBE2C (ubiquitin E2 ligase C) and miR-483 in flow-dependent AV endothelial function and AV calcification.

Approach and Results—Human AV endothelial cells and fresh porcine AV leaflets were exposed to stable flow or d-flow. We found that UBE2C was upregulated by d-flow in human AV endothelial cells in the miR-483–dependent manner. UBE2C mediated d-flow-induced endothelial inflammation and endothelial-mesenchymal transition (EndMT) by increasing the HIF-1α (hypoxia-inducible factor-1α) level. UBE2C increased HIF-1α by ubiquitinating and degrading its upstream regulator pVHL (von Hippel-Lindau protein). These in vitro findings were corroborated by immunostaining studies using diseased human AV leaflets. In addition, we found that reduction of miR-483 by d-flow led to increased UBE2C expression in human AV endothelial cells. The miR-483 mimic protected against endothelial inflammation and EndMT in human AV endothelial cells and calcification of porcine AV leaflets by downregulating UBE2C. Moreover, treatment with the HIF-1α inhibitor (PX478) significantly reduced porcine AV calcification in static and d-flow conditions.

Conclusions—These results suggest that miR-483 and UBE2C are novel flow-sensitive anti- and pro-calcific AV disease molecules, respectively, that regulate the HIF-1α pathway in AV. The miR-483 mimic and HIF-1α pathway inhibitors may serve as potential therapeutics of calcific AV disease.

4D Ultrasound of Murine Abdominal Aortic Aneurysms

Hannah L. Cebull[1], Daniel J. Romary[1], Craig J. Goergen[1]

[1] Weldon School of Biomedical Engineering, Purdue University, West Lafayette, Indiana, USA

Introduction

Current approaches for *in vivo* abdominal aortic aneurysm imaging focus on measuring maximum diameter, neglecting 3D vascular deformation and strain. Complex vessel geometries, heterogeneous wall compositions, and surrounding structures can all influence aortic strain over the cardiac cycle. Improved understanding of the complex kinematics and stresses within the aortic wall has the potential to increase our ability to predict aneurysm expansion and eventual rupture.

Methods

4D high frequency ultrasound data (Fig. 1) were collected from two murine AAA models: **1)** apolipoprotein E-deficient animals infused with angiotensin II (AngII) [1] and **2)** a combination of topical elastase applied to the adventitia with drinking water infused with β-aminoproprionitrile fumarate (BAPN) [2]. Deformation gradient tensors were estimated using a direct deformation analysis technique [3]. 3D Green-Lagrange strain was then calculated at each timepoint and visualized as a volume. We compared heterogeneous patterns of the first principal strain component with vessel composition for each animal [4]. Strain measurements were then compared to H&E and Movat pentachrome histology at similar locations.

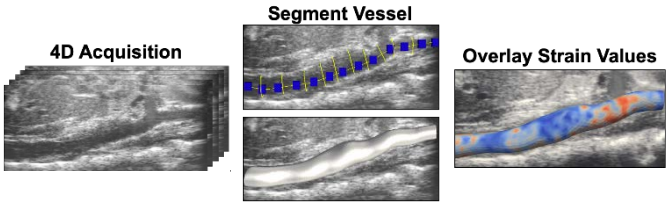

Figure 1: 4D ultrasound can be used to collect gated volumetric image data of the murine vasculature.

Results

Principal Green Lagrange strain is not evenly distributed throughout the vessel, and the range of strain values varied significantly between individual animals and groups. The elastase model led to tortuous infrarenal AAAs with intraluminal thrombus present in 60% of animals after 28 days (Fig. 2A). Further, we identified in the AngII model a general decrease in strain after focal breakage of the medial elastin, which was further exacerbated in animals with substantial formation of intramural thrombus (Fig. 2B). A slight increase in strain was noted in two mice with no focal elastin breakage, suggesting that intact medial elastin is correlated with greater aortic deformation, especially in hypertensive animals. Interestingly, a dissection that went undiagnosed via ultrasound imaging did show reduced strain, suggesting this animal experienced medial elastin breakage within its aorta, a finding that was later confirmed via histology.

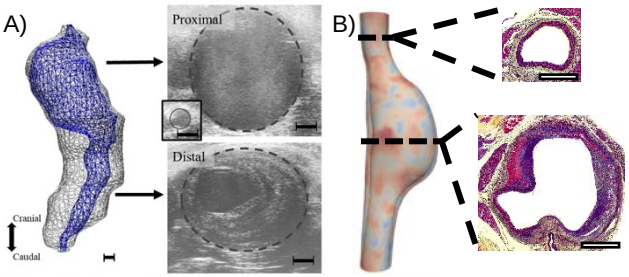

Figure 2: Elastase (A) and AngII (B) aneurysms compared to either raw ultrasound data (left) or histology (right).

Conclusions

These results highlight the relationship between *in vivo* 3D aortic strain and vessel composition. By quantifying a wide range of lesion severities and heterogeneous strain patterns, we showed that region-specific strain provided improved insight into aortic aneurysm dynamics and thrombus formation, illustrating the need for mouse-specific analysis. While further work is needed with both preclinical animal models and human imaging studies, these initial 4D imaging data indicate that incorporating *in vivo* vessel strain may be useful for developing an improved metric correlated with aneurysm growth and rupture.

References

[1] Daugherty, A., *et al.*, (2000). *J Clin Invest.* **105**(11):1605-1612. **[2]** Lu, G., et al., (2016). *J Vasc Surg*. **66**(1)p232-242.e4. **[3]** Boyle, J.J., *et al.*, (2018), *J Biomech*. **141**(1): 011010. **[4]** Cebull, H.L., *et al.*, (2019). *J Biomech*. Accepted.